DETERMINATION OF
EARTH RESISTIVITY PROFILE
IN MUL TI LAYER SOIL

A thesis submitted to the

Department of Electrical Engineering, University of Moratuwa

in partial fulfillment of the requirements for the

Degree of Master of Philosophy

by

IMAL-I THANUJA DHARMADASA

Supervised by: Prof. J.R. Lucas

Co-Supervised by: Dr. -V.K.D.L. Vdawatta

Mr. W.D.A.S. Wijayapala

Department of Electrical Engineering

University of Moratuwa, Sri Lanka

2009

93877

Abstract

Soil structure investigation is very important in many Engineering applications. The Electrical Engineers extensively use the soil structure information when designing grounding systems. The sub soil structure with its resistivity distribution has a direct impact on the performance of the grounding system, that is, the electrode resistance and the surface voltage distribution.

In Applied Geophysics a variety of soil structure investigation methods are used. Among these, the Electrical Resistivity Method has become very popular due to its simplicity. The resistivity method measures apparent resistivity of the ground to a direct current flow. The field data contain apparent resistivity values and geometry information. When the field data is interpreted, it detects the discontinuity of resistivity distribution in a location of interest. This interpretation can be done One dimensionally(lD), Two-dimensionally (2D) or Three-dimensionally (3D) depending on the application's necessity. The interpretation of resistivity field data using inversion techniques may be ambiguous. Conventional ID DC resistivity inversion techniques include graphical methods requiring interpolation and judgment and computer based iterative calculation methods.

The work presented in this thesis, investigates a new resistivity data inversion tool, Neural networks(NNs). Neural Networks are capable of solving several types of problems, including parameter estimation, parameter prediction, pattern recognition, classification and optimization. Also recently the use of Neural Networks in the Geophysics parameter estimation problems has Shown strong results. With this recent trend in the applicability of the NN's for the non linear geophysical inversion problems NN's is proposed as the inversion tool for parameter estimation or **Sub** surface interpretation. The main intention of this study is to investigate the applicability of NNs as a fast and accurate inversion tool for field resistivity data. The study considers the approach and capabilities of the NNs in inversion of field

resistivity data to interpret ID, 2D or 3D sub soil Structure with resistivity discontinuities.

List of Figures

List of Tables

1.1 Background

Earth resistivity surveying is commonly conducted to interpret the subsurface conditions (soil structure) for engineering applications. Soil structure investigation is very important in many Engineering applications such as Electrical Engineering, Civil Engineering and Earth Resource Engineering applications. For instance Civil Engineers investigate the soil structure for pile foundation constructions. Earth Resource and Mines Engineers apply them in mineral and groundwater exploration, Sand Gravel prospecting and oil exploration; and Electrical Engineers use soil structure knowledge for designing of grounding systems and for lighting protection design. Nowadays they are also extensively used to monitor groundwater contamination, locate subsurface cavities and fissure for various other engineering applications.

Sub soil structure investigations can be done by indirect methods and by direct methods. The latter includes the direct drilling of the earth which is time consuming and costly. Limitations do arise in physical excavations on subsurface study due to digging.

Indirect methods come under Geophysics, where, among other methods, they use electrical energy to gain knowledge of the interior of the earth. These methods are based on sound principles of physical science, which is Geophysics, and involves the application of physical theories and measurements to discover the properties of the earth or the soil structure.

Geophysics can be divided into two broad categories: Whole earth geophysics and applied geophysics. Whole earth geophysics involves the study of physical processes that span the whole earth, such as those associated with plate tectonics, earthquakes and the earth's magnetic field.

Applied geophysics is the use methods such as seismic, gravity, magnetic, electrical, and electromagnetic, in the search for oil, gas, metallic mineral deposits, and water. It also includes the investigation of subsurface structures and materials that have

engineering implications, the study of near-surface processes that impact the environment and society, and more, with the objective of economic exploitation. The variation in electrical conductivity and natural currents in the earth, rates of decay of artificial potential differences introduced into the ground, local changes of gravity, magnetism and radioactivity- all these provide information about the nature of structure below the surface, thus permitting geophysists to determine the most favorable places to search for the mineral deposits etc., that they seek. In short, geophysical exploration intends to create an image of the subsurface of the earth in terms of its physical properties. Unlike solid earth geophysics, exploration geophysics generally concentrates on finding lateral heterogeneities in a relatively small part of the earth's crust.

Applied Geophysics in the search for minerals, oil and gas may be divided into the methods of Exploration as given in Table 1.1.

Geophysical Method		Quantitative Measure (Experimental or observational data)
Gravity Method		Measures the variation in gravitational field of the earth
Magnetic Method		measures the earth's ambient magnetic field
Seismic Methods (reflection and refraction)		measures the response of seismic (sound) waves that are input into the earth
Electrical Methods	Spontaneous Potential	measures naturally occurring DC currents
	Electromagnetic Method	measure apparent resistance of ground to induced alternating current (AC) flow
	Field resistivity measurements	Measures apparent resistance/resistivity of ground to direct current flow.
	Induced Polarization	measures effect on current flow of charge storage in ground
Ground-penetrating radar		Measures changes in dielectric properties

Table 1.1 – Applied Geophysical Methods

It should be pointed out that geophysics techniques can detect only a discontinuity, that is, where one region differs sufficiently from another in some property. This, however, is a universal limitation, for we cannot perceive that which is homogeneous in nature: we can discern only that which has some variation in time and/or space [1]. The choice of techniques to locate a certain mineral depends on the nature of the mineral and of the surrounding rocks. Sometimes a method may give a direct indication of the presence of the mineral being sought, for instance, the magnetic method when used to find magnetic ores of iron or nickel; at other times the method may indicate only whether or not conditions are favorable to the occurrence of the mineral sought. For instance, the magnetic method is used in petroleum exploration as a reconnaissance tool to determine the depth to the basement rocks and thus determine the sediments are thick enough to warrant exploration.

1.2 Electrical Geophysical Methods and their applications

Electrical exploration methods may be subdivided into two main groups. One group is concerned with measurement of resistivity, or conductivity, of rocks, while the other group is concerned with measurement of their capacitance. The resistivity, induction and magneto-telluric methods belong to the first group, and the induced polarization methods belong to the second group.

1.2.1 Spontaneous Potential Method

The Spontaneous Potential or Self Potential method measures the natural variation of the ground voltage between two electrodes. The voltage variation is caused by electrochemical reactions at a conductive body.

Natural oxidation-reduction processes generate small electrical potentials that can be measured and mapped. Oxidation of a mineral such as pyrite, transforms iron sulfide into iron oxide; that liberates electrons, which produce a negatively charged electrical current that is normally under one volt. Spontaneous Potential methods take advantage of this phenomenon that contrasts zones with higher concentration of sulfides in oxidation which produce negative potential anomalies that stand out well below the local base level.

To measure small currents on the ground one needs special electrodes that do not polarize as they are introduced in the soil. Spontaneous potential (SP) is measured by an electrode in a borehole relative to a fixed reference electrode on the surface. In the field one probe of a voltmeter is placed at the Earth's surface (called surface electrode) and the other probe in the borehole (called down hole electrode), where the SP is to be measured. In fact, logging tools employ exactly this method. Since this measurement is relatively simple, usually the SP down-hole electrode is built into other logging tools.

1.2.2 Electromagnetic induction Method

The electromagnetic induction (EM) method measures the response of an induced alternating current. A current is induced into the ground by a transmitting coil. A receiving coil is placed a short distance away to measure the induced earth current. The size of the induced current depends on the geologic material (lithology) beneath the transmitter and receiver. By mapping changes in the induced current, it is possible to map out changes in lithology, in order to determine the potential presence of an aquifer. A map of subsurface conductivity can be produced from the data obtained in an electromagnetic induction survey. The map shows areas of disturbed soil, buried metallic objects, and changes in soil conductivity that may be related to disposal of highly conductive substances.

The EM method is also very sensitive to metal. Thus, the location of buried metal objects, such as drums or pipes, can be mapped with this technique.

1.2.3 Resistivity Method

All resistivity methods employ an artificial source of current, which is introduced to the ground through point electrodes. In practice, the current is introduced into the ground through one pair of electrodes. Current flow between these electrodes span out through the ground in a pattern and intensity that depends on the conductivity of the ground and any stratification or obstacles that lie in the vicinity of the electrodes. A second pair of electrodes is then used to quantitatively measure the voltage pattern on the surface resulting from the current flow pattern of the first set of electrodes. Finally an effective or apparent resistivity of the subsurface is determined.

Search for geothermal reservoirs normally involves resistivity surveying and is also employed routinely in groundwater exploration and in civil engineering.

The chief drawback of the method is its high sensitivity to minor variations in conductivity near the surface; in electronic parlance the noise level is high. This limitation added to the practical difficulties involved in dragging several electrodes and long wires through rough areas and due to cultural problems causing interference, e.g., power lines, pipelines, buried casings, fences has made the electromagnetic method popular than resistivity in mineral exploration. The resistivity method is not particularly suitable for oil prospecting.

The rapid development of the induced polarization technique, which includes resistivity data, has guaranteed the resistivity method's continuous use in spite of its limitations.

1.2.4.4 Induced Polarization Method

Induced Polarization (IP) is an Electrical method of geophysical surveying employing an electrical current to determine indications of mineralization. The induced polarization method has been developed for detecting small concentrations of disseminated mineralization in base metal exploration. With the IP surveys subsurface materials, such as ore's can be easily identified. This method has also found limited use for detecting other exploration targets, e.g., in groundwater exploration, geotechnical and environmental applications.

The method is similar to electrical resistivity surveys, in that an electric current is induced into the subsurface through two electrodes, and voltage is monitored through two other electrodes. In the Time domain IP method the slow decay of voltage or chargeability over a specified time interval after the induced voltage is removed. The integrated voltage is used as the measurement, when the injected current is stopped. The IP method therefore measures the bulk electrical chargeability of the rocks.

Frequency domain IP methods use alternating currents (AC) to induce electric charges in the subsurface, and the apparent resistivity is measured at different AC frequencies.

The induced polarization (IP) method was developed originally for ore exploration. The transition from electronic to electrolytic conduction causes strong polarization effects in ores. However, other porous materials also exhibit polarization effects. They are caused by electrochemical processes at the internal interface between the pore fluid and the mineral grains. Although these effects are one to two orders smaller in size, modern IP equipment is able to resolve.

1.3 Resistivity Method – The Inverse Problem

The inversion of field dc resistivity measurements to interpret the actual sub soil structure is presently a popular geophysical method. The scientific procedure for the study of such a physical system can be divided into the following three steps [2].

- *Parameterization of the system:*

The discovery of a minimal set of model parameters whose values completely characterize the system.

- *Forward modeling*

The discovery of the physical laws, which allows us to make predictions on the results of measurements on some observable parameters, when the model parameters are given.

- *Inverse modeling*

The use of the actual results of some measurements of the observable parameters to infer the actual values of the model parameters.

Strong feedback exists between these steps, and a dramatic advance in one of them is usually followed by advances in the other two. While the first two steps are mainly inductive, the third step is deductive. Inverse modeling of the Geophysical Resistivity Method constitute to the determination of the actual variation of the Soil resistivity from the collected apparent resistivity (discussed in section 2.8.1) data from the field. The field data contain apparent resistivity values together with the geometry information.

In Sub surface interpretations, three main topographies are used, namely One Dimensional (1D) interpretation, Two Dimensional (2D) interpretation and Three Dimensional (3D) interpretation. In each of these interpretations the amount of sub soil conditions revealed is different. In the present study in the context of Electrical Engineering we are interested mainly in 1D and 2D interpretations to achieve successful earthing of a system.

In a 1D study the vertical variation beneath a point of interest is obtained. The field apparent resistivity values are inverted to produce a one dimensional plot of resistivity values (Figure 1.1) i.e. thickness and earth resistivity of each layer in a horizontally stratified multilayer earth structure. Early practitioners used several quantitative graphical representation methods such as Curve matching, Ohm-meter method, Moore-cumulative method and Barnes layer method [3]. Other conventional 1D DC resistivity inversion techniques include graphical methods requiring interpolation and judgment and computer based iterative calculation methods [4], [5], [6], [7]. Recently Artificial Intelligence approaches such as Genetic Algorithms [8] and Artificial Neural Networks [9], [10], [11] have been used.

Layer 1	ρ_1	h_1
Layer 2	ρ_2	h_2
Layer 3	ρ_3	h_3

| Layer N-1 | ρ_{N-1} | h_{N-1} |
| Layer N | ρ_N | h_N |
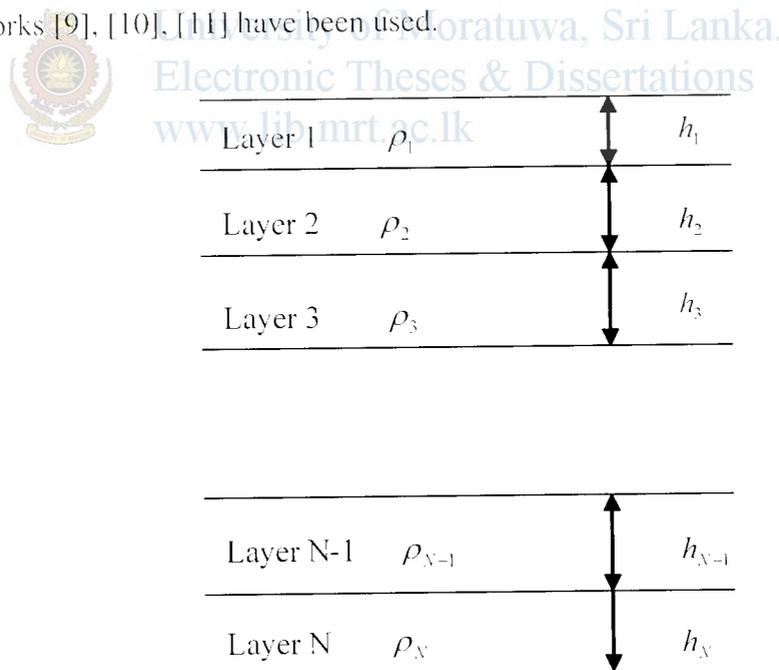
Figure 1.1 - One Dimensional Interpretation of a N-layer horizontally stratified soil structure

But a 1D interpretation will not generally reveal the actual sub soil structure of a complex earth model. However 1D inversion results are very useful in constructing

initial models for multidimensional interpretations. Then presently, two-dimensional (2D) interpretations are also widely used. In order to adequately resolve complex soil structures with arbitrary resistivity distributions, the regularized least squares optimization is frequently used [12] in the 2D inversion of electrical imaging data. Simulated annealing [13], Maximum entropy [14], Conjugate Gradient [15] and Neural Networks [11], [16] are other techniques used in the complex structure 2D inversions of geophysical data.

In areas where the geological structures are approximately two-dimensional (2D), conventional 2D electrical imaging surveys have been successfully used. The main limitation of such surveys is probably the assumption of a 2D structure. In areas with complex structures, there is no substitute for a full 3D survey. Researchers have observed that 2D and 3D resistivity surveys at the same location produced very different images on the same cross section. This discrepancy causes much confusion among practitioners about effectiveness of resistivity imaging methods.

Neural Networks are capable of solving several types of problems, including parameter estimation, parameter prediction, pattern recognition, classification and optimization. Also recently the use of Neural Networks in the Geophysics parameter estimation problems has shown strong results [10]. In the past decade and even earlier, there has been research done on the application of Neural Networks in the area of geophysics. Examples of such research are, Electromagnetic [17], Seismic data processing [18], Seismic velocity estimation [19], and 3D resistivity interpretation of controlled-source audio-magnetotelluric (CSAMT) data [20], inversions of magneto telluric (MT) data [21].

With these research showing a great potential in Neural Networks as a inversion tool for geophysics applications lately Neural Networks were applied for 1D and 2D inversion of resistivity data [9][10][11][16].

In the present study Neural Networks is proposed as the inversion tool for parameter estimation in the resistivity problem (discussed in Chapter 3).

1.4 Objectives of the Present Study

The objective of this study is to address the inverse problem of the geophysical resistivity method to implement the one dimensional (1D), two dimensional (2D) and three dimensional (3D) earth structures from a set of field resistivity measurements. This is proposed to be achieved by developing a user friendly software tool with fast response, at low cost to suit current requirements using Artificial Intelligent concepts.

Soil Resistivity is a major factor influencing the performance of an earthing system. In the present study special attention is given to evaluate this with the use of the resistivity method.

Preliminary a study on the resistivity methods Forward Modeling problem was carried out to study how the currents flowing in the different earth structures give rise to the measurable potentials on the earth's surface, that is, how the current flow inside different earth structures behaves. Secondly, the inverse problem for 1D, 2D and 3D cases is implemented with the application of Neural Networks.

1.5 Organization of the Chapters

The rest of the thesis is divided in to eight chapters.

Chapter 2 deals with the Resistivity Method's Forward Modeling equations and the general theories/terminologies in acquiring field measurements.

Chapter 3 deals with a general discussion on Neural Network architecture, algorithms and training.

Chapter 4 discusses the One Dimensional Interpretation of the resistivity problem. A literature survey of the one dimensional problem and Neural Network programs and optimizations together with the interpretation results are given.

Chapter 5 discusses the practical importance (for Earthing) of the resistivity interpretation.

Chapter 6 gives the Two Dimensional resistivity data inversion is presented. The chapter outlines practical field measurement techniques and existing forward modeling approaches and inversion strategies.

Chapters 7 discuss the capability of Neural Networks for Three Dimensional resistivity inversions with the use of synthetic examples. Practical field measurement techniques and existing forward modeling approaches and inversion strategies are outlined.

Chapter 8 presents the results of the NN optimization and theoretical and practical results obtained with NN Inversion.

Chapter 9 gives the conclusion of the study and further recommendations to be added in future work.

Chapter 2
Resistivity Method Forward Modeling

2.1 Introduction

In the context of Electrical Engineering, the purpose of resistivity testing is to obtain a set of measurements which may be interpreted to yield an equivalent model for the electrical performance of the earth, as seen by the particular earthing system. When defining the properties of a portion of the earth, a distinction between the geoelectric and the geologic model is required. In the geoelectric model the boundaries between the layers are determined by changes in resistivity, being primarily dependent upon water and chemical content as well as texture. The geologic model based upon such criteria as fossils and texture may contain several geoelectric sections. The converse is also common.

Electrical resistivity investigations are based on the principle of applying electric current to the earth through two electrodes and measuring the potential difference between two or more other electrodes. The distance between the electrodes and the measured potential difference are the data used to make interpretations of subsurface conditions.

When a set of observational data or experimental data from the physical world are systematically collected there must be ways of explaining or coordinating them. For that it is required to understand the relationship between these properties of the physical system and the observable geophysical response. The system of equations that describes this relationship constitutes the forward theory.

This chapter deals with how the Direct current introduced to earth would distribute in the earth and the theoretical equations governing the current flow and the potential build up in the soil. i.e. the geophysical response for the direct current injection into the earth. Also the chapter includes a study on soil mechanics, the practical field measurement techniques and terminologies.

2.2 Soil Resistivity

Resistance is that property of a conductor which opposes electric current flow when a voltage is applied across the two ends. In electrical circuit, the electrical resistance R of a wire in which current I is flowing is given by Ohm's Law (2.1).

$$R = V/I \tag{2.1}$$

Where,

V - Potential difference across wire.

R - Measured in ohms, V in volts, and I in amps.

Resistance is not a fundamental characteristic of the material. The Resistance of a conductor depends on the atomic structure of the material or its Resistivity which is that property of a material which measures the ability to conduct electricity.

The Resistance of a block of material of length L and cross section A, can be derived from the resistivity as (2.2),

$$R = \rho L/A \tag{2.2}$$

Where,

ρ - Resistivity (Ωm) of the conductor material

Resistivity is an intrinsic property of a material. This affords an opportunity of distinguishing one type of material from another. Resistivity is also sometimes referred to as 'Specific Resistance' since from (2.2), Resistivity is the Resistance in ohms between opposite faces of a unit cube of material.

Consequently 'Soil Resistivity' is the measure of the resistance between the opposite sides of a with a cube of soil with a side dimension of 1m.

Factors that effect Soil Resistivity may be summarized as,
- Type of Earth (e.g. clay, granite, sandstone, loam)
- Stratification i.e. layers of different types of soil (eg. Loam backfill on a clay base)
- Moisture content
- Temperature
- Chemical composition and concentration of dissolved salt

- Presence of metal or concrete structures (e.g. pipes, cable ducts, rail tracks)

When designing an earthing system to meet safety and reliability, an accurate reisitivity model of soil is required (discussed under Chapter 5).

2.3 Soil Mechanics

In order to model the soil, it was critical to know how the current flows through soil. To study the current flow through soil, a study of Soil mechanics was done.

2.3.1 Current flow in soil

The three main mechanisms of current flow can be stated as follows.

1) Electrolytic Conduction
   - Occurs by relatively slow migration of ions in a fluid electrolyte.
   - Controlled by type of ion, ion concentration, and ionic mobility.
2) Electronic Conduction (as in metal wire)
   - Occurs in metals by rapid movement of electrons.
   - Found in native metals and some metal oxides and sulphide ores
3) Dielectric Conduction
   - Occurs in weakly conducting materials, or insulators, in presence of external alternating current
   - Atomic electrons are shifted slightly relative to nucleus

Electrical current can flow, (i.e. electrical charges can move), in rocks and soils, but process is usually different from the current flowing in a metal wire. Rocks are usually porous and pores are filled with fluids, mainly water. As a result, rocks are electrolytic conductors.

The flow of electricity through a soil is a composite of
   - Flow through the soil particles alone(small due to solid phase is a poor conductor)
   - Flow through the pore fluid alone
   - Flow through both pore fluid and solids
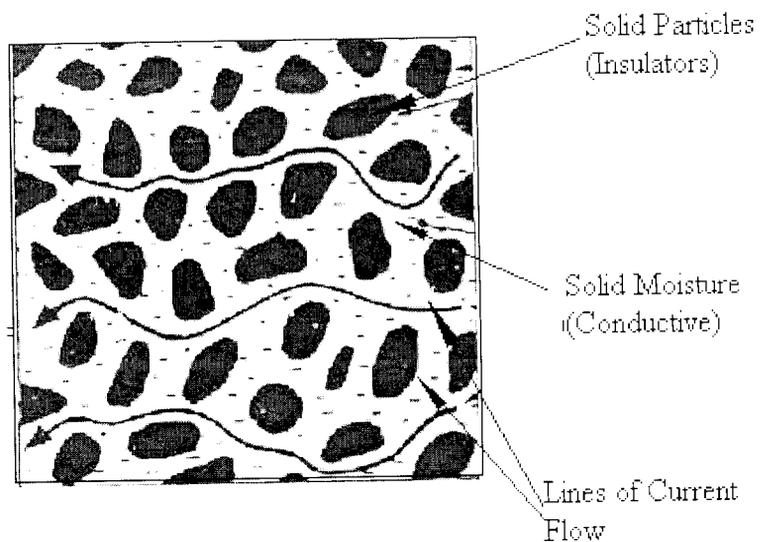
Figure 2.1 - Current flow through the soil

Electrical current is carried through a rock mainly by the passage of ions in por waters (Figure 2.1). In most rocks a dc current flow is by electrolytic conductio rather than ohmic processes.

The total electrical flow is influenced by,

- The porosity of flow paths (pore fluid and pore geometry)
- Condition of the interfaces between solid and liquid phases.

2.3.1.1 Archie's Law

In sedimentary rocks, resistivity of pore fluid is probably the single most importa factor controlling resistivity of the whole rock. Archie (1942) developed empiric formula for effective resistivity of rock (2.3)

$$\rho = a\phi^{-m} s^{-n} \rho_w$$

(2.

Where,

ρ - Porosity

s - Volume fraction of pores with water

ρ_w - Resistivity of pore fluid.

a, m, and n are empirically determined constants. ($0.5 < a < 2.5$, $1.3 < m < 2.5$,

$n \sim 2$).

ρ_w is controlled by dissolved salts and can vary between 0.05 ohm-m for saline groundwater to 1000 ohm-m for glacial melt water. Archie's Law ignores the effect of pore geometry, but is a reasonable approximation in many sedimentary rocks.

With these current flow properties, soil is therefore treated (modeled) as a *Lossy media.*

2.4 Soil Model

Soils behaving as Lossy media can be modeled as a conductor of resistance r and as a dielectric (Figure 2.2). Therefore the behavior of current flow for buried ground electrodes in soil can be analyzed by means of the soil model below.
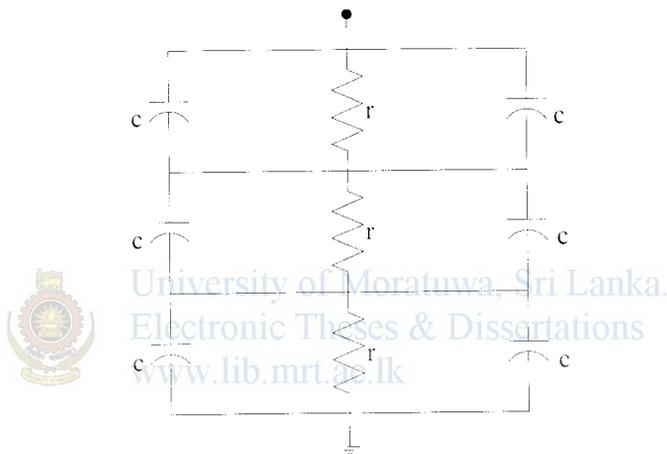
Figure 2.2 - Soil, Modeled as a lossy media

Except for high frequency and steep front waves penetrating a very resistive soil material, the charging current is negligible in comparison to the leakage current and the earth can be represented by a pure resistance.

2.5 Current flow and Potentials in Homogeneous media due to single electrode at surface

Current spread out in homogeneous soil vertically and horizontally (radially), somewhat in the manner in which water from a garden hose would flow into porous sand layer. If the soil was homogeneous then hemispherical equipotential surfaces will develop and a point source current flow in earth can be shown as in Figure 2.3.
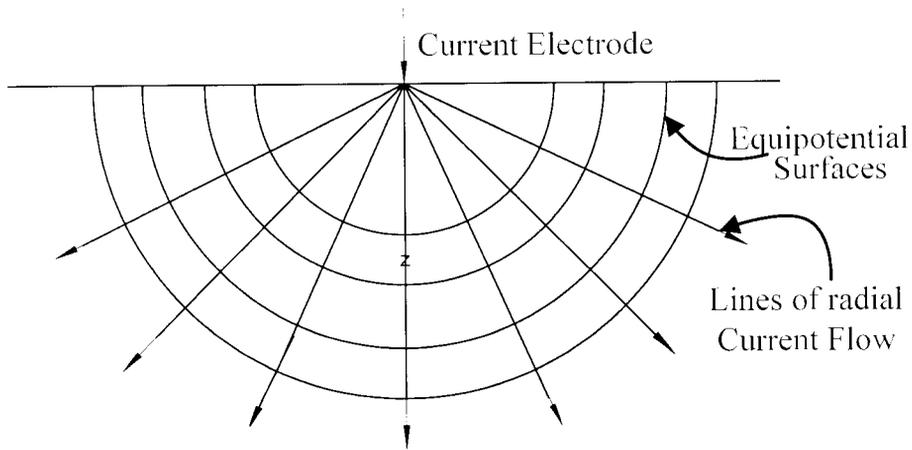
Figure 2.3 - Current Flow and developed equipotential surfaces in homogeneous soil due to a point source of current on the surface

The potential at any point of earth due to a current I flowing through a point Electrode situated on the surface of a half space can be expressed with Spherical Coordinates system as,

$$V = \frac{\rho I}{2\pi r} \qquad (2.4)$$

Which is the voltage at a distance r from a point source of current (electrode) at the surface of a half-space.

The same can be expresses with the Cartesian coordinates [8] as,

$$V = \frac{\rho I}{2\pi} \int_{0}^{\infty} e^{-\lambda|z|} J_0 (\lambda x) d\lambda \qquad (2.5)$$

The derivation of equation (2.4) and (2.5) are given in Appendix A.

In the resistivity measuring arrangements (discussed under Appendix C) two current electrodes are used (Figure 2.4). In such a situation current flow paths and the field lines in homogeneous soil can be shown as in Figure. 2.5.
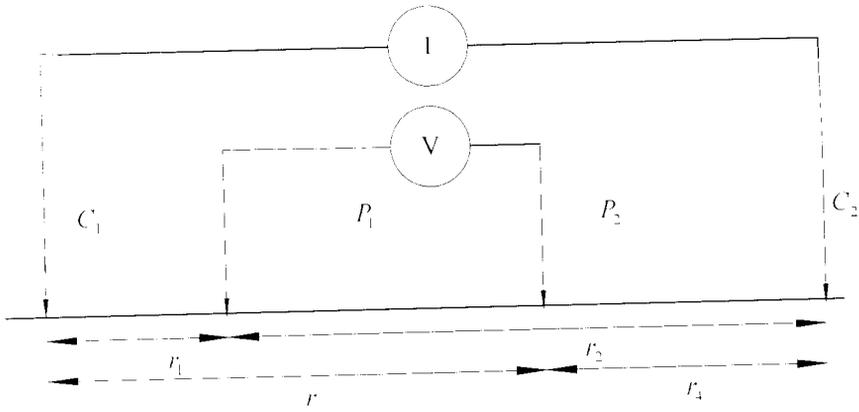
Figure 2.4 - Field Survey Electrode arrangement with two current and two potential electrodes on the surface of homogeneous soil.

When the distance between the two current electrodes is finite, the potential at any nearby surface point will be affected by both current electrodes. Referring Figure 2.4 the potential due to C_1 at P_1 is,

$$V_1 = -\frac{A_1}{r_1} \quad \text{where } A_1 = -\frac{I\rho}{2\pi} \tag{2.6}$$

Because the currents at the two electrodes are equal and opposite in direction the potential due to C_2 at P_1 is,

$$V_2 = -\frac{A_2}{r_2} \quad \text{where } A_2 = \frac{I\rho}{2\pi} = -A_1 \tag{2.7}$$

Thus, the potential at P_1 due to both the current electrodes is,

$$V_1 + V_2 = \frac{I\rho}{2\pi}\left(\frac{1}{r_1} - \frac{1}{r_2}\right) \tag{2.8}$$

Similarly with a second potential electrode at P_2, the potential difference between P_1 and P_2 is given by,

$$\Delta V = \frac{I\rho}{2\pi}\left\{\left(\frac{1}{r_1} - \frac{1}{r_2}\right) - \left(\frac{1}{r_3} - \frac{1}{r_4}\right)\right\} \tag{2.9}$$
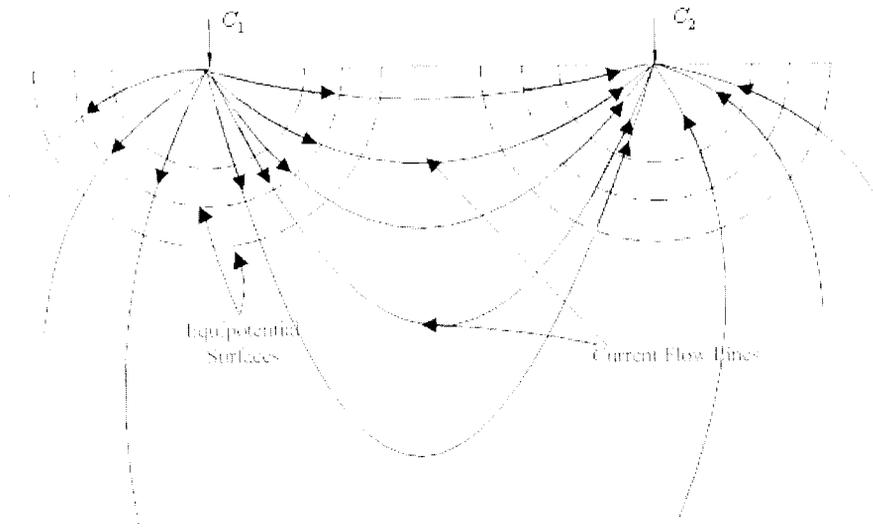
(a)
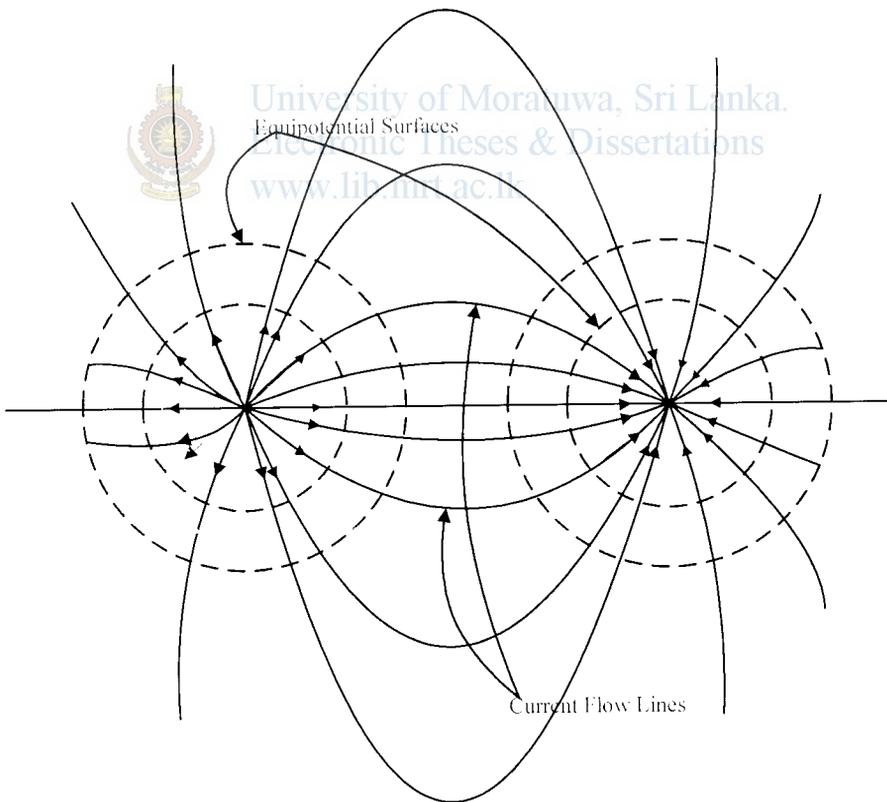
(b)

Figure 2.5 - Equipotentials and current flow lines for two point sources of current on the surface of homogeneous soil (a) vertical section (b) plan view

2.6 Current Flow in Non-Homogeneous Earth

Often, the earth structure will have resistivity layers related to the physical layers such as topsoil, sub-soil, and bedrock. Clearly these layers or divisions in soil structure will have a considerable impact on both soil resistivity and earth resistance/impedance.

Deviation from uniform to a platy structured soil will cause changes in the pattern of current flow. At the boundary of two different resistivity layers the current tends to deviate it's flow path, and the equipotential surfaces developed will be affected by the current densities distribution. Considering the fact that current flow in the direction of a good conductor a model can be drawn as in Figure 2.6 to show how the current flow is expected to change in non-uniform soil.
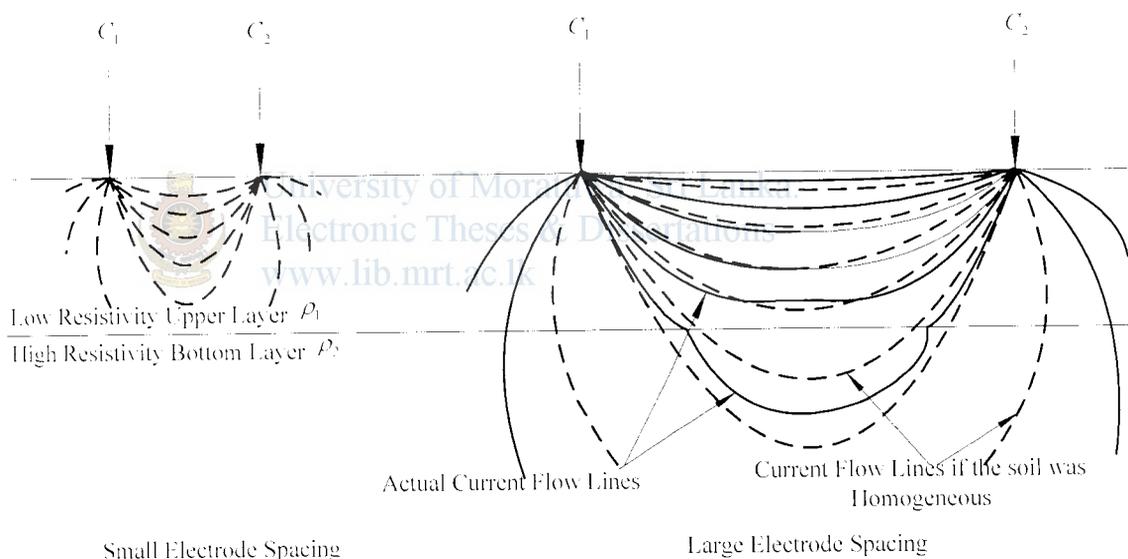
Figure 2.6 – Two layer model with low resistivity layer over high resistivity layer (a) for small electrode spacing (b) for large electrode spacing

2.6.1 Current density variation between boundaries

For simplicity, we consider harmonic EM field with time dependence of $\exp(j\omega t)$ at the interface between two lossy media.

The first medium is characterized by a real positive permittivity ε_1 and a real positive conductivity σ_1. The second medium is characterized by a real positive permittivity

19

ε_2 and a real positive conductivity σ_2. The first medium is equivalent to a dielectric

with complex permittivity $\varepsilon_1 - \sigma_1/j\omega$. The second medium is equivalent to a dielectric

with complex permittivity $\varepsilon_2 - \sigma_2/j\omega$.
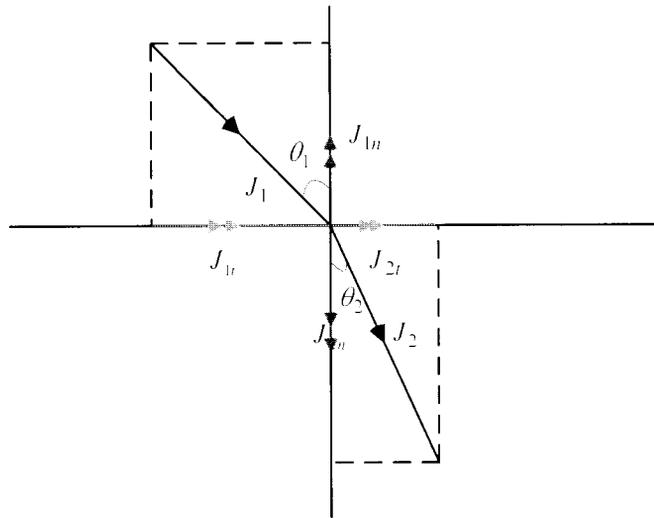
Figure 2.7 - Behavior of EM field at the boundary between two lossy medias

Since the normal component of electric flux density is continuous across the interface, it is easy to know the normal component of electric current density is also continuous across the interface.

$$J_{1n} = J_{2n} \tag{2.10}$$

The tangential component of current density is not continuous if σ_1 is not equal to σ_2 since the tangential component of E is continuous.

$$J_{1t} / \sigma_1 = J_{2t} / \sigma_2$$

$$\therefore \frac{J_{1t}}{J_{2t}} = \frac{\sigma_1}{\sigma_2}$$

$$\therefore \frac{J_{1t}}{J_{2t}} = \frac{\rho_2}{\rho_1} \tag{2.11}$$

Dividing the above 2 expressions we have,

$$\frac{J_{1t}/J_{1n}}{J_{2t}/J_{2n}} = \frac{\rho_2}{\rho_1}$$

$$\frac{\tan\theta_1}{\tan\theta_2} = \frac{\rho_2}{\rho_1} \tag{2.12}$$

Thus the current lines are bent when crossing the boundary. Clearly if the current flow is distorted in passing from a medium of one resistivity into another, the equipotentials also will be distorted.

2.6.2 Potential at a point on the surface of a half-space with horizontal beds

To determine the potential field of a non homogeneous earth, many mathematical methods exist including the solving of the Laplace equation. But a simpler approach will be to use the analogy of optical images to solve the problem. With the optical image technique it can be shown that the potential at a point on the surface (with two layers) where the current electrode is fixed, is affected by infinite set of images above and below the current electrode (discussed in Appendix B).

The expression (B.8) for the potential of a point on surface over two beds may be expressed in the integral form as [7],

$$V = \frac{I\rho_1}{2a\pi}\left\{1 + 2a\int_0^r f(\lambda)J_0(\lambda a)d\lambda\right\} \tag{2.13}$$

Where,
J_0 - Zero order Bessel Function of first kind

$$f(\lambda) = \frac{ke^{-2h\lambda}}{1 - ke^{-2h\lambda}}$$

The equation (2.13) can be illustrated as the general equation for the surface voltage at a point on the surface of a horizontally stratified for N-layer soil structure (Figure 2.8) where in that case $f(\lambda)$ will be generalized as follows.

$$f(\lambda) = \frac{K_{N1}e^{-2\lambda h_1}}{1 - K_{N1}e^{-2\lambda h_1}}$$

$$K_{N1} = \frac{k_1 + K_{N2}e^{-2\lambda h_2}}{1 + k_1 K_{N2}e^{-2\lambda h_2}}$$

$$K_{Ns} = \frac{k_s + K_{Ns+1}e^{-2\lambda h_{s+1}}}{1 + k_s K_{Ns+1}e^{-2\lambda h_{s+1}}}$$

$$K_{NN-1} = k_{N-1}$$

and

$$k_1 = \frac{\rho_2 - \rho_1}{\rho_2 + \rho_1}, k_s = \frac{\rho_{s+1} - \rho_s}{\rho_{s+1} + \rho_s}, k_{N-1} = \frac{\rho_N - \rho_{N-1}}{\rho_N + \rho_{N-1}}$$

(2.14)

Layer 1	ρ_1	h_1
Layer 2	ρ_2	h_2
Layer 3	ρ_3	h_3
Layer N-1	ρ_{N-1}	h_{N-1}
Layer N	ρ_N	h_N
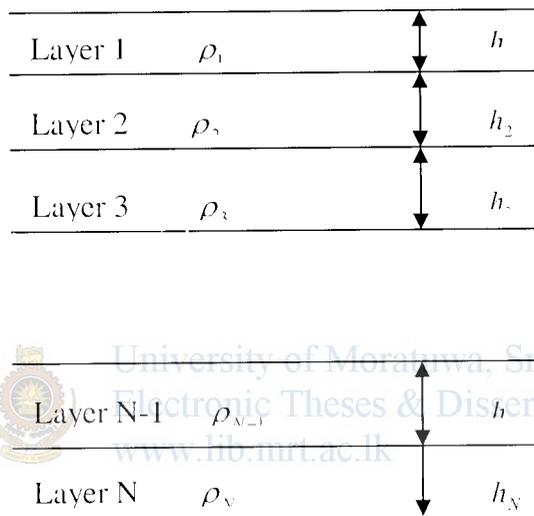
Figure 2.8 - Multilayer Earth Model

2.7 Field Procedures of Soil Resistivity Tests

In practice the soil resistivity measurements are collected with a collinear array. With these arrays what is actually measured is an 'Apparent Resistivity'.

2.7.1   Apparent resistivity

Rearranging the equation (2.9),

$$\rho = \frac{2\pi\Delta V}{I} \frac{1}{\left\{ \left(\frac{1}{r_1} - \frac{1}{r_2} \right) - \left(\frac{1}{r_3} - \frac{1}{r_4} \right) \right\}}$$

$$\rho = \left(\frac{2\pi\Delta V}{I} \right) p \tag{2.15}$$

Where,

p - parameter depending on the electrode geometry

By measuring the potential difference ΔV and current I and knowing the electrode configuration a value for ρ can be obtained.

The resistivity of the soil varies widely from site to site. If the soil was homogenous and isotropic it would be expected that this resistivity will be constant for any current and electrode arrangement irrespective of the location considered.

Unfortunately, in practice, the earth exhibits a far from uniform structure. Therefore in non-homogeneous soil when the electrode spacing is varied or the spacing remained fixed while the whole array is moved, the ratio in general will change. This results in different values of ρ for each measurement. The magnitude is intimately related to the electrode geometry. This measured quantity is known as the 'Apparent Resistivity', ρ_a.

Other important facts on resistivity field procedures such as types of resistivity surveys and electrodes arrays are discussed in Appendix C.

2.8 Basic Formula for Wenner array Apparent Resistivity in horizontally stratified N-layer soil

For the present study the Wenner array is considered. Starting with the integral form given in equation (2.13) for the voltage at a point on the surface in horizontally stratified N-layer Soil, a formula for apparent resistivity is derived as follows.

Referring Figure C.1 the potential due to C_1 at P_1 is,

$$V_{11} = \frac{I\rho_1}{2a\pi} \left\{ 1 + 2a \int_0^\infty f(\lambda) J_0(\lambda a) d\lambda \right\} \tag{2.16}$$

$$V_{11} = \frac{I\rho_1}{2a\pi} \left\{ 1 + F_N(a) \right\} \tag{2.17}$$

Where,

$$F_N(a) = 2a \int_0^\infty f(\lambda) J_0(\lambda a) d\lambda$$

$f(\lambda)$ is in the same form as in equation (2.14).

Because the currents at the two electrodes are equal and opposite in direction the potential due to C_2 at P_1 is,

$$V_{12} = \frac{(-I)\rho_1}{4a\pi}\{1 + F_N(2a)\} \tag{2.18}$$

Thus, the potential at P_1 due to both the current electrodes is,

$$V_1 = V_{11} + V_{12}$$

$$V_1 = \frac{I\rho_1}{2a\pi}\left\{\frac{1}{2} + F_N(a) - \frac{F_N(2a)}{2}\right\} \tag{2.19}$$

Similarly with a second potential electrode at P_2, the potential difference between P_1 and P_2 is given by,

$$\Delta V = \frac{I\rho_1}{2a\pi}\{1 + 2F_N(a) - F_N(2a)\} \tag{2.20}$$

Substituting equation (2.20) into equation (C.1) the theoretical expression for the apparent resistivity ρ_a is obtained,

$$\rho_a = \frac{2\pi a}{I}\left(\frac{I\rho_1}{2a\pi}\{1 + 2F_N(a) - F_N(2a)\}\right)$$

$$\rho_a = \rho_1\{1 + 2F_N(a) - F_N(2a)\} \tag{2.21}$$

Equation (2.21) is the general equation for calculating the apparent resistivity in the case of a horizontally stratified multi layer earth for a wenner array.

2.8.1 Basic Formula for Schlumberger array Apparent Resistivity in horizontally stratified N-layer soil

For the Shlumberger array the above equation (2.21) is written as,

$$\rho_a = \rho_1 \left\{ 1 + 2L^2 \int_0^{\infty} f(\lambda) J_1'(\lambda L) d\lambda \right\}$$ (2.22)

$$J_1'(\lambda L) = -J_0'(\lambda L)$$

Where,

$J_1(\lambda L)$ - First order Bessel Function

$J_0'(\lambda L)$ - First derivative of J_0

L - Half the current electrode separation

2.9 Current Density

The general theory as developed above has considered the earth homogeneous and of the same resistivity . The actual condition encountered in the field is a heterogeneous material vertically and often laterally as well. The actual measurements as made in the field only involve a small element of material between the potential electrodes (Figure 2.9).

Resistivity theory states that the lines of current flow will be deflected toward a good conductor, that is, one with a lower resistance or higher conductance. This is similar to ground-water flow where the flow lines are denser in the aquifer of higher permeability. The potential difference **between** the potential electrodes is proportional to the current density and the true resistivity of the small near surface element of material between the potential electrodes [3]. Stated mathematically:

$$V \propto \rho_0 i$$ (2.23)

Where,

V - Voltage drop

ρ_0 - True resistivity

I - Current density

This equation is substituted to equation (C.1), since $2\pi a$ is a constant,

$$\rho_a \propto \left(i / I \right) \rho_0$$ (2.24)

Which states that, the apparent resistivity ρ_a is proportional to the true resistivity multiplied by the ratio of the current density to the current. The current density is directly proportional to the total current; therefore, the measured apparent resistivity is independent of the total current applied.
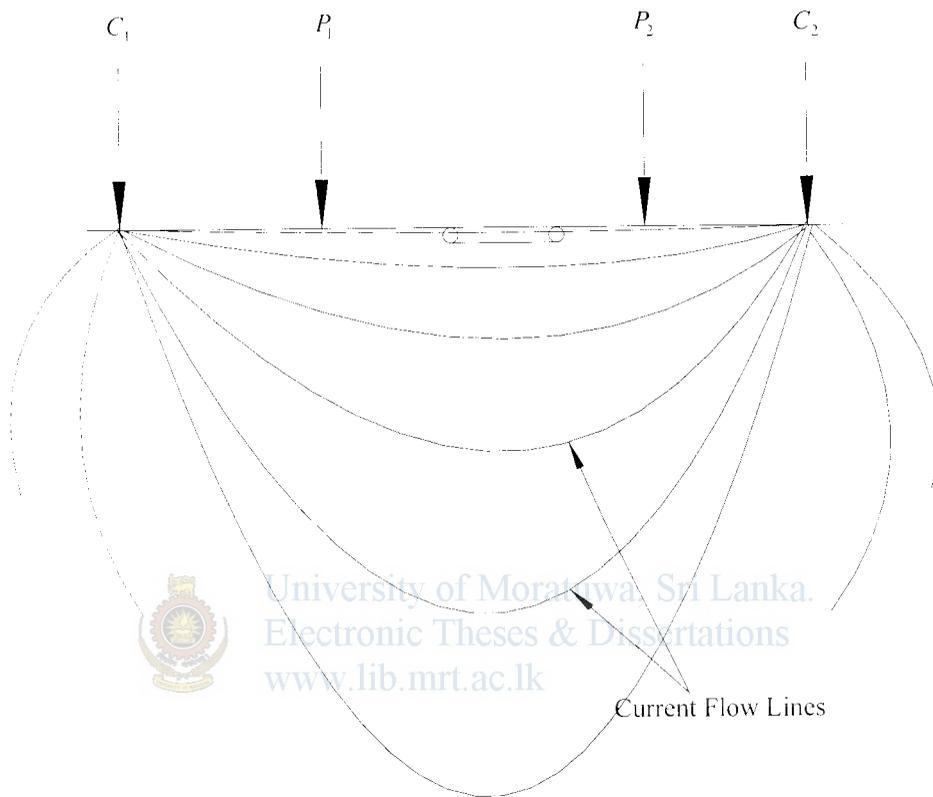
Figure 2.9 - Small Element of material

According to [3] the equation (2.24) contains the key to the qualitative interpretation of resistivity effects. This key may also be stated in these words: "Different subsurface conditions will produce different apparent resistivity readings. If a small volume element is imagined as extending along the earth surface between the two potential electrodes shown in Figure 2.9, then it will have a certain current density i , and a certain true resistivity ρ_0. The measured apparent resistivity will be directly proportional to these two quantities."

So, deviation from a homogeneous earth structure, the current density will be effected by the actual sub surface condition. This will in turn affect the current density in the small volume element considered between the potential electrodes. Similarly the

actual subsurface conditions will affect the true resistivity between the potential electrodes.

2.10 Depth of current penetration

For a homogeneous material, consider a vertical plane at the midpoint between electrodes. One half the current flows through this plane at a depth equal to one half the electrode spacing and one half flows at a greater depth.

If we consider a wenner array the resistivity determined by the equation (C.1) applies to a volume of material that depends on the electrode spacing, and as the spacing is increased, the current penetrates deeper in to the earth.

As the electrode spacing is increased, the current flows through a greater volume of material both horizontally and vertically and the deeper materials will have an effect on the apparent resistivity. Thus, if the deeper material is of higher resistance the current flow lines will be deflected upward and the current density in the near surface volume element is increased. If the deeper material is of lower resistivity the current flow lines will be deflected downward and the current density will be decreased. The increase or decrease in current density is measured by the resistivity apparatus. Interpretation of the apparent resistivity changes with change in electrode spacing will indicate changes in and types of material at certain depths.

Empirical observations have shown that for the Wenner electrode configuration changes in apparent resistivity are considered to occur at the depth equal to the spacing between adjacent electrodes.

To find out the depth of current penetration as a function of current electrode spacing, L (Figure 2.10) lets consider the current flow in a homogeneous medium between two point electrodes C_1 and C_2. The horizontal current density at point P is,

$$J = \left(-\frac{1}{\rho}\right)\frac{\partial V}{\partial x} \qquad (2.25)$$
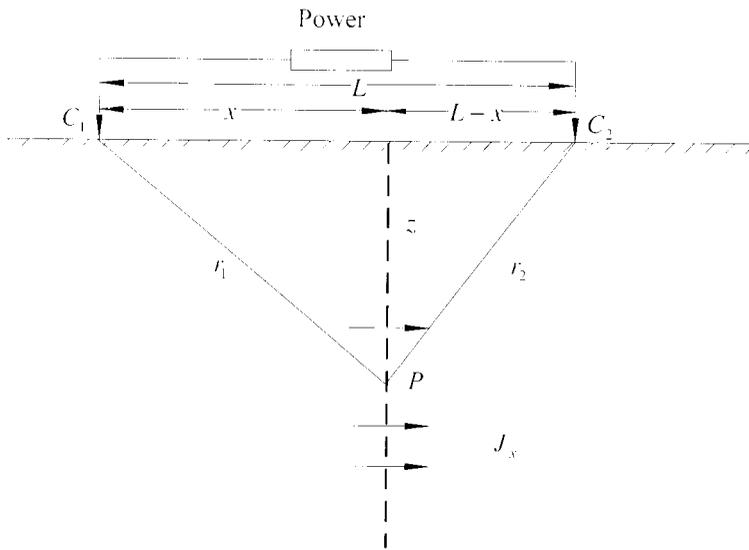
Figure 2.10 - Determining the current density in uniform ground below two surface electrodes

Substituting for voltage V at due to both the current electrodes from equation (2.8),

$$J_x = \left(-\frac{1}{2\pi}\right)\partial/\partial x\left(\frac{1}{r_1} - \frac{1}{r_2}\right)$$

$$= \left(\frac{1}{2\pi}\right)\left\{\frac{x}{r_1^3} - \frac{(x-L)}{r_2^3}\right\} \qquad (2.26)$$

If point P is on the vertical plane midway between C_1 and C_2, now $r_1 = r_2 = r$ and,

$$J_x = \frac{I}{2\pi}\frac{L}{\left(z^2 + L^2/4\right)^{3/2}} \qquad (2.27)$$

The total current flowing in the x direction through a cross section $dy\,dz$ is,

$$\partial I_x = J_x\,dy\,dz = \frac{I}{2\pi}\frac{L}{\left(L^2/4 + y^2 + z^2\right)^{3/2}}\,dy\,dz \qquad (2.28)$$

The total current falling below some depth Z_1 is,

$$I_z = \int_{Z_1}^{\infty}\int_{-\infty}^{\infty} \frac{I}{2\pi}\frac{L}{\left(L^2/4 + y^2 + z^2\right)^{3/2}}\,dy\,dz$$

$$I_z = I\left(1 - \frac{2}{\pi}\tan^{-1}\frac{2Z_1}{L}\right) \qquad (2.29)$$

Figure 2.11 shows the percentage of current flowing below depth Z_1 for electrode spacing L. Only about 15% of the current penetrates below a depth of twice the

28

electrode spacing. Also we see that when $L = 2Z_1$ half the current flows in the top layer and half below it.
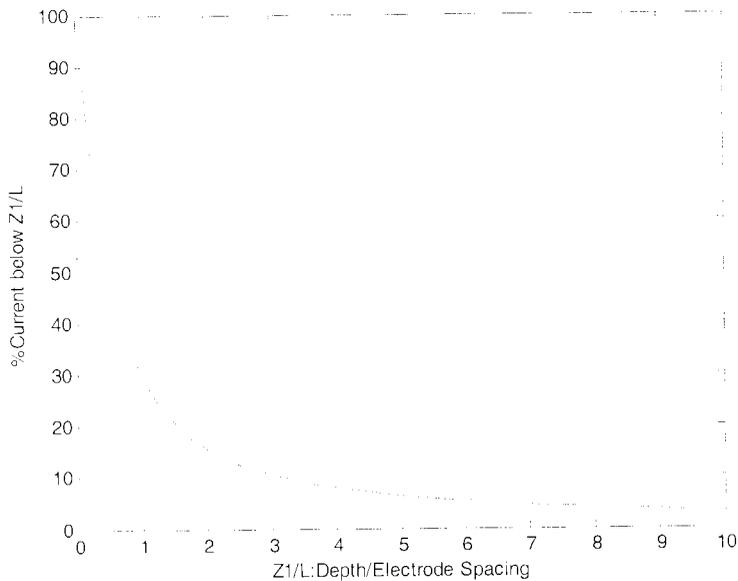
Figure 2.11 - Percentage of current flowing below depth Z_1 for current electrode spacing L

Since the variation in potential measured at surface are proportional to the current flow below, it is desirable to get much current in to the ground as possible. For good penetration we must us large enough spacing that sufficient current reaches the target depth.

2.11 Master curves

The master curves are prepared in a dimensionless form for a number of reflection coefficients $k = \left(\dfrac{\rho_2 - \rho_1}{\rho_2 + \rho_1} \right)$ or for ρ_2 / ρ_1. Figure 2.12 shows the master curves represented on a single plot for a two layer earth structure.

Chapter 3
Neural Networks as the Inversion Tool

3.1 Introduction

Inverse theory is the use of the actual results of some measurements of the observable data to infer the actual values of the model parameters (properties of the physical system). The field data contain apparent resistivity values and geometry information. These data are then inverted to produce a plot of resistivity values. This resistivity inversion section is then used to interpret subsurface lithology.

Different subsurface conditions will produce different apparent resistivity readings. Inverse modeling of the Geophysical Resistivity Method is determination of the actual variation of the Soil resistivity from the collected apparent resistivity data from the field. However, the one-dimensional (1D) and two- dimensional (2D) inversion in terms of vertical variation of resistivity is a difficult task. Practitioners use many software packages as the inversion tool with complex mathematical algorithms and huge sequential codes when it comes to interpretation of the field data. Section 1.3 discusses some of the methods where most of them based on iterative calculation methods.

Artificial Neural Networks (ANNs) are capable of solving several types of problems, including parameter estimation, parameter prediction, pattern recognition, classification and optimization. Also recently the use of neural networks in the geophysics parameter estimation problems has shown strong results (discussed under 1.3). With this recent trend in the applicability of the ANN's for the non linear geophysical inversion problems ANN's is proposed as the inversion tool for parameter estimation or sub surface interpretation in the resistivity problem. MatLab is used as the software tool for the modeling of the neural network and generation of synthetic data. Several MatLab commands and functions available in the Neural Network Tool Box are used for the programs written. This chapter carries a general discussion about the Neural Networks (NN's) and the function selection for the Neural Network modeling and optimization.

3.2 Selection of Neural Networks for the Present Study

As discussed earlier many geophysical applications have used neural networks as an inversion tool, and have shown strong results. In spite of this latest trend in applying Neural Networks for inversion following discussed are some more reasons for choosing NN's as the inversion tool for present study.

- Elimination of lengthy sequential codes

A neural network can be trained with a set of example data pairs. So this will eliminate complex mathematical algorithms and huge sequential codes required for converting an input to output. Rather to train the network all what we need is a collection of representative examples of the desired translation. The NN then adopts itself to produce the desired outputs when presented with the example inputs.

In addition, the NN will also produce an output for the inputs, which it has never seen. This is because of the inherent ability of the network to deal with noise or obscured patterns. This has significant advantage of as NN approach over a traditional algorithmic approach.

So, now if we consider the 1D inversion case the basic intention behind the use of neural networks is to first train the program with a synthetic data set generated using the equations (2.50). Then input a set of field collected resistivity measurement data to the network to obtain the actual earth structure with the layer parameters i.e. the layer thicknesses and the individual layer resistivities.

- Omission of a initial model estimation

NN's do not need a 'good' initial solution set of parameters as an input for their program, where in other inverse algorithm based programs developed they need to determine the initial values properly, for the speed of convergence of the iterative solution [5]. In [5] the initial guess for a three layer model is based on the two-end limit property. With this determines the top layer and bottom layer resistivities, with the argument that selected probe spacing (a) is small enough and large enough to obtain almost unchanging apparent resistivity with further change of a.

- Possibility of training the network in place of human visual inspection

One thing noted in literature was that after every measurement set is taken before applying it to an inverse algorithm based program for parameter optimization, the measured data is plot with apparent resistivity Vs probe spacing. So with the curve shape or the trend of the curve a model to fit namely two layers, three layers, four layers is determined first. This is done with a visual inspection of the curves and by matching them approximately with the standard curve shapes.

So a similar classification base can be used for the neural network approach. Where the neural network can be trained to classify the apparent resisitivity measurement set under the suitable model first as two layers, three layers and so on. Here again with the reference to the standard curve types a broad classification can be given based on the resistivity variation of soil models more than two layers (e.g. for three layers Low-high-low model, high-medium –low model etc.)

So after training the network for a determined well selected set of such curve types the time consuming visual inspection and initial guess determination can be taken off from the humans. After training the neural networks they will perform excellent at real time solely for the measured field data.

3.3 Biological Neural Networks

The human brain is a highly complicated machine capable of solving very complex problems. Although we have a good understanding of some of the basic operations that drive the brain, we are still far from understanding everything there is to know about the brain.

In order to understand Artificial Neural Networks (ANN), it is necessary to have a basic knowledge of how the internals of the brain work. The brain is part of the central nervous system and consists of a very large NN. The NN is actually quite complicated, but I will only include the details needed to understand ANN, in The NN is a network consisting of connected neurons. The center of the neuron is called the nucleus. The nucleus is connected to other nucleuses by means of the dendrites and the axon. This connection is called a synaptic connection.

33
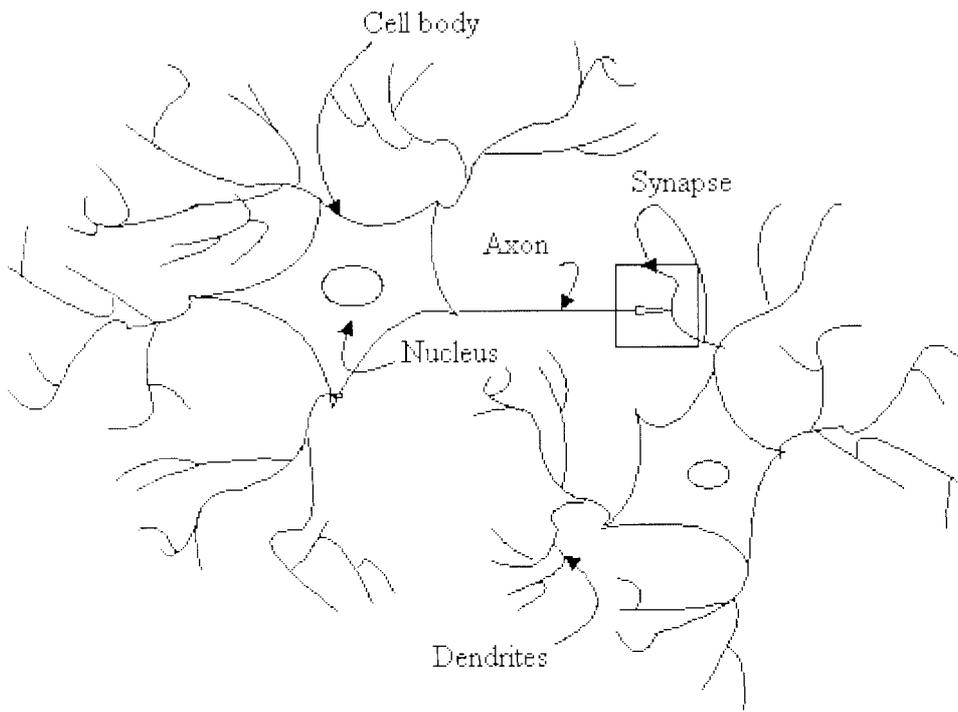
Figure 3.1 - Simplified biological neuron

The neuron can fire electric pulses through its synaptic connections, which is received at the dendrites of other neurons. Figure 3.1 shows how a simplified neuron looks like.

When a neuron receives enough electric pulses through its dendrites, it activates and fires a pulse through its axon, which is then received by other neurons. In this way information can propagate through the NN. The synaptic connections change throughout the lifetime of a neuron and the amount of incoming pulses needed to activate a neuron (the threshold) also change. This behavior allows the NN to learn.

The human brain consists of around 10^{11} neurons which are highly interconnected with around 10^{15} connections [22] these neurons activates in parallel as an effect to internal and external sources. The brain is connected to the rest of the nervous system, which allows it to receive information by means of the five senses and also allows it to control the muscles.

3.4 Artificial Neural Networks (ANN)

Basically the neural network concept can be referred to as the "computer learning by experience". Conventionally a computer program is a set of sequential set of

34

instructions carried out by the computer, which is written by a human. But these sequential computer systems will be experiencing difficulties in performing inherently parallel tasks. The case of visual patterns recognition can be given as an example.

Comparative to the conventional computer the individual neural cell is capable of handling massive parallelism and interconnectivity, together with a high response time to typically a few tens of milliseconds. Therefore the biological system accompanying the brain has the ability to perform complex pattern recognition in hundreds of milliseconds.

We will need our computers to perform complex pattern recognition problems in the real world applications. But since the conventional computers are not suited for these applications, we therefore borrow features form the physiology of the brain as the basis of a new processing model. Hence the technology is known as Artificial Neural Systems (ANS) or Neural Networks. Ultimately the conventional computer is now capable of handling and interpreting the complex pattern recognition
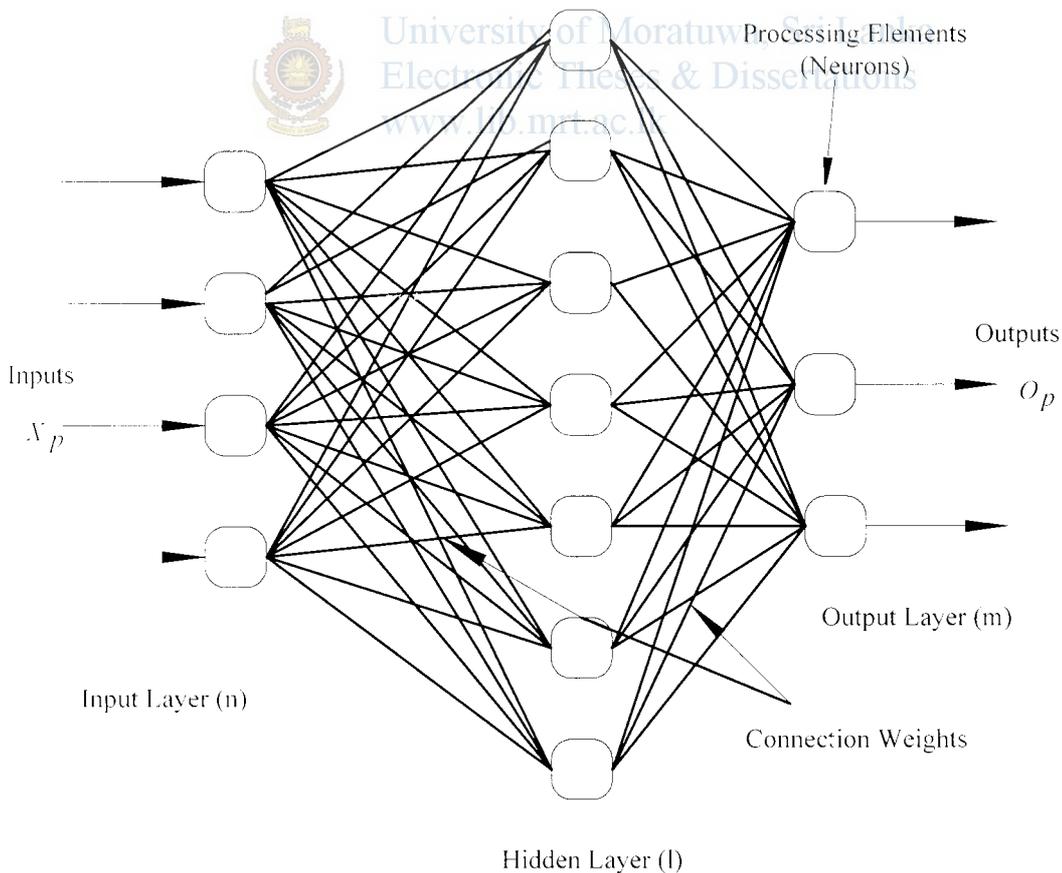
Figure 3.2 - an Artificial Neural Network

Figure 3.2 shows a General Neural Network. The Neural network shown above has three layers, namely the input layer, hidden layer and output layer. The layers consist of neurons or Processing Elements (PE's). PE's are simple elements operating in parallel and they are inspired by biological nervous systems. The number of input and output layer neurons is decided on the application and the hidden neurons are decided on a trial and error basis.

A NN is specified by architecture: a set of neurons and links connecting neurons. Each link has a weight, a neuron model: the information processing unit of the NN, a learning algorithm: used for training the NN by modifying the weights in order to solve the particular learning task correctly on the training examples.

The layers are interconnected with a set of connections. Where each neuron in the input layer is connected to each neuron in the hidden layer i.e. the network is fully interconnected. These connections are assigned with a value called weights. The network function is determined largely by the connections between elements. The input layer is connected to the external world or the raw data.

An ANN is not programmed; rather, it is trained by showing it a range of example inputs. The ANN builds up a configuration based on the examples that allows it to function as an adaptive filter. This configuration is an internal representation or generalization of the examples, based on regression. The ANN uses the generalization to match other input patterns against, within a range of tolerance. For example, an ANN could be trained on a variety of data sets that represent a known sample. With enough training, the ANN can recognize and identify data from unknown samples. The level of resolution varies with the threshold and the resolution of the training examples.

Each node in an ANN sees a different component of the data set. The components may overlap. The different nodes make decisions based on their components. Then a consensus of these decisions results in a final, global decision, recognition, or identification.

3.4.1 Neuron Model

Figure 3.3 shows an artificial neuron. The neuron is the basic information processing unit of an ANN.

36
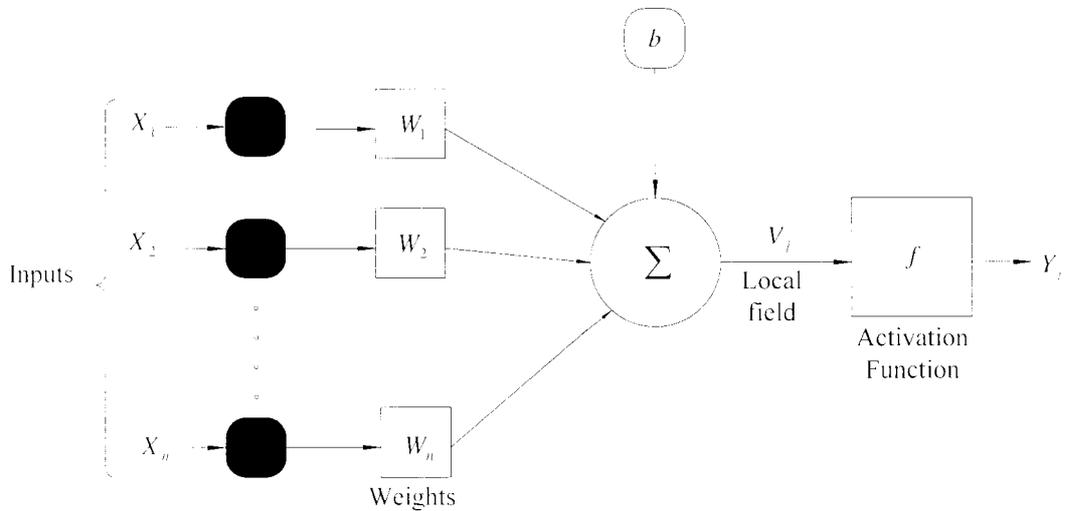
Figure 3.3 - Artificial Neuron Model

Equation 3.1 represents the mathematics of the behavior of a single neuron. Inputs X_1 through X_n are multiplied by weights W_1 through W_n for this specific node and then summed. This weighted sum is referred to as the induced field of the neuron. Output of the summing function is then sent into a transfer function. This function then turns this number into a real output via some algorithm. The output, Y_i results when the weighted sum of the inputs exceeds the given threshold defined by a nonlinear transfer function. Bias is a constant input with certain weight. The bias **b** has the effect of applying an affine transformation to the weighted sum. It can be modeled by adding an extra input.

$$V_i = W_1 \times X_1 + W_2 \times X_2 + W_3 \times X_3 + \ldots\ldots + W_n \times X_n + b \qquad (3.1)$$

The Neuron transfer function or the Activation function (squashing function) is for limiting the amplitude of the neuron output. The most common activation functions used are shown in Figure 3.4.The result of the transfer function is usually the direct output of the processing element.

The Hard Limiter function can be given mathematically as,

$$f(v) = \begin{cases} 1 \text{ if } v \geq 0 \\ 0 \text{ if } v < 0 \end{cases}$$

The Piece-Wise Linear function can be given mathematically as,

$$f(v) = \begin{cases} 1 & \text{if } v \ge 1/2 \\ v & \text{if } 1/2 > v \ge -1/2 \\ 0 & \text{if } v \le 1/2 \end{cases}$$

The Sigmoid Function is similarly given as,

$$f(v) = \frac{1}{1 + \exp(-av)}$$

The hyperbolic Tangent is similarly given mathematically as,

$$f(v) = \tanh(v)$$
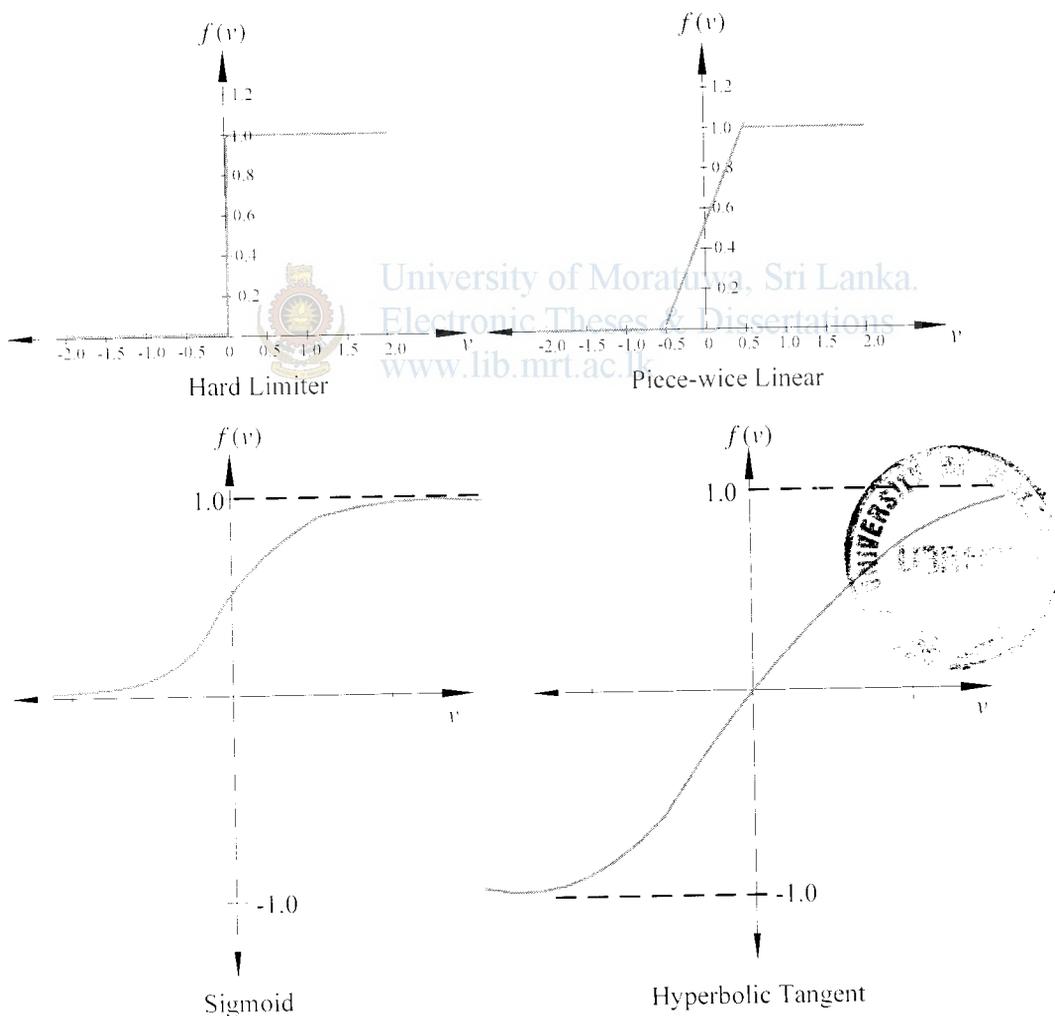
Figure 3.4 - Common Activation Functions

3.4.2 Learning Algorithm

There are several types of networks based on the algorithm used by them to learn (or to train the network). The term 'learn' refers to the adjusting or updating the connection weights. Every neural network possesses knowledge which is contained in the values of the connections weights. Modifying the knowledge stored in the network as a function of experience implies a learning rule for changing the values of the weights. The Adaptive network learns under supervised or unsupervised learning.

3.4.2.1 Supervised learning

Supervised learning is a technique for learning a function from training data. The training data consist of pairs of input objects (typically vectors), and desired outputs. The output of the function can be a continuous value or can predict a class label of the input object (called classification). The task of the supervised learner is to predict the value of the function for any valid input object after having seen a number of training examples (i.e. pairs of input and target output). To achieve this, the learner has to generalize from the presented data to unseen situations in a "reasonable" way. This parallel task in human and animal psychology is often referred to as concept learning.

Paradigms of supervised learning include error-correction learning, reinforcement learning and stochastic learning. An important issue concerning supervised learning is the problem of error convergence, i.e. the minimization of error between the desired and computed unit values. The aim is to determine a set of weights which minimizes the error. One well-known method, which is common to many learning paradigms, is the least mean square (LMS) convergence.

3.4.2.2 Unsupervised learning

Unsupervised learning studies how systems can learn to represent particular input patterns in a way that reflects the statistical structure of the overall collection of input patterns. By contrast with supervised learning, there are no explicit target outputs or environmental evaluations associated with each input; rather the unsupervised learner brings to bear prior biases as to what aspects of the structure of the input should be captured in the output.

Unsupervised learning is important since it is likely to be much more common in the brain than supervised learning. The only things that unsupervised learning methods have to work with are the observed input patterns, which are often assumed to be independent samples from an underlying unknown probability distribution. With unsupervised learning it is possible to learn larger and more complex models than with supervised learning. If the causal relation between the input and output observations is complex, it is often easier to bridge the gap using unsupervised learning instead of supervised learning. This is because in supervised learning one is trying to find the connection between two sets of observations. The difficulty of the learning task increases exponentially in the number of steps between the two sets and that is why supervised learning cannot, in practice, learn models with deep hierarchies.

In unsupervised learning, the learning can proceed hierarchically from the observations into ever more abstract levels of representation. Each additional hierarchy needs to learn only one step and therefore the learning time increases (approximately) linearly in the number of levels in the model hierarchy.

Unsupervised competitive learning is used in a wide variety of fields under a wide variety of names, the most common of which is "cluster analysis". Hebbian learning is the other most common variety of unsupervised learning. Hebbian learning minimizes the same error function as an auto-associative network with a linear hidden layer, trained by least squares, and is therefore a form of dimensionality reduction. Perhaps the most novel form of unsupervised learning in the NN literature is Kohonen's self-organizing (feature) map .SOMs combine competitive learning with dimensionality reduction by smoothing the clusters with respect to an a priori grid.

3.5 Backpropagation Learning

The learning algorithm used for the present study is the 'Feed forward back propagation' algorithm where the Generalized Delta Rule is used. It adjusts the weights of the NN in order to minimize the average squared error.

During the Feed Forward Step, an input patter is applied to the network as a stimulus at the first layer, of the network it is propagated through each successive layer until an output is generated. This output is compared to the desired output and an error signal is computed for each unit.

This error signal is transmitted backwards to each unit in the intermediate layers. The units receive only a portion of the total error based on their contribution made to the original output. Based on error signal received, connection weights are updated by each unit to cause the network to converge towards a state that all training patters to be encoded. This is the backward step.

3.5. 1 Feed Forward Step

Let's consider the input vector as,

$$X_p = \left(x_{p1}, x_{p2}, \ldots, x_{pi}, \ldots, x_{pn} \right) \tag{3.2}$$

Where x_{pi} is the input to the ith unit of the input layer.

Then these inputs are activated by an activation function, and presented as the activation vector of the layer. Let us assume that activation functions at all the cases are equal to its net input.

Now the input to the jth hidden unit, net^h_{pj} can be calculated as follows from equation (3.1).

$$net^h_{pj} = \sum_{i=1}^{n} W^h_{ji} x_{pi} + \theta^h_j \tag{3.3}$$

Where,

W^h_{ji} – Weights from i^{th} input unit to j^{th} hidden unit

θ^h_j – Bias input to j^{th} hidden unit

The output of the node is,

$$i_{pj} = f^h_j (net^h_{pj}) \tag{3.4}$$

Where, f^h_j - the transfer function of the jth hidden unit.

Similarly equations for the output nodes are,

$$net^o_{pk} = \sum_{j=1}^{L} W^o_{kj} i_{pl} + \theta^o_k \tag{3.5}$$

$$O_{pk} = f^o_k(net^o_{pk}) \tag{3.6}$$

Where "o" superscript refers to quantities in the output layer.

Now after the output for the pth input is calculated an error measure is taken. Where the error for the pth input vector of the kth unit of the output layer ε_{pk} is given by,

$$\varepsilon_{pk} = d_{pk} - O_{pk} \tag{3.7}$$

Where,

d_{pk} - Desired output of the kth output node for p^{th} training vector

The error that is minimized by the Generalized Delta Rule is the sum of the squares of the error for all output units. The Mean square error function for the pth training vector can thus be given by,

$$E_p = \frac{1}{2} \sum_{k=1}^{m} (d_{pk} - O_{pk})^2 \tag{3.8}$$

3.5.2 Back Propagation Step

In order to adjust the weights to minimize E_p, the weights are changed in the negative gradient of the above error function. This is done first with respect to the output layer weights, where $\dfrac{\partial E_p}{\partial W^o_{kj}}$ is evaluated.

3.5.2.1 Weight update for the Output layer

By using the chain rule for partial derivatives,

$$-\frac{\partial E_p}{\partial W^o_{kj}} = (d_{pk} - O_{pk}) \frac{\partial f^o_k}{\partial(net^o_{pk})} \frac{\partial(net^o_{pk})}{\partial W^o_{kj}} \tag{3.9}$$

From equation (3.5),

$$\frac{\partial(net^o_{pk})}{\partial W^o_{kj}} = \left(\frac{\partial}{\partial W^o_{kj}} \sum_{j=1}^{L} W^o_{kj} i_{pj} + \theta^o_k \right) = i_{pj} \tag{3.10}$$

42

The functions f_j^h and f_k^o can take many forms as discussed under the section 3.2.1 two commonly used forms are,

$$f_k^o(net_{pk}^o) = net_{pk}^o \tag{3.11}$$

$$f_k^o(net_{pk}^o) = (1 + e^{net_{pk}^o})^{-1} \tag{3.12}$$

Where (3.11) and (3.12) are linear transfer function and sigmoid transfer function respectively. In the sigmoid function the output is within zero and one.

From equation (3.11),

$$f_k^{o'} = 1 \tag{3.13}$$

From equation (3.12),

$$f_k^{o'} = f_k^o \left(1 - f_k^o\right) = o_{pk}\left(1 - o_{pk}\right) \tag{3.14}$$

Combining equations (3.10) and (3.11) the negative gradient is,

$$-\frac{\partial E_p}{\partial W_{kj}^o} = (d_{pk} - O_{pk})f_k^{o'}(net_{pk}^o)i_{pj} \tag{3.15}$$

Finally the weight change value $\Delta_p W_{kj}^o$ can be given by

$$\Delta_p W_{kj}^o == -\eta \frac{\partial E_p}{\partial W_{kj}^o} \tag{3.16}$$

Where,

η is the learning rate parameter

Therefore the updated weights can be given by,

$$W_{kj}^o(t+1) = W_{kj}^o(t) + \Delta_p W_{kj}^o(t) \tag{3.17}$$

Combining equations (3.15), (3.16) and (3.17) the general weight update equation is given as,

$$W_{kj}^o(t+1) = W_{kj}^o(t) + \eta(d_{pk} - O_{pk})f_k^{o'}(net_{pk}^o)i_{pj} \tag{3.18}$$

Now combining equation (3.18) and (3.13) the weight update equation for linear output units is,

43

$$W_{kj}^{o}(t+1) = W_{kj}^{o}(t) + \eta(d_{pk} - O_{pk})i_{pj} \tag{3.19}$$

The weight update equation for sigmoid output units combining (3.18) and (3.14) is,

$$W_{kj}^{o}(t+1) = W_{kj}^{o}(t) + \eta(d_{pk} - O_{pk})o_{pk}\left(1 - o_{pk}\right)i_{pj} \tag{3.20}$$

The above equation is summarized by defining a quantity,

$$\varepsilon_{pk}^{o} = (d_{pk} - O_{pk}).f_{k}^{o'}(net_{pk}^{o})$$

$$= \varepsilon_{pk}.f_{k}^{o'}(net_{pk}^{o}) \tag{3.21}$$

Combining equation (3.18) and (3.21) the weight update equation can be finally summarized as,

$$W_{kj}^{o}(t+1) = W_{kj}^{o}(t) + \eta\varepsilon_{pk}^{o}i_{pj} \tag{3.22}$$

3.5.2.2 Weight update for the Hidden layers

The weight update for the hidden layer is done in a similar manner by evaluating the error gradient with respect to the hidden layer weights W_{ji}^{h} .

$$\frac{\partial E_{p}}{\partial W_{ji}^{h}} = \frac{1}{2}\sum_{k}\frac{\partial}{\partial W_{ji}^{h}}\left(d_{pk} - o_{pk}\right)^{2}$$

$$\frac{\partial E_{p}}{\partial W_{ji}^{h}} = -\sum_{k}\left(d_{pk} - o_{pk}\right)\frac{\partial o_{pk}}{\partial\left(net_{pk}^{o}\right)}\frac{\partial\left(net_{pk}^{o}\right)}{\partial i_{pj}}\frac{\partial i_{pj}}{\partial\left(net_{pj}^{h}\right)}\frac{\partial\left(net_{pj}^{h}\right)}{\partial W_{ji}^{h}} \tag{3.23}$$

Referring section 3.3.2.1 for the evaluation of similar partial derivatives, above equation can be given as,

$$\frac{\partial E_{p}}{\partial W_{ji}^{h}} = -\sum_{k}\left(d_{pk} - o_{pk}\right).f_{k}^{o'}\left(net_{pk}^{o}\right)W_{kj}^{o}f_{j}^{h'}\left(net_{pj}^{h}\right)x_{pi} \tag{3.24}$$

The hidden layer weights are updates in proportion to the negative of equation (3.24),

$$\Delta_{p}W_{ji}^{h} = \eta f_{j}^{h'}\left(net_{pj}^{h}\right)x_{pi}\sum_{k}\left(d_{pk} - o_{pk}\right)f_{k}^{o'}\left(net_{pk}^{o}\right)W_{kj}^{o} \tag{3.25}$$

Using equation (3.21), (3.25) can be written as,

$$\Delta_p W_{ji}^h = \eta f_j^{h'}\left(net_{pj}^h\right) x_{pi} \sum_k \varepsilon_{pk}^o W_{kj}^o \tag{3.26}$$

From equation (3.25) it is evident that every weight update on the hidden layer depends on all the error terms ε_{pk}^o on the output layer. This result is where the notation of backpropagation arises. The known errors on the output layer are propagated back to the hidden layer to determine the appropriate weight changes on that layer.

To make the hidden layer weight update equation analogous to equation (3.22), the weight update equation of the output layer, a hidden layer error term is defined,

$$\varepsilon_{pi}^h = f_j^{h'}\left(net_{pj}^h\right) \sum_k \varepsilon_{pk}^o W_{kj}^o \tag{3.27}$$

Finally the weight update equation for the hidden layer becomes,

$$W_{ji}^h(t+1) = W_{ji}^h(t) + \eta \varepsilon_{pj}^h x_i \tag{3.28}$$

3.6 Neural Network Modeling Process

The MatLab7 was used as the software tool for the modeling of the Neural Network. Several MatLab 7 commands and functions in accordance with the above described backpropagation theory; available in the Neural Network Tool Box is used for the programs written. The network architecture optimization, improving the generalization and database processing are some important sections paid special attention during the modeling process and finalization process.

The following sections carry a general discussion about the selection of functions for the modeling.

3.6.1 Neural Network Architecture

As described early in the chapter the neural network consists of an input layer, output layer and one or more intermediate layers referred to as hidden layers.

3.6.1.1 Input and Output Neurons

Though the no of input neurons and the no of output neurons are directly related to the specific problem, hidden layers and hidden neuron determination is not so straight

45

forward. But this is the section which has to be done with a lot of emphasis, since the performance of a Neural Network model is essentially determined by a successful optimization of the number of neurons in the network so that a minimum error level is achievable in least computational time [23].

3.6.1.2 Optimizing the Network Architecture

Determination of the number of hidden layers and hidden units in layers are looked into in this section. Heuristics exist for determining the number of units in the hidden layers.

3.6.1.2.1. Effect of the size of hidden layers

The function of a hidden layer of a well trained three layer network is that it views the input pattern to determine which features are present in the pattern, and the output layer considers what output should be generated for the particular combination of features identified by the hidden layer [23].

Increasing the size of hidden layer usually improves the network's accuracy on the training set. Also the hidden layer may memories the input patterns rather than learning the features, especially the number of neurons in the hidden layer exceeds the number of training cases. Thus will lose the predictability on an unseen set. i.e. the network will lose its generalization capability. For a network with a single hidden layer it is common practice to initially make the number of neurons equal to about two-third of the number in the input layer. For a well generalized neural network model, there should be about 10 times as many training data points as there are weights in the network. By using this heuristic we can set an upper limit on the number of hidden units in the model.

Decreasing the size of the hidden layer generally improves generalization and hence the performance on the new cases.

But a perfect fit of hidden neurons i.e. a just large enough network design is however for each application is basically a process of trial and error. In the present study the No of hidden neurons and no of hidden layers are determined by monitoring the training error. The selection criteria is given in the under the results.

3.6.2 Inputs and outputs to the network (The Database)

Presenting data for training the NN is a critical factor, when considering the NN's final performance. The training database should be *sufficiently* and *properly* selected [24]. But this selection has no hard and fast rules. In general one can use as many data available to train the network, although it is not necessary to use them all. If the network is trained to perform in a noisy environment then including some noisy input vectors in the data set will help the network to converge even if no noise is expected at the input.

From the available training data, a small sub set is often sufficient to train a network successfully. The remaining data can be used to test the network to verify the network's generalization capability. Often the available database is splitted in to three sub sections such as,

- The training set - which is used for computing the gradient and updating the network weights and biases
- The validation set – The error on the validation set is monitored during the training process With early stopping(discussed in section 3.6.3.2), the choice of the validation set is important. The validation set should be representative of all points in the training set.
- The test set

The training set is used to train the network and the validation set is used as a checking data set which is used to monitor the over fitting of the network to the training data. A separate Testing set (previously unseen by the network during training) generated on the same sampling strategy was used to evaluate the performance of the network.

3.6.2.1 Pre-Post Processing of data

In neural Network learning, data with different scales often leads to instability of neural networks [25]. This can be addressed by making the training data set representative of the kind of patterns the operational network will have to recognize [26]. Since they are sensitive to absolute magnitudes all inputs to the neural network

47

usually the input variables are standardized so that they are all on the same order of magnitude [26].

Data may have to be converted into another form to be meaningful to the network i.e. since neurons operate with numeric inputs and outputs that corresponds to the activation values of the neurons usually 0 to 1 or -1 to +1, variables are standardized to ranges between these values.

The general data processing techniques include,

- Data Normalization

    Dividing all values of a set by the maximum value in the set. This can result in loss of information with anomalous spikes [26].

- Data Scaling

    Mapping the variable with a range between the minimum and maximum values to the full working range of the network input.

    $$X_{scaled} = \frac{X - X_{min}}{X_{max} - X_{min}}$$

- Z-Scores

    Converts each example value to a Z score by subtracting the mean and dividing the difference by the standard deviation. This compensates for both different magnitudes and variability.

It has been found that standardizing the input variables to means of zero and units of standard deviations has consistently led to better results in Neural Networks so that in the present study Z Score standardization is used [27].

Not only the magnitudes and the variability, but also the existence of high degree of redundancy in the data from the monitored variables of a system can have an adverse effect on the results of neural network modeling.

3.6.3 Avoiding Overtraining (Improving Generalization)

Overtraining is probably the most common error in neural networks. There is no perfect method for determining the number of training iterations or where to stop training. Overtraining will result in the network to adjust it self to the minor details in the training set similarly as in the case of a very large network compared to the training set. The most basic method to improve generalization is to select a network that is just large enough to provide an adequate fit (also discussed in section 3.6.2.2.1).If the network is too large then it can learn or create complex functions. If we use a small enough network, it will not have enough power to over fit the data.

Various methods can be used to determine when to stop training in neural networks.

1. Early stopping based on cross validation
2. Stopping after a user defined error level is reached or after the error levels off
3. Use of a test data set

The problem with the second method is that it is difficult to decide on what this error level is. Often this level is chosen when the error levels off and does not change. The error during training usually drops until a certain number of iterations where it levels off and does not get much smaller, however at this point the network may be overtrained.

Use of a test data set is not independent of model development. Though this method may give the best model for that set of data it does not give the generalizability of the system.

There are two other methods for improving generalization

- Regularization
- Early stopping

Both these generalization techniques are implemented in the Matlab7 Neural Network tool Box. There are used in combination with the different training functions and eliminates the guesswork required in determining the optimum network size. The two

49

methods with the implemented strategies in the Matlab7 Neural Network tool box are discussed below.

3.6.3.1 Regularization

Bayesian regularization method of improving the generalization is implemented in the function 'trainbr' which is an inbuilt training function in the Neural networks tool Box.

This involves modifying the performance function, which is normally chosen to be the sum of squares of the network errors on the training set.

This function updates the weight and bias values according to Levenberg-Marquardt optimization. It minimizes a combination of squared errors and weights, and then determines the correct combination so as to produce a network that generalizes well. The process is called Bayesian regularization.

One feature of this algorithm is that it provides a measure of how many network parameters (weights and biases) are being effectively used by the network. This effective number of parameters should remain approximately the same, no matter how large the total number of parameters in the network becomes. (This assumes that the network has been trained for a sufficient number of iterations to ensure convergence.)

The trainbr algorithm generally works best when the network inputs and targets are scaled so that they fall approximately in the range [-1, 1].

When using trainbr, it is important to let the algorithm run until the effective number of parameters has converged. You can also tell that the algorithm has converged if the sum squared error (SSE) and sum squared weights (SSW) are relatively constant over several iterations. When this occurs we can stop training manually.

3.6.3.2 Early Stopping

With early stopping methods some of the data is removed before training begins. Then when training is done, the data that was removed can be used to test the performance of the learned model on ``new" data. This is the basic idea for a whole class of model evaluation methods called *cross validation*.

The error reduces on the training data as the training proceeds. To evaluate the network training is stopped periodically and substitute the test set for one epoch and record the sum squared error. The error also initially goes down on the hold out data (validation set) but then the error level rises again as the model becomes over trained.

In the Matlab7 Neural Network tool box early stopping can be used with any of the inbuilt training functions. You simply need to pass the validation data to the training function.

When the validation error increases for a specified number of iterations, the training is automatically stopped, and the weights and biases at the minimum of the validation error are returned.

Requirement of a large example data set is one drawback of this method. Another problem is that it doesn't guarantee that the minimum error found is a global minimum rather than a local minimum.

Two main approaches exist for evaluation (testing) model performance with the early stopping technique.

1. Use a single set to train and test the model using cross validation, leave-one-out, jack-knife or bootstrapping when a large set of example data are not available.
2. Use of an independent data set for testing. If the data set is split into two parts with one part for testing, it is called a split-sample approach or hold out method. However the independent test is optimal if the two data sets originate from two different sampling strategies.

3.6.3.2.1 Hold-out method

Split-sample or hold-out method is commonly used for early stopping in Neural Networks. This is the simplest kind of cross validation. The data set is separated into two sets, called the training set and the testing set. The function approximator fits a function using the training set only. Then the function approximator is asked to predict the output values for the data in the testing set (it has never seen these output values before). The advantage of this method is that it is usually preferable to the residual

method and takes no longer to compute. However, its evaluation can have a high variance. The evaluation may depend heavily on which data points end up in the training set and which end up in the test set, and thus the evaluation may be significantly different depending on how the division is made.

3.6.3.3 Regularization Vs Early Stopping

Both regularization and early stopping can ensure network generalization when properly applied.

When using Bayesian regularization, it is important to train the network until it reaches convergence. The sum squared error, the sum squared weights, and the effective number of parameters should reach constant values when the network has converged.

For early stopping, you must be careful not to use an algorithm that converges too rapidly.

- When using a fast algorithm **trainlm** (training with Levenberg-Marquardt backpropagation) set the training parameters so that the convergence is relatively slow
- The training functions **trainscg** (Scaled conjugate gradient backpropagation) and **trainrp** (Resilient backpropagation) usually work well with early stopping

Based on experience, Bayesian regularization generally provides better generalization performance than early stopping, when training function approximation networks. This is because Bayesian regularization does not require that a validation data set be separated out of the training data set. It uses all of the data. This advantage is especially noticeable when the size of the data set is small.

In the present study since data is synthetically generated a large example database is available. Therefore Early stopping with a Hold out cross validation is used. Also the automated training termination is more reliant than monitoring convergence in the Regularization method.

3.6.4 Determining Network Parameter

Network parameters are the Learning Rate, Weight Ranges that influence the model performance by affecting the weights.

The weight should be initialized to small positive random values.

Selection of a value for the learning rate parameter η has a significant effect on the network performance. Usually η must be a small number on the order of 0.05-0.25 to ensure that the network will settle to a solution [24]. If a small value of η is selected the network will have to make a large number of iterations to converge. It is possible to increase the value of η while training proceeds, to speed convergence by increasing the step size as the error reaches a minimum, but the network may bounce around too far from the actual minimum value if η gets too large.

'Momentum' is another technique to increase the speed of convergence. For that a modification is done to the weight update equation: when calculating weight change value, $\Delta_p W$ a fraction of the previous change is added. This additional term tends to keep the weight changes going in the same direction. With the momentum term the weight change equation (3.22) of the output layer become,

$$ W_{kj}^{o}(t+1) = W_{kj}^{o}(t) + \eta \varepsilon_{pk}^{o} i_{pj} + \alpha \Delta_p W_{kj}^{0}(t-1) $$
(3.29)

Where α is the momentum parameter and is usually set to a positive value less than 1.

3.7 MatLab Function Selection in the Modeling

In the earlier sections some MatLab7 Neural Network functions used for the program development was mentioned and discussed. In this section the Training function selection etc. will be discussed. The MatLab inbuilt functions provide a compact set of functions which eliminates the lengthy programs written in the C or C++ language.

3.7.1 Pre and Post processing of the training database

There are several pre and post processing techniques available.

- Postmnmx   Unnormalize data which has been normalized by premnmx
- Postreg   Post process network response with linear regression analysis
- Poststd   Unnormalize data which has been normalized by prestd
- Premnmx   Normalize data for maximum of 1 and minimum of –1
- Prepca   Principal Component analysis on input data
- Prestd   Normalize data for unity standard deviation and zero mean
- Tramnmx   Transform data with precalculated minimum and max
- Trapca   Transform data with PCA matrix computed by prepca
- Trastd   Transform data with precalc. mean & standard deviation

3.7.2 Creating a Neural Network

'Newff' Create a feed-forward backpropagation network. The functions with input parameters are,

net = newff(PR,[S1 S2...SNl],{TF1 TF2...TFNl},BTF,BLF,PF)

This returns an N layer feed-forward backpropagation network (net).

Where,

PR - R x 2 matrix of min and max values for R input elements

Si - Size of ith layer, for Nl layers

TFi - Transfer function of ith layer, default = 'tansig'

BTF - Backpropagation network training function, default = 'traingdx'

BLF - Backpropagation weight/bias learning function, default = 'learngdm'

PF - Performance function, default = 'mse'

3.7.3   Transfer Functions

The transfer functions TFi can be any differentiable transfer function such as,

54

- Tansig   Hyperbolic tangent sigmoid transfer function
- Logsig   Log sigmoid transfer function
- Purelin   Linear transfer function

3.7.4 Training Algorithms

A large number of backpropagation algorithms exist [7] the training function BTF can be any of the backpropagation training functions such as,

- Trainlm   Levenberg-Marquardt backpropagation
- Trainbfg   BFGS quasi-Newton backpropagati
- Trainbr   Bayesian regularization backpropagation
- Trainrp   Resilient backpropagation (network training function that

                updates weight and bias values according to the resilient

                backpropagation algorithm (RPROP))

- Traingd   Gradient descent backpropagation
- Traingdm   Gradient descent with momentum backpropagation
- Traingda   Gradient descent with adaptive learning rate backpropagation
- Traingdx   Gradient descent with momentum and adaptive learning rate

                Backpropagation.

- trainc   Cyclical order incremental update
- traincgb   Powell-Beale conjugate gradient backpropagation
- traincgf   Fletcher-Powell conjugate gradient backpropagation
- traincgp   Polak-Ribiere conjugate gradient backpropagation
- trainoss   One step secant backpropagation
- trainr   random order incremental update
- trains   Sequential order incremental update
- trainscg   Scaled conjugate gradient backpropagation

'Trainlm' is the default training function because it is very fast, but it requires a lot of memory to run. Function 'trainbfg', is slower but more memory-efficient than 'trainlm'. 'Trainrp', is slower but more memory-efficient than trainbfg.

Function Characteristics as described in [28] are,

- On function approximation problems, for networks that contain up to a few hundred weights, the Levenberg-Marquardt algorithm will have the fastest convergence this advantage is especially noticeable if very accurate training is required. In many cases, **trainlm** is able to obtain lower mean square errors than any of the other algorithms tested. However, as the number of weights in the network increases, the advantage of the trainlm decreases.

- In addition, **trainlm** performance is relatively poor on pattern recognition problems. The storage requirements of trainlm are larger than the other algorithms tested. By adjusting function parameters the storage requirements can be reduced, but at a cost of increased execution time.

- The **trainrp** function is the fastest algorithm on pattern recognition problems. However, it does not perform well on function approximation problems. Its performance also degrades as the error goal is reduced. The memory requirements for this algorithm are relatively small in comparison to the other algorithms considered. The performance of Rprop is not very sensitive to the settings of the training parameters.

- The conjugate gradient algorithms, in particular **trainscg,** seem to perform well over a wide variety of problems, particularly for networks with a large number of weights. The SCG algorithm is almost as fast as the LM algorithm on function approximation problems (faster for large networks) and is almost as fast as trainrp on pattern recognition problems. Its performance does not degrade as quickly as trainrp performance does when the error is reduced. The conjugate gradient algorithms have relatively modest memory requirements.

- The **trainbfg** performance is similar to that of trainlm. It does not require as much storage as trainlm, but the computation required does increase geometrically with the size of the network, since the equivalent of a matrix inverse must be computed at each iteration.

- The variable learning rate algorithm **traingdx** is usually much slower than the other methods, and has about the same storage requirements as trainrp, but it can still be useful for some problems. There are certain situations in which it is better to converge more slowly. For example, when using early stopping you may have inconsistent results if you use an algorithm that converges too

quickly. You may overshoot the point at which the error on the validation set is minimized.

3.7.4.1 Choosing a training Algorithm

Multilayer networks typically use sigmoid transfer functions in the hidden layers. These functions are often called "squashing" functions, since they compress an infinite input range into a finite output range. Sigmoid functions are characterized by the fact that their slope must approach zero as the input gets large.

The basic backpropagation algorithm adjusts the weights in the steepest descent direction (negative of the gradient).This causes a problem when using steepest descent to train a multilayer network with sigmoid functions, since the gradient can have a very small magnitude; and therefore, cause small changes in the weights and biases, even though the weights and biases are far from their optimal values.

The purpose of the resilient backpropagation (Rprop) training algorithm is to eliminate these harmful effects of the magnitudes of the partial derivatives. Only the sign of the derivative is used to determine the direction of the weight update; the magnitude of the derivative has no effect on the weight update.

Also it turns out that, although the function decreases most rapidly along the negative of the gradient, this does not necessarily produce the fastest convergence.

In the conjugate gradient algorithms a search is performed along conjugate directions, which produces generally faster convergence than steepest descent directions.

In most of the training algorithms a learning rate is used to determine the length of the weight update (step size). In most of the conjugate gradient algorithms, the step size is adjusted at each iteration. A search is made along the conjugate gradient direction to determine the step size, which minimizes the performance function along that line.

57

Chapter 4
One Dimensional Resistivity Inversion

4.1 Introduction

In a One Dimensional (1D) study the vertical variation beneath a point of interest is obtained. This is referred to as Vertical Electrical Sounding (VES) by most practitioners. The field apparent resistivity values are inverted to produce a one dimensional plot of resistivity values   i.e. thickness and earth resistivity of each layer in a horizontally stratified multilayer earth structure as shown in Figure.1.1.

4.2 Literature Survey

Following is a brief outline of the methods used in 1D interpretation, as discussed under section 1.3.

4.2.1 Qualitative Interpretation

The qualitative interpretation depends on two principles: the lines of current will be deflected towards a good conductor and potential difference between the potential electrodes is produced by the current flow along the lines joining them (discussed under section 2.9).

4.2.1.1 Two Layer Structure -High Resistivity layer over low resistivity layer

Consider the earth model shown in Figure 4.1, a high resistivity layer over a lower resistivity layer. When the current electrodes are closely spaced, in the region surrounding the potential electrode positions (between the two current electrodes), most of the current flows through the upper layer along paths that are close to those that they would have flown along if the model were homogeneous. That is, in this electrode configuration, current flow is not significantly perturbed near the potential electrodes to distinguish between this layer model and a homogeneous Earth model with a resistivity equal to the resistivity of the top layer. Thus, the computed apparent resistivity will be close to the resistivity of the upper layer, ρ_1 .

C₂   C₂   C₁   C₂

High Resistivity Upper Layer P
Low Resistivity Bottom Layer P

Actual Current Flow Lines   Current Flow Lines if the soil was
                                            Homogeneous

Small Electrode Spacing   Large Electrode Spacing
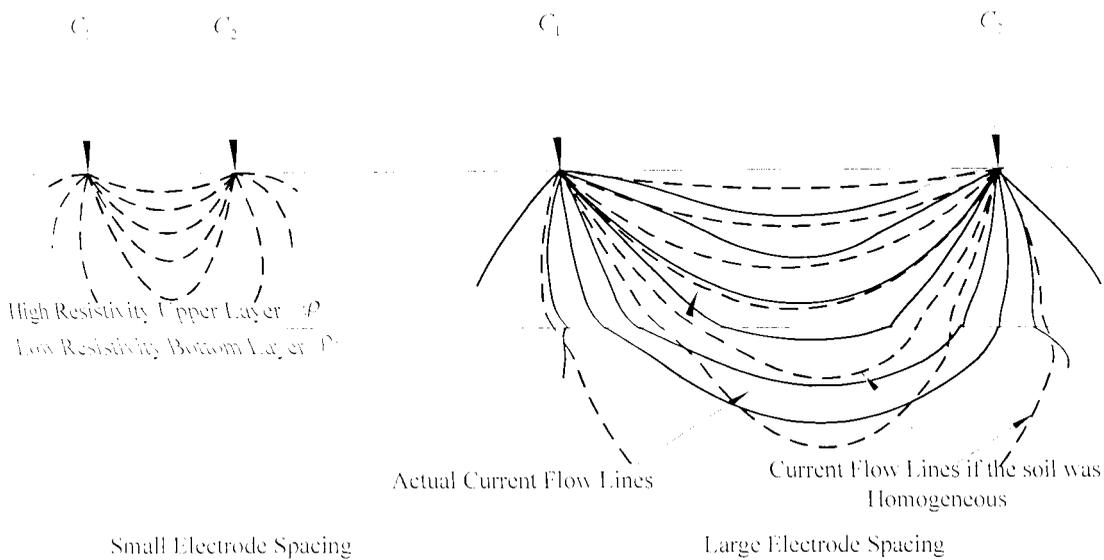
Figure 4.1 - Two layer model with high resistivity layer over low resistivity layer
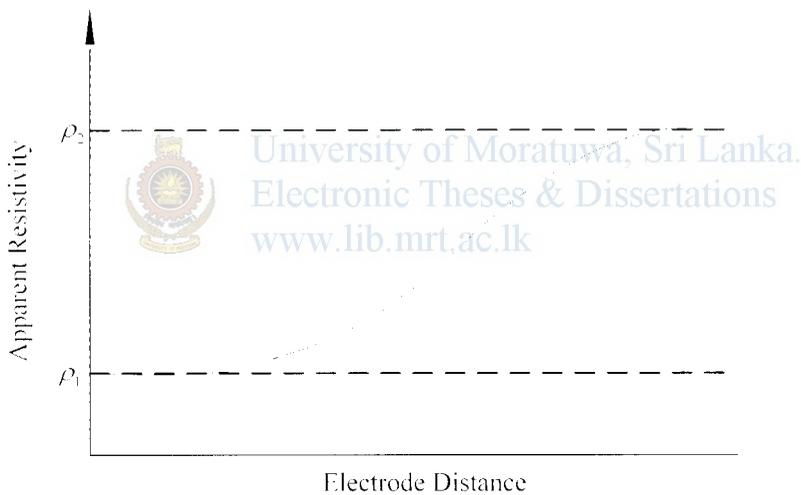

Figure 4.2 - Field Curve pattern for two layer model with high resistivity layer over low resistivity layer

Now, when increasing the current electrode spacing, the current flow near the potential electrodes is significantly altered by the presence of the subsurface boundary. In this case, current is preferentially drawn downward into the lower resistivity layer, decreasing the current density between the two current electrodes. This decrease in current density will cause the computed value of apparent resistivity to gradually decrease from ρ_1.

At very large current electrode spacing, underneath the potential electrodes, the pattern of current flow is again similar to that which we would observe in a

homogeneous Earth model. In this case, however, the media has a resistivity of ρ_2. Thus, the expected resistivity curve will have a pattern as shown in Figure 4.2.

4.2.1.2 Two Layer Structure -Low Resistivity layer over high resistivity layer

Consider the earth model shown in Figure 2.6. In this case, a low resistivity layer overlies a higher resistivity half space. The behavior of apparent resistivity is shown in Figure 4.3. Similar to the above discussion, when the electrode spacing is small compared to the depth of the top layer the current density is unaffected by the bottom layer. Therefore, thee resistivity reading s will be unaffected by the high resistivity layer and the apparent resistivity will give a reading equal to ρ_1, the resistivity of the top layer.

When the electrode spacing is gradually increased the current starts to enter the high resistivity bottom layer. The current is deflected away from the high resistivity substratum as the current seeks to follow a low resistance path. The current density in the top layer will increase, where the current density between the current electrodes is increased. Therefore the corresponding apparent resistivity reading will gradually increased from ρ_1. Finally at very large electrode spacing compared to the top layer height the apparent resistivity reading will gradually approach the bottom layer resistivity, ρ_2 as shown in Figure 4.3.

Thus with respect to geological formation of earth, certain field curves can be drawn.
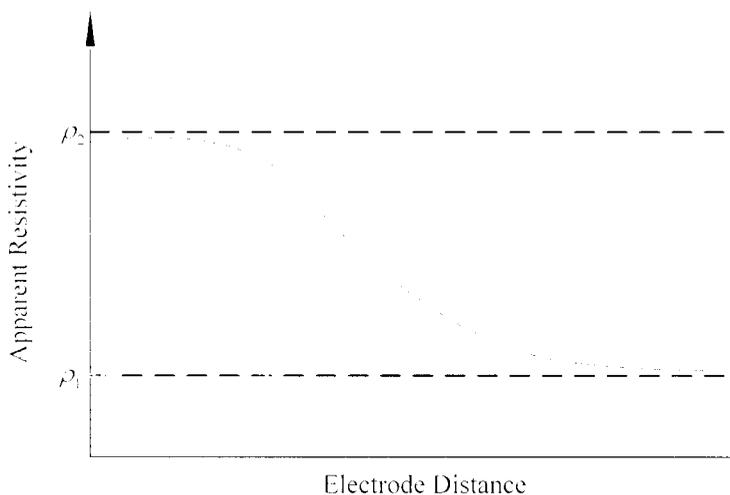
Figure 4.3 - Field Curve pattern for two layer model with low resistivity layer over high resistivity layer

4.2.1.3 Three layer Structure standard curves

The geological formation of a three layer structure defines 4 curve types namely Type A, Q, K and H (Figure 4.4). Table 4.1 gives the resistivity combination of the four types.

Curve Type	Top layer resistivity	Intermediate layer resistivity	Bottom layer resistivity
A	Low	Medium	High
Q	High	Medium	Low
K	Low	High	Medium
H	High	Low	Medium

Table 4.1 - Geological formation for three layer structure

Type A
a : $h_2 > h_1$, $\rho_1 \ll \rho_3$
b : $h_2 < h_1$, $\rho_1 < \rho_3$

Type Q
a : $h_2 < h_1$, $\rho_1 > \rho_3$
b : $h_2 > h_1$, $\rho_1 > \rho_3$

Type K
a : $h_2 < h_1$, $\rho_1 \gg \rho_3$
b : $h_2 > h_1$, $\rho_1 \gg \rho_3$
c : $h_2 > h_1$, $\rho_1 > \rho_3$
d : $h_2 > h_1$, $\rho_1 < \rho_3$

Type H
a : $h_2 > h_1$, $\rho_1 > \rho_3$
b : $h_2 > h_1$, $\rho_1 < \rho_3$
c : $h_2 > h_1$, $\rho_1 \ll \rho_3$
d : $h_2 < h_1$, $\rho_1 < \rho_3$
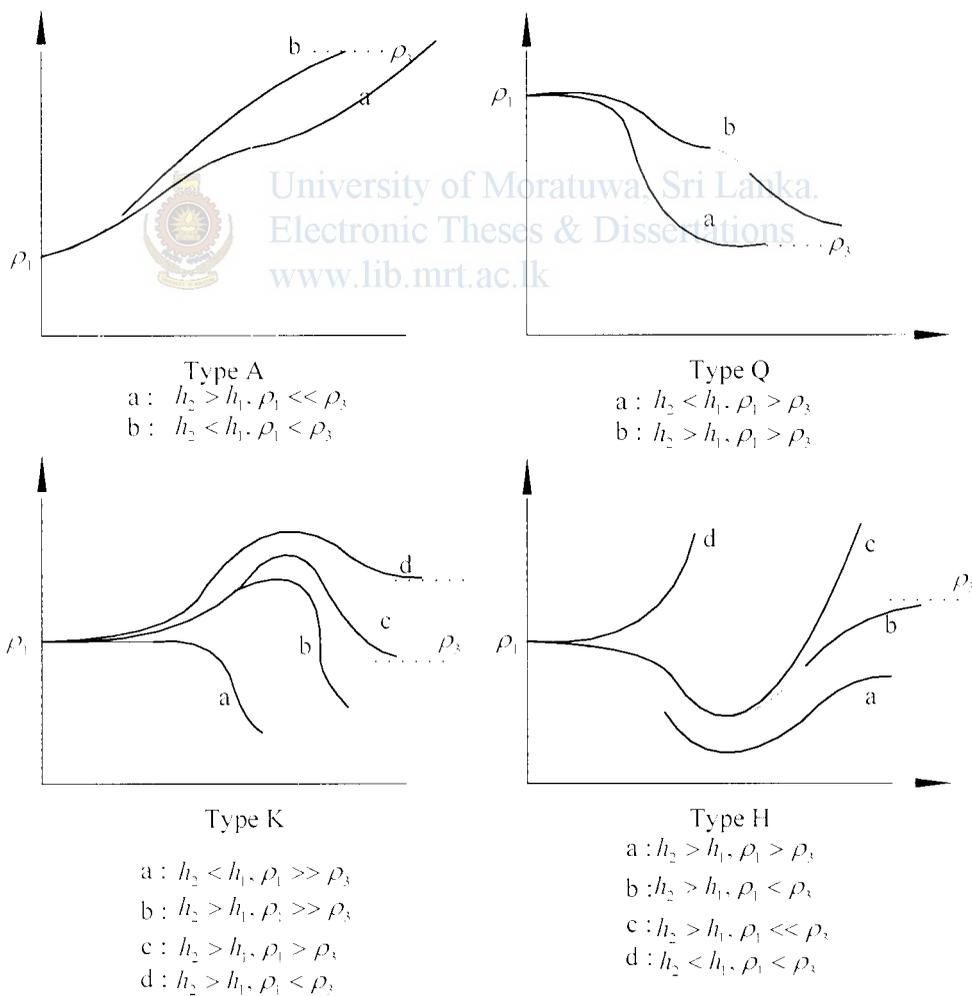
Figure 4.4 - Field curve patterns for three layer structure

Types H & K have distinct maximum/minimum and indicate anomalously high/low resistivity respectively. Types A & Q show steady change indicating middle layer has

61

intermediate resistivity between upper and lower layer. As with the two layer case, the current density will be affected by the multiple layers as the electrode spacing increases.

First part of curve at small electrode separations can be analyzed as two layer case to see if r_a increase or decreases into second layer. Comparing curve at small and large spacing indicates resistivity of lower layer relative to upper. Character of mid-part of curve indicates nature of middle layer.

But the drawback is that layer only shows up in curve if it is sufficiently thick and resistivity sufficiently different from others.

4.2.1.4 Four layer structure Standard Curves

Obviously the above four curves also may be combined. It is generally possible to say from the shapes of the adjacent parts of the profile which layer corresponds to the maximum or minimum on the K and H curve types. Therefore the standard curves for a four layer model can be classified in to six curve types as HK, HA, KH, KQ, QH and AK representing different geological formations. Figure 4.5 shows two example curves.

Type HK
$\rho_1 > \rho_2 < \rho_3 > \rho_4$
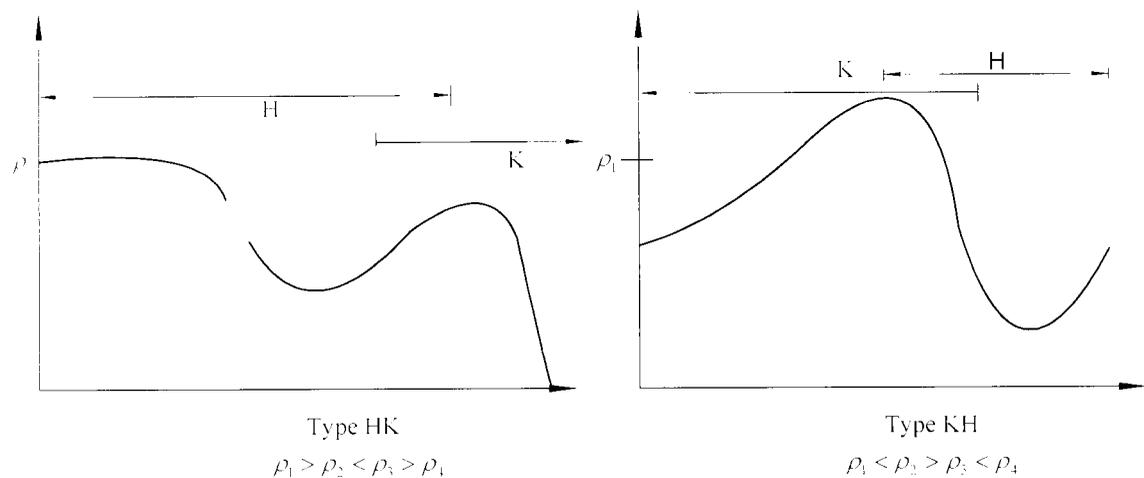
Type KH
$\rho_1 < \rho_2 > \rho_3 < \rho_4$

Figure 4.5 - Four layer Type HK and Type KH curve patterns

In general, number of detectable layers equal to number of turning points in sounding curve plus one. Turning point due to an interface, so number of layers is one greater.

Electrode separation, at which turning points occur, has no connection with depth to interface

4.2.2 Quantitative Interpretation

Ohm-meter method, Moore-cumulative method and Barnes layer method are some earliest used 1D interpretation techniques. Ohm-meter method is the earliest, simplest and poorest method of interpretation [3]. The field collected apparent resistivity values are plotted versus depth in feet and a curve is drawn through the points. Interpretation consists of noting the depths at which breaks occur in the shape of curve.

4.2.2.1 Curve matching

Before the availability of personal computers, the curve-matching process was done. The use of standard or master curves (discussed in section 2.11) requires an identification of the curve type followed by a comparison with standard curves of that type to obtain the best match. Two-layer and three-layer curves can be used for complete interpretation of VES curves of more layers by the Auxiliary Point Method, which requires the use of a small set of auxiliary curves and some constructions.
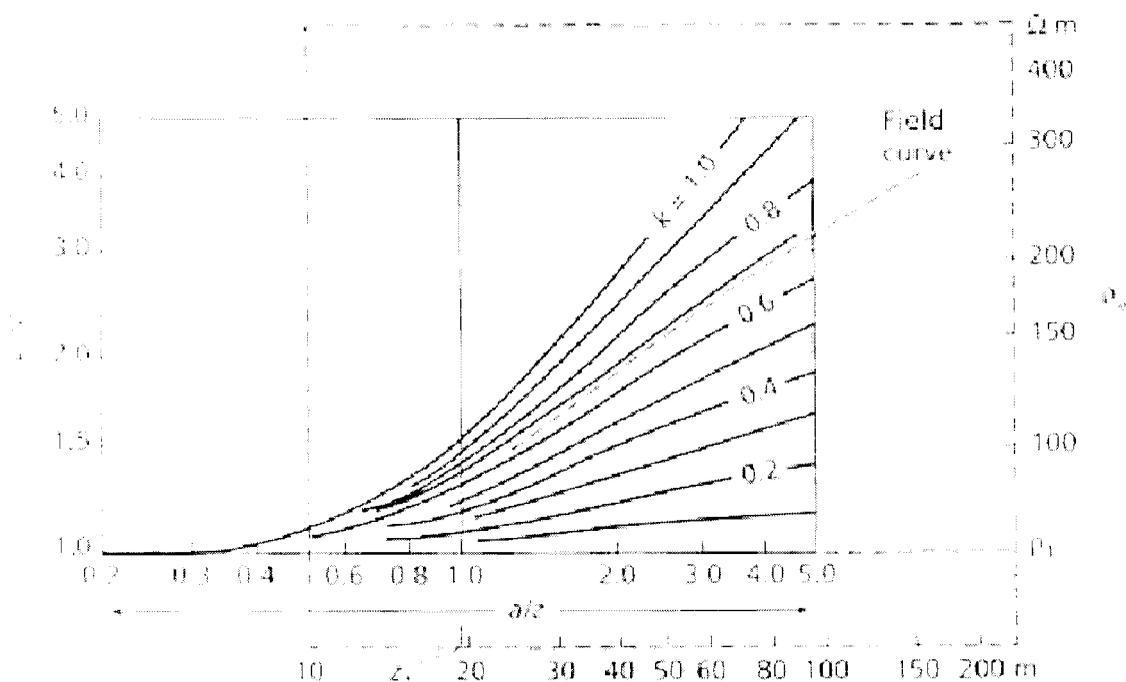

Figure 4.6 - The interpretation of a two layer apparent resistivity graph by comparison with a set of master curve. The upper layer resistivity is 68 and its thickness is 19.5 m.

The field curve to be interpreted is plotted on transparent logarithmic paper with the same modulus as the master curve. It is then shifted over the master curve keeping the coordinate axes parallel, until a reasonable match is obtained with one of the master curves or with an interpolated curve as shown in Figure 4.6.

Then the Electrode spacing on transparency at which $a/z = 1$ to get interface depth h. Apparent resistivity on transparency at which $\rho_a/\rho_1 = 1$ to get resistivity of layer 1, ρ_1. Read the value of k, i.e. the reflection coefficient and calculate ρ_2, the resistivity of layer 2 using equation (B.3).
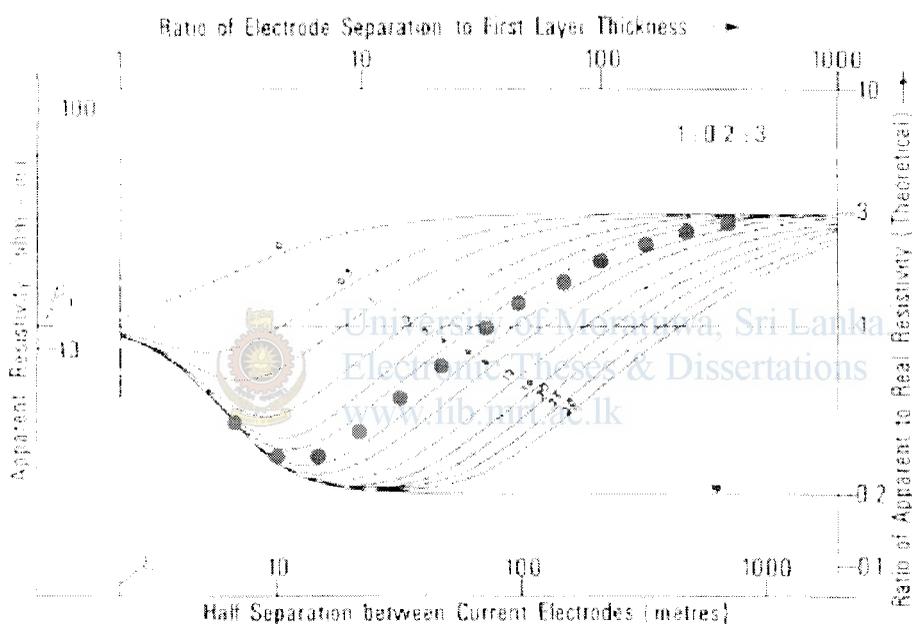

Figure 4.7 - the interpretation of a three layer apparent resistivity graph by comparison with a
Set of master curve.

3 layer case: Much larger sets of curves are required to represent the increased number of possible combinations of resistivities and layer thicknesses. Direct curve fitting is time consuming, better use auxiliary point techniques. Figure 4.7 shows a 3 layer curve matching example problem.

Dashed lines are the axes of the theoretical curves. Thick lines are the axes of the field curve. The number on curves are values of z_2/z_1 the points of intersection of these two axes give the field values of ρ_1 and z_1. ρ_2 and ρ_3 follow from the ratios given

from this family of curves where $\rho_2/\rho_1 = 0.2$ and $\rho_3/\rho_1 = 3$. z_2 is found from the ratios given on the best fitting curve. In this case an interpolation has been made between curves for 4 and 6. Final results therefore give: $\rho_1 = 13\Omega m$, $\rho_2 = 1.6\Omega m$, $\rho_3 = 39\Omega m$, $z_1 = 2.2m$ and $z_2 = 11m$

4.2.2.2 Computer based iterative calculation methods

With the introduction of linear filter theory [29] [30] [31] to develop a fast numerical method for computing apparent resistivity values from the resistivity transforms, and vice versa many computer based interpretation programs were developed. With these methods, new standard curves or trial VES curves can be computed as needed, with a computer, either to match the curves or to check the validity of an interpretation of the field data. Thus, trial-and-error interpretation of VES data is feasible. Trial values of the layer parameters can be guessed, checked with a computed apparent resistivity curve, and adjusted to make the field and computed curves agree (Figure 4.8). After a suite of sounding curves has been individually interpreted in this manner, a second pass can be made where certain layer thicknesses and/or resistivities can be fixed to give a more consistent project-wide interpretation.

ρ_a

Measured Apparent
Resistivities

ρ_a

Calculated Apparent
Resistivities

INPUTS

INVERSION

OUTPUTS

Start Model/ Initial Guess
(eg. For a three layer case)

ρ_1, h_1
ρ_2, h_2
ρ_3

Final Model/ Estimated
Earth parameters

ρ_1, h_1
ρ_2, h_2
ρ_3
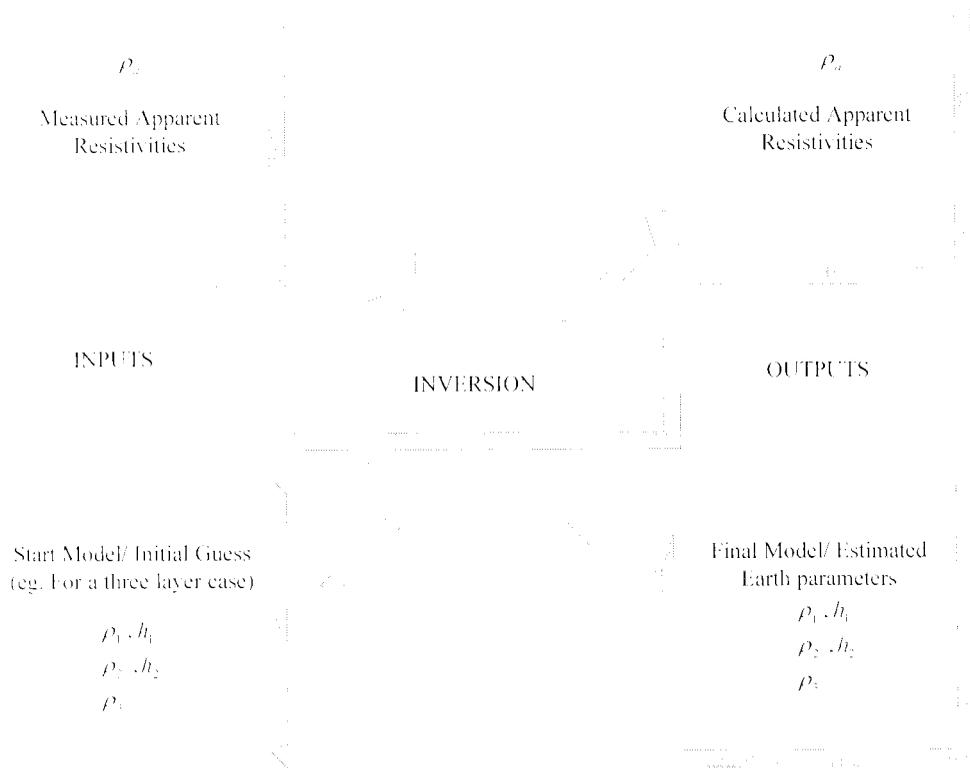
Figure 4.8 - Computer based iterative solution method.

In order to estimate on the correct parameters of the model through inversion first an error function is developed.

$$F_g = \sum_{i=1}^{N} \frac{|M_i - P_i|}{M_i}$$
(4.1)

Where,

M_i^m - i^{th} measurement of electrical property

P_i - Calculated value of the electrical property in a forward modeling calculation.

The calculation of parameters of two layer earth is a three parameter optimization problem, parameters being the resistivity of both layers and the depth of the top layer while the depth of the lower layer is taken as infinity. Also parameter calculation for three layer soil is a five parameter optimization problem, the parameters being, resistivities of the three layers and the depth of the upper layers while the depth of the third layer is taken as infinity. Similarly for N layers the problem is an optimization of (2N-1) parameters.

Computer programs have been written by [4] [5] [6] [7] [32] [33] and several commercial software companies for the use of this method to obtain the layer parameters automatically by iteration, starting with an initial estimate obtained by an approximate method. The process will be much faster, of course, if the initial guess is guided by a semi quantitative comparison with two- and three-layer curves. Most computer programs require a user-supplied initial estimate (model), whereas some programs can optionally generate the initial model.

In general all the computer based solutions presented is based on minimization of the above error function (4.1) which ultimately leads to recovery of unknown parameters giving an optimal solution.

4.3 Limitations of the 1D Interpretation

The major limitations of the electrical resistivity method are resolution, suppression and equivalence. They are all associated with the concept of relative thickness (RT), which is defined as the ratio of the thickness of a layer to the depth to the top of the layer.

4.3.1 Resolution

As a general rule, the resistivity method cannot resolve thin layers (RT < 0.1). It follows that the method can resolve considerable detail near the surface, but can see only bulk zones at depth.

4.3.2 Equivalent models

The interpretation of resistivity data is ambiguous. It is possible to find different combinations of thicknesses and resistivities which when substituted in equation (2.21) would yield the same theoretical resistivity sounding curve i.e. an apparent resistivity curve can be interpreted by different resistivity models.

The principle of equivalence states: The thickness and resistivity can not be derived independently. The geophysicist has to select the model, which agrees best with the known geological and hydro geological structures of the ground. Another selective criterion is the comparison with neighboring soundings.

4.3.3 Suppression

Usually, soundings can resolve no more than six to eight layers. Even a reasonably thick layer (0.1 < RT < 1) may not be detected if resistivity contrast is inadequate. This is likely to happen with a layer of intermediate resistivity which is sandwiched between one layer which is more conductive (less resistive) and another layer which is more resistive. Such a layer is said to be suppressed, as there may be no hint of the layer in the field data.
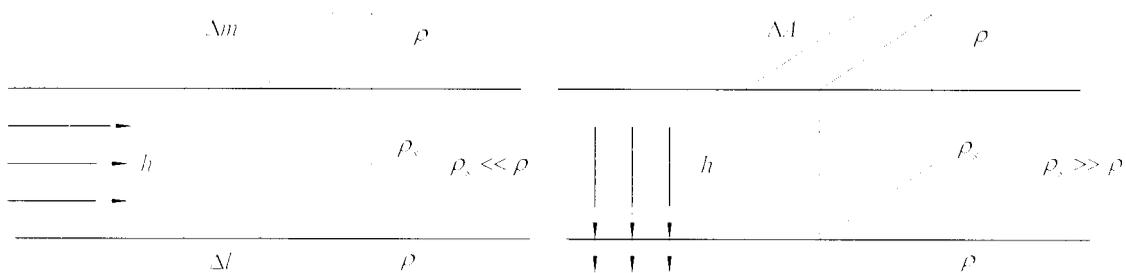
Figure 4.9 - Illustrates the problem of a "sandwiched layer"

To illustrate the above problem, Figure 4.9 is used, considering refraction at the boundary. If $\rho_s >> \rho$ the current flows nearly parallel then the resistance of the layer is,

$$R = \frac{\rho_s \Delta l}{h \Delta m} \tag{4.2}$$

$$S = \frac{h \sigma_s \Delta m}{\Delta l} \equiv \frac{S_L \Delta m}{\Delta l} \tag{4.3}$$

Where,

$\quad\quad S_L$ - longitudinal conductance

If $\rho_s << \rho$ the current flows nearly perpendicular (shortest path through layer). Then the layer resistance is,

$$R = \frac{\rho_s h}{\Delta A} \equiv \frac{R_t}{\Delta A} \tag{4.4}$$

Where,

$\quad\quad R_t$ - Transverse Resistance

It is evident that for any combination of ρ_s and h with the same ratio for equation and for same product for equation gives the same result.

4.3.4   The effect of Anisotropy

In sediments such as clay or shale the resistivity perpendicular to the layering is usually greater than parallel to the direction of layering.

Other than the error of equivalence one other reason for the ambiguity is, that in deriving equation (2.21) it was assumed that the earth is made of N homogeneous, isotropic, and horizontally continuous layers of resistivities $\rho_1, \rho_2, \ldots, \rho_N$. If the layers are anisotropic (i.e., the resistivity of each layer in the vertical direction ρ_t differs from that in the direction parallel to bedding ρ_q) as shown in Figure 4.10. In such a case the interpreted resistivity from sounding data, of each layer is equal to neither ρ_t nor ρ_q but equal to,

$$\rho_{t} = \sqrt{\rho_{t}\rho_{q}}$$ (4.5)

And its thickness is equal to,

$$h' = \lambda h$$ (4.6)

Where,

   h' - the interpreted thickness

   λ - Anisotropy coefficient equal to $\sqrt{\rho_{t}/\rho_{q}}$ e.g. for sand ,gravel $\lambda = 1.3$,coal $\lambda = 2$

Since ρ_{t} is generally greater than ρ_{q} for horizontally layered media, the interpreted thickness would be greater than the true thickness.
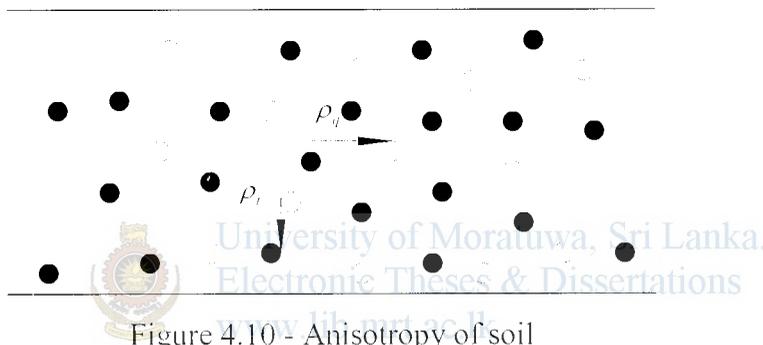
Figure 4.10 - Anisotropy of soil

The transverse resistance T and the longitudinal conductance S of this model are given by:

$$T = \sum_{i=1}^{n} \rho_{i} h_{i}$$ (4.7)

$$S = \sum_{i=1}^{n} h_{i}/\rho_{i}$$ (4.8)

Clearly, there is an infinite number of homogeneous and anisotropic single layered models possessing the same values of T and S. Thus, depending on the chosen thickness h of the model, it is possible to find values for ρ_{t} nor ρ_{q} which satisfy the following relations:

$$T = \rho_{t} h$$ (4.9)

$$S = h/\rho_{q}$$ (4.10)

Where,

$$h = \sum_{i=1}^{n} h_i$$

4.3.5 Non Horizontal layering

1D interpretation is valid, if the dip of the layers is not greater than 15°. Figure 4.11 shows a situation where the 1D interpretation is not valid.

a   b
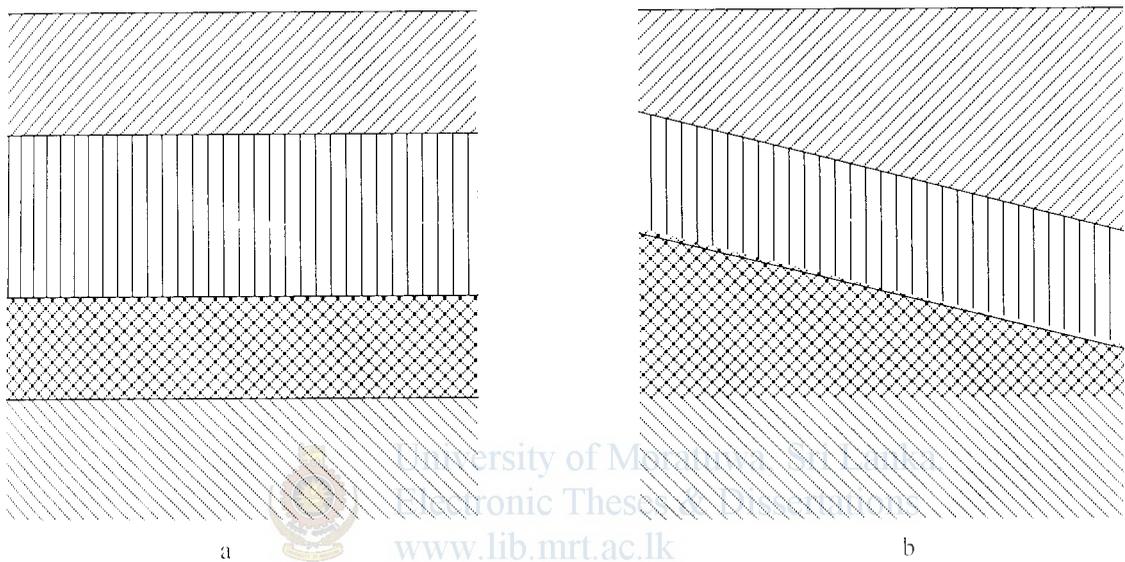
Figure 4.11 - (a) valid 1D interpretation (b) 1D interpretation is not valid

4.4 Synthetic Data generation

In order to train the Neural network an available example set is essential. Since no field measurements were available the neural network was decided to be trained with synthetic data. The data was generated by solving the infinite integral (2.21) of the apparent resistivity measured by a wenner array for the N- layers, which is in the generalized integral form given by,

$$\rho_a = \rho_1 \{1 + 2F_N(a) - F_N(2a)\} \tag{4.11}$$

Where,

$$F_N(a) = 2a \int_0^\infty \frac{K_{N1}e^{-2\lambda h_1}}{1 - K_{N1}e^{-2\lambda h_1}} J_0(\lambda a)d\lambda$$

And,

$$K_{N1} = \frac{k_1 + K_{N2}e^{2\lambda h_2}}{1 + k_1 K_{N2}e^{-2\lambda h_2}}$$

$$K_{Ns} = \frac{k_s + K_{Ns-1}e^{2\lambda h_{s-1}}}{1 + k_s K_{Ns-1}e^{-2\lambda h_{s-1}}}$$

$$K_{NN-1} = k_{N-1}$$

and

$$k_1 = \frac{\rho_2 - \rho_1}{\rho_2 + \rho_1} . k_s = \frac{\rho_{s+1} - \rho_s}{\rho_{s-1} + \rho_s} . k_{N-1} = \frac{\rho_N - \rho_{N-1}}{\rho_N + \rho_{N-1}}$$

$J_o(\lambda a)$ - Bessel function of First kind of order zero

Figure 4.1 shows the representation of a two layer one dimensional representation. During the two layer curve generation layer resistivities are varied between $10\,\Omega m$ and $1000\,\Omega m$. The top layer height is varied between 1-10m. The resistivity values used for database preparation are given in Table 4.2 where ρ_1 is the Upper layer resistivity and ρ_2 is the Bottom layer resistivity. For each combination of resistivity the first layer height is varied as, 1 m, 2.5m, 5m, 3m, 7.5m, 4.25m, 6m, 8.3m, 9.2m and 10m.
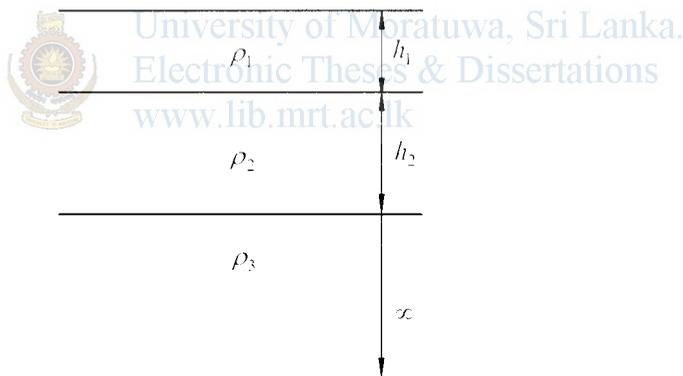

Figure 4.12 - Three layer one dimensional representation

Figure 4.12 shows a three layer one dimensional representation. For the three layer curve generation different resistivity combinations and layer height combinations were used. Table 4.3 gives the layer resistivity values used for the four types of curve generation. Here ρ_1 is the First layer resistivity, ρ_2 is the second layer resistivity and ρ_3 is the bottom layer resistivity.

	ρ_1	ρ_2
1.	10	100
2.	98	300
3.	175	520
4.	325	600
5.	475	500
6.	545	650
7.	725	1000
8.	840	1000
9.	100	400
10.	220	600
11.	420	750
12.	50	250
13.	935	1000
14.	620	700
15.	250	500
16.	300	250
17.	450	100
18.	1000	100
19.	220	20
20.	500	350
21.	650	400
22.	900	300
23.	725	500
24.	1000	200
25.	850	400
26.	600	300
27.	700	100
28.	500	175
29.	350	200
30.	1000	300

Table 4.2 - Resistivity value combinations of the two layer curve generation

	Type A			Type H			Type K			Type Q		
	ρ_1	ρ_2	ρ_3	ρ_1	ρ_2	ρ_3	ρ_1	ρ_2	ρ_3	ρ_1	ρ_2	ρ_3
1.	10	300	1000	300	100	700	245	500	100	800	300	100
2.	100	235	300	450	100	800	350	450	20	750	420	250
3.	120	400	520	500	100	100	725	1000	400	1000	600	345
4.	210	456	600	220	20	467	120	800	10	975	750	472
5.	300	350	500	500	350	879	685	950	350	1000	600	560
6.	125	543	650	650	400	743	400	575	100	998	800	630
7.	175	700	1000	900	300	1000	100	300	25	800	450	200
8.	500	642	1000	725	500	865	195	660	78	700	100	20
9.	350	377	400	452	200	678	720	1000	200	675	350	70
10.	475	532	600	850	400	975	500	750	340	900	675	300
11.	250	500	750	600	300	700	830	950	250	700	100	10
12.	220	240	250	700	100	1000	900	1000	620	1000	750	420
13.	420	800	1000	500	175	775	200	620	20	700	500	150
14.	50	400	700	350	200	920	475	800	300	1000	700	485
15.	400	675	800	750	300	1000	540	720	210	750	560	100

Table 4.3 - Resistivity value combinations of the three layer curve generation

	Type A/Type H		Type K		Type Q	
	h_1	h_2	h_1	h_2	h_1	h_2
1.	1	4	2	1	4	1
2.	2.5	6.75	5.5	1.5	6	1.5
3.	5	3.8	8	4	7.2	4
4.	3	9.4	1.5	2	1	2
5.	7.5	2	9.25	5	10	5
6.	4.25	10	6.4	20	7.5	20
7.	6	3.5	3.6	15	3.25	15
8.	8.3	7.4	4.4	9	4.4	30
9.	9.2	8.3	7	100	5	100
10.	10	10	10	50	2.67	45

Table 4.4 - Layer height combinations of the three layer curve generation

The layer height combinations are given in Table 4.4. For each combination of resistivity, the layer height combinations are varied from 1-10. Here h_1 is the first layer height and h_2 is the height of the second layer.

4.4.1 Hankel Transform's for solving the infinite integral

The equation that appears in the integral form,

$$E_r = \int_0^\infty G(\lambda) J_v(\lambda r) d\lambda \tag{4.12}$$

Are referred to as Hankel Transform (HT) or a Bessel Transform:

Here,

$J_v(\lambda r)$ - Bessel function of real order v of the first kind

$G(\lambda)$ - kernel function

Digital linear filter operators are widely used for carrying out the above type of numerical integrations [34]. A digital linear filter consist of,

- n abscissa values to sample the input defined with two constants. Sampling interval or spacing (s) and shift (a).The shift specifies the placing of the starting point for sampling the input function while the spacing specifies the interval which the remaining samples are to be taken.
- n filter weights

The value of the output function is determined by the sum of products of n samples of the input function with the corresponding filter weights.

The sampling points are calculated as follows,

$$\lambda_i = (1/r) \times 10^{[a-(i-1)s]}, i = 1,2,...,n \tag{4.13}$$

The function $G(\lambda)$ is then evaluated for these values of λ and the values of E_r computed from,

$$rE = \sum_{i=1}^{n} G(\lambda_i)W_i \qquad (4.14)$$

Where W_i are the n filter weights, by dividing the sum on the right hand side of the equation (4.14) by r.

Based on Dr. Brian Borchers's MatLab implemented routines [35] for numerical approximation of Hankel transforms of order 0 and 1 described from Walt Anderson's FORTRAN code [36], the routines are modified as to suite the present resistivity forward modeling problem with some additional routines. Appendix D gives the descriptive MatLab functions for the apparent resistivity curve generation for two layer case and three layer cases.

Table 4.5 compares the results obtained for the equation (4.11) evaluated with the MATLAB programs which uses the 801 Anderson filter weights; with the results given in [4] to calculate the error. It is evident that it reveals close agreement with the results obtained in [4] with maximum error in the order of 0.08% .Thus through the use of the programs I proceeded to calculate the synthetic data.

	Electrode Spacing	Results from [4] :SPEF:R	Using 801 Anderson Weights:R1	(R-R1)/R (%)
Case 1	1.0	693.74	694.01	-0.039
	2.0	251.62	251.80	-0.072
	3.0	84.56	84.62	-0.071
	4.0	37.64	37.67	-0.080
	5.0	25.32	25.34	-0.079
Case 2	2.0	123.33	123.33	0.000
	4.0	189.99	189.99	0.000
	6.0	258.93	258.99	-0.023
	8.0	320.27	320.35	-0.025
	10.0	374.13	374.21	-0.021
Case 3	2.0	102.26	102.26	0.000
	4.0	113.07	113.07	0.000
	6.0	129.77	129.77	0.000
	8.0	147.52	147.52	0.000
	10.0	163.95	163.95	0.000

Table 4.5 - Error of calculated Wenner Four Probe Data

Where.

Case 1 : $\rho_1 = 1000\Omega m$, $\rho_2 = 20\Omega m$, $h = 1.0m$

Case 2: $\rho_1 = 100\Omega m$, $\rho_2 = 1000\Omega m$, $h = 2.5m$

Case 3: $\rho_1 = 100\Omega m$, $\rho_2 = 300\Omega m$, $h = 5.0m$

4.4.2 Network Structure for 1D interpretation

Two Neural Networks are proposed in the inversion procedure (Figure 4.14). First Network will identify the curve type and will pass on the inputs to the second network to determine the 1D parameters. Figureure 4.13 shows the general Network structure used for inversion.
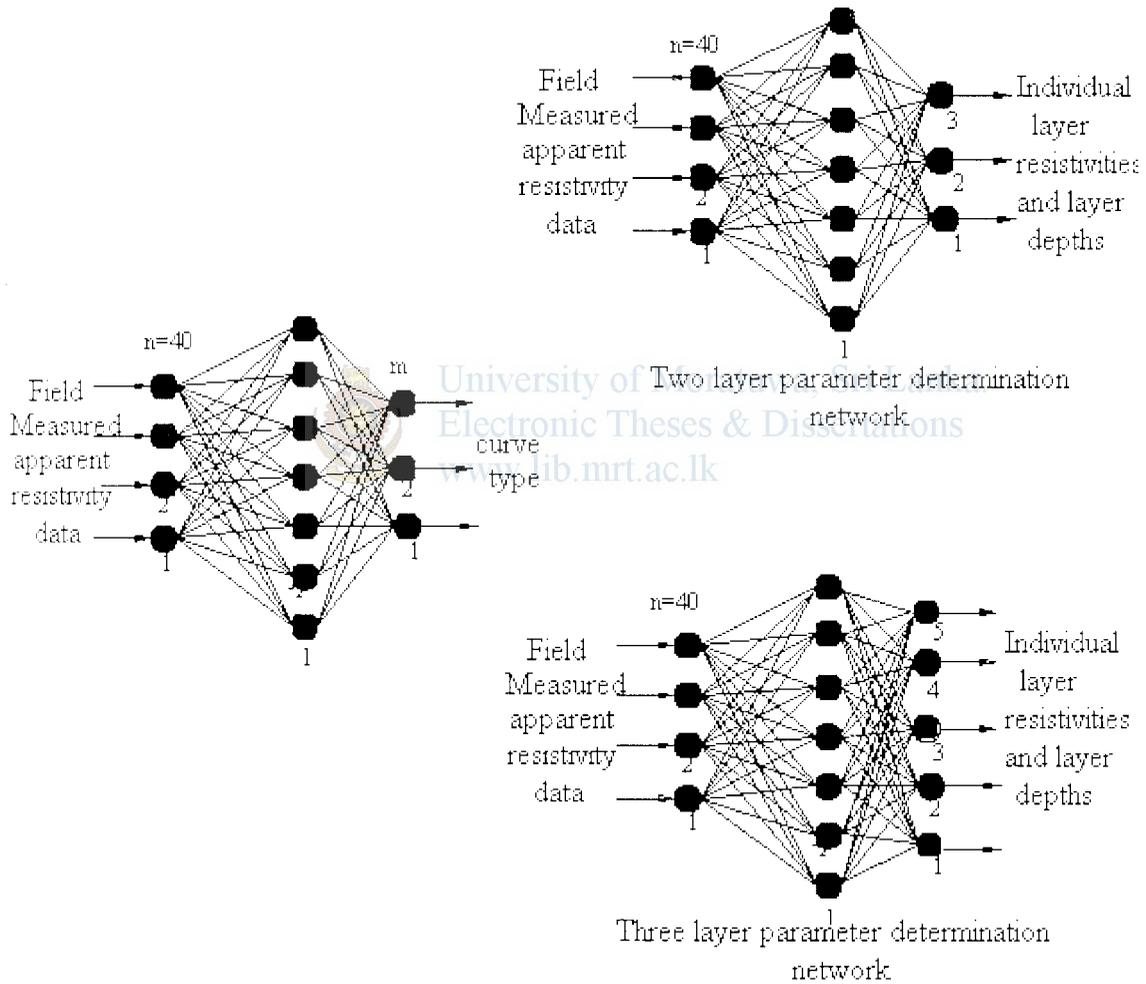
Figure 4.13 - Proposed Neural Network Structure

4.4.3 Inputs and outputs to train the Network (The Database)

The synthetically generated data for different curve types are used as the training data for the Neural Network. 900 examples of apparent resistivity curves are generated at 40 electrode spacing (a) of the Wenner array ranging from 0.001m to 390m in

successive 10m steps. Thus n of Figure 3.2 is set to 40. An example three layer curve with the 40 sampling points is shown in Figure 4.14.

Apparent Resistivity Vs Electrode Spacing
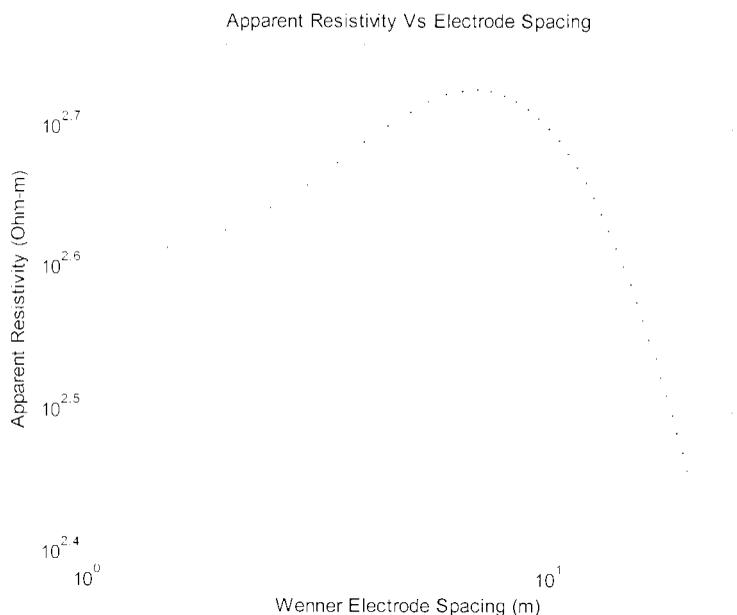
Figure 4.14 - sampling points of a three layer synthetically generated apparent resistivity curve.

$$\rho_1 = 400\Omega m, \rho_2 = 1000\Omega m, \rho_3 = 100\Omega m, h_1 = 3m, h_2 = 5m$$

The database includes 150 examples for each two layer and three layer curve types, with different resistivities and thicknesses .A 600 example training set and a 300 example validation set is separated.

The training set is used to train the network and the validation set is used as a checking data set which is used to monitor the over fitting of the network to the training data. A separate Testing set of 150 test sets (previously unseen by the network during training) generated on the same sampling strategy was used to evaluate the performance of the network.

Six curve types will be indentified by the curve identification network. The curve identification network will act as a classifier, therefore 6 output neurons are selected, i.e. m of Figure 3.2 is set to 6. Here a single neuron will switch to give a '1' output and the others a '0' output. Then, none zero output will tell the curve type.

The model parameter determination networks will give resistivities and thicknesses as outputs. The two layer model parameter optimization network has 3 output neurons while the three layer model parameter determination network has 5 output neurons.

5.1 Introduction

In general resistivity methods can be applied for studying variations of resistivity with depth (depth sounding methods) or for studying lateral changes in resistivity (horizontal profiling methods) as long as the units have a resistivity contrast. Often this is connected to rock porosity and fraction of water saturation of the pore spaces.

The electrical resistivity method is one of the most useful techniques in groundwater hydrology exploration because the resistivity of a rock is very sensitive to its water content. In turn, the resistivity of water is very sensitive to its ionic content. Other applications include studies on Water table depth, Groundwater quality, Aquifer exploration, mineral Exploration, Detection of cavities, Waste site exploration and General stratigraphic mapping.

In the context of Electrical Engineering Soil Resistivity studies have become utmost important in the design of Earthing or Grounding Systems. This chapter discusses about the practical considerations on Earthing and the impact of a Multi layer soil on the Earth Electrode Resistance.

5.2 Requirements of an Earthing System

Earthing or Grounding may be described as a system of electrical connections to the general mass of earth. This system of electrical connections consists of components of an electrical system and metal works associated with equipment, apparatus and appliances. Earth is a conductor covered with the resistive material, soil. The purpose of grounding is to provide direct path for the fault currents to the soil while maintaining the step and touch voltages at acceptable values, i.e. for limiting potential with respect to the general mass of earth in order to ensure safety.

A good grounding system is important for the protection of an overall system facility. From a good earthing system we anticipate on Protection of buildings and installations against lightning, Safety of human and animal life by limiting touch and step voltages to safe values , Electromagnetic compatibility (EMC) i.e. limitation of electromagnetic

disturbances and Correct operation of the electricity supply network and to ensure good power quality.

All these functions are provided by a single earthing system that has to be designed to fulfill all the requirements. Some elements of an earthing system may be provided to fulfill a specific purpose, but are nevertheless part of one single earthing system. Standards require all earthing measures within an installation to be bonded together, forming one system. A complete grounding system might include only one earth electrode, an entire group of electrodes with a grounding grid, or anything in between and beyond.

There are many factors that determine how well a grounding system performs. Two major parameters are its resistance to remote earth and the resistivity of the local soil. Each of these values can be measured to help determine and design the best solution for the grounding system. The resistance to remote earth of the grounding system needs to be at a minimum in order to sustain its effectiveness. A few of the components that make up this resistance are the physical properties of the material used to make the electrode and conductor, all connections made, contact resistance between the electrode and the soil, and the soil resistivity.

In many of the applications of grounding, low earth resistance is essential to meet electrical safety standards. The intention of keeping the earth resistance low is to provide a path back to the supply of sufficiently low impedance to permit the protective devices to operate properly. The resistance figures also vary from industry to industry. Accepted industry standards stipulate that transmission substations should be designed not to exceed $1\,\Omega$. In distribution substations, the maximum recommended resistance is for $5\,\Omega$ or even $1\,\Omega$. In most cases, the buried grid system of any substation will provide the desired resistance. In light industrial or in telecommunication central offices, $5\,\Omega$ is often the accepted value. For lightning protection, the arrestors should be coupled with a maximum ground resistance of $1\,\Omega$.

5.3 Electrical properties of the earthing system

The electrical properties of earthing system depend essentially on two parameters: Earthing resistance and Configuration of the earth electrode. Earthing resistance determines the relation between earth voltage and the earth current value. The

79

configuration of the earth electrode determines the potential distribution on the earth surface, which occurs as a result of current flow in the earth. The potential distribution on the earth surface is an important consideration in assessing the degree of protection against electric shock because it determines the touch and step potentials.

5.3.1 Earthing resistance

This has two components: the Dissipation Resistance R_D, which is the resistance of the earth between the earth electrode and the reference earth and resistance R_L of the metal parts of the earth electrode and of the earthing conductor. The resistance R_L is usually much smaller than the dissipation resistance R_D. Thus, usually the earthing resistance is estimated to be equal to the dissipation resistance R_D.

Also In AC circuits one must consider essentially the impedance of an earthing Z_E, which is the impedance between the earthing system and the reference earth at a given operating frequency. The reactance of the earthing system is the reactance of the earthing conductor and of metal parts of the earth electrode. At low frequencies such as the 50Hz supply frequency and associated harmonics, reactance is usually negligible in comparison to earthing resistance, but must be taken into account for high frequencies such as lightning transients. Thus, for low frequencies, it is assumed that the earthing impedance Z_E is equal the dissipation Resistance R_D, which is in turn assumed to be approximately equal to the earthing resistance, R.

$$Z_E \approx R_D \approx R \tag{5.1}$$

The earthing resistance R, of an earth electrode depends on the earth resistivity ρ as well as the electrode geometry.

5.3.2 Electrode configuration

In order to achieve low values of Earth Resistance the current density flowing from the electrode metal to earth should be low, i.e. the volume of earth through which the current flows is as large as possible. Once the current flows from metal to earth it spreads out, reducing current density. If the electrode is physically small, e.g. a point, this effect is large, but is very much reduced for a plate where spreading is only

effective at the edges. This means that rod, pipe, or wire electrodes have a much lower dissipation resistance than, for example, a plate electrode with the same surface area. Moreover, it is well documented in literature that DC and AC induced corrosion increases with current density. Low current density extends electrode life.

5.3.2.1 Hemisphere type electrode
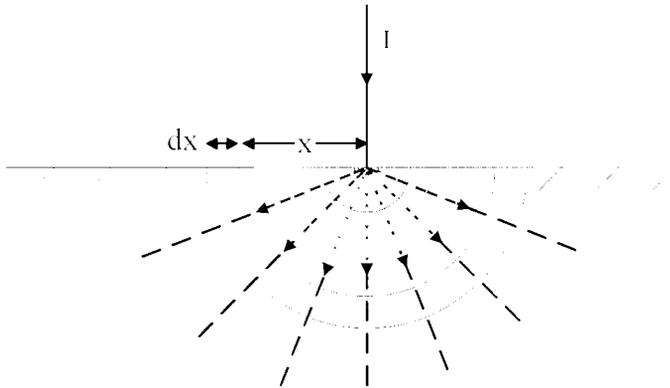
Figure 5.1 - Hemispherical Electrode –Cross Sectional elevation

The current entering into the electrode will flow radially and the potentials will gradually decrease as it goes outwards from the surface of the electrode. Now if we consider a hemispherical element of thickness dx at a distance x, the resistance of the elemental hemisphere dR is,

$$dR = \frac{\rho.dx}{2\pi x^2}$$
(5.2)

Where,

ρ - Resistivity of the homogeneous soil

Total electrode resistance is the resistance between the point of entry of current and the general mass of the earth. To obtain this integrate from the electrode surface to infinity,

$$R = \int \frac{\rho.dx}{2\pi x^2}$$

$$R = \frac{\rho}{2\pi r}$$
(5.3)

5.3.2.2 Plate type
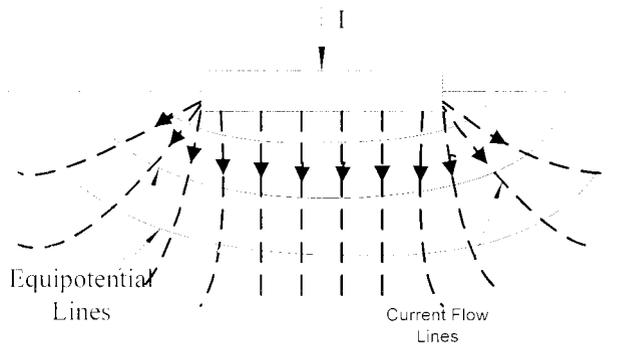
Figure 5.2 - Plate Electrode –Cross Sectional elevation

Consider a circular plate electrode of radius r, lying on the surfce of the earth of homogeneouse resistivity ρ. Making the assumtions that all currents coming out from below the plate are vertical and all current coming out from the edges go out radially from the edge, the resistance of an elemental area of thickness dx at distance x is given by,

$$dR = \frac{\rho.dx}{\pi(\pi rx + 2x^2 + r^2)} \tag{5.4}$$

Thus to obtain the total Electrode Resistance,

$$R = \int_{0}^{\infty} \frac{\rho}{2\pi r}\left[\frac{1.4628}{x+0.4436r} - \frac{1.4628}{x+1.1272r}\right]dx$$

$$= \left[\frac{\rho}{4.295r}\ln\frac{x+0.4436r}{x+1.1272r}\right]_{0}^{\infty} = \frac{\rho}{4.295r}\ln\frac{1.1272}{0.4436}$$

$$= \frac{\rho}{4.6r} \tag{5.5}$$

Let's consider the area of the plate to be A. Now $A = \pi r^2$,

$$r = \sqrt{\frac{A}{\pi}} \tag{5.6}$$

Therefore substituting (5.6) in (5.5),

$$R = \frac{\rho}{4.6} \sqrt{\frac{\pi}{A}}$$
(5.7)

Since approximations are used in the calculation, it would have yielded a higher value than the answer from equation (5.7). So, the following equation is conveniently used as the Electrode Resistance of a circular plate.

$$R = \frac{\rho}{4} \sqrt{\frac{\pi}{A}}$$
(5.8)

5.3.2.3 Rod/pipe type electrode
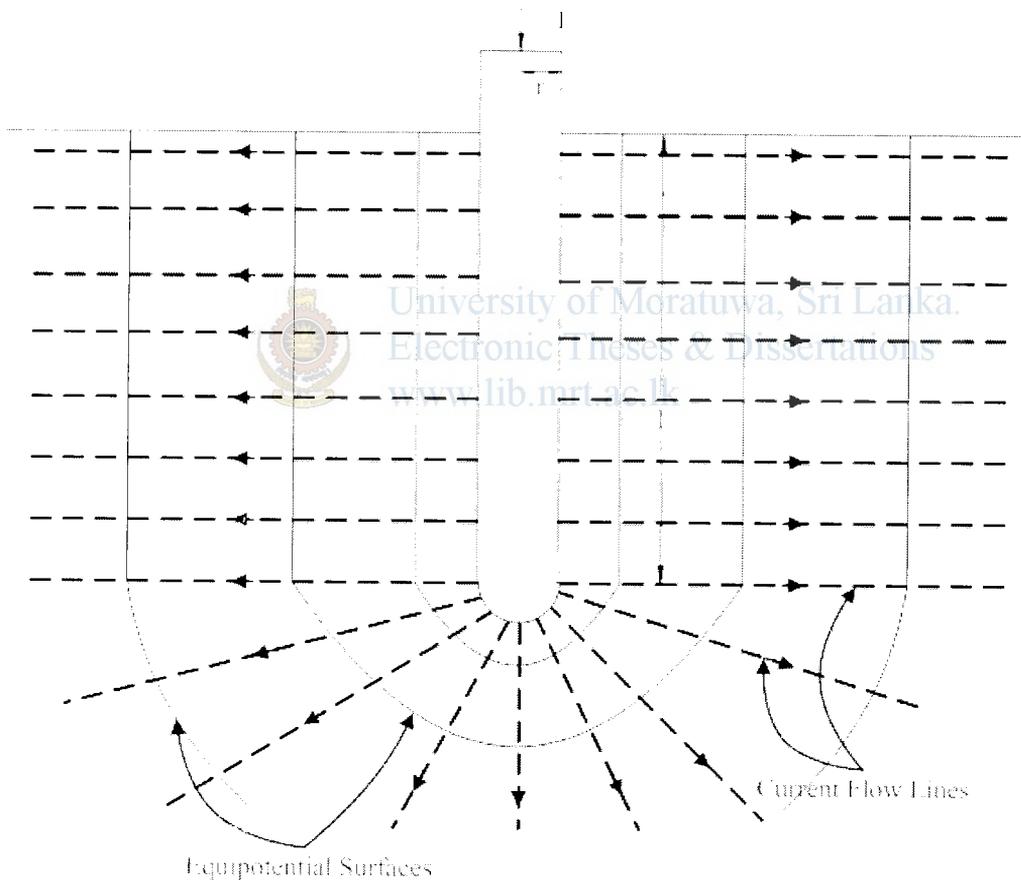
Figure 5.3 - Rod Electrode –Cross Sectional elevation

Let's consider a rod electrode of radius r and length l. Let's assume that the current flow outwards from the vertical section is horizontal and from the lower hemispherical end is radial outwards. Consider an elemental area at distance x , now the resistance of the elemental area is,

$$dR = \frac{\rho.dx}{2\pi xl + 2\pi x^2} \tag{5.9}$$

Total resistance of the Rod Electrode is,

$$R = \int_r^l \frac{\rho}{2\pi l}\left(\frac{1}{x(x+l)}\right)dx$$

$$= \left[\frac{\rho}{2\pi l}\ln\frac{x}{x+l}\right]_r^l$$

$$R = \frac{\rho}{2\pi l}\ln\frac{r+l}{r} \tag{5.10}$$

Generally $l \gg r$ so,

$$R = \frac{\rho}{2\pi l}\ln\frac{l}{r} \tag{5.11}$$

The above equation (5.11) for the Resistance of a Rod Electrode is given in BS7430 as follows,

$$R = \frac{\rho}{2\pi l}\left[\ln\left(\frac{8L}{d}\right) - 1\right] \tag{5.12}$$

Where,

L - Buried Length of the Electrode in m

d - Diameter of the Electrode in m

The earth resistance depends significantly on how deep the electrode is sunk in the ground. This is because the moisture content is higher and more stable for deeper ground layers than for shallow layers. Layers near the surface are influenced more by seasonal and short-term weather variations and are subject to freezing.

The most versatile type of earth electrode is the driven rod. On sites where soil resistivity is high, the use of deep driven rods to lower the resistance is one option. Figure 5.4 shows for a rod earth electrode how the earthing resistance reduces considerably as the depth of a rod electrode increases. However, it is not always possible to place electrodes at the preferred depth for geological reasons, for example,

where there are rocks or obstructions close to the surface or where the electrode system covers a large area.

Electrode Resistance Vs Buried Length
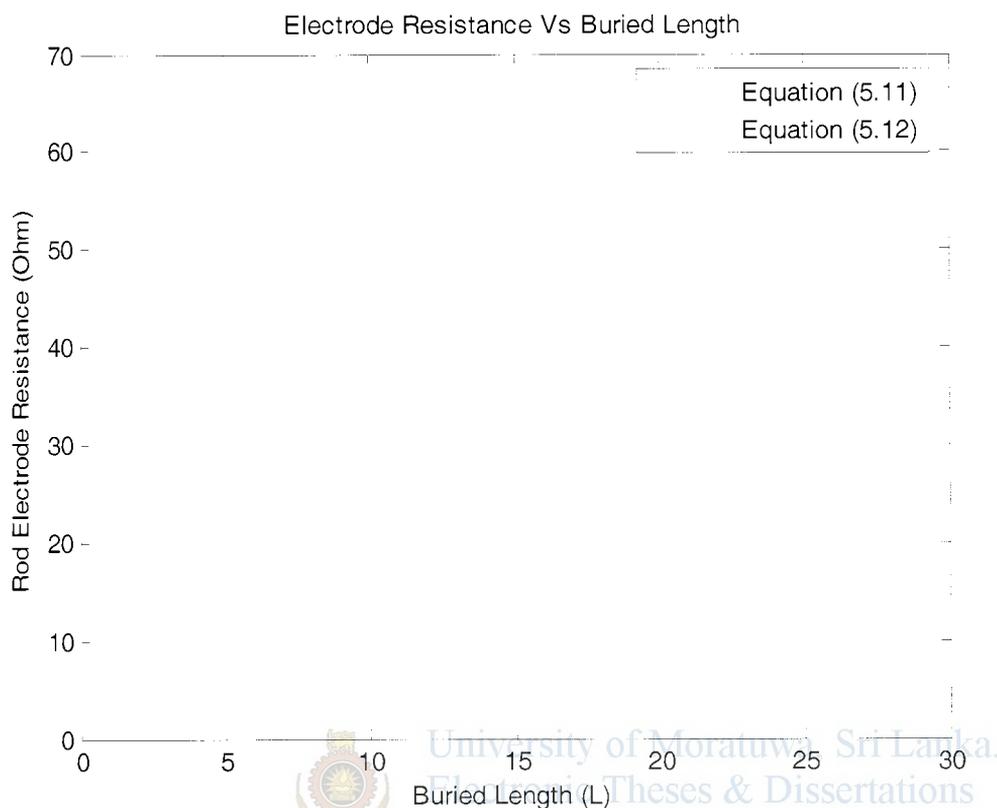
Figure 5.4 - Dissipation Resistance of a Rod Electrode as a function of its buried length ($\rho = 100\Omega m$ and $r = 25mm$)

(*Original is in color*)

The advantage of these is that they pass through soil layers of different conductivity and are particularly useful in places where the shallow layers have poor conductivity. In this way it is easy to obtain an expected electrode resistance as seen in Figure. 5.4. Another advantage of rod electrodes is that they can be installed in places where there is a limited surface area available to install the electrode. However, surface potential distribution of rod electrodes is unfavorable, so in practice a combination of rod and surface earth electrodes are also used, in order to obtain both a good resistance and desirable surface potential distribution.

5.3.2.3.1 Effective Resistance Area of a Rod electrode

The current flowing from the earth electrode goes through layers of soil immediately surrounding the electrode. Also the cross sectional area s of the soil layers nearest to the electrode is rather small and the soil is relatively a poor conductor of electricity.

Therefore, the effective resistance of the conductor is concentrated mainly in the first few meters of soil immediately surrounding the electrode. This fact can be illustrated as follows,

Using equation (5.11) the resistance R_x of the electrode up to a distance x from the electrode is,

$$R_x = \left[\frac{\rho}{2\pi l} \ln \frac{x}{x+l} \right]_r^x$$

$$R_x = \frac{\rho}{2\pi l} \ln \frac{x(r+l)}{r(x+l)} \tag{5.13}$$

Now lets consider a numeric example where $l = 2.5m$ and $r = 25mm$ and soil resistivity $\rho = 100\Omega m$, Substituting in equation (5.11) the total resistance of the electrode is,

$$R = \frac{100}{2\pi \times 2.5} \ln \frac{2.5}{0.025} = 29.3174\Omega$$

Using equation (5.13),

$$R_x = \frac{100}{2\pi \times 2.5} \ln \frac{x(2.525)}{0.025(x+2.5)}$$

$$R_x = \frac{100}{2\pi \times 2.5} \ln \frac{x(2.525)}{0.025(x+2.5)}$$

$$R_x = 29.3808 - 6.3662 \ln (x+2.5)/x \tag{5.14}$$

The resulting plot of R_x vs. x is shown in Figure 5.5. From Figure 5.5 it can be observed that 50% of the resistance is from just 0.28m, 75% in 1.14m, 90% in 4.15m, 95%in 9.21m and 99% in 43.4m. Increase in resistance is very slow after 90% value. Thus in general it is considered that the resistance of a rod electrode has a resistance area having a radius of approximately twice the length, i.e. for this particular example it is 5m's where the value is 91.4%. This is the reason why when an electrode is planted it should not be closer than 2 Or 3 times its length from other major earths.The area within this distance of the rod is the so-called effective resistance area.

Distance from Electrode,x Vs Resiatnce at diatance x

X: 4.152
Y: 26.38

X: 1.139
Y: 21.98

X: 0.2789
Y: 14.67

Earth Resistance at distance x, Rx (Ohms)

Distance from Electrode,x (m)
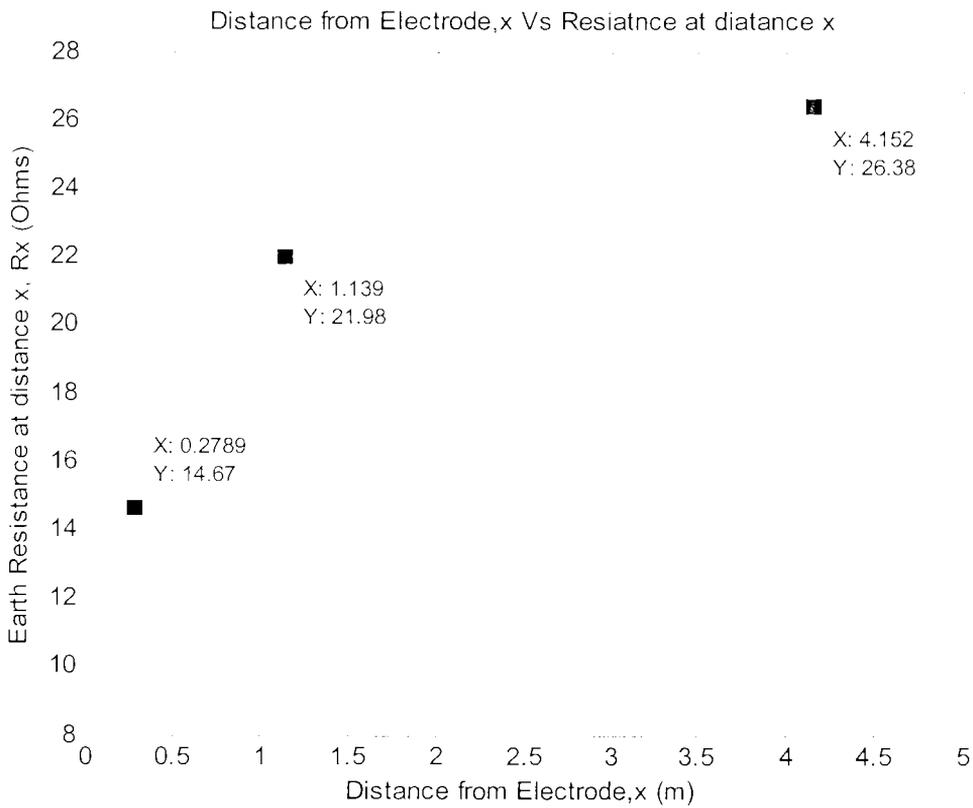
Figure 5.5 - Variation of Earth Resistance at distance *x* from the electrode

5.3.2.4 Slip or conductor type

Equipotential
lines

Current
flow lines

(a)

(b)
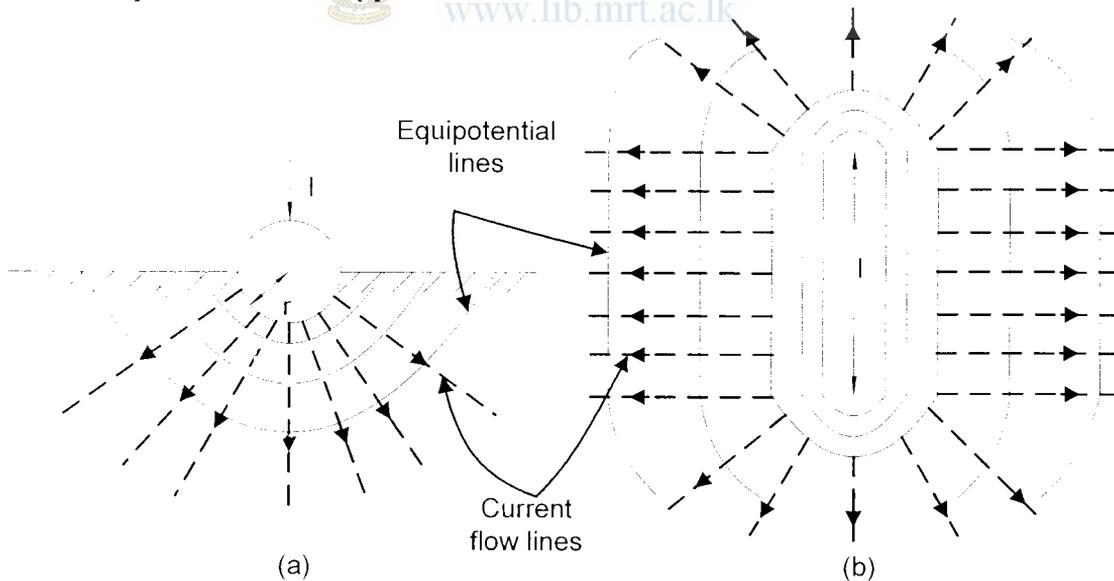
Figure 5.6 - Conductor Electrode (a) Cross Sectional elevation (b) Plan

Trench Electrodes, conductors buried horizontally under the surface of the ground, also make very good connections to earth. They are particularly effective when a

down-conductor is connected to a point in the middle of the trench electrode. These horizontal electrodes have special advantage where high resistivity soil has a shallow layer of low resistivity soil above it. The Strip Electrode is similar to a rod electrode of circular cross section buried horizontally such that a hemispherical cross section is below the soil (Figure 5.6).

Lets consider an elemental half cylinder with half hemispherical ends, at a distance x, below and thickness dx. Now the resistance of the elemental considered is,

$$dR = \frac{\rho.dx}{\pi xl + 2\pi x^2} \tag{5.15}$$

The total circular conductor Electrode Resistance is,

$$R = \frac{\rho}{\pi} \int_r^l \frac{dx}{x(2x+l)}$$

$$= \frac{\rho}{\pi l} \int_r^l \left[\frac{1}{x} - \frac{1}{x+l/2} \right] dx$$

$$= \left[\frac{\rho}{\pi l} \ln \frac{x}{x+l/2} \right]_r^l$$

$$R = \frac{\rho}{\pi l} \ln \frac{l+2r}{2r} \tag{5.16}$$

When $l \gg r$,

$$R = \frac{\rho}{\pi l} \ln \frac{l}{2r} \tag{5.17}$$

When the circular conductor of radius r is replaced by a strip of width μ, this becomes,

$$R = \frac{\rho}{\pi l} \ln \frac{l}{\mu} \tag{5.18}$$

If the tape is buried at a depth t, instead at surface,

$$R = \frac{\rho}{2\pi l} \ln \frac{2l^2}{\mu t} \tag{5.19}$$

5.3.2.5 Meshed electrodes

Another example of the use of conductors buried under the surface of the earth is the ground-grid mesh. These are constructed as a grid placed horizontally at shallow depth cable with exposed metal sheath or amour which behaves similarly to a strip-type earth electrode. Grid meshes are often used to complement rods or can be used separately when deep driven rods are impractical due to soil and terrain considerations.

Grid meshes are often used for the earthing in substations to create an equipotential platform and also to handle the high fault currents returning to the transformer neutrals. They are particularly useful when multiple injection points are required, at a substation for example. In this case a number of items will be connected to the grid at various locations; the mesh provides a good earth irrespective of the injection point of the fault current. Earthing resistance of buried grid meshes can be considerably lower than those implemented using vertical earth spikes. Increasing the area of the grid coverage can also significantly reduce the earth resistance.

5.3.2.6 Foundation earth electrodes

These are formed from conductive structural parts embedded in concrete foundation providing a large area contact with the earth.

5.4 Electrical properties of the ground

The calculation of the earthing resistance requires a good knowledge of the soil properties. The electrical properties of the ground are characterized by the earth resistivity ρ. Therefore the soil stratum is required to be analyzed to determine the soil Resistivity, at the design stage.

Soil resistivity has a direct effect on the resistance of the grounding system. The evaluation of the resistivity of the local soil can determine the best location, depth, and size of the electrodes in a grounding system, and can also be used for many other applications. As discussed in earlier chapters geological survey uses the soil resistivity to locate ore, clay, gravel, etc. beneath the earth's surface. Depth and thickness of bedrock can also be determined. The degree of corrosion of the local soil also can be

obtained from its resistivity value. Due to these many reasons, it is necessary to measure the resistivity of the local soil.

A large variation in the value of ρ is a problem. In many practical situations, a homogenous ground structure will be assumed with an average value of ρ, which must be estimated on the basis of soil analysis or by measurement. The determination of ρ is often a complicated task for the ground does not have a homogenous structure, but is formed of layers of different materials and the resistivity of a given type of ground varies widely (Table 5.1) and is very dependent on moisture content. Where no information is available about the value of ρ it is usually assumed $\rho = 100\Omega m$. However, as Table 5.1 indicates, the real value can be very different; one important point is that the current distribution in the soil layers used during measurement should simulate that for the final installation. Consequently, measurements must always be interpreted carefully. So acceptance testing of the final installation, together with an assessment of likely variations due to weather conditions and over lifetime, must be undertaken.

5.4.1 The Approximate resistivity values of common rock types

Material	Resistivity (Ωm)
Air	∞
Pyrite	0.3
Galena	0.002
Quartz	$4 \times 10^{10} - 2 \times 10^{14}$
Calcite	$1 \times 10^{12} - 1 \times 10^{13}$
Rock Salt	$30 - 1 \times 10^{13}$
Mica	$9 \times 10^{12} - 1 \times 10^{14}$
Granite	$100 - 1 \times 10^{6}$
Gabbro	$1 \times 10^{3} - 1 \times 10^{6}$
Basalt	$10 - 1 \times 10^{7}$
Limestones	$50 - 1 \times 10^{7}$
Sandstones	$1 - 1 \times 10^{8}$
Dolomite	$100 - 10000$
Sand	$1 - 1000$
Clay	$1 - 100$
Ground Water	0.5-300
Sea Water	0.2

Table 5.1 - Resistivities of Some materials
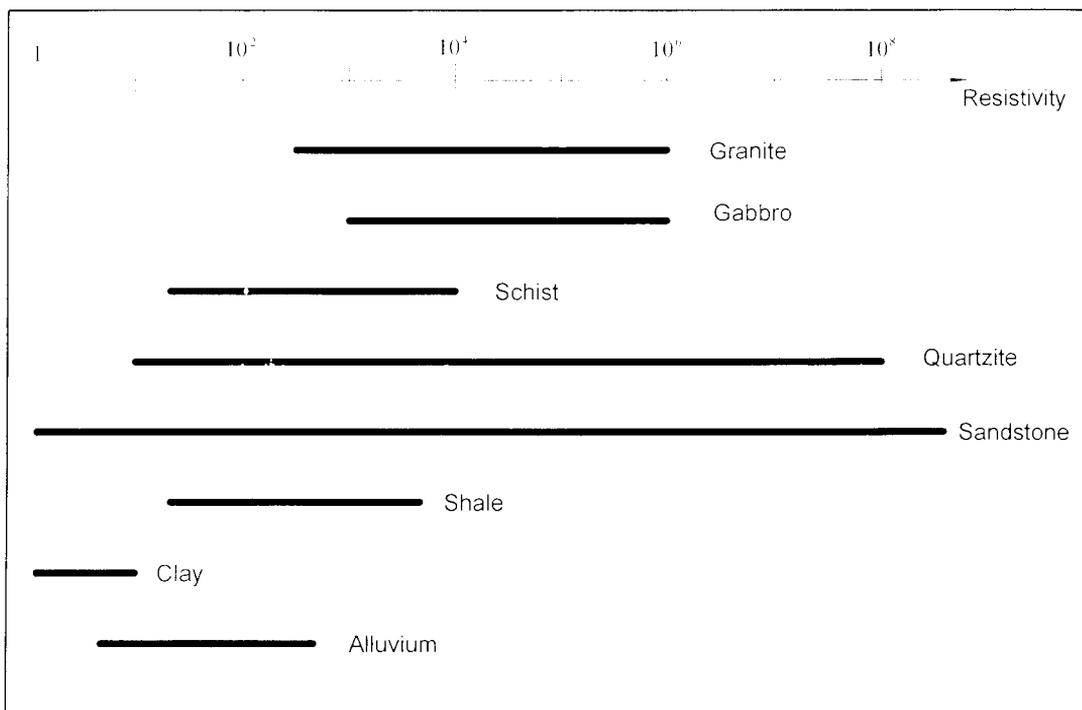
Figure 5.7 - Resistivities of some common rock types

Although some native metals and graphite conduct electricity, most rock-forming minerals are electrical insulators. Measured resistivities in Earth materials are primarily controlled by the movement of charged ions in pore fluids. Although water itself is not a good conductor of electricity, ground water generally contains dissolved compounds that greatly enhance its ability to conduct electricity. Hence, porosity and fluid saturation tend to dominate electrical resistivity measurements. In addition to pores, fractures within crystalline rock can lead to low resistivities if they are filled with fluids.

5.4.2 Principle factors effecting soil resistivity

5.4.2 1 Type of Soil

The soil composition can be clay, gravel, loam, rock, sand, shale, silt, stones, etc. In many locations, soil can be quite homogenous, while other locations may be mixtures of these soil types in varying proportions. As discussed in earlier chapters very often, the soil composition is in layers or strata.

5.4.2.2 Climate

Obviously, arid and good rainfall climates are at opposite extremes for conditions of soil resistivity.

5.4.2.3 Seasonal Conditions

The effects of heat, moisture, drought and frost can introduce wide variations in "normal" soil resistivity. Soil resistivity increases few percent with moisture content while soil temperatures below freezing greatly increase soil resistivity.
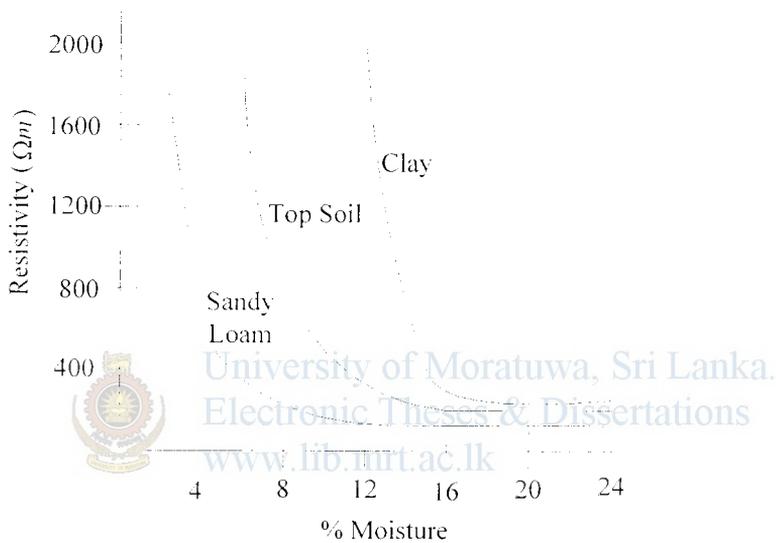
Figure 5.8 - Influence of moisture content

The moisture content can change over a wide range, depending on geographical location and weather conditions, from a low percentage for desert regions up to about 80% for swampy regions. Moisture content can be a significant factor in determining the resistivity of the local soil. Figure 5.8 shows the influence of the moisture content on the resistivity value. The drier the soil, the higher the resistivity. The soil resistivity remains relatively low (and constant) if the moisture content of the soil is greater than 15% (by weight,) and skyrockets for lower values of moisture content.

Also the effect of freezing is similar to that of drying, the resistivity increases significantly at higher freezing levels.

It should be noted that however the moisture alone is not the predominant factor in the low resistivity soils. If the water is relatively pure, it will be high resistivity unless the soil contain sufficient natural element to form a conducting electrolyte, the abundance

92

of water will not provide the soil with adequate conductivity. The value of high moisture content is advantageous in increasing the solubility of existing natural elements in the soil, and in providing for the solubility of ingredients which may be artificially introduced to improve the soil conductivity.
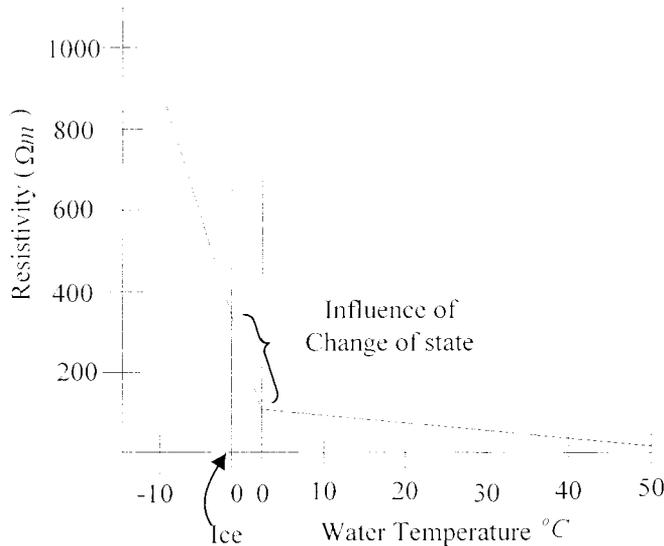
Figure 5.9 - Influence of temperature

Figure 5.9 shows the influence of varying temperature on the soil resistivity value. The temperature coefficient of resistivity for soil is negative, but is negligible for temperature above freezing point. At about $20^\circ C$, the resistivity change is about 9% per $1^\circ C$. With temperature, the colder the soil is, the higher the resistivity. Due to seasonal changes where the temperature can change drastically for a particular area, the resistivity of the local soil can also change drastically

5.4.2.4 Other Factors

Grain size and distribution, and closeness of packing are also contributory factors since they have much to do with retention of soil moisture, as well as providing good conditions for a closely packed soil in good contact with the earth rod.

Another significant factor in the determination of soil resistivity is the content of minerals, such as salts or other chemicals dissolved in the contained water. For values of 1% (by weight) salt content, the soil resistivity remains low (and constant,) and skyrockets for lower values of salt content.

93

Many of these factors (moisture content, mineral content, compactness, and temperature,) of the local soil can change during the life of the grounding system, and therefore change the resistance to remote earth of that grounding system. For these reasons the calculations of earth resistance and the planning of electrodes can be performed up to a limited level of accuracy.

5.5 Surface potential distribution

Earthing voltage, as well as distribution of the earth surface potential during the current flow in the earthing system, is important parameters for protection against electric shock. Earthing voltage (V_E), is equal to the earthing potential (assuming that the potential of the reference earth is equal zero). Using equation (5.10), the earthing potential can be described as follows,

$$V_E = I_E R_E = \frac{\rho I_E}{2\pi l} \ln \frac{r+l}{r} \tag{5.20}$$

Where,
I_E - Earth Current

Under fault conditions, the earth electrode is raised to a potential with respect to the general mass of earth. This results in the existence of voltages in the soil around the electrode that may be injurious to telephone and pilot cables, whose cores are substantially at earth potential, owing to the voltage to which the sheath of such cables are raised . This happens mainly in connection with large electrode systems as at power stations and sub stations.

The voltage gradient at the surface of ground may also constitute a danger to life, specially where the cattle are concerned. This occurs principally with pole mounted sub stations with low voltage systems.

5.5.1 Surface Potential Distribution due to a Rod Electrode buried in a homogeneous medium

The potential of any point located at distance x from the middle of earth electrode, in which earth current I_E flows, can be formulated with the following equation using starting with the equation (2.13) and equation (2.14).

94

Since it is assumed that the current flows outwards from the vertical section is horizontal and from the lower hemispherical end is radial outwards the total current I_E crossing a cylindrical plus hemi- spherical surface is given by,

$$I_E = \left(2\pi x l + 2\pi x^2\right) J \tag{5.21}$$

Thus from (2.14),

$$\frac{A}{x^2} = \rho J = \frac{I_E \rho}{\left(2\pi x l + 2\pi x^2\right)} = \frac{I_E \rho}{2\pi x\left(l + x\right)} \tag{5.22}$$

Therefore,

$$A = -\frac{\rho I_E x}{2\pi(l + x)} \tag{5.23}$$

Hence from (2.13),

$$V = \frac{\rho I_E}{2\pi(x + l)} \tag{5.24}$$

Which is the voltage at a distance x due to current flowing in the center of a rod electrode buried to a distance L from the surface.

Following is an illustration of the surface potential distribution due to a current flowing in a rod type electrode. Figure 5.10 shows a rod type electrode embedded in a homogeneous ground.

With Figure 5.10 it is possible for us to calculate the step and touch potentials due to certain earth fault condition to evaluate the degree of expected shock at a specified distance from the electrode. Step and touch voltage situations arise when it is possible for a person to make simultaneous contact with a part of an electrical system which is not live under normal conditions but has become live due to the passage of a fault current, and another conductive part which is at a different potential. This situation is described as 'indirect contact' with live parts.
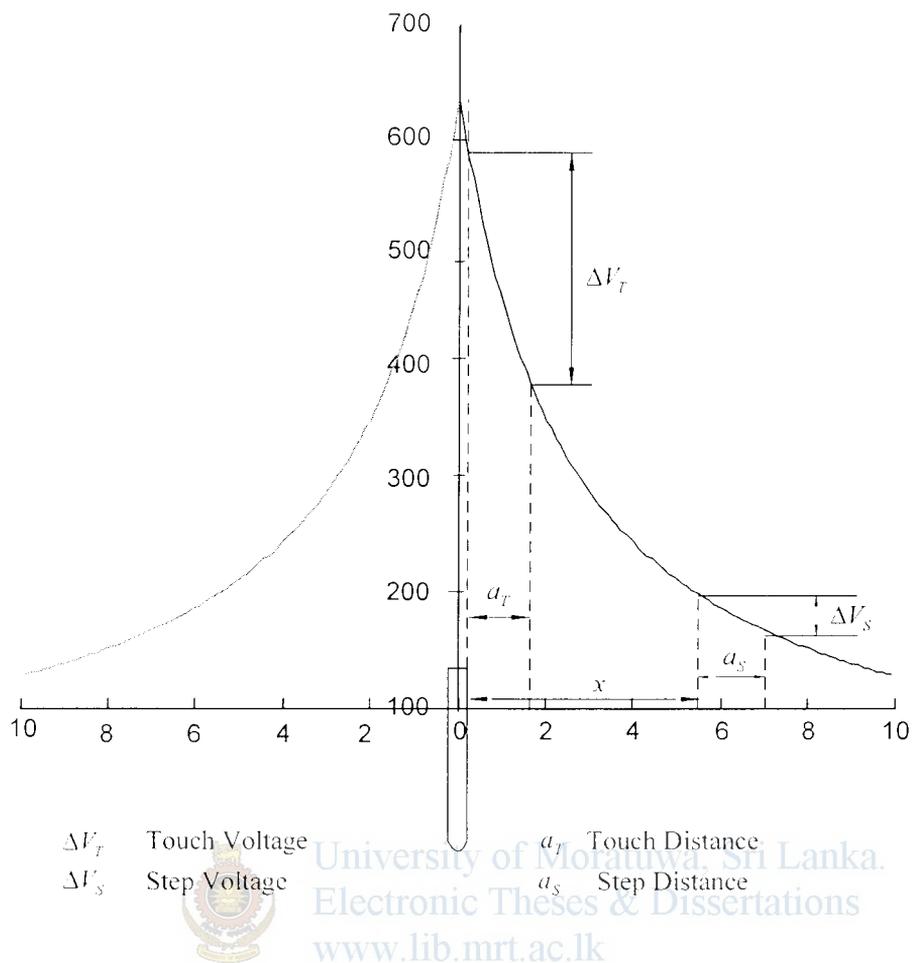
Figure 5.10 - Notational representation of Surface Potential distribution of a rod electrode buried in a homogeneous medium.

$$(l = 2.5m, r = 25mm, \rho = 100\Omega m, I_E = 100A)$$

A common step and touch voltage situation arises in and around substations under earth fault conditions wherein the earth fault current flows through the earth electrode and grid system, and it is possible for a person to make simultaneous contact with two parts which are at a different potential due the passage of the earth fault current.

5.5.2 Touch Potential

Touch potential is the voltage between the energized object and the feet of a person in contact with the object, , i.e. the voltage between a palm and a foot of a person who is just touching the earth electrode or metal parts connected to it (Figure 5.10). It is equal to the difference in voltage between the object (which is at a distance of 0m's) and a point 1m distance away. It should be noted that the touch potential could be

nearly the full voltage across the grounded object if that object is grounded at a point remote from the place where the person is in contact with it.

5.5.3 Step Potential

Step potential is the voltage between the feet of a person standing near an energized grounded object. It is equal to the difference in voltage, given by the voltage distribution curve, between two points at $1m$ distances from the "electrode" (Figure 5.10). A person could be at risk of injury during a fault simply by standing near the grounding point.

5.6 Methods of Earth Electrode Resistance Measurements of a single Electrode

When an electrode system has been designed and installed, it is usually necessary to measure and confirm the earth resistance between the electrode and reference earth. Grounding systems should be tested upon installation and then annually during their service life. The initial testing establishes a performance baseline, confirms that the design specification is met and validates the quality of the installation. Annual testing ensures the continued integrity of the system and provides protection against degradation prior to equipment damage or performance problems.

The most commonly used method of measuring the earth resistance of an earth electrode is the 3-point measuring technique. Other more complex methods, such as the *Slope Method* or the *Four Pole Method*, have been developed to overcome specific problems associated with this simpler procedure, mainly for measurements of the resistance of large earthing systems or at sites where space for locating the test electrodes is restricted.

Regardless of the measurement method employed, it should be remembered that the measurement of earth resistance is as much an art as it is a science, and resistance measurements can be affected by many parameters, some of which may be difficult to quantify. As such, it is best to take a number of separate readings and average them, rather than rely on the results of a single measurement.

5.6.1 Fall of Potential Method

The 3-point method or the Fall of Potential method is the most recognized method for measuring the resistance to earth of a grounding system, and is best suited to small

systems that don't cover a wide area. It is simple to carry out and requires a minimal amount of calculation to obtain a result. This method is generally not suited to large earthing installations, as the stake separations needed to ensure an accurate measurement can be excessive, requiring the use of very long test leads.

This method comprises the Earth Electrode to be measured and two other electrically independent test electrodes, usually labeled P (Potential) and C (Current) (Figure 5.11). An alternating current (I) is passed through the outer electrode C and the voltage is measured, by means of an inner electrode P, at some intermediary point between them. The Earth Resistance is simply calculated using Ohm's Law; $R_E = V/I$.
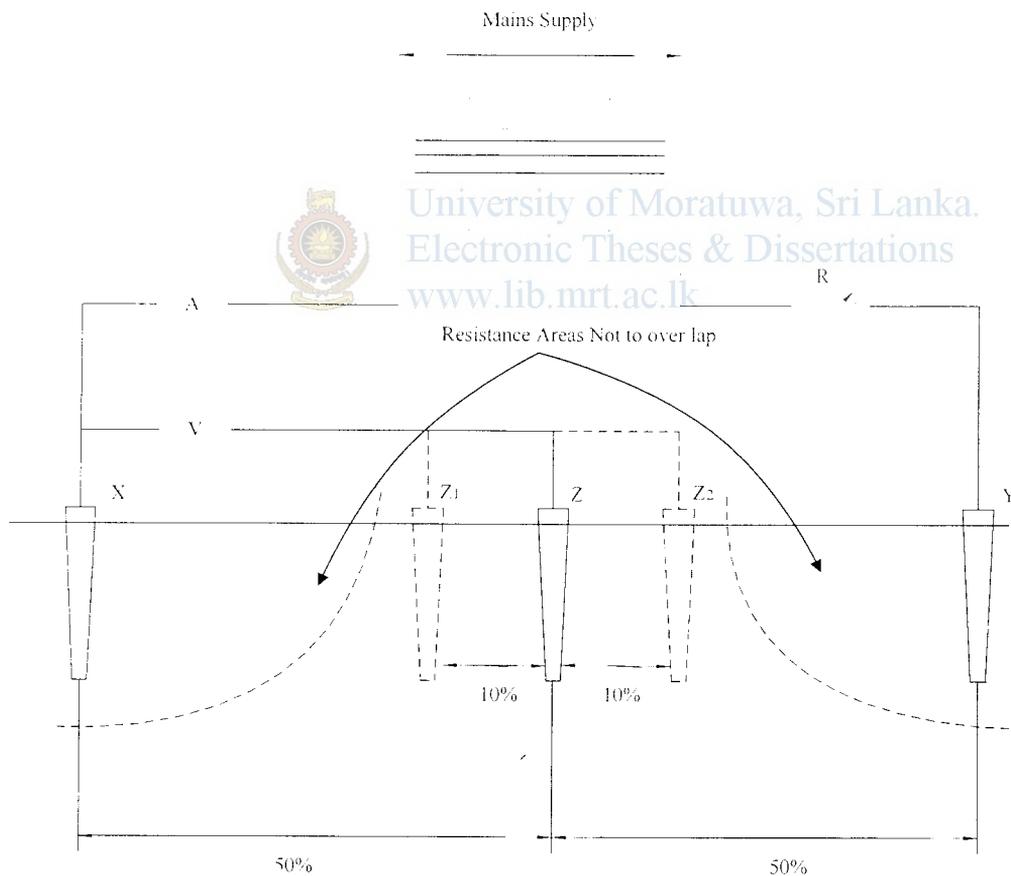
Figure 5.11 - 3-Point Method of Earth Resistance Measurement

When performing a measurement, the aim is to position the auxiliary test electrode C far enough away from the earth electrode under test so that the auxiliary test electrode P will lie outside the effective resistance areas of both the earth system and the other

test electrode (Figure 5.11). If the current test electrode C is too close, the resistance areas will overlap and there will be a steep variation in the measured resistance as the voltage test electrode is moved (Figure 5.12(b)). If the current test electrode is correctly positioned, there will be a 'flat' (or very nearly so) resistance area somewhere in between it and the earth electrode (Figure 5.12(a)).
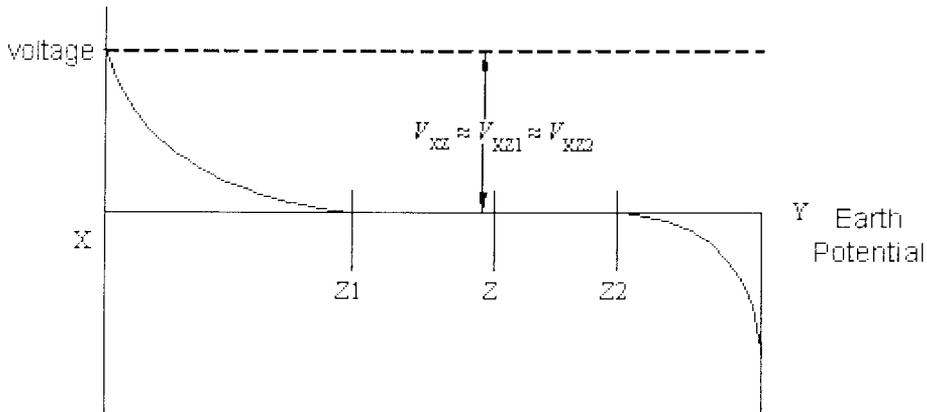
(a)
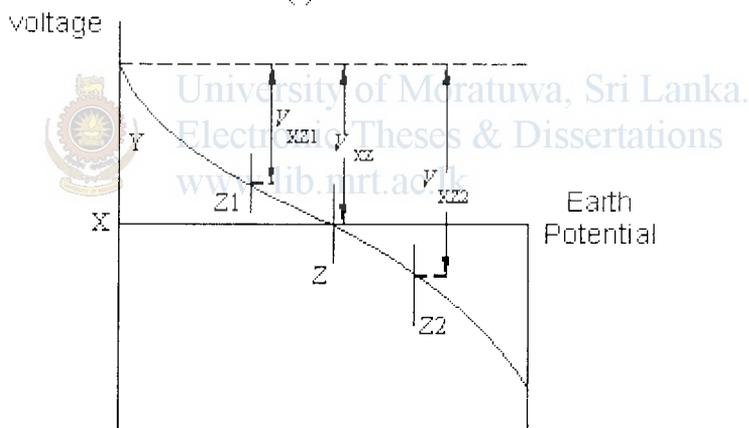
(b)

Figure 5.12 - (a) Successful plot due to correct spacing (b) Effect of resistance area overlap due to insufficient spacing between earth electrode and current electrode

The Fall of Potential method incorporates a check to ensure that the test electrodes are indeed positioned far enough away for a correct reading to be obtained. It is advisable that this check be carried, as it is really the only way of ensuring a correct result. To perform a check on the resistance figure, two additional measurements should be made; the first with the voltage test electrode (P) moved 10% of the original voltage electrode-to-earth system separation *away* from its initial position, and the second

with it moved a distance of 10% closer than its original position, as shown in Figure 5.11.

If these two additional measurements are in agreement with the original measurement, within the required level of accuracy, then the test stakes have been correctly positioned and the DC resistance figure can be obtained by averaging the three results. However, if there is substantial disagreement amongst any of these results, then it is likely that the stakes have been incorrectly positioned, either by being too close to the earth system being tested, too close to one another or too close to other structures that are interfering with the results. The stakes should be repositioned at a larger separation distance or in a different direction and the three measurements repeated. This process should be repeated until a satisfactory result is achieved.

5.6.2 The 62% Method

The Fall of Potential method can be adapted slightly for use with medium sized earthing systems. Based on empirical data the ohmic value measured at 62% of the distance from the ground-under-test to the remote current probe, is taken as the system ground resistance. Therefore this adaptation is often referred to as the *62% Method*, as it involves positioning the inner test stake at 62% of the earth electrode-to-outer stake separation (recall that in the Fall-of-Potential method, this figure was 50%).

All the other requirements of test stake location - that they be in a straight line and be positioned away from other structures - remain valid. When using this method, it is also advisable to repeat the measurements with the inner test stake moved ±10% of the earth electrode-inner test stake separation distance, as before.

The main disadvantage with this method is that the theory on which it is based relies on the assumption that the underlying soil is homogeneous, which in practice is rarely the case. Thus, care should be taken in its use and a soil resistivity survey should always be carried out. Alternatively, one of the other methods should be employed.

5.6.3 Other Test Methods

Many other methods exist for taking earth resistance measurements. Many of these methods have been designed in an attempt to alleviate the necessity for excessive

electrode separations, when measuring large earth systems, or the requirement of having to know the electrical centre of the system.

5.6.3.1 The Slope Method

This method is suitable for use with large earthing systems, such as sub-station earths. It involves taking a number of resistance measurements at various earth systems to voltage electrode separations and then plotting a curve of the resistance variation between the earth and the current. From this graph, and from data obtained from tables, it is possible to calculate the theoretical optimum location for the voltage electrode and thus, from the resistance curve, calculate the true resistance.

The additional measurement and calculation effort tends to relegate this system to use with only very large or complex earthing systems.

5.6.3.2 The Star-Delta Method

This technique is well suited to use with large systems in built up areas or on rocky terrain, where it may be difficult to find suitable locations for the test electrodes, particularly over long distances in a straight line.

Three test electrodes, set up at the corners of an equilateral triangle with the earth system in the middle, are used and measurements are made of the total resistance between adjacent electrodes, and also between each electrode and the earthing system.

Using these results, a number of calculations are performed and a result can be obtained for the resistance of the earth system.

5.6.3.3 The Four Potential Method

This technique helps overcome some of the problems associated with the requirement for knowing electrical centre of the earthing systems being tested. The main draw back with the Four Potential method is that, like with the Fall of Potential method, it can require excessive electrode separation distances if the earthing system being measured is large.

This method is similar in set up to the standard Fall of Potential method and measurements are made with the voltage electrode at different positions and a set of equations are used to calculate the theoretical resistance of the system.

5.7 Limitations on calculating the Electrode Resistance

The calculation of earthing resistance is usually performed under the assumptions that the ground is boundless and of uniform structure with a given value of resistivity. It is possible to determine exact equations for earthing resistance but, in practice, their usefulness is very limited, especially in the case of complex and meshed earth electrodes where the mathematical relations become very complicated.

Furthermore, even a small inaccuracy in the value of the resistivity has a significant influence on the actual earthing resistance of meshed earth electrodes and it is often very difficult to determine the earth resistivity with the accuracy required. Because of this, the theoretical equations of earthing resistance derived in sections 5.3.2.1 - 5.3.2.4 usually used only for homogeneous earth structure. When it comes to the actual sub soil with a layered structure the Earth Resistance and the surface potential distribution will be effected due to the changes in current flow in the non-homogeneous media. Therefore it is essential to study the resistance of a rod electrode buried in a multi layer media since ultimately it can be more accurately estimated the depth of boring or the length of a rod electrode in a multi layer situation.

5.7.1 Surface Potential Distribution due to a Rod Electrodes buried in a Multi Layer Media.

Figure 5.13 shows a rod electrode driven in a multi layer earth. $I_1, I_2, ..., I_N$ are considered to be current sources in the respective layers, due to current I entering into the electrode.

The work presented in paper [37] gives theoretical formulas for calculating the electrode resistance and surface potential distribution. In order to present the equations here, I start with the potential at the earth surface due to individual current sources in the layered structure.

The potential V_1 due to current source, I_1 in the 1st Layer,

102

$$V_1 = \frac{\rho_1 I_1}{2\pi} \int_0^\infty \frac{\alpha_{N1} e^{-\lambda t} + \beta_{N1} e^{-2\lambda h_2} e^{\lambda t}}{\alpha_{N1} - \beta_{N1} e^{-2\lambda h_1}} J_0(\lambda x)\, d\lambda \qquad (5.25)$$
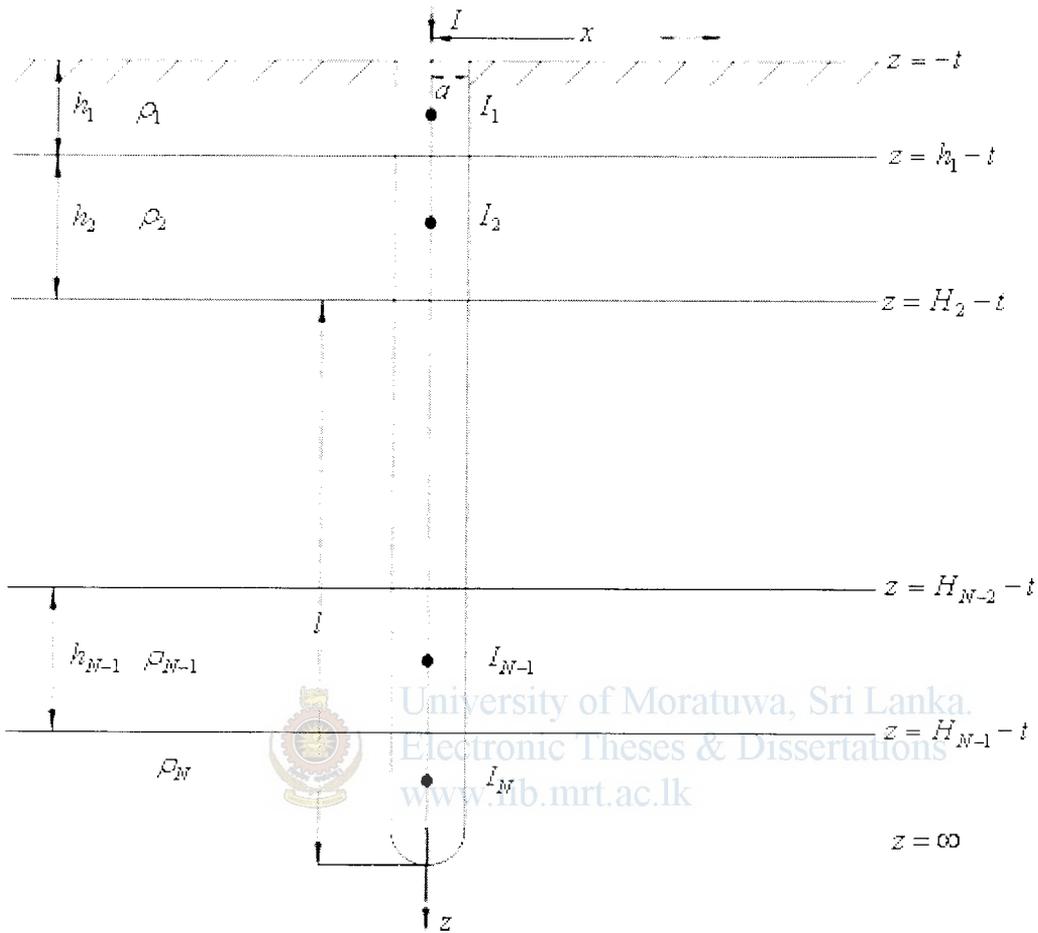
Figure 5.13 - Driven rod in multi layer earth

And the general equation of the potential V_N due to current source, I_N in the Nth Layer is given as,

$$V_N = \frac{\rho_N I_N}{2\pi} (1 - k_1)(1 - k_2)\ldots(1 - k_{N-1}) \int_0^\infty \frac{e^{-2\lambda t}}{\alpha_{N1} - \beta_{N1} e^{-2\lambda h_1}} J_0(\lambda x)\, d\lambda \qquad (5.26)$$

Where.

$$\alpha_{N1} = \alpha_{N2} + \beta_{N2} e^{-2\lambda h_2}$$

$$\alpha_{N2} = \alpha_{N3} + \beta_{N3} e^{-2\lambda h_3}$$

$$\vdots$$

$$\beta_{N1} = k_1 \alpha_{N2} + \beta_{N2} e^{-2\lambda h_2}$$

$$\beta_{N2} = k_1 \alpha_{N3} + \beta_{N3} e^{-2\lambda h_3}$$

103

Accordingly, the surface potential $V_N(x)$ at distance x from the center of the electrode, due to a deep driven rod in an N-layer earth structure is given as,

$$V_N(x) = \int_0^{h_1} V_1 dt + \int_0^{H_2} V_2 dt + \ldots + \int_{H_{N-1}}^{l} V_N dt \tag{5.27}$$

$$= \frac{\rho_1 I_1}{2\pi} \sum_{s=1}^{N} \left[\prod_{i=0}^{s-1} (1-k_i) \int_{H_{s-1}}^{H_s} \int_0^{\infty} \frac{\alpha_{Ns} e^{-\lambda t} + \beta_{Ns} e^{-2\lambda H_s} e^{\lambda t}}{\alpha_{N1} - \beta_{N1} e^{-2\lambda h_1}} J_0(\lambda x) d\lambda dt \right] \tag{5.28}$$

Where,

$$H_s = \sum_{i=1}^{s} h_i , H_0 = 0 , H_N = l$$

$$\alpha_{NN} = 1 , \beta_{NN} = 0$$

When it come to calculations the current I_1 should be determined. For that it is assumed that the current density is inversely proportional to the resistivity, ρ so that it can be considered that the current in each layer is uniform. Thus,

$$\rho_1 I_1 = \rho_2 I_2 = \ldots = \rho_N I_N \tag{5.29}$$

$$I_1 h_1 + I_2 h_2 + \ldots + I_N (l - h_1 - h_2 \ldots h_{N-1}) = I \tag{5.30}$$

Solving the above equations,

$$\rho_1 I_1 = \frac{I}{\sum_{i=1}^{N-1} \frac{h_i}{\rho_i} + \frac{l - H_{N-1}}{\rho_N}} \tag{5.31}$$

Where,

$$H_{N-1} = \sum_{i=1}^{N-1} h_i$$

I - Current Flowing in the rod electrode

ρ_N - Resistivity of layer N

Finally the general equation to calculate surface potential $V_N(x)$ at distance x from the center of the electrode, due to a deep driven rod in a N-layer earth structure is given as,

$$V_N(x) = \frac{1}{2\pi} \frac{I}{\sum_{i=1}^{N-1} \frac{h_i}{\rho_i} + \frac{l - H_{N-1}}{\rho_N}} \sum_{s=1}^{N} \left[\prod_{i=0}^{s-1} (1-k_i) \int_{H_{s-1}}^{H_s} \int_0^{\infty} \frac{\alpha_{Ns} e^{-\lambda t} + \beta_{Ns} e^{-2\lambda H_s} e^{\lambda t}}{\alpha_{N1} - \beta_{N1} e^{-2\lambda h_1}} J_0(\lambda x) d\lambda dt \right]$$

$$\tag{5.32}$$

104

5.7.2 Rod Electrode Resistance buried in a Multi layer Media

From [37] the earth resistance for a deep driven rod can be expressed as the ratio between the potential at the surface of the rod and the current flowing in the rod. That is,

$$R = \frac{V_N(a)}{I} \qquad (5.33)$$

Where,

a - radius of the rod

Therefore, from equation (5.32),

$$R = \frac{1}{2\pi} \frac{1}{\sum\limits_{i=1}^{N-1} \frac{h_i}{\rho_i} + \frac{l - H_{N-1}}{\rho_N}} \sum\limits_{s=1}^{N} \left[\prod\limits_{i=0}^{s-1} (1 - k_i) \int\limits_{H_{s-1}}^{H_s} \int\limits_{0}^{\infty} \frac{\alpha_{Ns} e^{-\lambda t} + \beta_{Ns} e^{-2\lambda H_s} e^{\lambda t}}{\alpha_{N1} - \beta_{N1} e^{-2\lambda h_1}} J_0(\lambda x) d\lambda dt \right] \qquad (5.34)$$

In order to evaluate the theoretical values for the Case Study in section 5.8 the equations (5.32) and (5.34) are used. The Mathematica 5.0 software is used for the calculations. To evaluate the compatibility of using Mathematica, the software output is compared with the results given in [37].

Table 5.2 compares the calculated results from equation (5.34) using the Mathematica 5.0 software and the results given in [37]. The results obtained from Mathematica calculations reveal close agreement with the results in [37] with maximum error in the order of 0.7%. Thus, through the use of the Software I proceeded to calculate the earth resistance for the earth electrode.

h/l	Tagg:R	Takahashi & Kawase :R1	Mathematica:R2	(R-R1)/R%	(R-R2)/R%
0.1	0.537661	0.536923	0.538217	0.137261211	-0.103410885
0.3	0.206955	0.206692	0.205311	0.127080766	0.794375589
0.5	0.130679	0.13052	0.130769	0.121672189	-0.06887105
0.7	0.09623	0.096116	0.0963525	0.118466175	-0.127299179
0.9	0.076474	0.076384	0.0765701	0.117687057	-0.125663624

Table 5.2 - Error of calculated Electrode Resistance

105

Chapter 6
Two Dimensional Resistivity Inversion

6.1 Introduction

1D interpretation will not always reveal the actual sub soil structure of a complex earth model. A discussed under section 4.3 one-dimensional (1D) interpretations have certain limitations; therefore in areas where the geological structures are approximately two-dimensional (2D), conventional 2D electrical imaging surveys have been successfully used.

Electrical inversion techniques have progressed from approximate inverse methods using a series of 1-D inversion steps [38] to 3-D inversion methods. The latter have been developed using linearized and backprojection methods and non-linear optimization. However 1D inversion results are very useful in constructing initial models for multidimensional interpretations. Therefore presently two-dimensional (2D) interpretations are widely used. Applications of resistivity 2D inversion techniques are vastly found in hydrogeology.

In the present work three 2D scenarios are experimented. They are,

CASE 1: Detection of an anomalous body of arbitrary size $100\,\Omega m$ in a homogeneous medium of $1000\ \Omega m$

CASE 2: Detection of an anomalous body of arbitrary resistivity in a homogeneous medium

CASE 3: Detection of an anomalous body of arbitrary resistivity in a three layer medium

6.2 Literature Survey

2D electrical surveys are usually carried out using multi electrode arrays and in order to be able to model complex 2D structures adequately a cell based inversion is commonly used. When dealing with a 2D problem though there is a 2D earth model the electrical field due to a point source is 3D. It has become a standard practice to

solve the 2D and 3D resistivity forward modeling problem using numerical methods by discretization of the domain of investigation [12] [39] [40].

In order to adequately resolve such complex soil structures with arbitrary resistivity distributions, the regularized least squares optimization is frequently used [12] for shulmberger [39] for pole pole data [40] in the 2D inversion of electrical imaging data. Simulated annealing applied for very low frequency resistivity data (VLF-R) inversion, described in [13] , Maximum entropy [14], Conjugate Gradient [15] and Neural Networks (NN) [11],[16] are other techniques used in the complex structure 2D inversions of geophysical data.

In the work presented in [12], the use of two different constraints of regularized least squares optimization is discussed. L_2 norm based least squares optimization minimizes the sum of squares of spatial changes in the model resistivity while the L_1 norm based optimization or blocky inversion minimizes the sum of absolute values of the spatial changes of model resistivity.

Furthermore, approximations to the equations describing the physics of the forward and inverse problem of electrical prospecting are frequently employed to make the inverse problem more manageable on current computers [41]. The approximations usually allow the conductivities to vary only by a 'small' amount around a background or starting model. This allows a low-contrast approximation to be used, thus speeding up the computation. However, it has also been shown that current computers are sufficiently fast to invert field scale data sets within a reasonable time while solving the full non-linear inversion problem using an accurate forward model [15].

A FORTRAN code for the 2D Schlumberger inversion based on the finite-element forward modeling and the nonlinear least-squares scheme is presented in [39]. The program utilizes two kinds of meshes: a model mesh and a finite-element calculation mesh. The model mesh describes the 2D resistivity section beneath a survey line by dividing it into many rectangular blocks. The calculation mesh is formed for each sounding station by substituting the resistivity value of each element from the corresponding block on the model mesh. A smoothing procedure is incorporated for

the spatial resistivity distribution in order to reduce the spurious resistivity features on the 2D model.

The smoothing procedure is referred to as Smoothness constrained inversion. The resultant cross section of the 2D model often shows a rough spatial resistivity distribution. i.e. the resistivity changes abruptly between two neighboring blocks and extraordinary low or high resistivities appear. Although the rough model could result numerical closely matching the observed data, it often does not seem to represent the true structure. In order to avoid these phenomena and to reduce the non-uniqueness of model, smoothing factor is introduced.

In the above works it has been shown that the quality of inversion greatly depends on the smoothing factor and the number of unknown resistivity blocks.

6.3 Forward Modeling of a 2D earth Structure

6.3.1 Acquiring Field Measurements for a 2D study
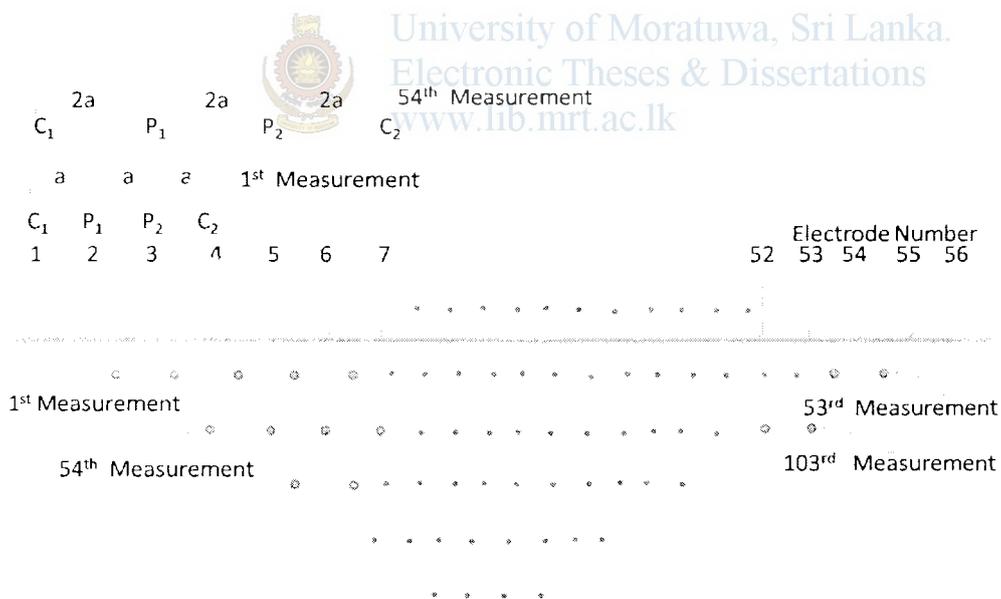
Figure 6.1 – Apparent resistivity pseudo section for 1m spaced 56 multi electrode array

The field measurements for a 2D study is obtained first by moving an electrode array laterally along the field line of interest with a fixed electrode spacing, secondly the array electrode intervals is increased in steps and the measurements are repeatedly taken. Presently automatic field measurement acquiring instruments are available,

which these instruments operate in a multi electrode mode to acquire a set of field measurements at once.

In the present study a 56 multi electrode Wenner array with 1m spacing is considered. The initial electrode spacing (a) is set to 1m and the spacing is increased in 1m steps. This adopts an apparent resistivity pseudo section with 495 field measurements (Figure 6.1).

6.3.2 Construction of a 2D structure

The 2D structure, after the inversion of the field data is interpreted with a cell or block based model. A model mesh is used for this purpose. This model mesh describes a 2D resistivity structure along the survey line by initially dividing the surface medium into many rectangular blocks. A constant resistivity will be assigned to the individual cells in the inverted 2D model.

The mesh discretization for the present study is given in Table 6.1. The block boundaries in the horizontal direction are at the position of an electrode. These results in a mesh with 385 mesh divisions or blocks (Figure 6.2).

Number of mesh divisions sets the minimum number of cells between the electrodes. If this is set to a larger value a finer mesh of higher accuracy will result for the inverted model whilst longer run time of the program. This is due to the number of output nodes in the output layer of the Neural network is set to the number of mesh divisions.

Thickness incremental factor is applicable to surface resistivity surveys where model resolution degrades with the depth. A large thickness incremental factor will reduce the runtime of training the Neural Network since this factor too decides on the number of mesh divisions. Therefore the number of mesh divisions and the thickness incremental factor are set such that to minimise the training time of the neural network.

Depth factor determines the depth of the inverted model The depth of the inverted model is determined by the maximum median depth times the depth factor. Median depth is a function of electrode spacing and array type.

109

Modeling Parameter	Parameter Value
No of mesh divisions (individual cell/block width)	1 m
Starting thickness of the cells/blocks	0.9 m
Thickness incremental factor	1.15
Depth Factor	1.1
Maximum Electrode spacing for field data (a_{max})	18.67 m
Median depth of measurements ($a_{max}/2$)	9.33 m
Depth of inverted model (Median depth × Depth Factor)	10.3 m

Table 6.1 – Model Mesh discretization factors
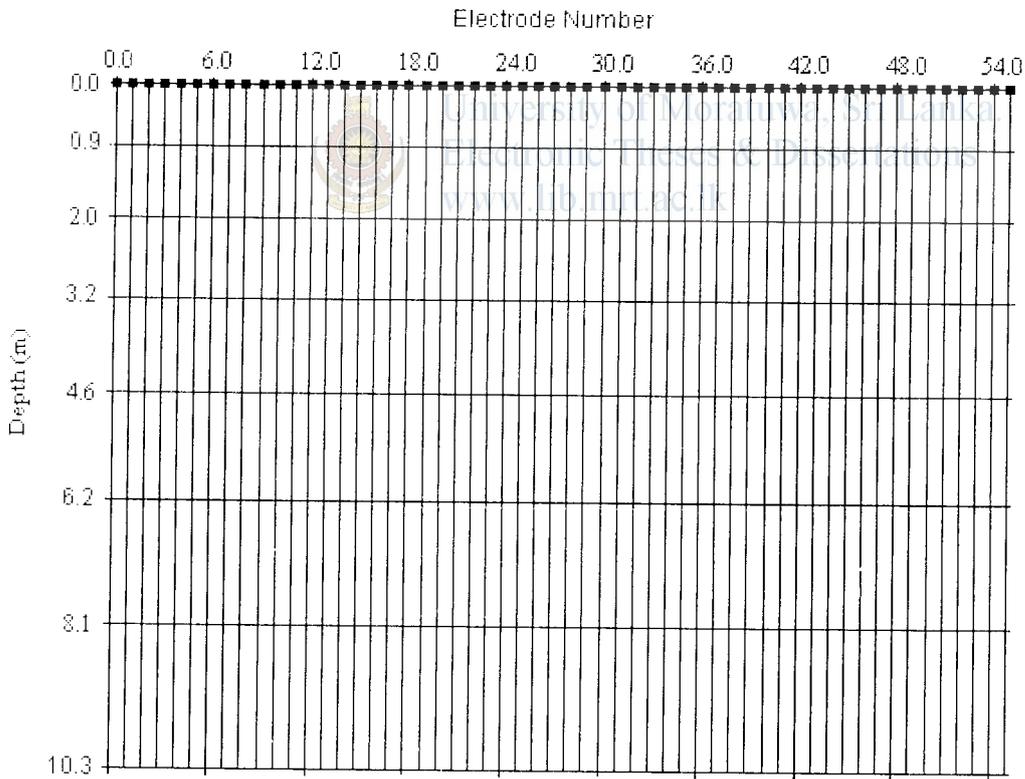
Figure 6.2 – Mesh discretization for the inverted sub surface model

In the present study the wenner array with 56 electrodes spaced at 1m is considered. Therefore,

Maximum electrode spacing (a_{max}) = 56/3 m

$$= 18.67\text{m}$$

Median depth for a wenner array ($a_{max}/2$) $= 18.67/2$ m

$$= 9.33 \text{ m}$$

Depth of inverted model

(Median depth × Depth Factor) $= 9.33 \times 1.1$

$$= 10.3 \text{ m}$$

6.3.3 Forward Response of 2D Earth Structure- Theoretical equations

Starting with equation (A.6) the dc response of a 2D earth is given by the Poisson's equation (now, σ is the conductivity of the medium in siemens per meter (S/m)),

$$-\sigma(x,z)\nabla^2 V(x,y,z) = J(x,y,z) \tag{6.1}$$

Where $\sigma(x,z)$ is the conductivity, $V(x,y,z)$ is the electrical potential and $J(x,y,z)$ is the current density.

For a 2D distribution the electrical conductivity in which resistivity varies along x and z axes for a point source $A(x,0,0)$ of current I at $z=0$, the DC response is the solution of (C.1).

By applying the Fourier transform to (C.1) with respect to y coordinate [39], we obtain,

$$\nabla \cdot \left[\sigma(x,y)\nabla \hat{V}(x,k_y,z)\right] + k_y^2 \sigma(x,z)\hat{V}(x,k_y,z) = \hat{I}(x,k_y,z) \tag{6.2}$$

where $^\wedge$ indicates the Fourier transform and k_y the Fourier transform variable. The equation (6.2) can be solved for 2D structures with finite element method or finite differences. We use the finite element method to compute the forward response for the Wenner array.

6.4 Synthetic data Generation

Synthetic data generation is done with a commercial software, *AGI EarthImager 2D Demo (Version 2.1.8(Build 507)), Copyright 2002-2006.* A 30 days demo version of this resistivity inversion software was downloaded from the website of the program developer, AGI Advanced Geosciences Inc, 2121 Geoscience Dr., Austin, TX 78726,

USA at the web address www.agiusa.com. This data is used for the Neural network training and testing.

Several commercial software's available for 2D resistivity inversion was examined and trial studies were carried out with them to choose the most reliable software package for the synthetic data generation for my present study. To generate the forward response for a given earth model it was required to supply the resistivity values of each cell in the 2D mesh, by coloring the individual cells.
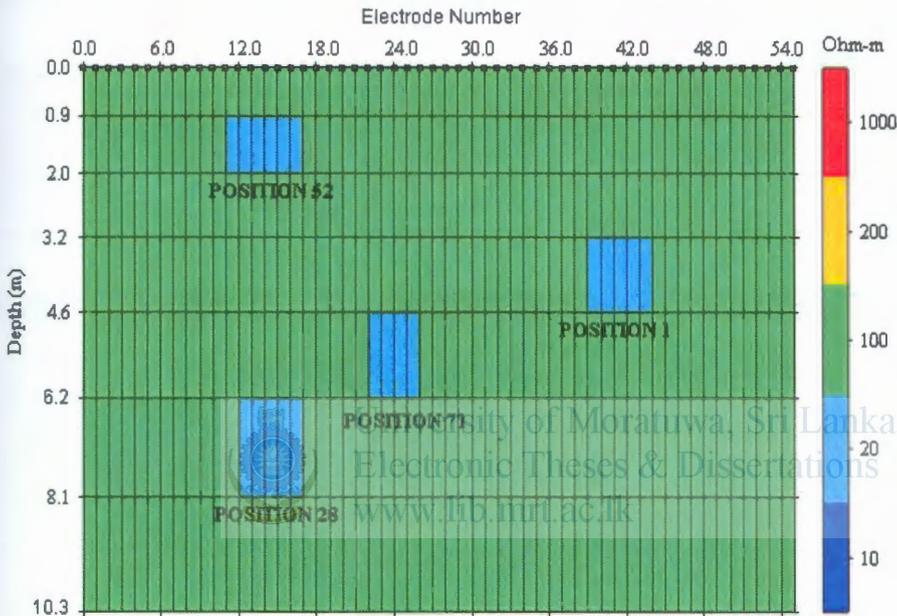
Figure 6.3 - Anomalous body assignments to generate synthetic data
(Original is in color)

For CASE 1 database generation was done by moving a 100 Ωm anomalous body of different size to different mesh positions as shown in Figure 6.3. The 130 number of entire body assignments used for the database are given in Appendix F. A constant resistivity is assigned to each of the blocks. With the commercial software the forward response is then generated and the results are saved in the '.stg' format (Figure 6.4). Then with a Visual Basic program the relevant data for the training is extracted from the .stg file and stored in .txt format as a text file.

For CASE 2 synthetic data generation was done by changing both the homogeneous medium resistivity and the anomalous body's resistivity. Homogeneous medium or the background resistivity is varied between 50 Ωm and 1000 Ωm . The anomalous body resistivity is varied between 100 Ωm and 10000 Ωm and it is moved to different mesh positions with variable sizes. CASE 2 mesh assignments included the 130 mesh

assignments given in Appendix F. The data is saved and processed similarly as in CASE 1. Table 6.2 gives the Resistivity Combinations used for CASE 2 training database preparation.
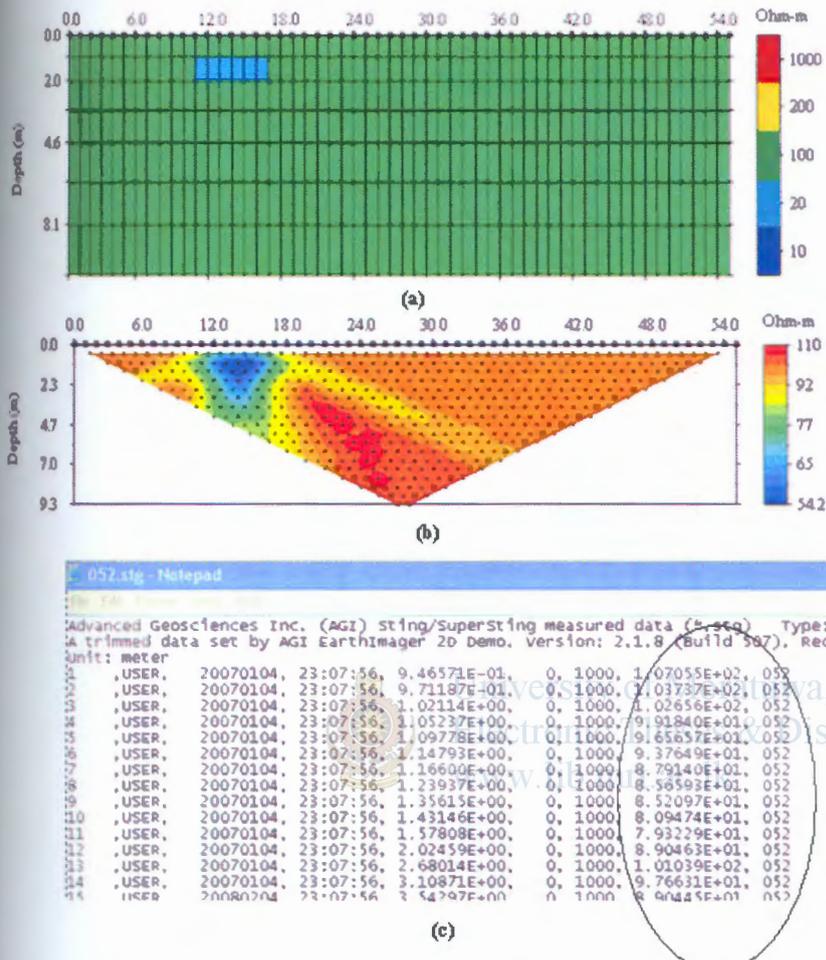
Figure 6.4- Synthetic data generating software outputs (a) Synthetic Model (b) Calculated apparent resistivity pseudo section (c) data saved in .stg format
(Original is in Color)

For CASE 3, i.e. Detection of an anomalous body of arbitrary resistivity in a three layer medium synthetic data generations is done by changing both the layer parameters (resistivities of the three layers and the height of the top two layers) and the anomalous body's resistivity. The layer resistivities are varied between $100\,\Omega m$ and $1000\,\Omega m$. Table 6.3 gives the resistivity combinations used for CASE 3 training database preparation

The top layer and the mid layer heights are varied between 0.9-6.2m and 1.2-5.8m respectively. The anomalous body resistivity is varied between $1000\,\Omega m$ and $5000\,\Omega m$ and it is moved to different mesh positions with variable sizes. The mesh

113

ssignments are as same as in Appendix F. Table gives the combinations of the layer resistivity values used. Appendix G shows the layer height combinations used for the database generation.

Background resistivity (Ωm)	Anomalous body's resistivity (Ωm)
50	1000
50	3000
100	1000
100	2500
100	7000
150	5000
200	8500
275	8000
300	10000
350	100
350	4000
400	1500
400	7000
450	3400
550	5000
575	100
600	2500
625	9500
650	7500
700	4250
800	100
825	2000
900	7500
950	3500
1000	100

Table 6.2 – Resistivity Combinations used for CASE 2 training database preparation

	ρ_1	ρ_2	ρ_3
1.	100	235	300
2.	300	350	500
3.	500	700	1000
4.	250	500	800
5.	425	650	900
6.	300	1000	725
7.	450	260	850
8.	600	320	975
9.	540	100	1000
10.	750	300	1000
11.	800	300	100
12.	1000	600	350
13.	700	400	100
14.	675	350	225
15.	900	650	430
16.	350	450	100
17.	120	800	350
18.	720	1000	360
19.	400	900	250
20.	625	875	300

Table 6.3 – Resistivity Combinations used for CASE 3 training database preparation

The anomalous body resistivity values used for database generation are, $1000\,\Omega m$, $1500\,\Omega m$, $2000\,\Omega m$, $2500\,\Omega m$, $2750\,\Omega m$, $3100\,\Omega m$, $3600\,\Omega m$, $4000\,\Omega m$, $4500\,\Omega m$ and $5000\,\Omega m$.

6.4.1 Database for network training

For CASE 1 the database consists of 1040 examples generated by adding Gaussian noise of 0%, 0.5%, 1%, 1.25%, 1.5%, 2%, 2.5% and 2.75% for 130 different mesh assignments. The noise values are selected such that the measurement noise and numerical errors are usually below 3% [42].

For CASE 2 the databases consists of 13000 examples (20 resistivity combinations × 130 mesh assignments × 5 noise levels), all generated by varying the Gaussian noise level at 0%, 1%, 1.5%, 2% and 2.5%.

For CASE 3 the databases consists of 9750000 examples (20 resistivity combinations ×75 layer height combinations ×130 mesh assignments ×10 anomalous body resistivities× 5 noise levels), all generated by varying the Gaussian noise level at 0%, 1%, 1.5%, 2% and 2.5%.

The input data is pre processed to give normalized data with unity standard deviation and zero mean. The database is then split to three sections to use with the generalized training of the Network. Table 6.4 gives the sizes of the training set, test set and the validation set.

Case Number	Size of			
	Database	Training Set	Validation Set	Test Set
1	1040	640	200	200
2	13000	7000	3000	3000
3	9750000	5750000	2000000	2000000

Table 6.4 - Data set separation

6.5 Neural Network Modeling and Optimization

Referring Figure 3.2 of the general neural network architecture, for the three cases of interest n is set to 495 (apparent resistivity pseudo section datum points), and m is set to 385 (individual cell resistivity assignments). The no of hidden layers and hidden neurons (l) are finalized on a trial and error basis after monitoring the training and testing error.

When observing the synthetically generated pseudo sections for an arbitrary resistivity distributions certain data patterns can be recognized. The 'Trainrp' function (discussed under section 3.7.4) is the fastest algorithm on pattern recognition problems [28] among the available set of neural network training functions in MATLAB7s' Neural Network tool Box. Therefore 'Trainrp', the network training function that updates weight and bias values according to the resilient backpropagation algorithm (RPROP) is used for the 2D resistivity data inversion.

116

In the present study since data is synthetically generated a large example database is available. Therefore in order to improve generalization or to avoid overtraining, Early stopping with a Hold out cross validation is used. i.e. for the network optimizing procedure the automated training termination is used.

7.1 Introduction

In areas where the geological structures are approximately two-dimensional (2D), conventional 2D electrical imaging surveys have been successfully used. The main limitation of such surveys is probably the assumption of a 2D structure. In areas with complex structures, there is no substitute for a fully 3D survey. Researchers have observed that 2D and 3D resistivity surveys at the same location produced very different images on the same cross section. This discrepancy causes much confusion among practitioners about effectiveness of resistivity imaging methods.

When dealing with a 3D resistivity problem a 3D earth model with a 3D arbitrary resistivity distribution and 3D electrical field due to a point source is considered.

A Neural Network based inversion program is designed to invert data collected with a rectangular grid of electrodes with the pole-pole array. A seven by seven electrode grid is proposed for the present study with a total of 49 electrodes. The NN is trained to output to give a cell based inversion model for the pre defined mesh discretization. A paradigms of Backpropagation learning algorithm namely Resilient backpropagation is tested with different network architectures on trial and error to choose the best network with the lowest training and testing error to reproduce the 3D sub surface structure from the multi electrode field measurements.

A 3D case study of geological model of a two layer earth with an embedded Anomalous body is experimented.

7.2 Literature

Many resistivity imaging practitioners are interested in combining multiple 2D data sets collected along parallel survey lines into a pseudo 3D data set for 3D inversion. In such cases it is observed that most of the features on an extracted slice image from 3D inversion appeared on the image from 2D inversion, but the 2D inverted resistivity cross-section appeared more complicated with more anomalies and higher resistivity contrast [43]. The objects which did not intersect the imaging plane would be folded

onto the 2D inverted cross-section. This is why false anomalies are often seen on the 2D resistivity images. Therefore, 3D resistivity imaging methods are the better technology for subsurface imaging.

A 3D resistivity survey is carried out with a multi electrode array spanned in both x and y dimensions. Similarly as the 2D resistivity forward problem, it has become a standard practice to solve 3D resistivity forward modeling problem using numerical methods by discretization of the domain of investigation.

Now as multi-electrode, multi-channel resistivity imaging systems and commercial 3D resistivity inversion programs are readily available, more and more people are conducting 3D resistivity surveys.

7.3 Forward Modeling of a 3D earth Structure

7.3.1 Acquiring Field Measurements for a 3D study

Electrical resistivity surveys traditionally have been conducted with linear arrays, with electrodes evenly spaced. But three-dimensional (3D) surveys require the placement of parallel lines of electrodes.

7.3.1.1 Electrode Geometry
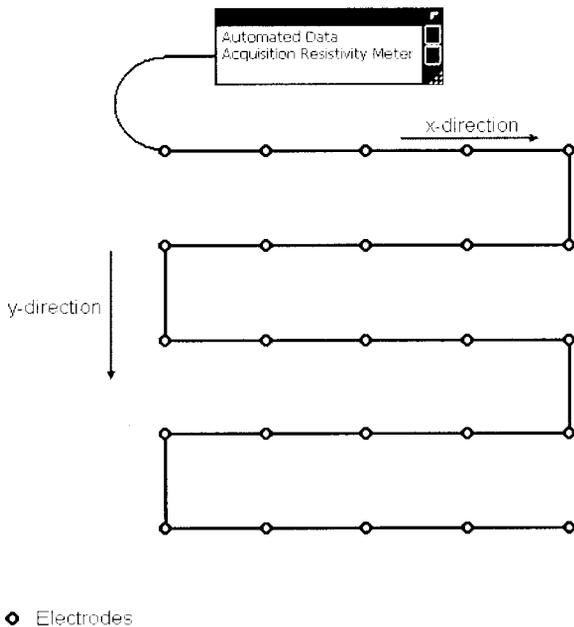
Figure 7.1 - one possible layout for a 3D survey

Ideally, the electrodes for a 3D survey are arranged in a rectangular grid (Figure 7.1). However, in practice depending on the available equipment, surface topography, survey time and budget, different types of survey procedures have been used.
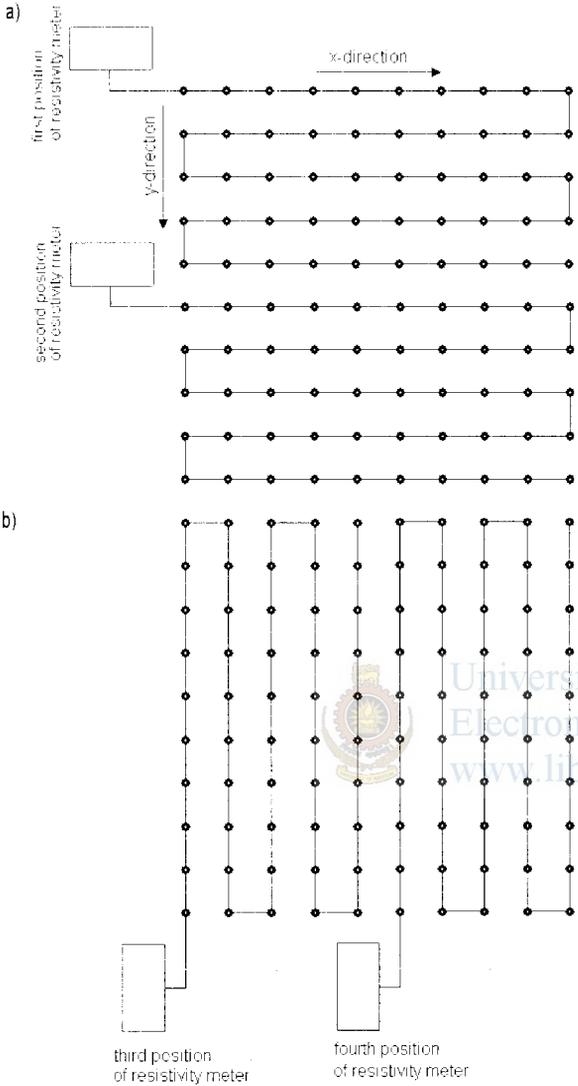
Figure 7. 2 - Using the roll-along method to survey a 10 by 10 grid with a resistivity-meter system with 50 electrodes. (a) Surveys using a 10 by 5 grid with the lines orientated in the x-direction. (b) Surveys with the lines orientated in the y-direction.

Most commercial 3D surveys will probably involve grids of at least 16 by 16 in order to cover a reasonably large area. A 16 by 16 grid will require 256 electrodes which is larger than many multi-electrode resistivity meter systems. To map large areas with a limited number of electrodes in a multi-electrode resistivity meter system, the roll-

120

along technique can be used [44]. Figure 7.2 shows an example of survey using a multi-electrode resistivity meter system with 50 electrodes to survey a 10 by 10 grid.

Initially the electrodes are arranged in a 10 by 5 grid with the longer lines orientated in the x-direction (Figure 7.2a) Measurements are made primary in the x-direction, with some possible measurements in the diagonal directions. Next the entire grid is moved in the y-direction so that the 10 by 5 grid now covers the second half of the 10 by 10 grid area. The 10 by 5 grid of electrodes is next orientated in the y-direction and the measurements are made between the electrodes in the y-direction (Figure 7.2b).

7.3.1.2 Array types

Some known electrode configurations such as wenner and shlumberger arrays are not applicable to 3D cross string measurements. The most common arrays used for 3-D surveys are the pole-pole (discussed in C.2.3), pole-dipole (discussed in C.2.4) and dipole-dipole (discussed in C.2.5) arrays. Other arrays might not provide sufficient data coverage for a full 3-D inversion [45].

7.3.2 Recording the field measurements

There are two popular methods for the 3D surveys, such as cross line or cross string measurements and pseudo 3D survey.

The electrode geometry can consist of several electrode strings. An electrode string is defined as a line of electrodes with consecutive addresses. It is not essentially a straight line. For a borehole resistivity survey a string is a borehole. For several lines on the surface electrodes on a survey line can be grouped together as one string. For electrodes laid out in an irregular shape such as some surface electrodes in a borehole resistivity imaging project, all surface electrodes are combined into one string. A cable may be oriented in either x or y directions.

To image a volume both same-string measurements and cross-string measurements should be collected. Same string measurements are acquired with the transmitting and receiving electrodes on the same string. But the cross string measurements are taken with transmitting electrode on one string and receiving electrode on another string. For efficient field surveys and data processing some pairs of string may not be used to collect data.

121

With a large number of cross-line measurements is an ideal approach for a 3D resistivity survey because it offers a better subsurface resolution than a pseudo 3D survey [1]. However, a pseudo 3D survey without any cross-line measurements is an acceptable alternative to a true 3D survey as far as the line spacing is equal to or less than twice the electrode spacing.

7.3.3 3D surveys with the pole-pole array

The pole-pole electrode configuration is commonly used for 3D surveys. The apparent resistivity value for the pole-pole array is given by (C.4),

$$\rho = 2\pi a R \tag{7.1}$$

Where R is the measured resistance, a is the spacing between the C1 and P1 electrodes. For a given number of electrodes, the pole-pole array gives the maximum number of independent measurements, n_{max} which is given by,

$$n_{max} = n(n-1)/2 \tag{7.2}$$

Where n is the number of electrodes.

In the measurement sequence shown in Figure 7.3, each electrode in turn is used as a current electrode and the potentials at all the other electrodes are measured. Because of reciprocity, only the potentials at the electrodes with a higher index number than the current electrode are measured. For a 5 by 5 electrode grid, a complete data set will have 300 datum points. For 7 by 7 and 10 by 10 electrode grids, the numbers of measurements are 1176 and 4500 respectively. It can be very time-consuming to make such a large number of measurements with typical single-channel resistivity meters commonly used for 2D surveys.

To reduce the number of measurements to about one-third of the maximum possible number required without seriously degrading the quality of the model obtained, an alternative measurement sequence has been tested (Figure 7.4). In this proposed "cross-diagonal survey" technique, the potential measurements are only made at the electrodes along the horizontal, vertical and the 45 degrees diagonal lines passing through the current electrode. The number of datum points with this arrangement for a 7 by 7 grid is reduced to 476.
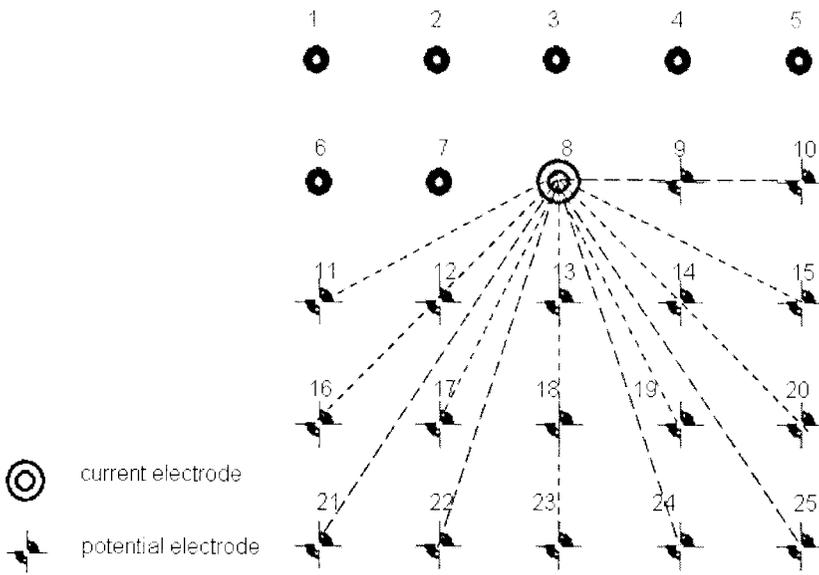
Figure 7.3 - The location of potential electrodes corresponding to a single current
electrode in the arrangement used by a survey to measure the complete data

In the case of a roll-along grid connection method all the possible measurements for
the pole-pole array or the cross diagonal measurements are made for each sub grid.
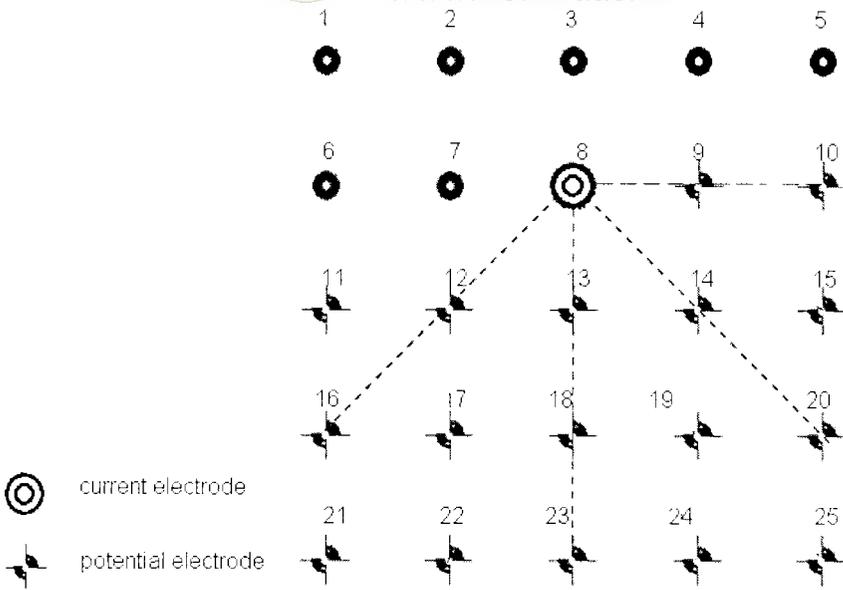
Figure 7.4 - The location of potential electrodes corresponding to a single current
electrode in the arrangement used by a cross diagonal survey

For practical reasons, the number of field measurements in some surveys might be even less than the cross-diagonal technique. Another common approach is to just make the measurements in the x- and y- directions only, without the diagonal measurements. This is particularly common if the survey is made with a system with a limited number of independent electrodes, but a relatively large grid is needed.

For relatively small grids of less than 12 by 12 electrodes, the pole-pole array has a substantially larger of possible measurements compared to other arrays. The loss of data points near the sides of the grid is kept to a minimum, and provides better horizontal data coverage compared to any other array. This is an attractive array for small survey grids with relatively small spacing (less than 10 meters) between the electrodes. However, it has the disadvantage of requiring two "far" electrodes that must be placed at a sufficiently large distance (at least 10 times the maximum electrode spacing used) from the survey grid. Due to the large distance between the two potential electrodes, this array is more sensitive to telluric noise. The pole pole array produces strong signals but a low model resolution.

In the present study a 7 by 7 electrode grid with 1m spacing is considered. The pole-pole array is considered and a cross diagonal data set acquiring option is considered. This adopts an apparent resistivity pseudo section with 476 field measurements.

7.3.4 Construction of a 3D Structure

The inverted 3D structure from the field data is interpreted with 2D slices equivalent to the no of layers in the z direction of the block based model (Figure 7.5).
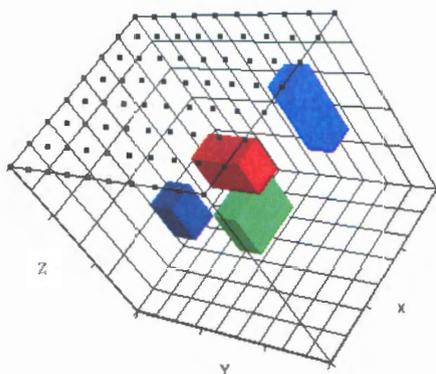
(a)
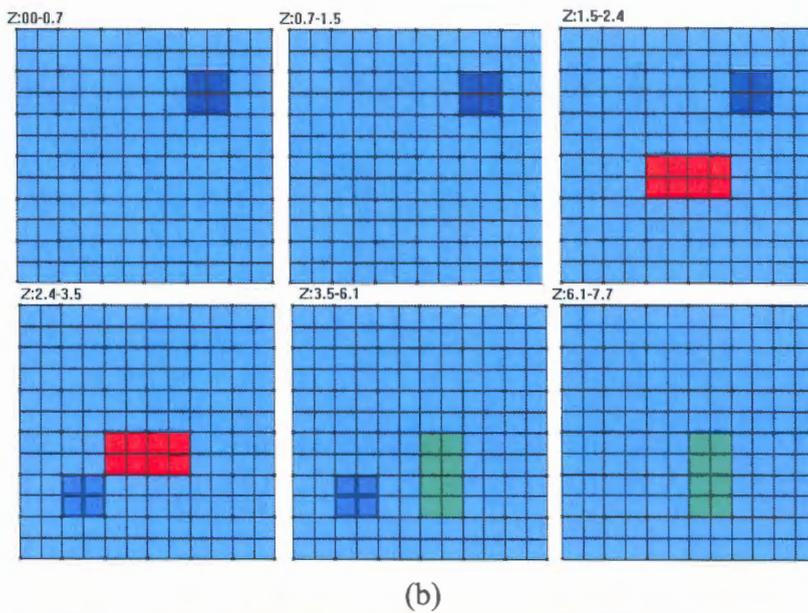
(b)

Figure 7.5 - Sample model with different sized and shaped anomalies,

for synthetic data generation (a) 3D mesh (b) 2D slices

(Original is in Color)

A 3D model mesh is used for this purpose. This model mesh describes a 3D resistivity structure by initially dividing the surface medium into many rectangular prisms. A constant resistivity will be assigned to the individual prisms in the inverted 3D model. Then 2D slices at predefined depths are used to interpret the 3D structure after inversion (Figure 7.5(b)).

The mesh discretization for the present study is as follows. The width of the rectangular blocks is set to the electrode spacing in the x and y directions. The number of model mesh levels is set to 7. Thickness of first layer is set to 0.7m. Since the resolution of the resistivity method decreases with depth, normally the thicknesses of the model layers are also increased with depth. A thickness incremental factor of 1.15 is selected. Hence the individual layer depths are 0.7m, 1.505m, 2.4307m, 3.4954m, 4.72m, 6.1276m and 7.7468m respectively. These results in a 7, 2D slices each with a 6 by 6 mesh, giving a 3D representation with a total of 252 ($6 \times 6 \times 7$) block divisions

.

7.3.5 Forward Response of a 3D structure

Using the Poisson's equation,

$$-\nabla.(\sigma \nabla V) = I \tag{7.3}$$

For a pole-pole array, the apparent resistivity can be calculated as,

$$\rho_a = 2\pi a \frac{\Delta V}{I} \tag{7.4}$$

Where a is the electrode spacing ΔV is the potential difference between the receiving electrodes.

For a 3D distribution the electrical conductivity forward solution can be obtained by solving the differential equation,

$$\frac{\partial}{\partial x}\left(\sigma \frac{\partial V}{\partial x}\right) + \frac{\partial}{\partial y}\left(\sigma \frac{\partial V}{\partial y}\right) + \frac{\partial}{\partial z}\left(\sigma \frac{\partial V}{\partial z}\right) = I(x, y, z)$$

$$\tag{7.5}$$

Where, V is the scalar electrical potential and ,I(x,y,z) is the electric current source. Finite difference or Finite Element method with an elemental volume was used to discretize the above partial differential equation.

7.4 Synthetic data generation

Similarly as in the two dimensional study a commercial software is used for the synthetic data generation. *RES3DMOD, version 2.14(April 2005), for Windows 95/98/Me/2000/NT*, a program for 3-D resistivity & IP forward modeling using the finite-difference and finite-element methods for Wenner, dipole-dipole, pole-pole, pole-dipole, Schlumberger, rectangular arrays by M.H.Loke was used for data generation. This demo version was downloaded from the website of Geotomo Software Sdn. Bhd., 115, Cangkat Minden Jalan 5, Minden Heights, 11700 Gelugor, Penang, Malaysia.
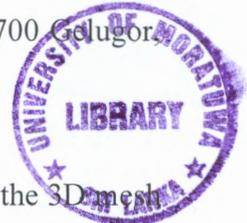
To use the program, user must supply the resistivity value of each cell in the 3D mesh using an input text file. Appendix H.1 gives a sample of a model file used for mesh assignments.

A two layer earth structure is considered with an embedded anomalous body. The layer resistivities are varied between $10\,\Omega m$ and $1000\,\Omega m$ while the top layer height is varied between 0.7-6.2m. The resistivity values used for database preparation are the

same as given in Table 4.2.The anomalous body resistivity is varied between 100-3000 Ωm and it is moved to different mesh positions with variable sizes(Figure 7.5). The synthetic data is generated by adding Gaussian noise of 0%, 1%, 1.5%, 2% and 2.5%.

For each combination of resistivity the upper layer height (h_1) is varied in the values of 0.7m, 1.5m, 2.43m, 3.5m, 4.72m and 6.13m.

The anomalous body was moved to different prism positions. The numbers of 65 body assignments used in the database generation are given in Appendix H.2. The anomalous body resistivity was varied in the values of 100 Ωm, 500 Ωm, 1000 Ωm, 1500 Ωm, 2000 Ωm, 2500 Ωm and 3000 Ωm.

With the commercial software the forward response is then generated and the results are saved in the '.dat' format (Figure 7.6). Then with a Visual Basic program the relevant data for the training is extracted from the .dat file and stored in .txt format as a text file.

Figure 7.6 - Apparent resistivity values (encircled) for the training database

7.4.1 Database for network training

The database consists of 409500 examples (30 resistivity combinations × 6 layer height combinations ×65 mesh assignments ×7 anomalous body resistivities× 5 noise levels). The input data is pre processed to give normalized data with unity standard deviation and zero mean. 225500 samples are separated as the training set while the test and validation sets are comprised for 92000 samples each.

In the 3D case considered the databases for Neural Network training and testing consists of input records of 476 datum points of the 3D measurement pseudo section. Individual output records consist of the constant resistivity values assigned to the 252 mesh divisions. That is referring Figure 3.2 n is set to 476 and m is set to 252.

Similarly as in the two dimensional cases the resilient backpropagation algorithm (RPROP),'**Trainrp**' function in MATLAB7s' Neural Network tool Box is used for network training. Also since a large example database is available, early stopping with hold out cross validation is used to ensure network generalization.

8.1 Neural Network Model Optimization Results for One Dimensional Inversion

Model Optimization i.e. selection of Hidden layers and hidden nodes was done with evaluating the Average Mean square Training Errors.

The network performance at each run was slightly different due to the random initializations. So at the network optimization session's 15 networks were trained and the performance was finalized on an average basis.

The weight initialization is randomly done in the application, the weights and biases are initialized to small positive values by a Matlab routine at each training session

Comparing all the factors discussed under the section 3.7.4 the 'Trainrp' function is preliminary used for training of the curve identification network. And also the training and test errors of both 'Trainrp' function and the 'Trainscg' function are compared to choose the best performing training algorithm.
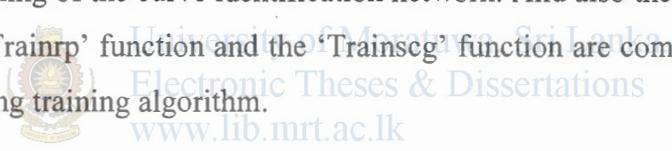
8.1.1 Curve Identification Network

Figure 8.1 shows the training performance of the Resilient Back propagation algorithm and the Scaled Conjugate Algorithm. With the average performance on 15 networks with different initializations the minimum training error is achieved with the 'Trainrp' function or the Resilient backpropagation algorithm.

Therefore the Resilient backpropagation algorithm is used there after for the trainings. In order to select the optimize network architecture i.e. to select the no of hidden nodes the training error of the resilient backpropagation function is compared. As seen in Figure 8.1 the training error variation with a Single hidden layer converges around 125 hidden nodes, however the training error level is converged to 0.4.

In order to check on the error level variation with two hidden layers several training sessions were carried out.

129
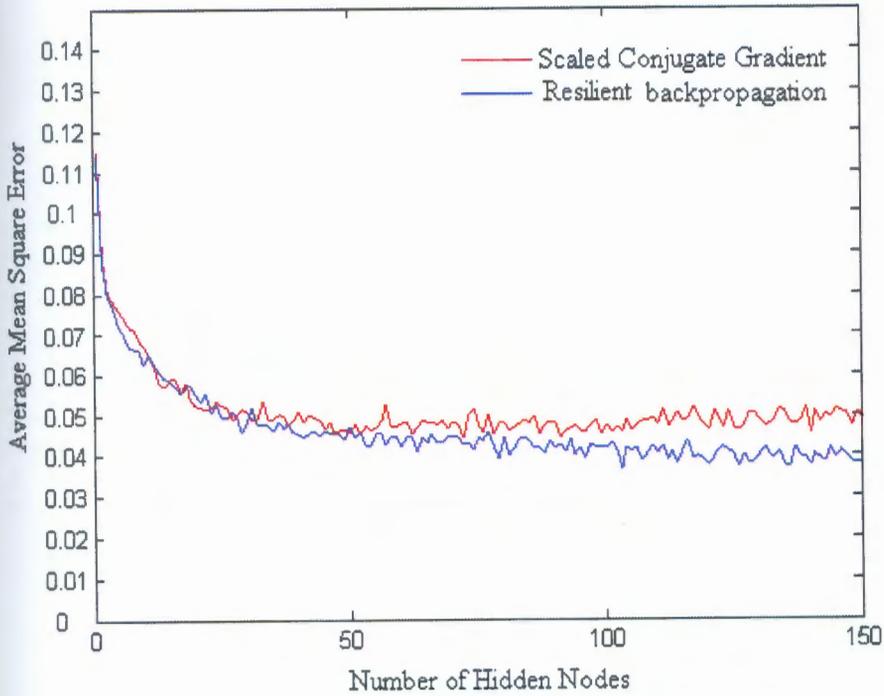
Figure 8.1 - Training Performance for the Training Function 'Trainrp' and 'Trainscg'with different no of hidden nodes (single hidden layer)
(Original is in Color)
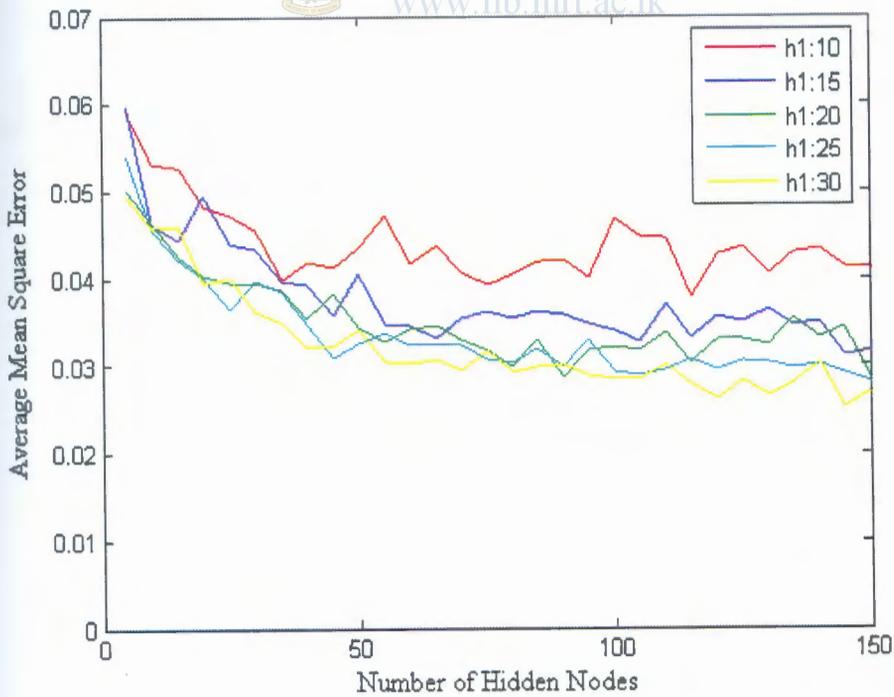
(a)
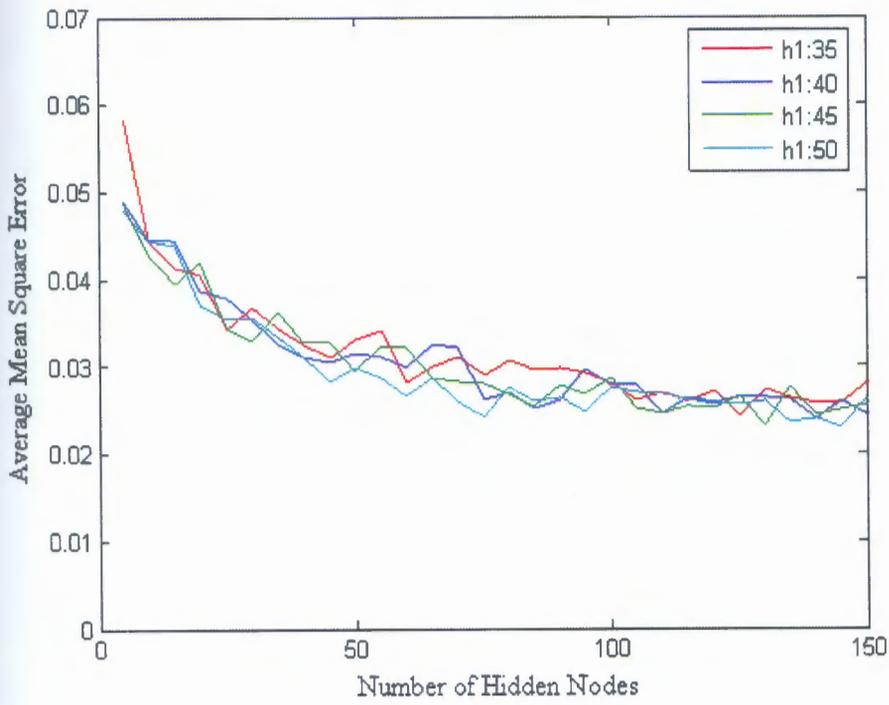
(b)
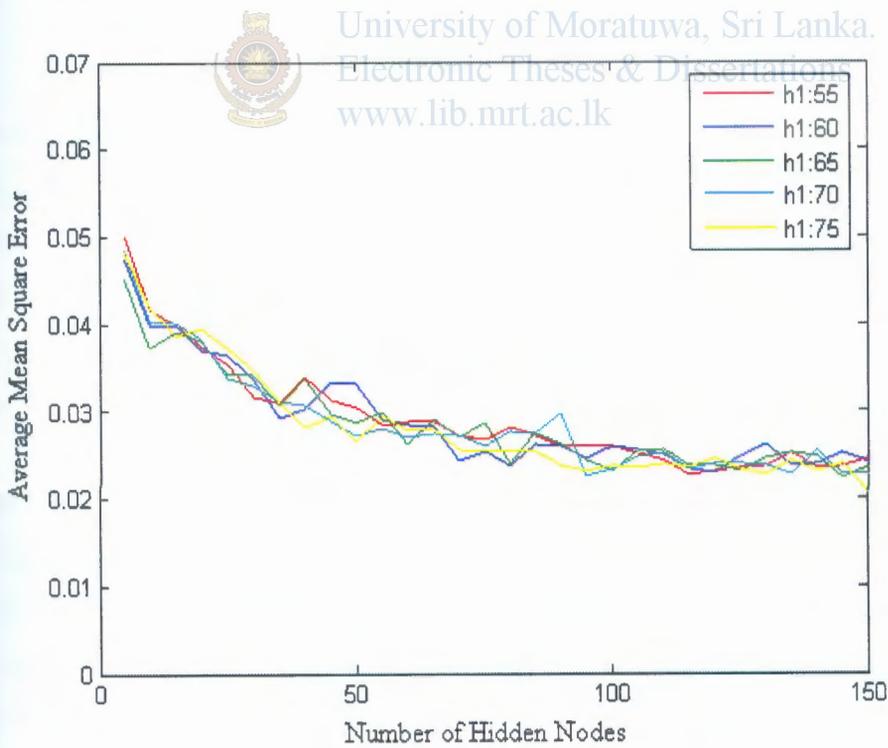
(c)
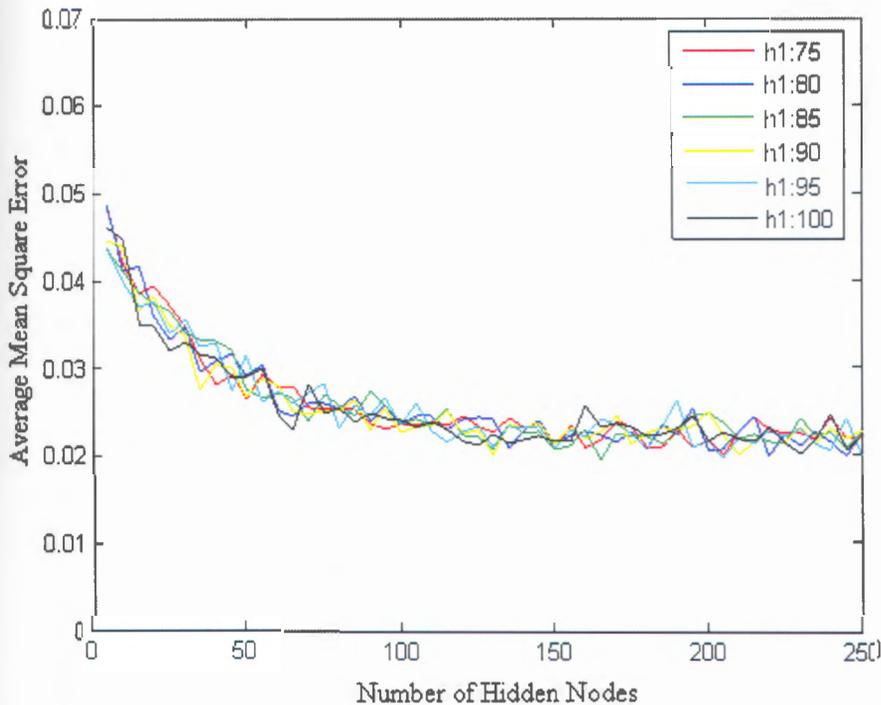
(d)

Figure 8.2 - Training Performance with two hidden layers for the curve identification
network

h1- No of Nodes in the first hidden layer

(Original is in Color)

Figure 8.2 (a) to Figure 8.2 (d) shows that the training error has reduced with the no of hidden nodes in the first layer and have converged with the increasing number of hidden nodes in the second layer. However the error reduction rate with the increment of the Hidden nodes is not significant. The average mean square error converges around 0.02 for 100 hidden nodes in the first layer. Therefore no further training is carried out with two hidden layers.

Further to check whether significant changes do occur with three hidden layers several training sessions were carried out. One such sample session results are given in Figure 8.3. The error level variation shows no improvement to the two hidden layer case. Since acceptable error levels are achieved with a two hidden layers the no of hidden layers is fixed to two, with 85 and 165 as the number of nodes in the first and second hidden layers respectively. The performance on the finalized network during training is shown in Figure 8.4. The training, validation and test error variation (on unseen data) is shown.

132
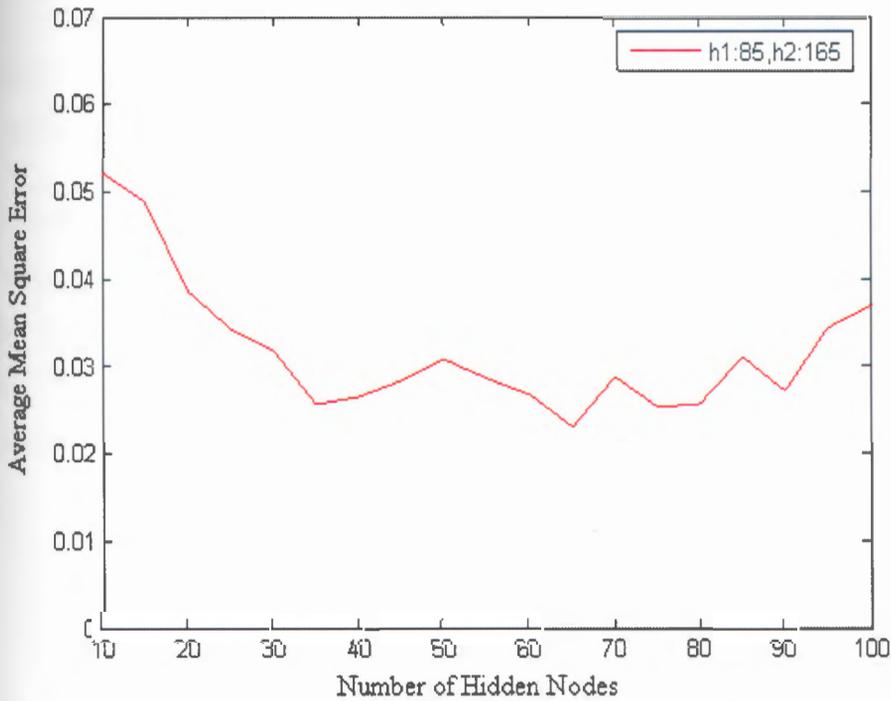
Figure 8.3 - Training Error variation of the curve identification network with three hidden layers
h1- nodes in the first hidden layer, h2- nodes in the second hidden layer
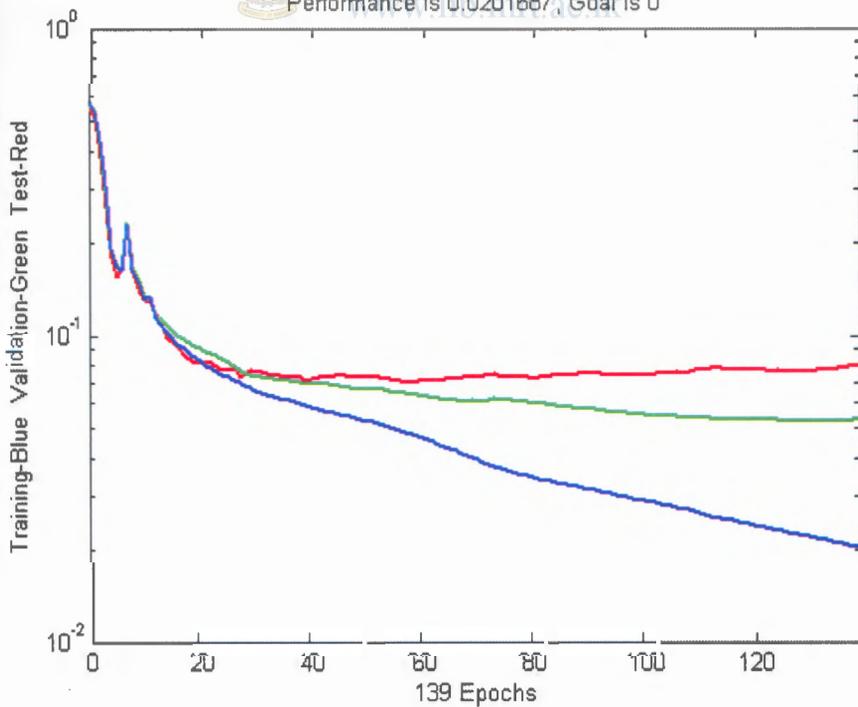
Figure 8.4 - Training, validation and Test performance of the finalized Network
(Original is in Color)

8.1.2 Two Layer Parameter Determination Network

In order to finalize the network architecture single hidden layer results and two hidden layer results for varying no of hidden neurons is compared for the 'Trainrp' function.

With referring the Figure 8.5 results the average training errors for a single hidden layer is converging around 0.07. Further training sessions was carried out to perceive whether any improvement can be done to the training error level with two hidden layers. Figure 8.6 (a) to Figure 8.6 (f) gives the training error variation with two hidden layers.
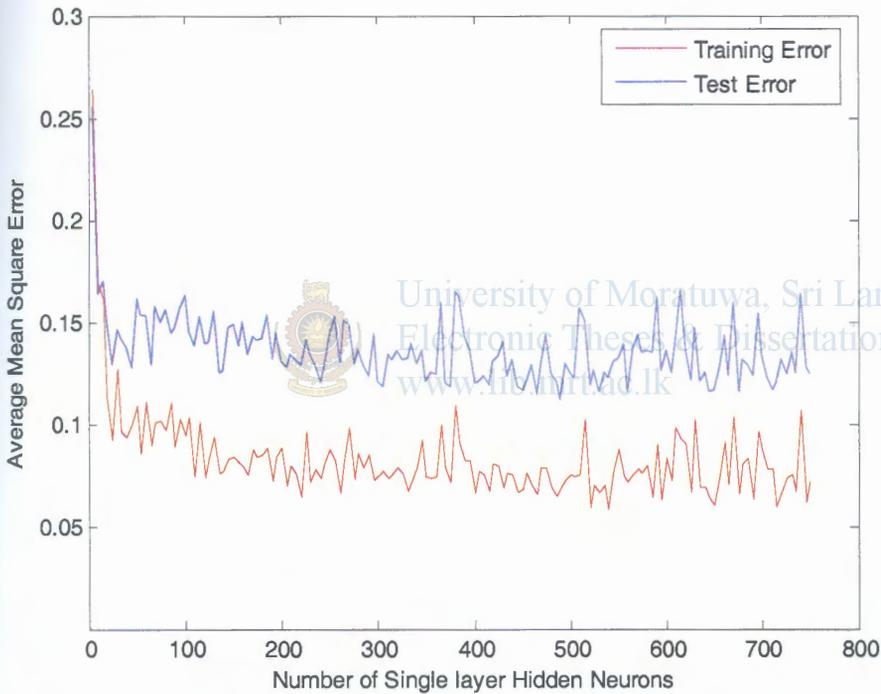
Figure 8.5 - Training Performance for the Training Function 'Trainrp' with different no of hidden nodes (single hidden layer and two hidden layers)
(Original is in Color)

With the results in Figure 8.6(a) it is seen that, when increasing the number of hidden nodes in the first layer from 25 to 100 the training error has decreased. But it is also seen that after 25 nodes in the second hidden layer the training error has tend to increase. Figure 8.6(b) shows the more detailed results of Figure 8.6(a).

But thereafter the training error levels are seen increasing with the increment of the number of nodes in the first layer. Therefore contrasting with the results of 8.1.1 here the error levels increased with the increment of nodes in the hidden layers.
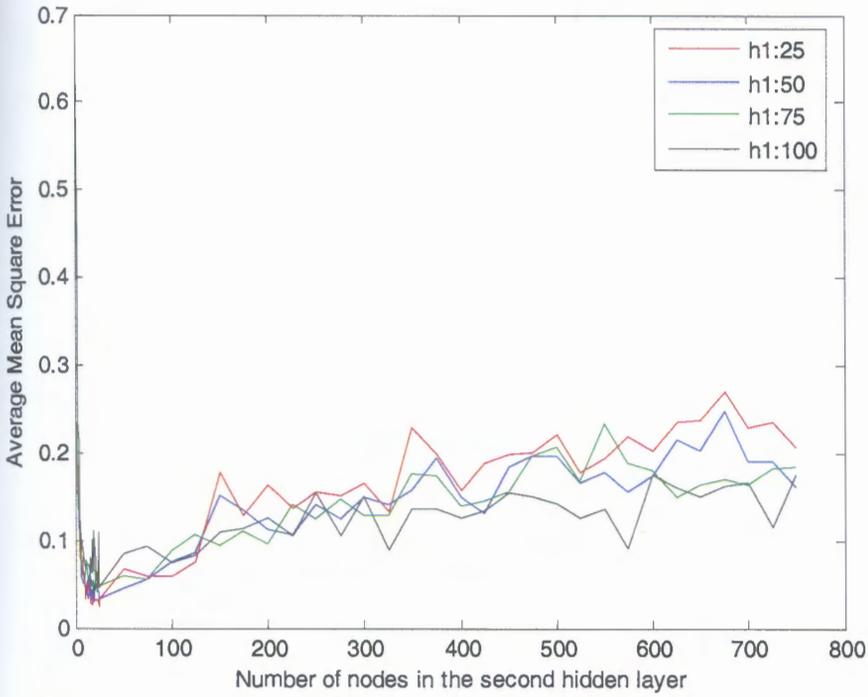
134

(a)
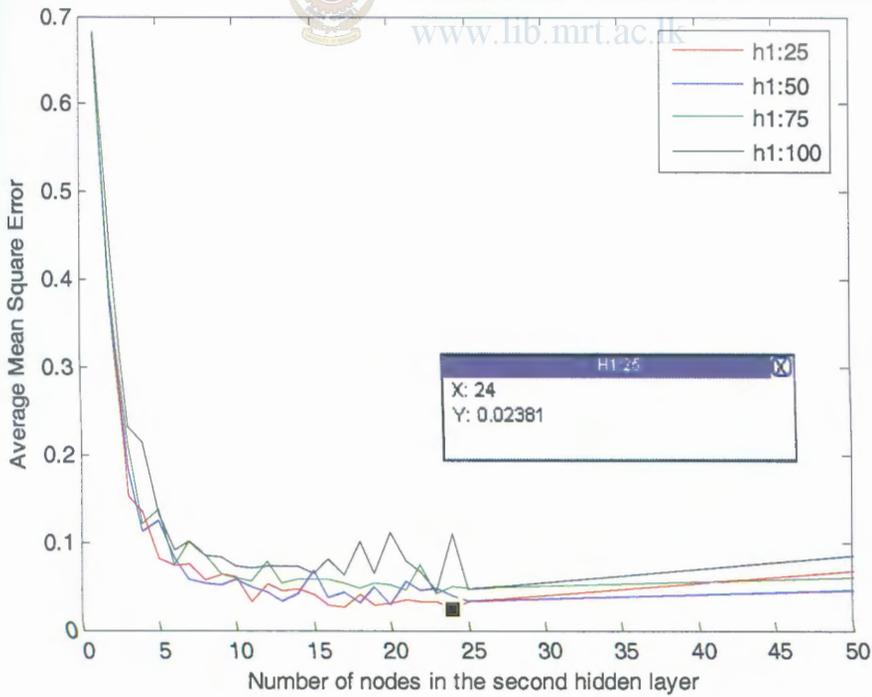
(b)
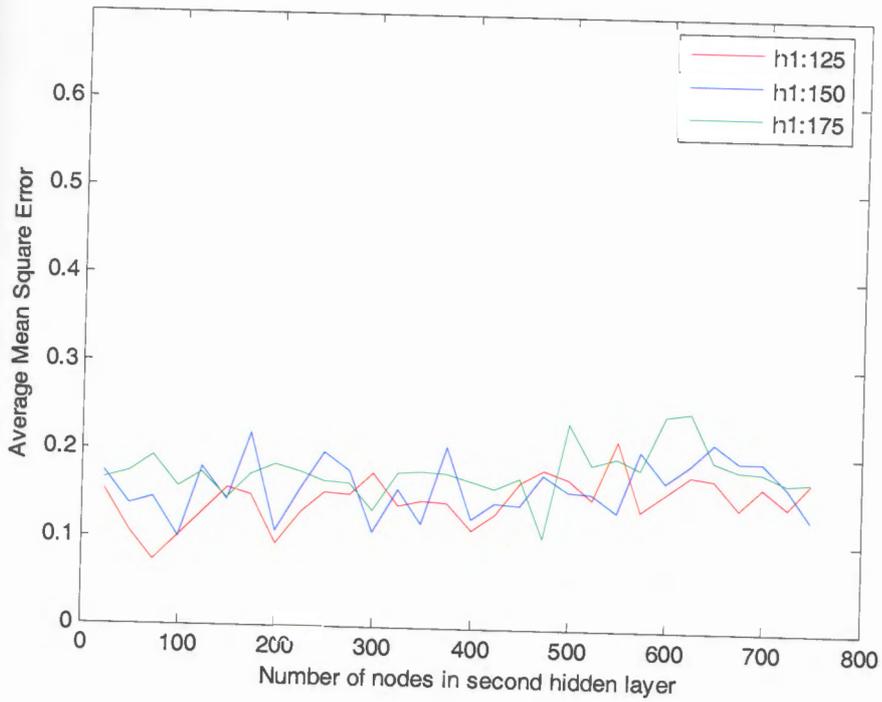
(c)
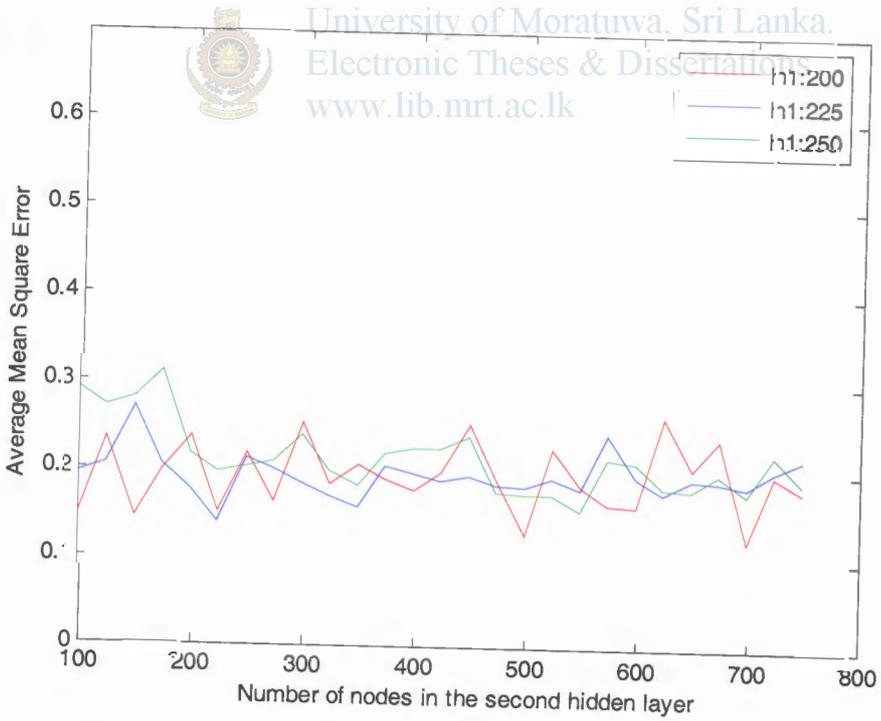
(d)
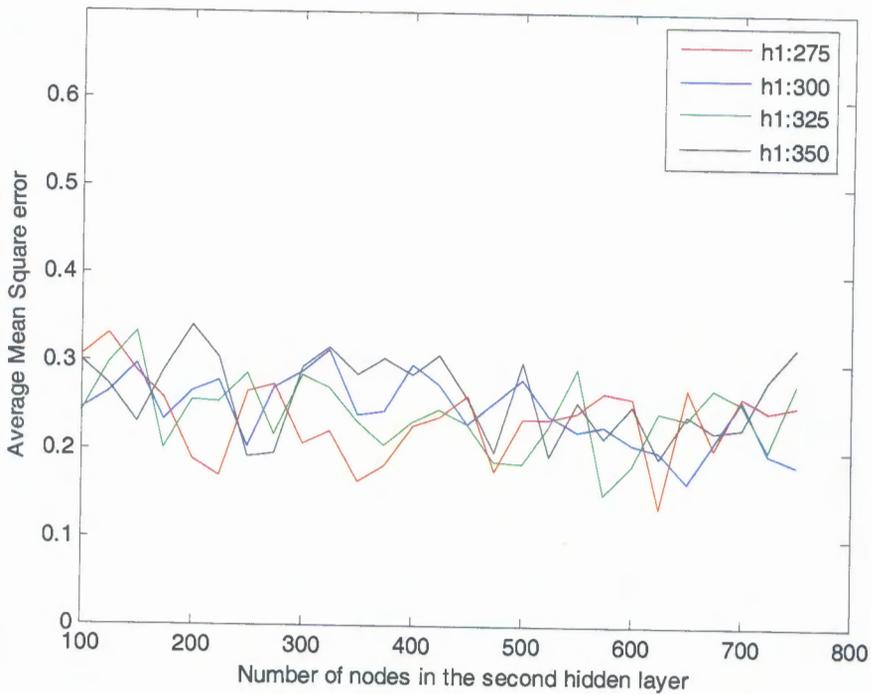
(e)
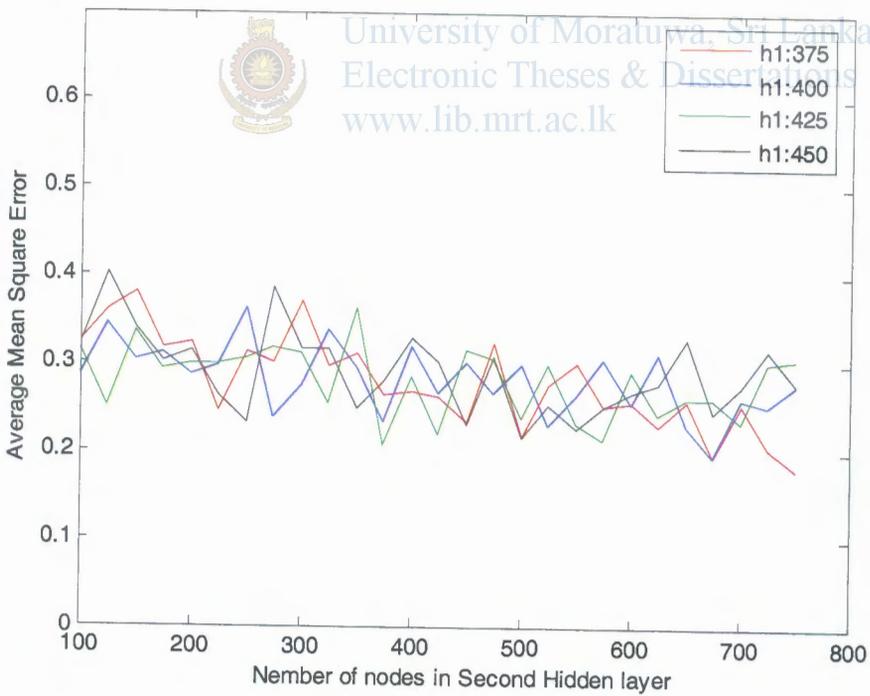
(f)

Figure 8.6 - Training Error variation of the two layer parameter determination network with two hidden layers (h1- nodes in the first hidden layer) *(Original is in Color)*

Finally by observing the performances the optimum network architecture was finalized as 25, 24 nodes in first and second hidden layer respectively (Figure 8.6(b)).

137

The minimum average mean square error achieved was 0.0238. The network performance for the finalized network is shown in Figure 8.7.

Performance is 0.0197243, Goal is 0
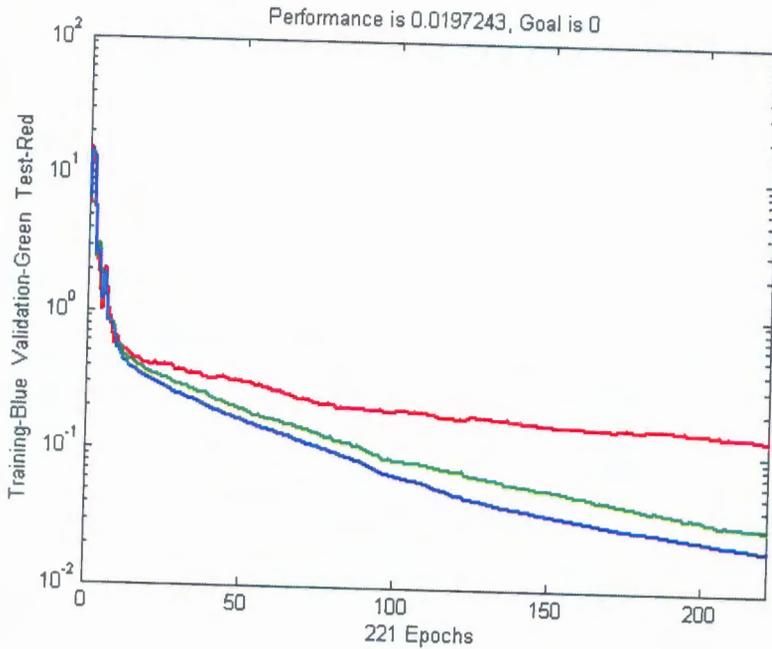
Figure 8.7 - Training, validation and Test performance of the two layer parameter determination, finalized Network *(Original is in Color)*

8.1.3 Three Layer Parameter Determination Network

Average Mean Square Error vs Number of Sinle Layer hidden Neurons
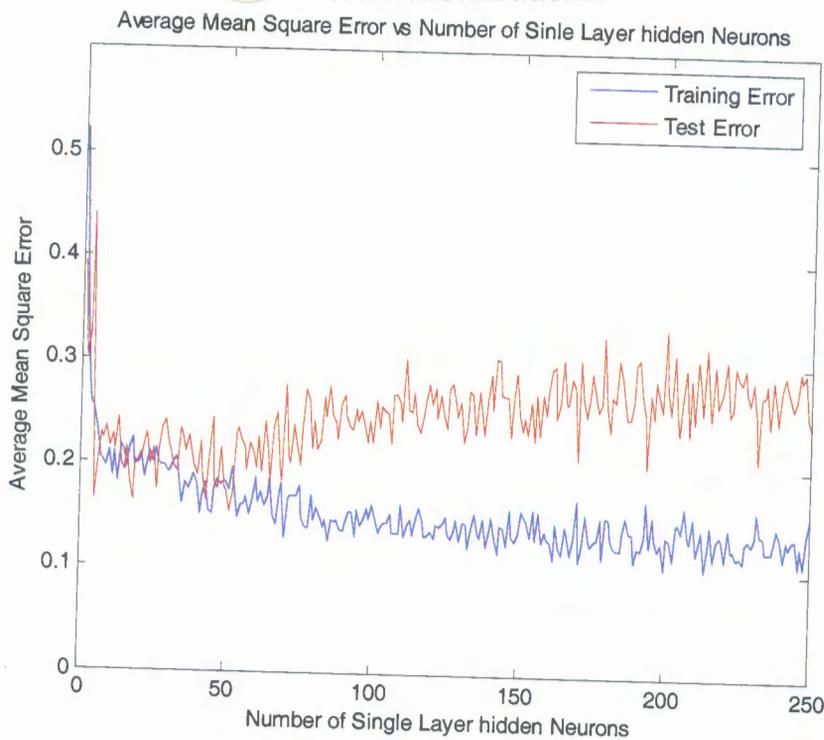
Figure 8.8 - Training and Testing Performance for the Training Function 'Trainrp' with different no of hidden nodes (single hidden layer) *(Original is in Color)*

Figure 8.8 shows the training and testing error variation with the varying number of nodes of a single hidden layer. Though the training error reduces and converge, the test set error starts increasing after about 50 nodes. However the training and testing error are high comparing to the previous training results. Therefore the training was preceded with two hidden layers.

Figure 8.9 (a) and (b) are the training performance of the network with two layers with different no of hidden node combinations. Figure 8.6(a) shows that the training error levels have decreased when increasing the number of hidden nodes in the first layer. Also the error levels has converged around 250 nodes in the second hidden layer.

Then proceeding further by increasing the number of hidden nodes the results given in Figure 8.6 (b) shows that error levels has started increasing with the increment in the number of both first and second layer hidden nodes. Therefore training was terminated and the referring Figure 8.6(a) the finalized network architecture was decided on the minimum training error of 0.014, at 100 and 260 hidden neurons for first hidden layer and second hidden layer respectively. The network performance for the finalized network is shown in Figure 8.10.
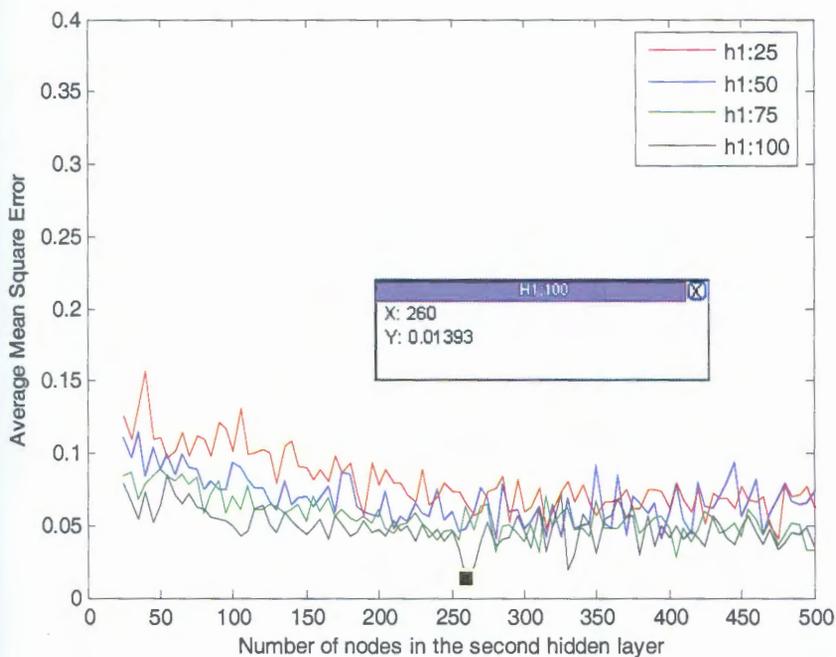
(a)
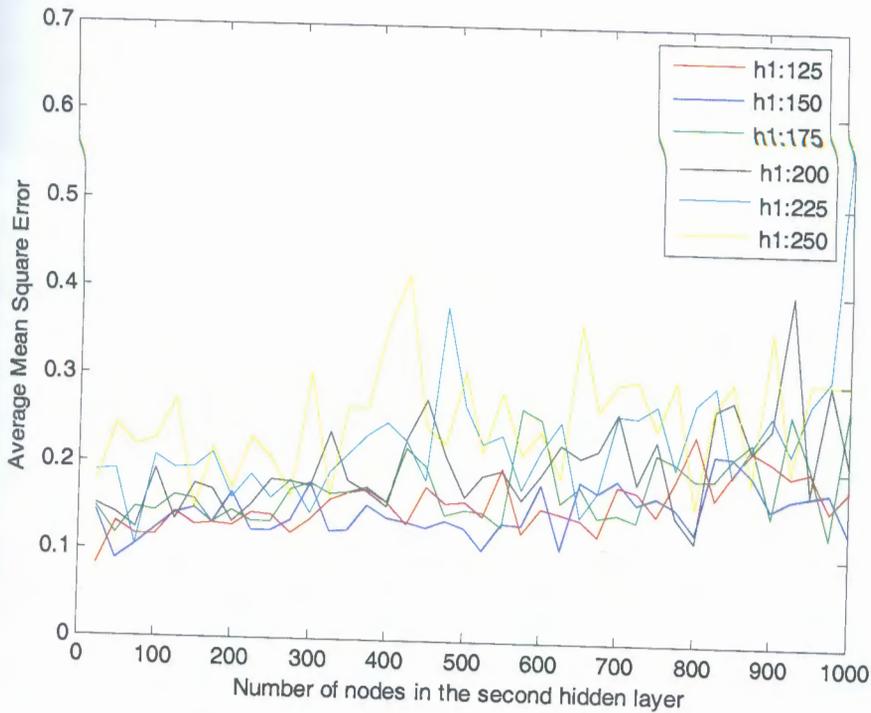
(b)

Figure 8.9 - Training Error variation of the three curve identification network with two hidden layers
h1- nodes in the first hidden layer
(Original is in Color)
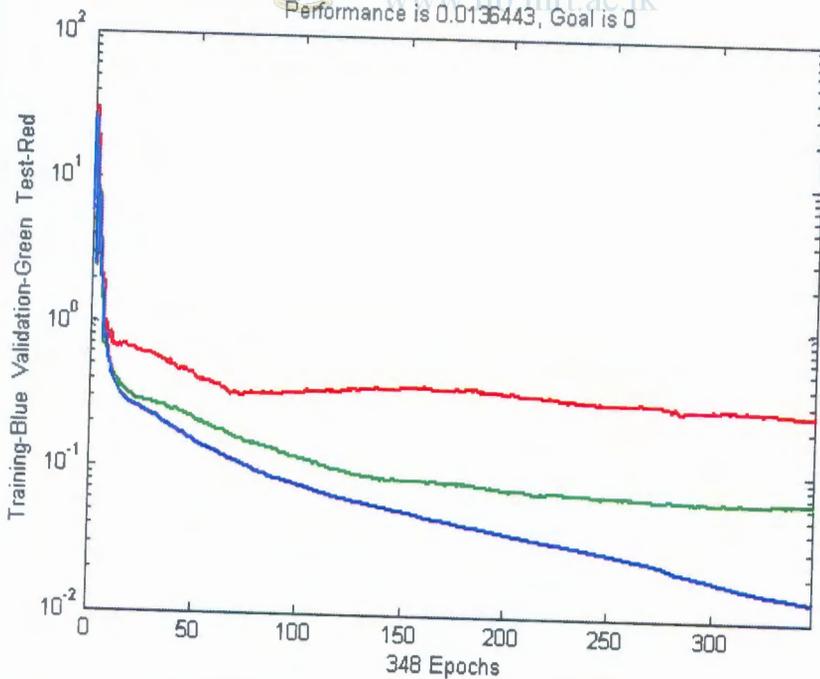
Figure 8.10 - Training, validation and Test performance of the finalized three layer parameter determination Network
(Original is in Color)

8.2 Simulation Results and Performance of the One dimensional Inversion

8.2.1 Curve Identification Network

To evaluate the Network performance on classification of the curve type the trained network with a two hidden layers with 85 and 165 hidden nodes in first and second hidden layers respectively, using the Resilient Backpropagation is used.

12 test data points with 2 for each curve type are used from the 150 example test data set for the performance evaluation. The One dimensional parameters of the test samples are given in Table 8.1. ρ_1, ρ_2 and ρ_3 are resistivity values of the first, second and the third layer while h_1, h_2 and h_3 are the heights of the first, second and third layer respectively. The network performance on the same test samples is evaluated with adding random noise.

Sample Number	Earth Parameters					
	ρ_1	ρ_2	ρ_3	h_1	h_2	h_3
Sample 01	25	630	-	6	∞	-
Sample 02	560	950	-	9.2	∞	-
Sample 03	300	100	-	1	∞	-
Sample 04	750	250	-	3	∞	-
Sample 05	110	500	900	2	5	∞
Sample 06	275	575	825	8.5	1	∞
Sample 07	560	100	800	5	2	∞
Sample 08	482	25	850	3	4	∞
Sample 09	150	400	75	3	5.4	∞
Sample 10	150	400	75	7	15	∞
Sample 11	625	400	150	2.5	4.1	∞
Sample 12	975	450	100	2.5	18	∞

Table 8.1 – One dimensional parameters of the test sets

8.2.1.2. Two layer curve Type 2
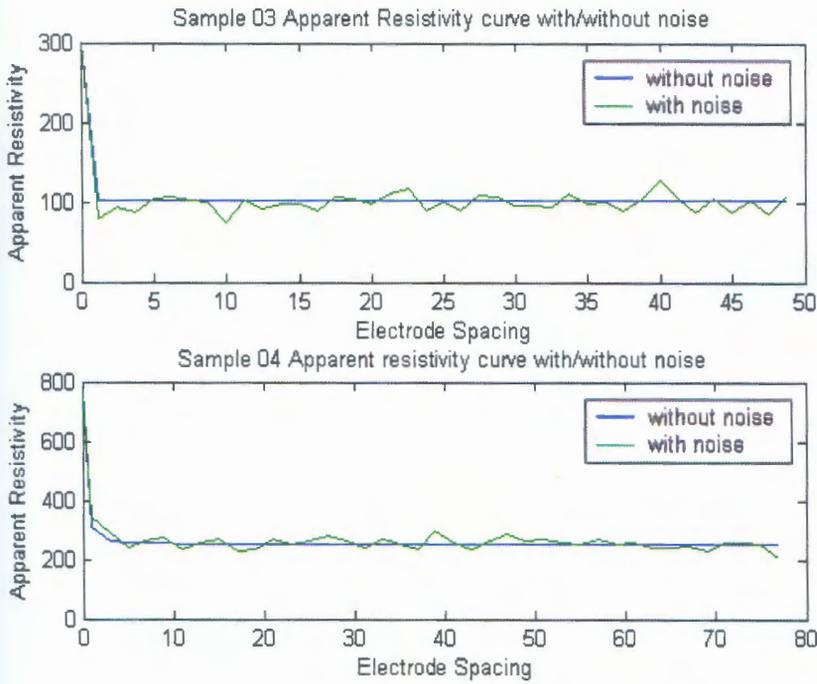
Figure 8.13 - Two layer curves used for evaluation (type 2)
(Original is in Color)
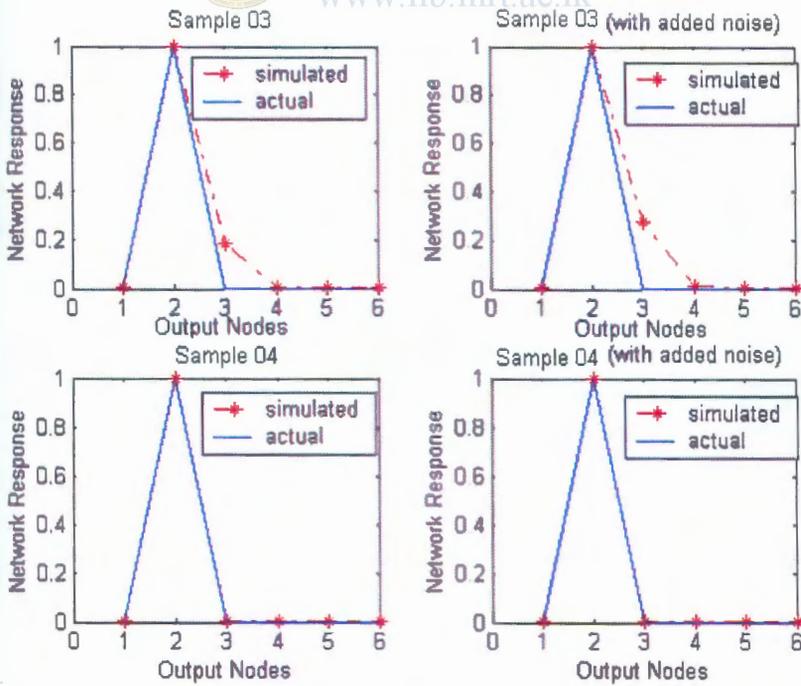
Figure 8.14 - Network Performance for two layer curves (type 2)
(Original is in Color)

143

8.2.1.4. Three layer curve Type H
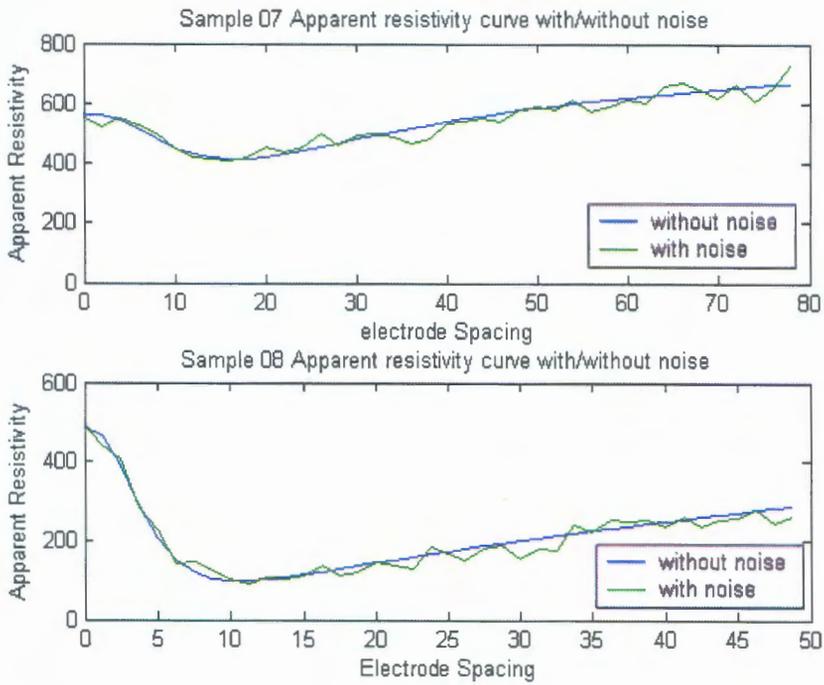
Figure 8.17 - Three layer Type H curves used for evaluation
(Original is in Color)
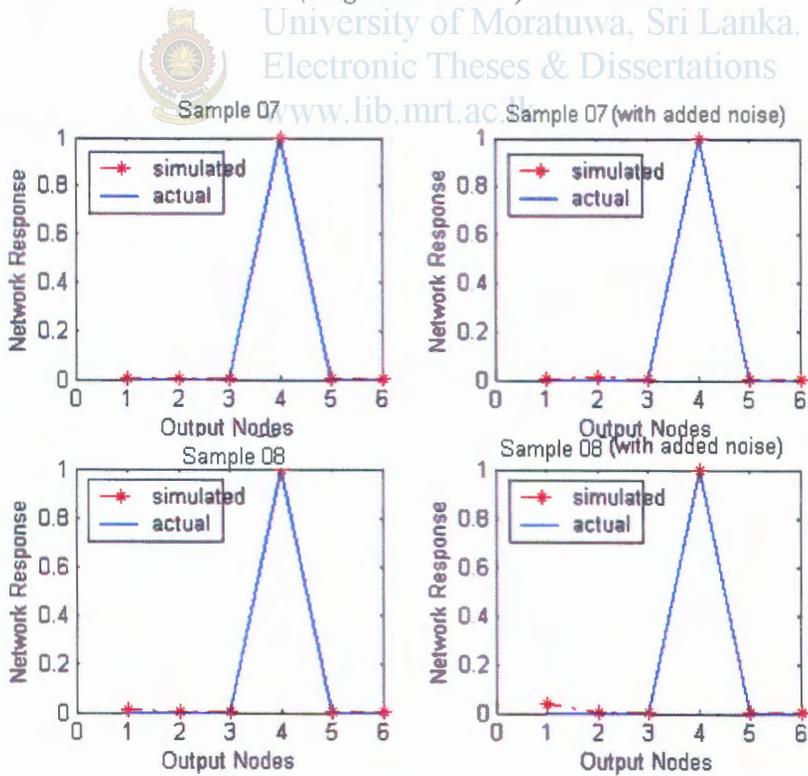
Figure 8.18 - Network Performance for Three layer Type H curves
(Original is in Color)

8.2.1.5. Three layer curve Type K
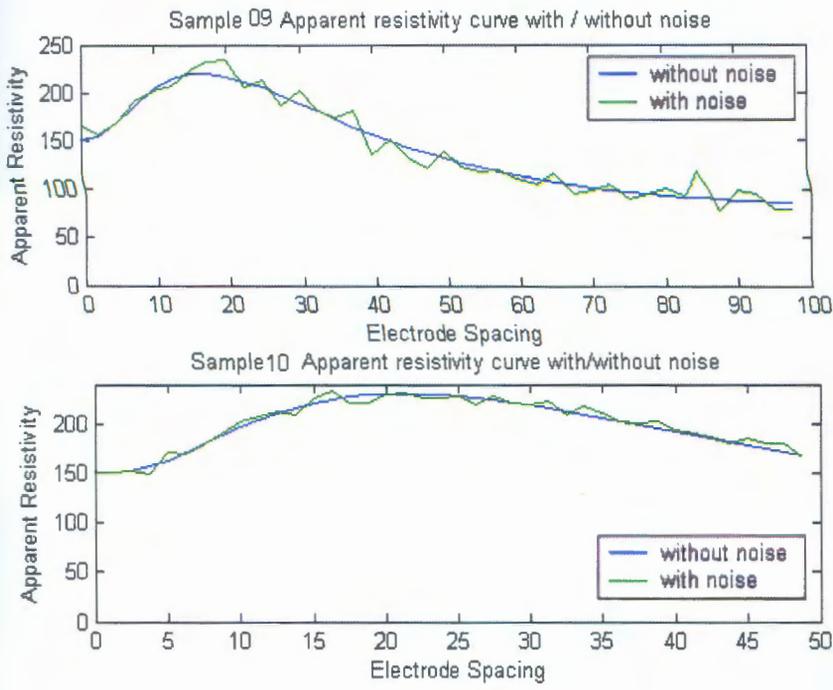
Figure 8.19 - Three layer Type K curves used for evaluation
(Original is in Color)
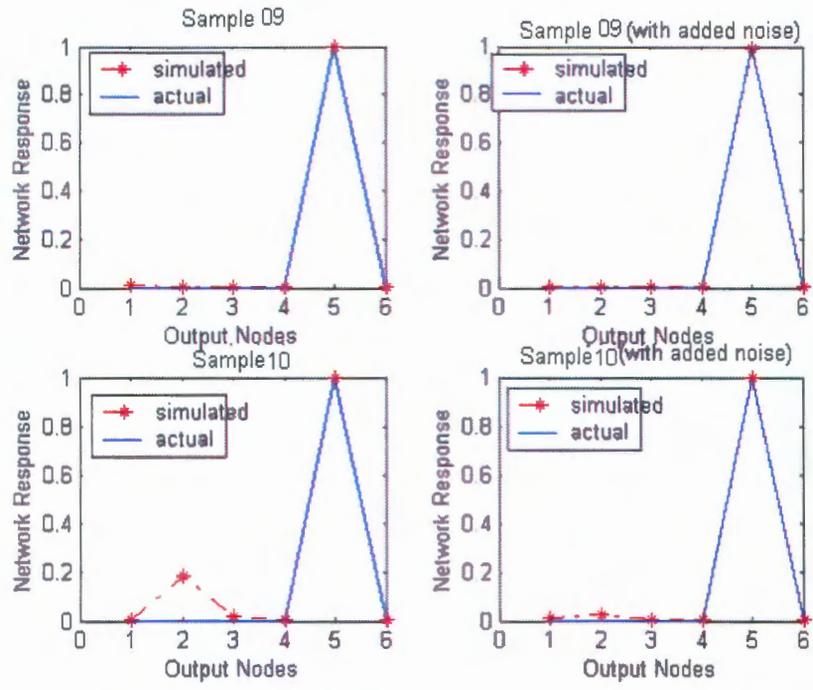
Figure 8.20 - Network Performance for Three layer Type K curves
(Original is in Color)

8.2.1.6. Three layer curve Type Q
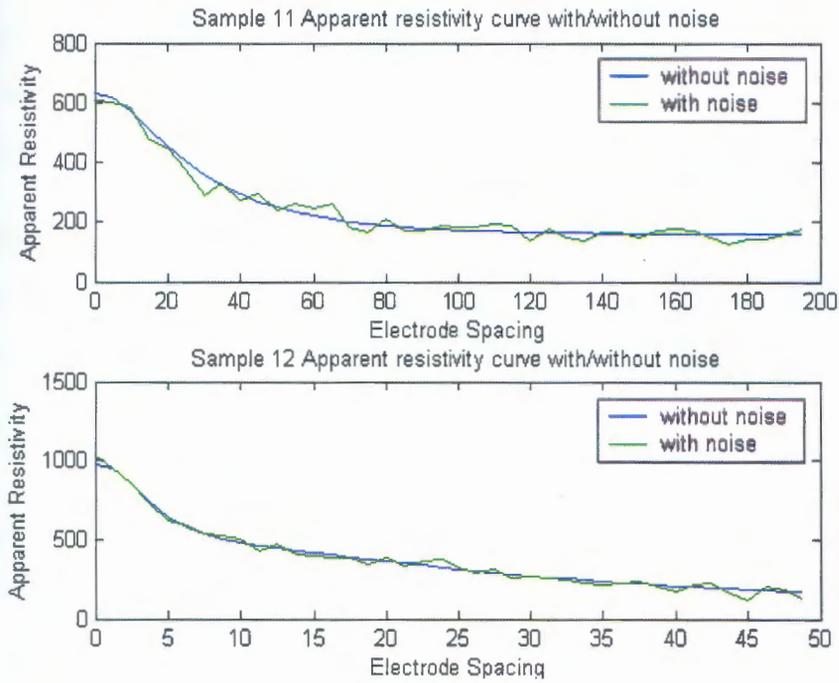
Figure 8.21 - Three layer Type Q curves used for evaluation
(Original is in Color)
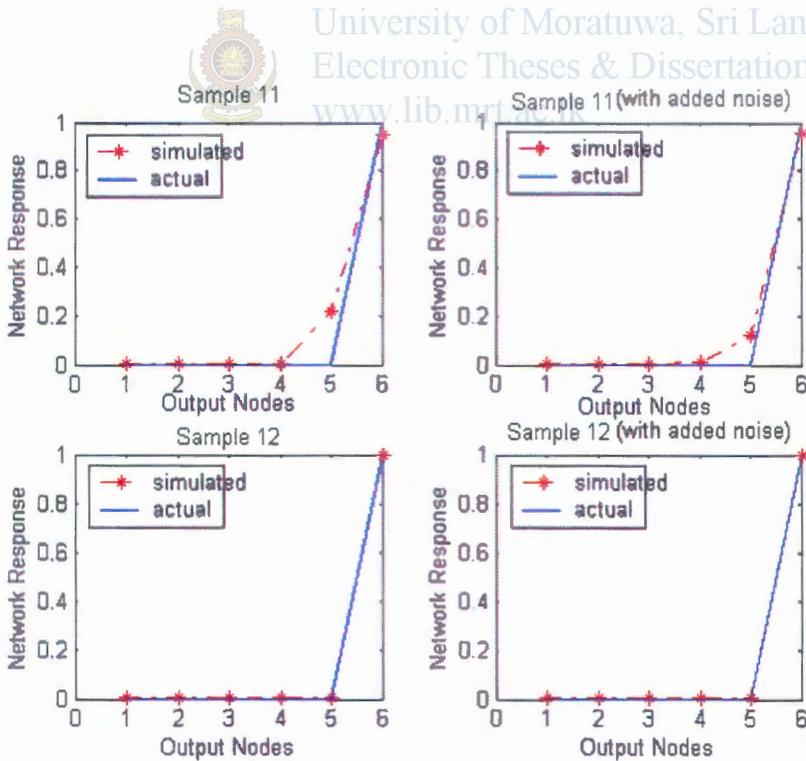
Figure 8.22 - Network Performance for Three layer Type Q curves
(Original is in Color)

8.2.2 Two Layer Parameter Determination Network

To evaluate the Network performance on determining two-layer parameter the trained network with two hidden layers with 25 and 24 hidden nodes using the Resilient Backpropagation is used.

Two of the above test data points (sample 01 and sample 03) for each curve type are used from the 150 example test data set for the performance evaluation. The network performance on the same test samples is evaluated with adding random noise.

8.2.2.1 Two Layer Curve Type1

The simulated and actual parameter values for sample 01 are presented below in Table 8.2 and on log log scale (Figure 8.23) with the actual parameters (in blue) and Neural Network output parameters (in red).
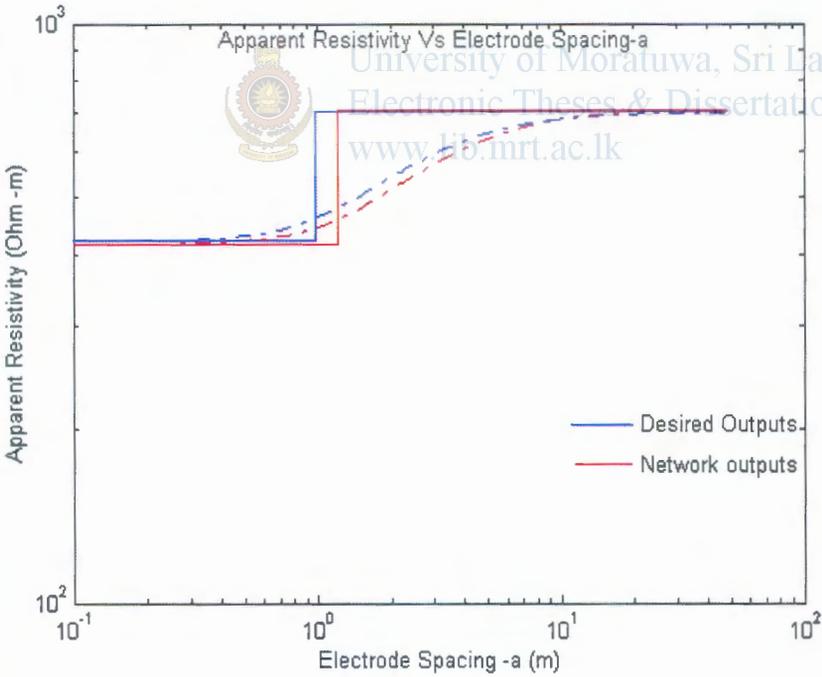
(a)
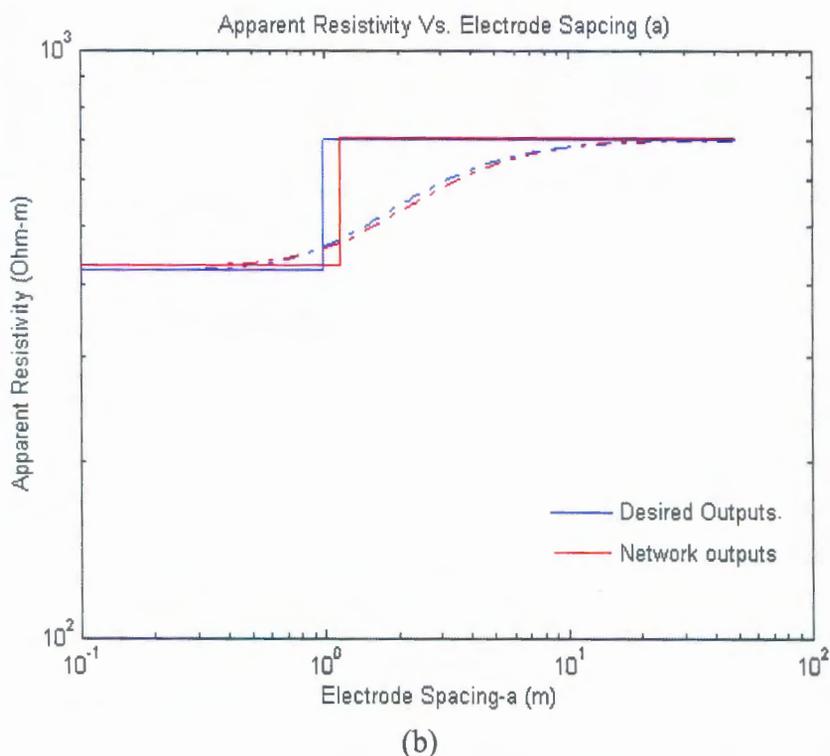
Figure 8.23 - Desired outputs and network outputs for sample 01
(a) Without noise (b) with added noise *(Original is in Color)*

	Parameter	Desired Value	Network Output	
			Noiseless Input	Noisy input
Sample 01	ρ_1	420	415.9854	428.2593
	ρ_2	700	708.7411	704.8135
	h	1.0	1.2078	1.1614

Table 8.2 - Two layer type 1 network output for samples 01 without/with noise inputs

.2.2.2 Two Layer Curve Type2

he simulated and actual parameter values for sample 03 are presented below in Table
.3 and on log log scale (Figure 8.24) with the actual parameters (in blue) and Neural
etwork output parameters (in red).

	Parameter	Desired Value	Network Output	
			Noiseless Input	Noisy input
Sample 03	ρ_1	300	304.6482	307.8346
	ρ_2	100	102.1155	107.3486
	h	1.0	1.0454	0.8240

able 8.3 - Two layer type 2 network output for samples 03 without/with noise inputs

149
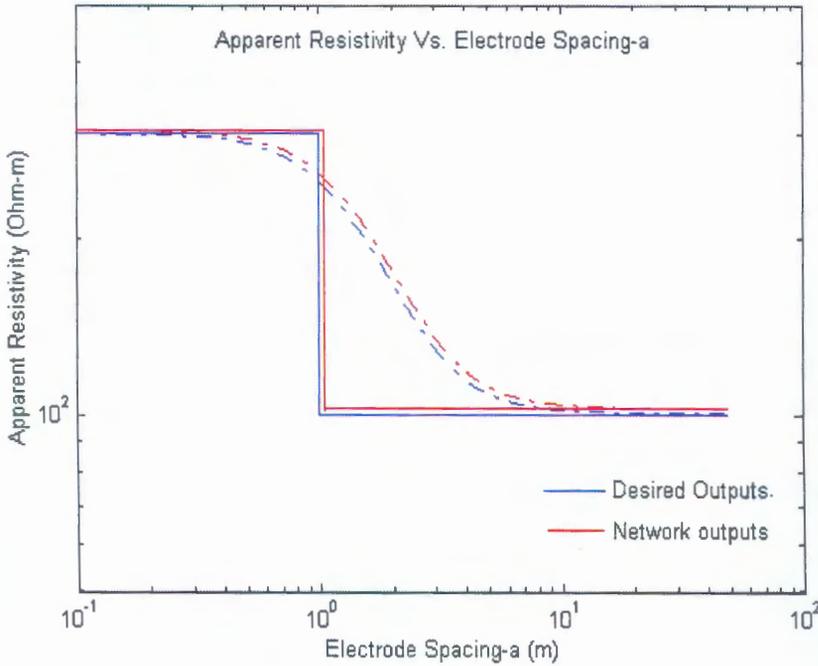
(a)
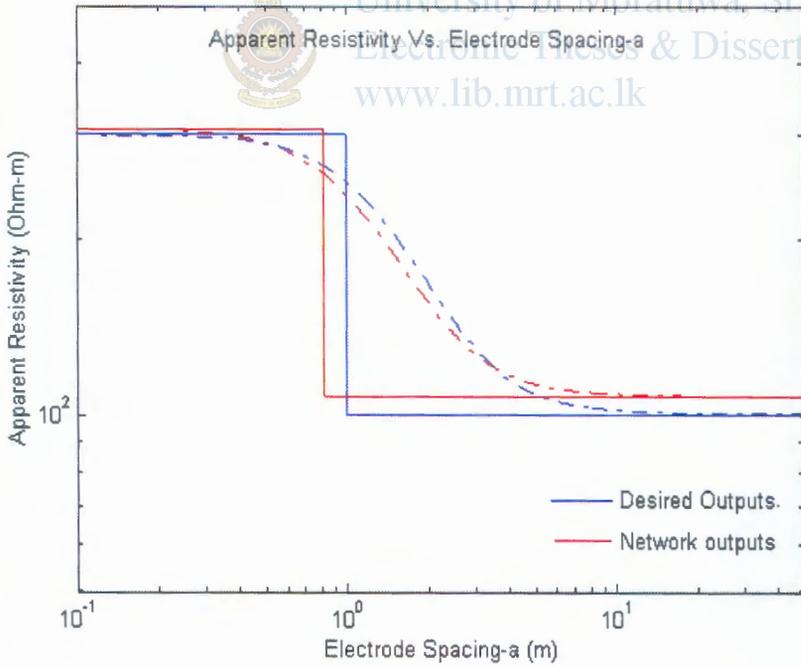
(b)

Figure 8.24 - Desired outputs and network outputs for sample 03
(a) Without noise (b) with added noise *(Original is in Color)*

8.2.3 Three Layer Parameter Determination Network

To evaluate the Network performance on determining three-layer parameter the trained network with two hidden layers with 100 and 260 hidden nodes using the

Resilient Backpropagation is used. The samples 05,07,09 and 11 are chosen from for each curve type A,H,K and Q respectively used from the 150 example test data set for the performance evaluation.

8.2.3.1 Three Layer curve Type A

The simulated and actual parameter values for sample 05 is presented below in Table 8.4 on log log scale (Figure 8.25) with the actual parameters (in blue) and Neural Network output parameters (in red).

| | Parameter | Desired Value | Network Output | |
			Noiseless Input	Noisy Input
	ρ_1	110	111.43	104.56
	ρ_2	500	496.98	513.29
Sample 05	ρ_3	900	905.07	908.73
	h_1	2	1.88	2.1
	h_2	5	5.21	4.7

Table 8.4 - Three layer type A network output for samples 05

(a)

Apparent Resistvity Vs Electrode Spacing
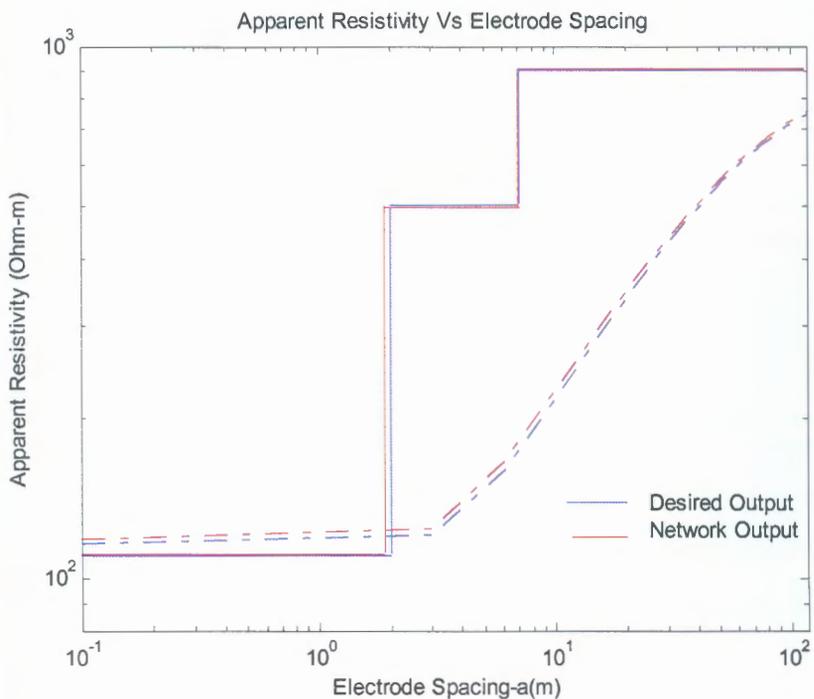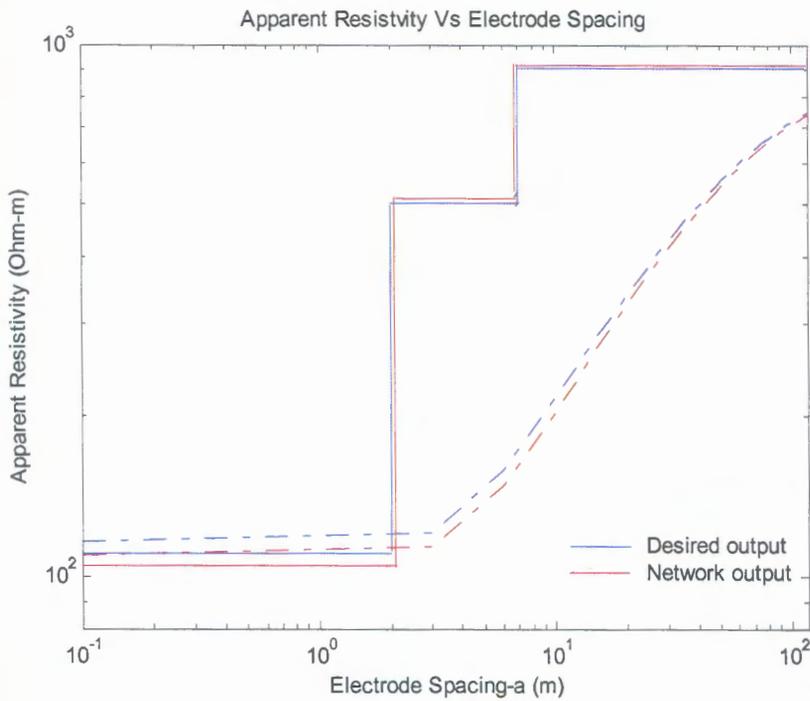
(b)

Figure 8.25 - Desired outputs and network outputs for sample 05
(a) Without noise (b) with added noise *(Original is in Color)*

8.2.3.2 Three Layer curve Type H

The simulated and actual parameter values for sample 07 is presented below in Table 8.5 and on log log scale (Figure 8.26) with the actual parameters (in blue) and Neural Network output parameters (in red).

| | Parameter | Desired Value | Network Output | |
			Noiseless Input	Noisy Input
	ρ_1	560	562.50	566.67
	ρ_2	100	103.27	99.98
Sample 07	ρ_3	800	812.04	797.88
	h_1	5	5.13	5.4
	h_2	2	2.01	1.87

Table 8.5 - Three layer type H network output for samples 07

152

Apparent Resistvity Vs Electrode Spacing

(a)

Apparent Resistivity Vs Electrode Spacing

(b)
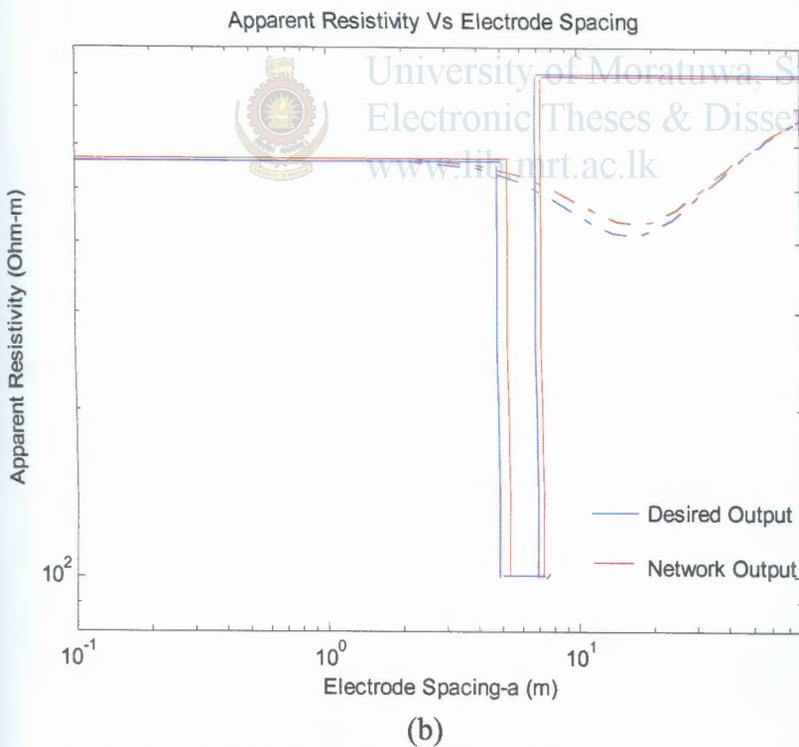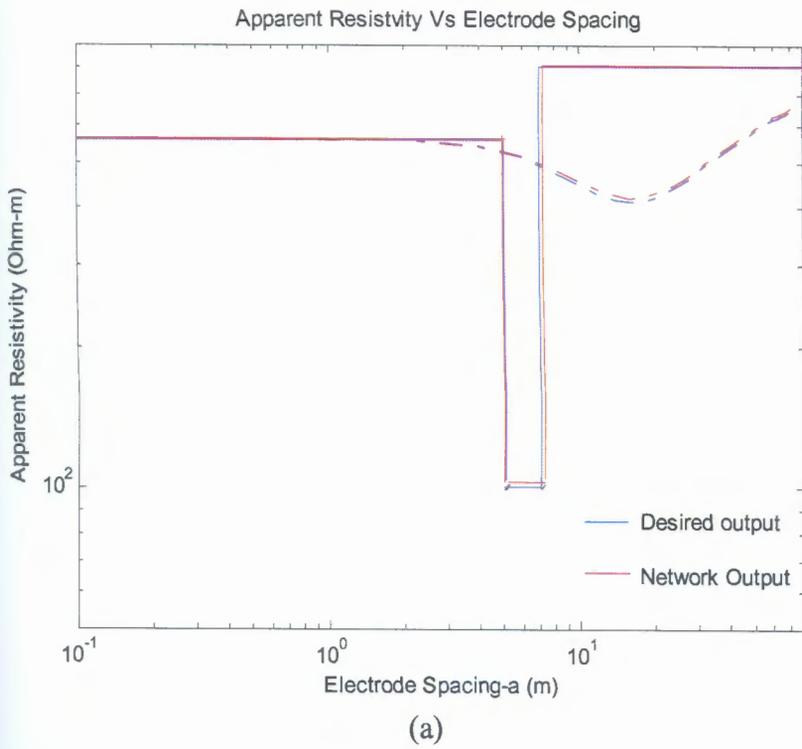
Figure 8.26 - Desired outputs and network outputs for sample 07
(a) Without noise (b) with added noise *(Original is in Color)*

8.2.3.3 Three Layer curve Type K

The simulated and actual parameter values for sample 09 are presented below in Table 8.6 and on log log scale (Figure 8.27) with the actual parameters (in blue) and Neural Network output parameters (in red).
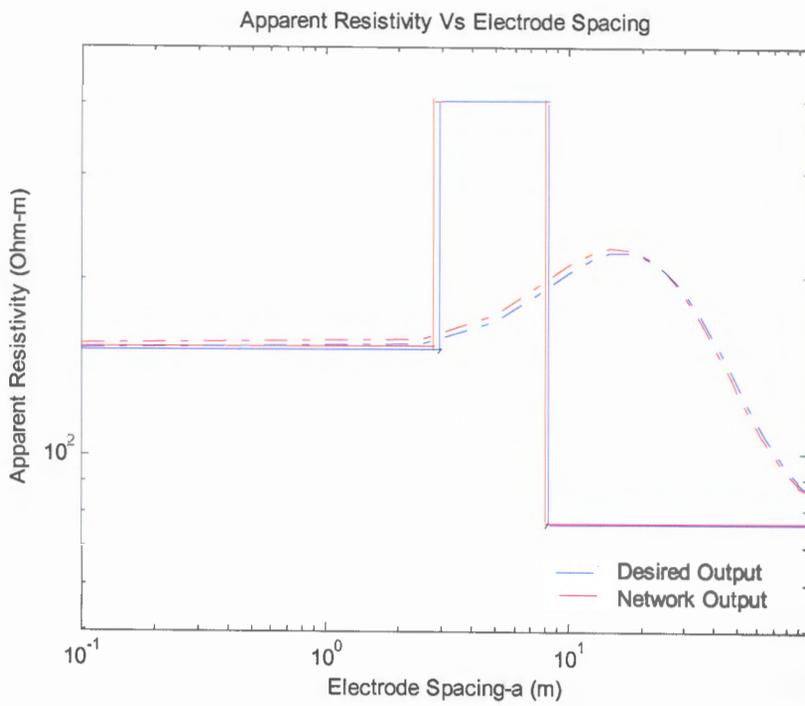
(a)
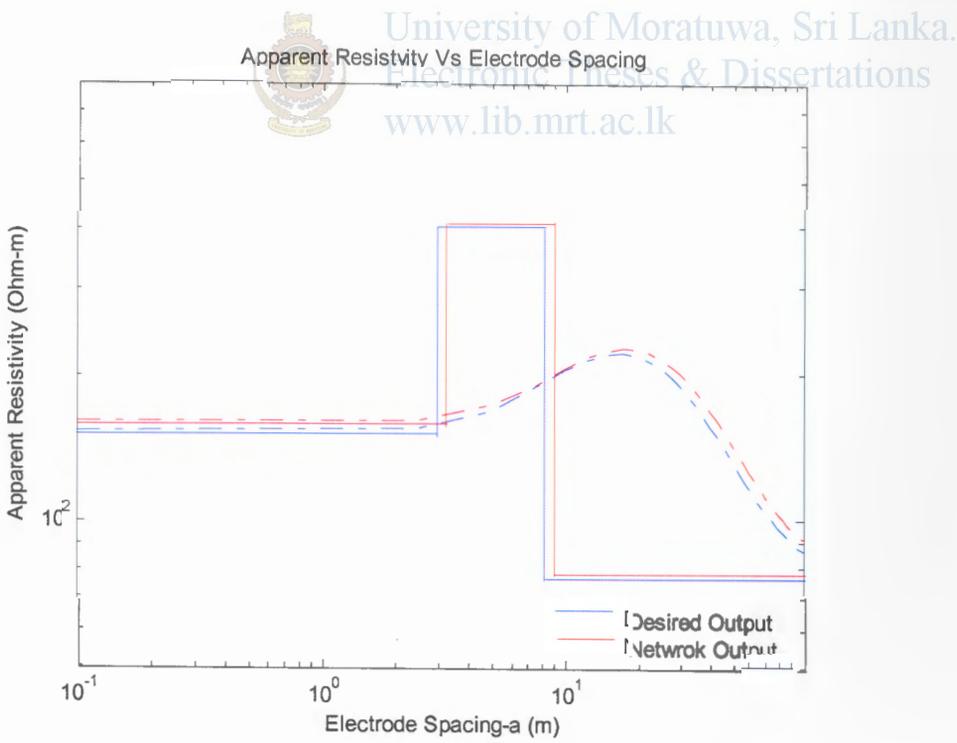
(b)

Figure 8.27 - Desired outputs and network outputs for sample 09
(a) Without noise (b) with added noise *(Original is in Color)*

	Parameter	Desired Value	Network Output	
			Noiseless Input	Noisy Input
Sample 09	ρ_1	150	152.33	158.00
	ρ_2	400	398.07	405.74
	ρ_3	75	75.70	77.34
	h_1	3	2.8	3.32
	h_2	5.4	5.28	5.75

Table 8.6 - Three layer type K network output for samples 09

8.2.3. Three Layer curve Type Q

The simulated and actual parameter values for sample 11 is presented below in Table 8.7 and on log log scale (Figure 8.28) with the actual parameters (in blue) and Neural Network output parameters (in red).

(a)

Apparent Resistivity Vs Electrode Spacing
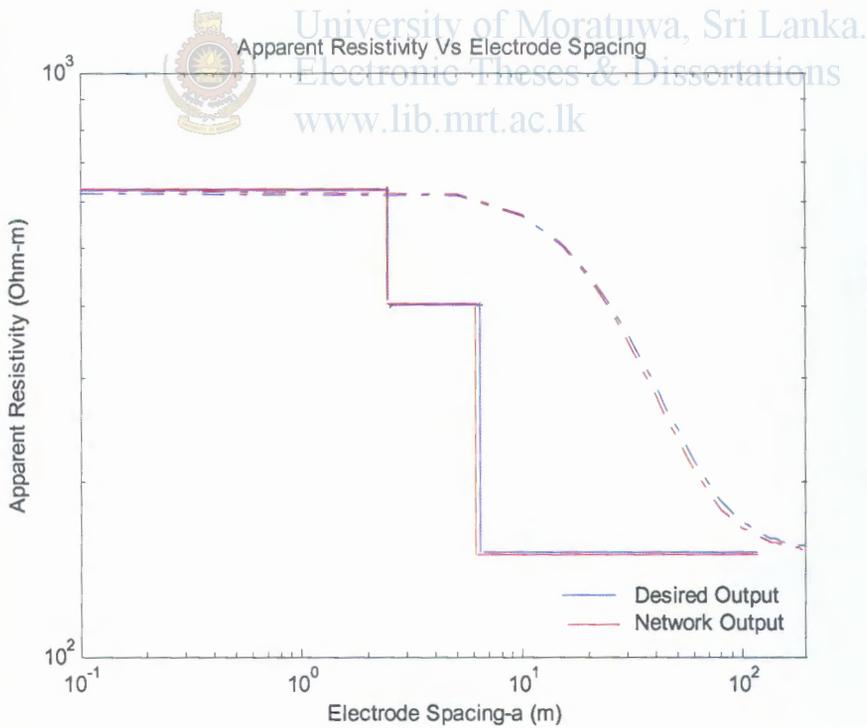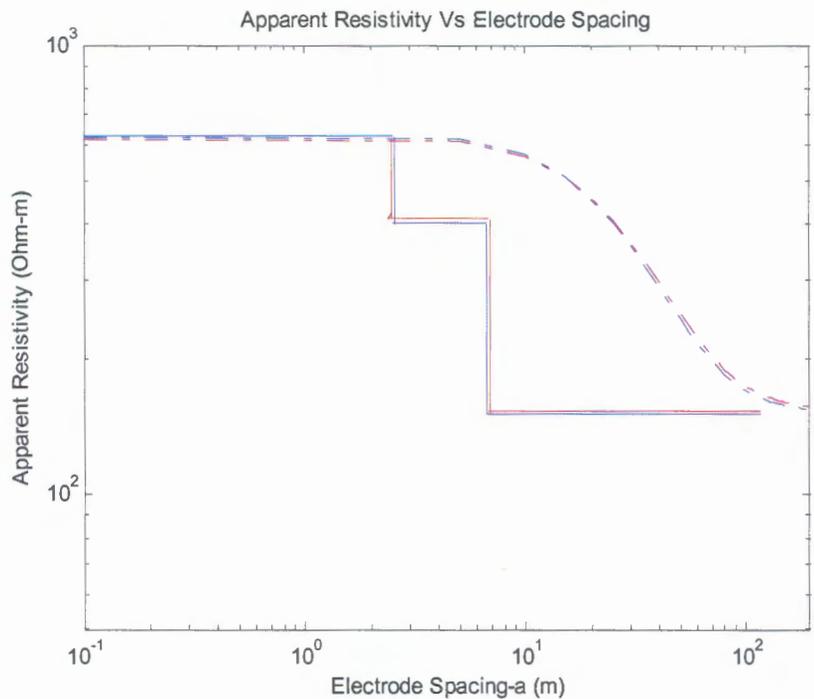
(b)

Figure 8.28 - Desired outputs and network outputs for sample 11
(a) Without noise (b) with added noise *(Original is in Color)*

	Parameter	Desired Value	Network Output	
			Noiseless Input	Noisy Input
	ρ_1	625	631.26	623.33
	ρ_2	400	402.04	411.50
Sample 11	ρ_3	150	149.0	152.54
	h_1	2.5	2.43	2.36
	h_2	4.1	3.8	4.36

Table 8.7 - Three layer type Q network output for samples 11

8.2.4 Network Performance for the Field Data

The playground of University of Moratuwa was selected as the field data acquisition site. The field data was collected with a Wenner array using the Fluke 1623 Earth/Ground Tester (Figure 8.29). Data was acquired in two perpendicular directions and the averaged value was used for simulations. Figure 8.30 shows the field arrangement used in the survey.

Figure 8.29 - Fluke tester used for data acquisition

Figure 8.30 - (a) Spike connection to earth (b) changing array spacing along the field line *(Original is in Color)*

The Field data is given in Table 8.8. Apparent resistivity for the measured Resistance is calculated using the equation (2.38). The Field data is plotted on log log scale (Figure 8.31).

Electrode Spacing (m)	Measured Resistance (Direction 1) (Ω)	Apparent Resistivity (Direction 1) ($\Omega\,m$)	Measured Resistance (Direction 2) (Ω)	Apparent Resistivity (Direction 2) ($\Omega\,m$)	Average Apparent Resistivity ($\Omega\,m$)
0.5	149.60	469.98	136.00	427.26	448.62
1.0	115.50	725.71	76.90	483.18	604.44
1.5	92.10	868.02	73.30	690.84	779.43
2.0	62.20	781.63	60.20	756.50	769.06
2.5	42.50	667.59	46.10	724.14	695.86
3.0	30.60	576.80	36.30	684.24	630.52
3.5	24.70	543.18	27.20	598.16	570.67
4.0	21.20	532.82	21.20	532.82	532.82
4.5	18.21	514.88	16.86	476.71	495.79
5.0	16.21	509.25	14.39	452.08	480.66
5.5	14.17	489.68	12.53	433.01	461.34
6.0	12.07	455.03	10.77	406.02	430.52
6.5	10.70	437.00	9.39	383.50	410.25
7.0	10.00	439.82	8.36	367.69	403.76
7.5	9.70	457.10	7.55	355.79	406.44
8.0	8.85	444.85	6.23	313.15	379.00
8.5	7.66	409.10	6.20	331.12	370.11
9.0	6.88	389.06	5.69	321.76	355.41
9.5	6.47	386.20	5.23	312.18	349.19
10.0	6.00	376.99	4.81	302.22	339.61
10.5	5.53	364.83	4.45	293.58	329.21
11.0	5.14	355.25	4.15	286.83	321.04
11.5	4.90	354.06	3.89	281.08	317.57
12.0	4.48	337.78	3.67	276.71	307.25
12.5	4.40	345.58	3.45	270.96	308.27
13.0	4.20	343.06	3.19	260.56	301.81
13.5	3.91	331.66	2.97	251.92	291.79
14.0	3.71	326.35	2.75	241.90	284.13
14.5	3.53	321.61	2.54	231.41	276.51
15.0	3.39	319.50	2.36	222.43	270.96
15.5	3.20	311.65	2.20	214.26	262.95
16.0	3.04	305.61	2.10	211.12	258.37
16.5	2.91	301.69	2.00	207.35	254.52
17.0	2.74	292.67	1.87	199.74	246.21
17.5	2.59	284.79	1.79	196.82	240.80
18.0	2.48	280.48	1.73	195.66	238.07
18.5	2.40	278.97	1.64	190.63	234.80
19.0	2.40	286.51	1.54	183.85	235.18
19.5	2.12	259.75	1.45	177.66	218.70
20.0	1.98	248.81	1.39	174.67	211.74

Table 8.8 - Field data and calculated averaged apparent resistivity values.
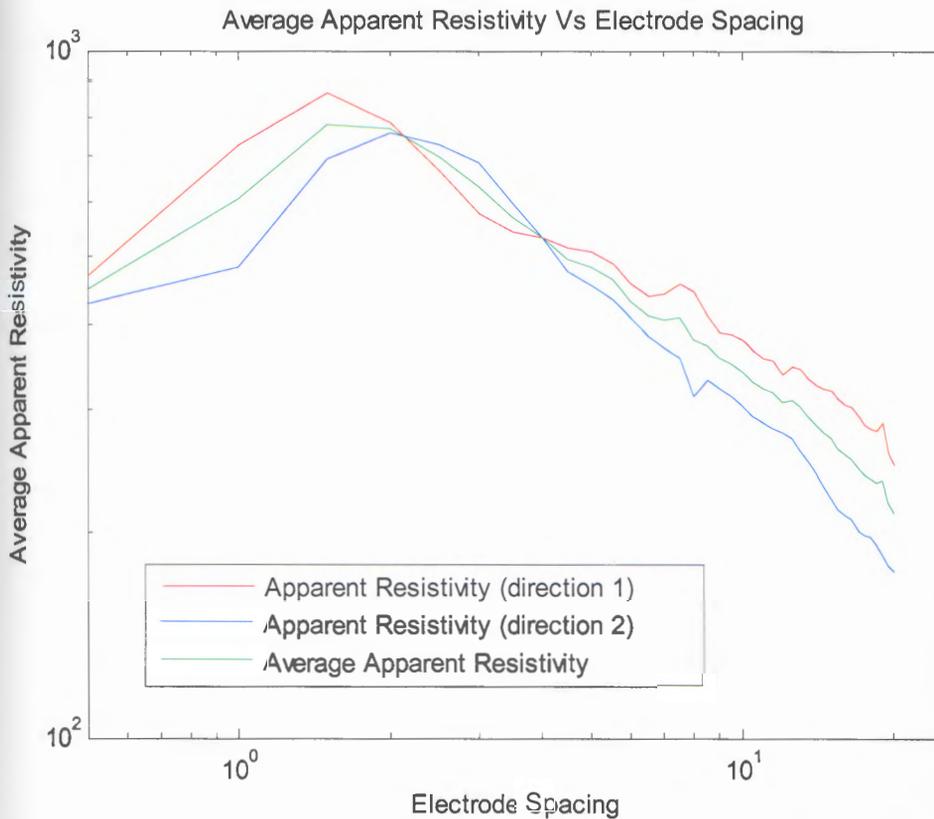
Figure 8.31- Resistivity curve of the field data *(Original is in Color)*

The average resisitivity measurements were then input to the neural network trained for curve identification. The results obtained are given in Figure 8.32; the network output classified the field data as a three layer type H with a 76.77% probability. Then to determine on the One dimensional parameters the same average resistivity values were input to the trained Three layer parameter estimating network, where the network output gave the following layer parameters given in Table 8.9.

In order to validate the network performance next step was to compare the theoretical and measured electrode resistance of an electrode buried in the point where the apparent resistivity measurements were taken. For this a 4.6 feet, 2 inch diameter GI pipe was buried and the earth resistance of the electrode was measured with the same Earth/Ground tester. The electrode arrangement was set up similar as shown in Figure 5.11. The electrode spacing between X and Y is set to 20.0m's, this was selected as to avoid the overlap of resistance areas. The electrode resistance measured is given in Table 8.10.
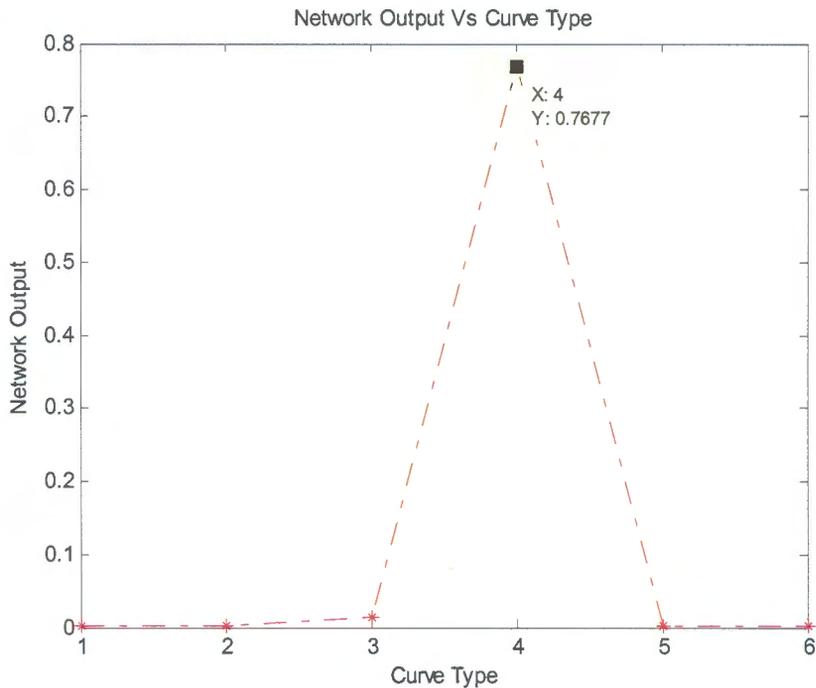
Figure 8.32 - Curve Identification network output for field data

Parameter	Network Output
First Layer Resistivity ρ_1	$800.45\,\Omega m$
Second Layer Resistivity ρ_2	$593.05\,\Omega m$
Bottom Layer Resistivity ρ_3	$897.87\,\Omega m$
First Layer height h_1	$5.71\,m$
Second Layer height h_2	$20.75\,m$

Table 8.9 - Earth parameters determined by the trained neural network

Electrode Spacing between X and Z (m)	Electrode Resistance (Ω)
8	452.01
10	452.01
12	452.02

Table 8.10 - Measured Electrode Resistance

Therefore the Electrode Resistance value was measured as $452.01\,\Omega$. Now using the theoretical equations in sections 5.7.1 and 5.7.2 the electrode resistance was calculated for the buried GI pipe using the parameters given in Table 8.9. The Mathematica 5.0 software was used for the electrode resistance calculations. The Mathematica codes

160

are given in Appendix I. Though it's a three layer predicted medium the electrode length (≈ 1.4m) is less than the First layer height ($5.71\,m$). Therefore the equation (5.25) was used for the calculations since the current source is now only in the first layer. Therefore the final equation used in the calculation is,

Substituting N=2,

$$V_1 = \frac{\rho_1 I_1}{2\pi l} \int_0^\infty \frac{e^{-\lambda t} + k_1 e^{-2\lambda h_2} e^{\lambda t}}{1 - k_1 e^{-2\lambda h_1}} J_0(\lambda x) d\lambda \tag{8.1}$$

$$R = \frac{V_1(a)}{I_1} \tag{8.2}$$

$$R = \frac{\rho_1}{2\pi l} \int_0^\infty \frac{e^{-\lambda t} + k_1 e^{-2\lambda h_2} e^{\lambda t}}{1 - k_1 e^{-2\lambda h_1}} J_0(\lambda x) d\lambda \tag{8.3}$$

The calculated Electrode resistance was $424.421\,\Omega$.

8.3 Neural Network Model Optimization Results for Two Dimensional Inversion

8.3.1 Two Dimensional CASE 1
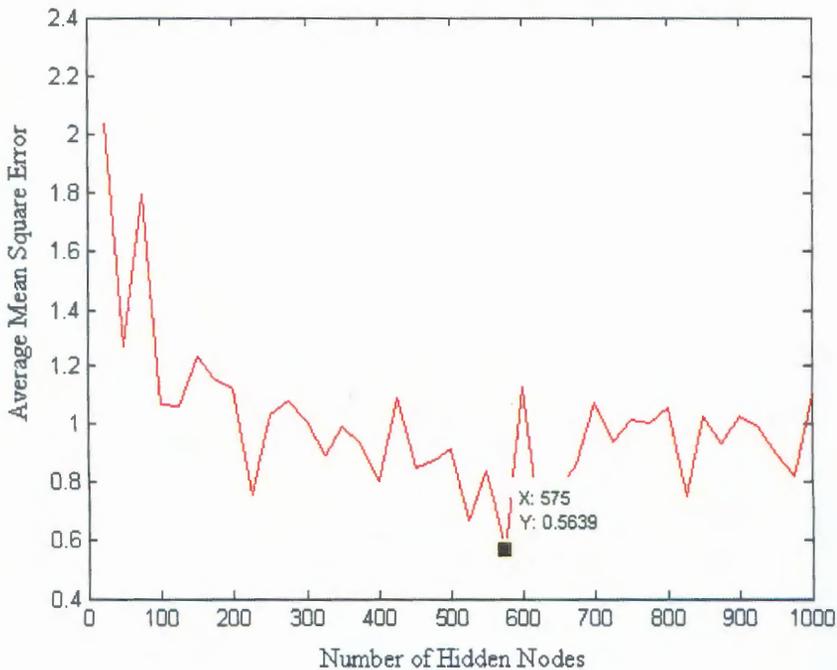
Figure 8.33 - Training Performance for the Training Function 'Trainrp' with different no of hidden nodes (single hidden layer)-2D CASE 1

Figure 8.33 shows the training performance of the Resilient Back propagation algorithm with Single hidden layer. The Mean square error is calculated with the average performance on 15 networks with different initializations. With the above results it is seen that the minimum error of 0.56 is achieved with 575 single hidden layer nodes of the network In order to seek for the ability of the network to achieve a much satisfactory error level secondly several training sessions are carried out with two hidden layers.

The training sessions with two layers was initiated with 200 nodes in the first layer. From Figure 8.34(a) it is seen that no considerable reduction of the error level is taken place while the nodes in the first layer are increased to 275 in 25 steps. But proceeding with 50 steps in nodes Figure 8.34(b) shows that the error levels have reduced satisfactorily. Further proceeding, the results shown in Figure 8.34(c) shows that after 500 nodes in the first hidden layer the error levels converge around 0.006.

Since an acceptable low error level is achieved training was terminated and the network was finalized, with two hidden layers the lowest average training error nearly

equal to 0.002 is achieved at 500 ,700 hidden nodes for the first hidden layer and second hidden layer respectively. The network performance for the finalized network is shown in Figure 8.35. The training, validation and test error variation (on unseen data) is shown.

(a)

(b)

163
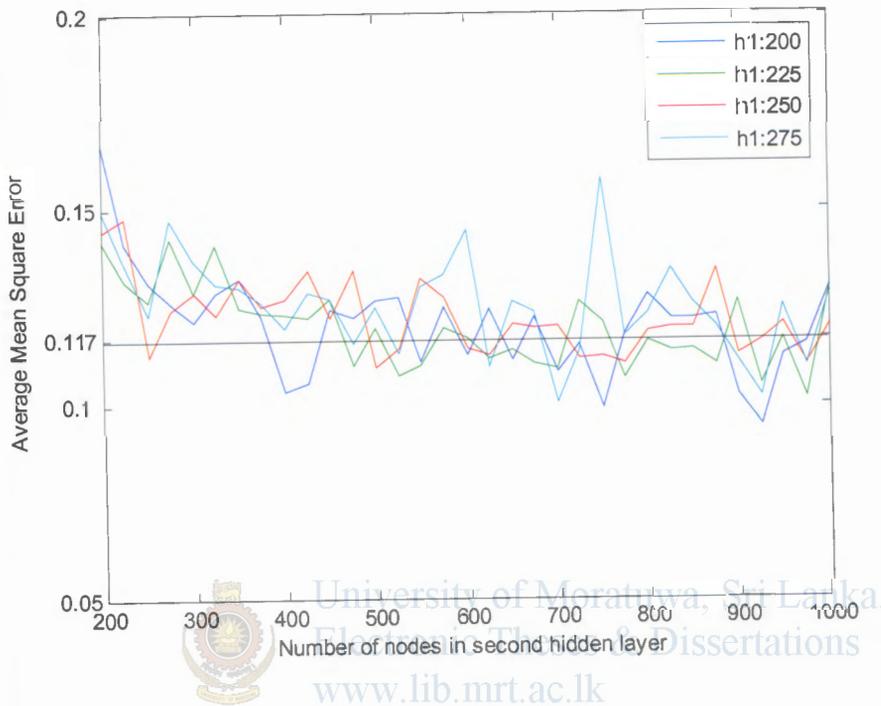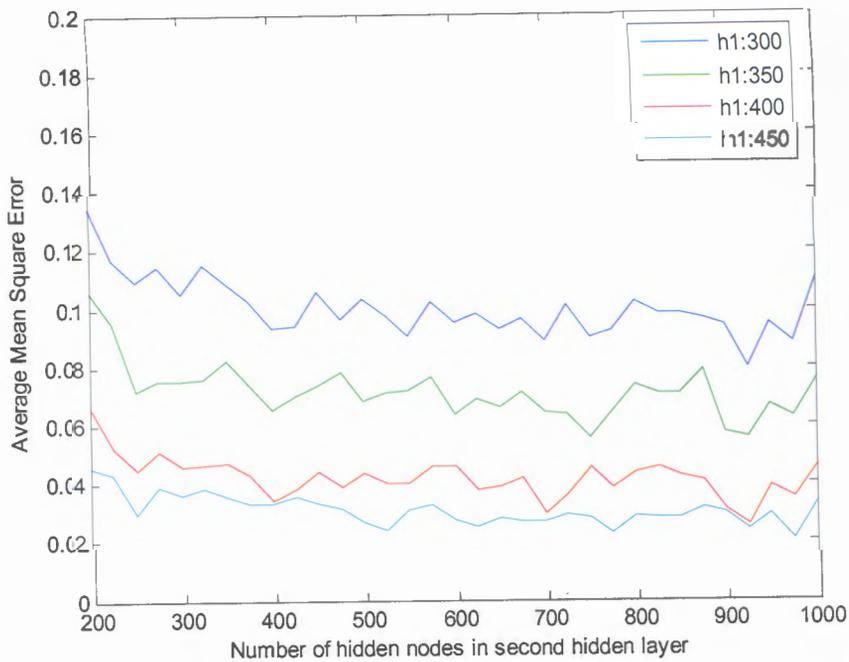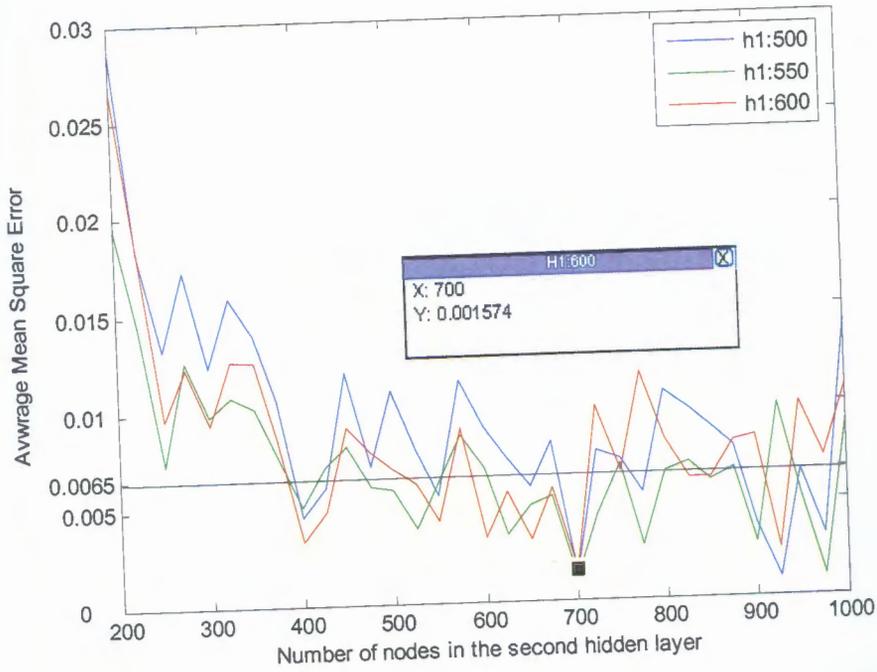
(c)

Figure 8.34 - Training Performance of two hidden layer network for 2D CASE 1.
h1: number of nodes in the first hidden layer
(Original is in Color)
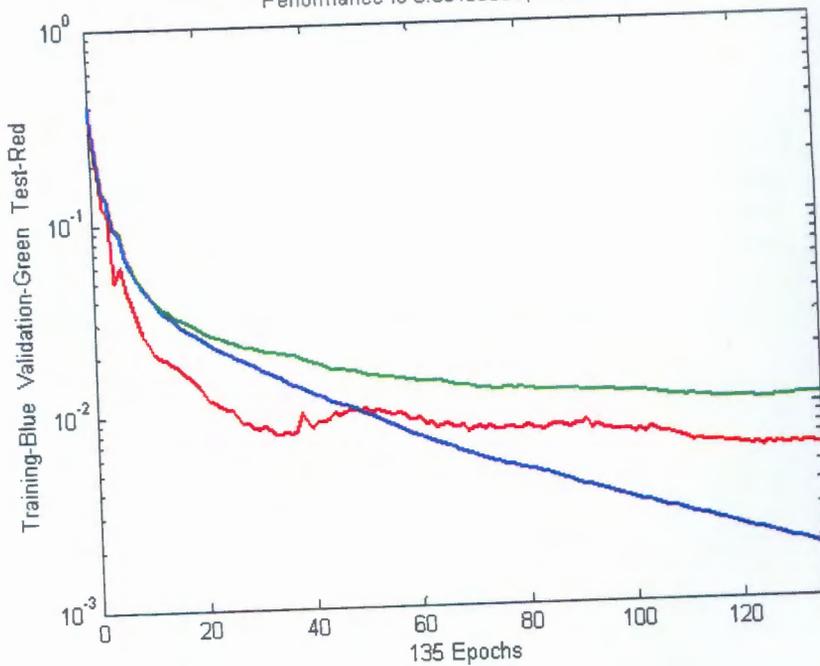
Figure 8.35 - Training, validation and Test performance of the
finalized Network-2D CASE 1
(Original is in Color)

8.3.2 CASE 2 Network Optimizing
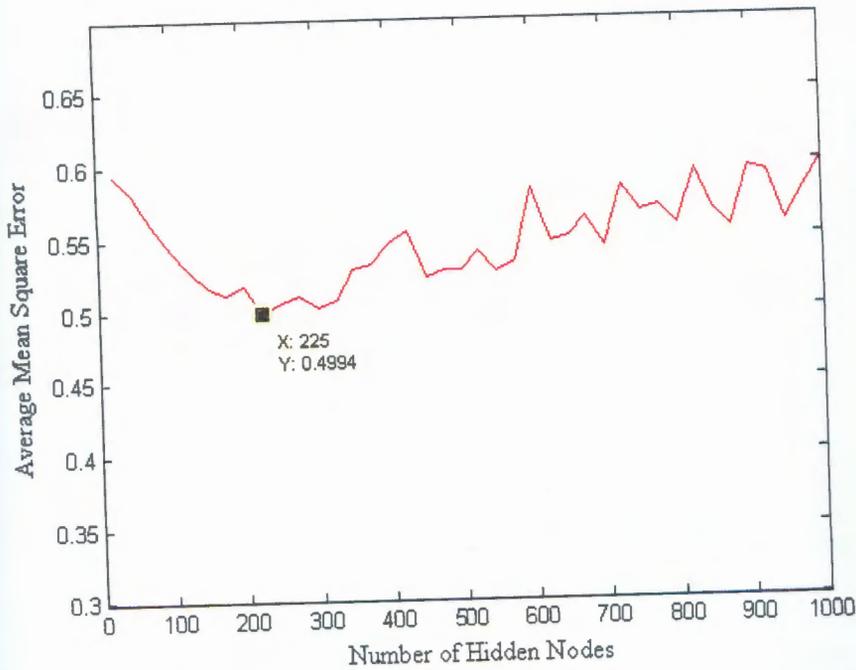
Figure 8.36 - Training Performance for the Training Function 'Trainrp' with different no of hidden nodes (single hidden layer) - 2D CASE 2

The Resilient backpropagation is used for the training and Figure 8.36 shows the Single hidden layer performance of the network. The minimum error of 0.5 is achieved at 225 hidden nodes.
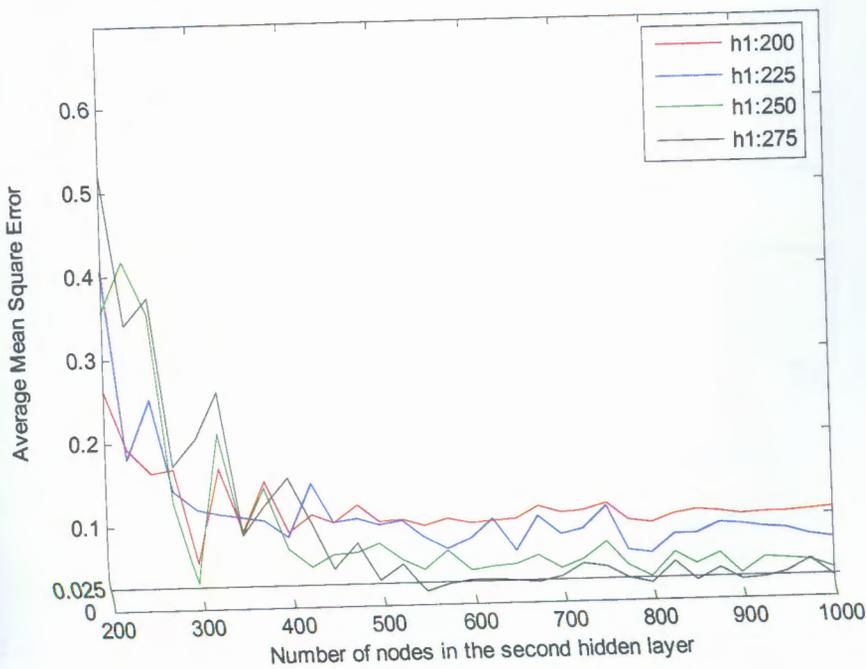
(a)
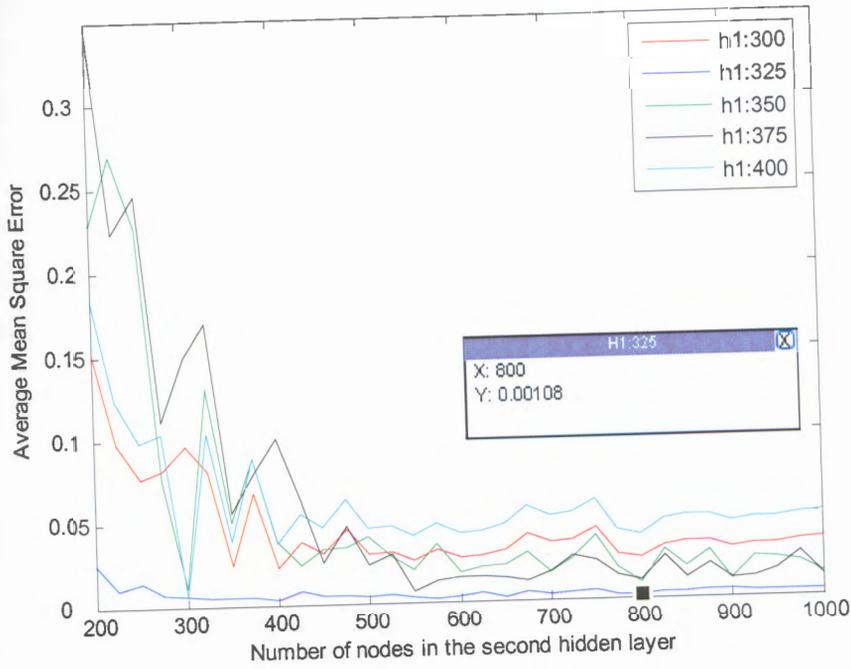
(b)

Figure 8.37 - Training Performance of two hidden layer network for 2D CASE 2
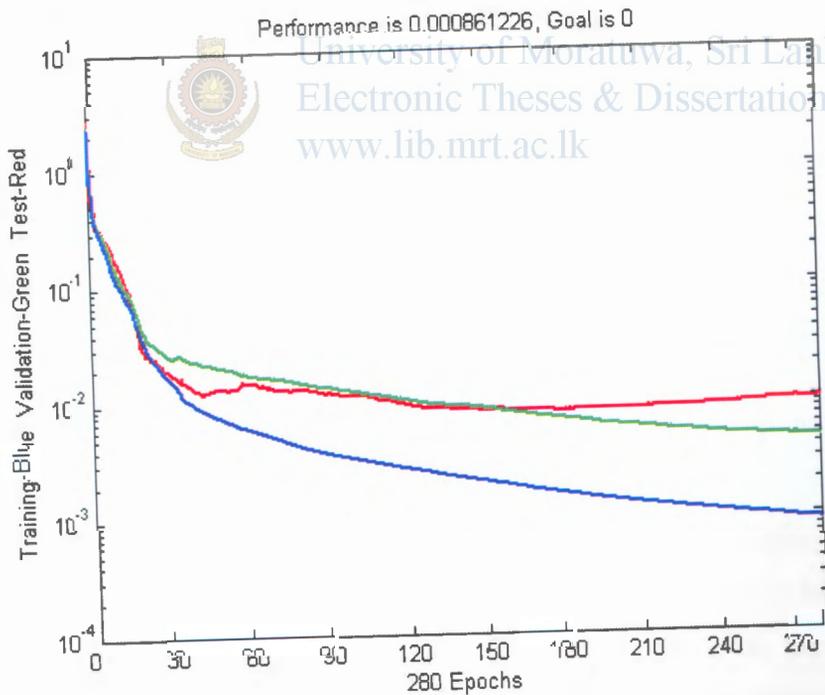
Figure 8.38 -Training, validation and Test performance of the
finalized Network-2D CASE 2 *(Original is in Color)*

For the 2D case 2, the training performance for two hidden layers with variable no of
hidden nodes is shown in Figure 8.37. Training was preceded from 200 hidden nodes
for the first hidden layer. First the training error levels tend to decrease with the

166

number of nodes in the first hidden layer and converged as the number of nodes in the second hidden layer increased (Figure 8.37(a)). But when the number of hidden nodes exceeded 325 in the first layer the training error levels are seen increasing, however converging when the number of second hidden layer nodes increases. From Figure 8.37(b), the minimum average training error is achieved with 325,800 nodes for first and second hidden layers respectively. Since the errors are within acceptable low values this architecture for 2D case 2 is finalized with two hidden layers. The network performance for the finalized network is shown in Figure 8.38.

8.3.3 CASE 3 Network Optimizing
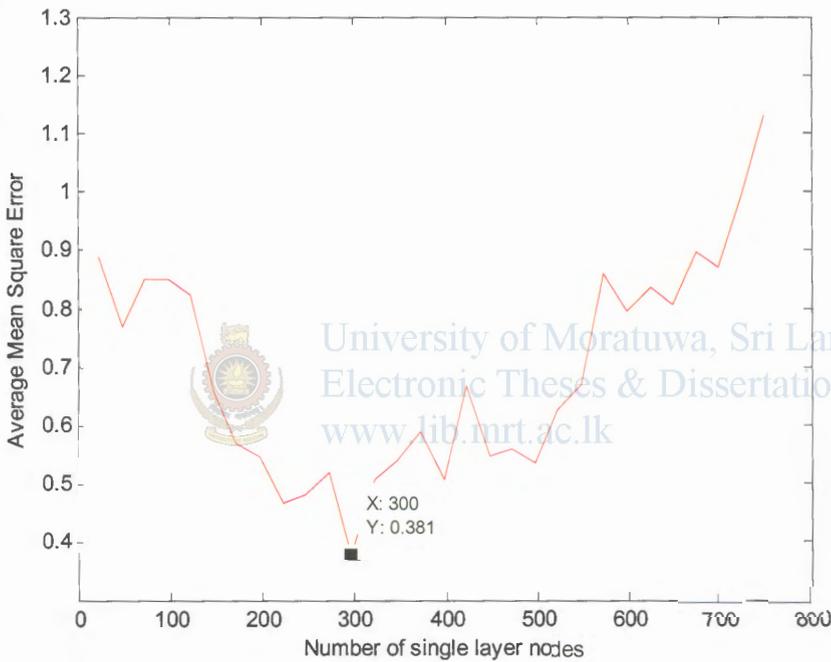
Figure 8.39 - Training Performance for the Training Function 'Trainrp' with different no of hidden nodes (single hidden layer) - 2D CASE 3

Similarly as in the previous cases the training was preceded with single hidden layer and two hidden layers preliminary. The single layer average minimum error of 0.381 was achieved at 300 hidden nodes (Figure 8.39). Figure 8.40 gives the two hidden layer training performance. The number of nodes in the first hidden layer was increased from 200 to 375 in 25 steps. The error initially reduced with the increasing number of hidden nodes in the second hidden layer and secondly converged. However the converging error levels were approximately equal to 0.04 irrespective of the number of nodes in the first hidden layer. Therefore training with two layers was terminated. The minimum average error in this case was 0.0198 at 250 and 700 nodes in the first and the second hidden layers respectively.

167
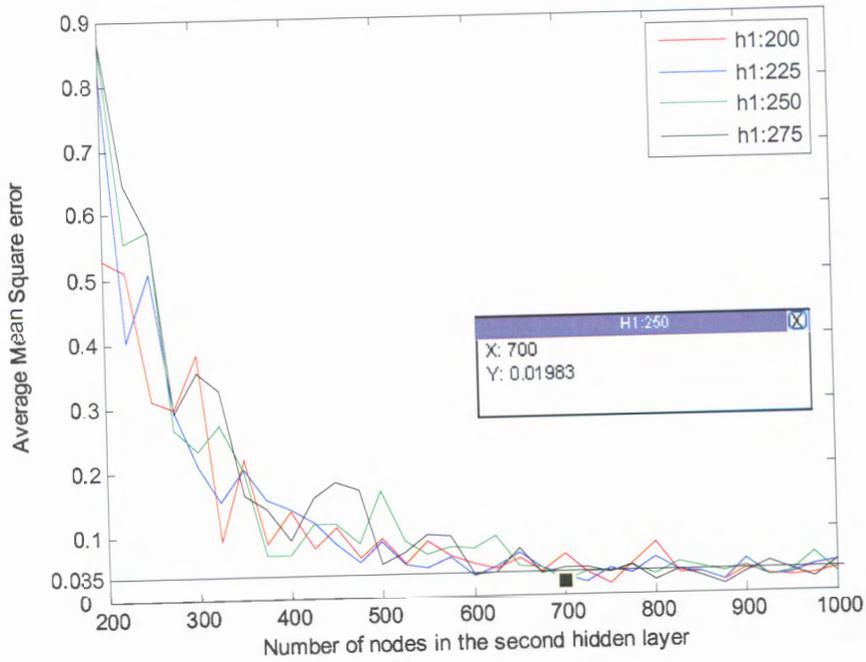
(a)
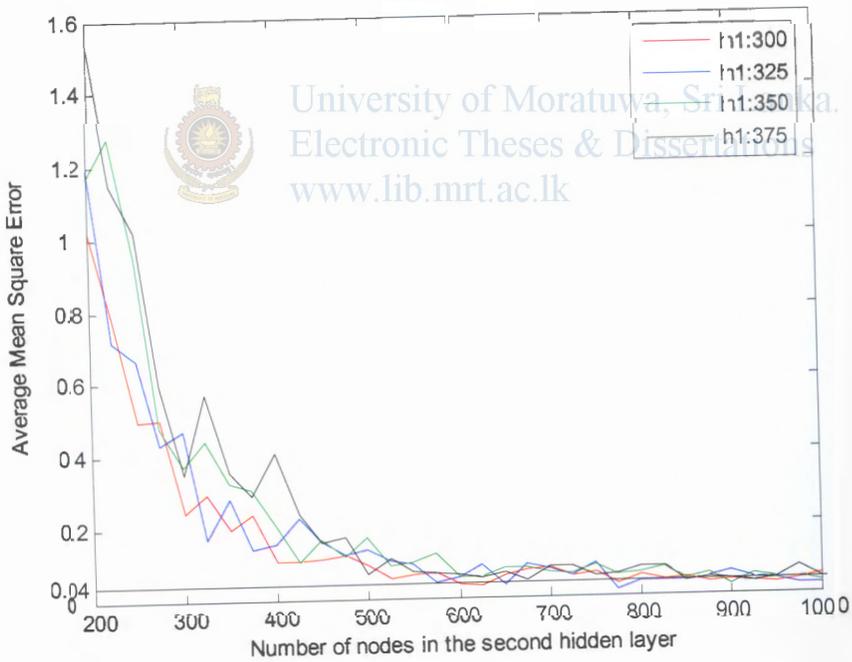
(b)

Figure 8.40 - Training Performance of two hidden layer network for 2D CASE 3
(Original is in Color)

In order to evaluate the error performance with an additional hidden layer, a third layer was introduced. Referring Figure 8.41(a) to Figure 8.41(c) it is evident that the average training error levels tend to reduce with the increasing number of hidden nodes in both the first and the second hidden layers. However the error level variation for a fixed first and second layer combination decreases preliminary and then starts

increasing giving an optimum point. But it is observed that these minimum average error values are still higher compared to the two layer performance, which is 0.064 being the minimum. Therefore further training was halted.
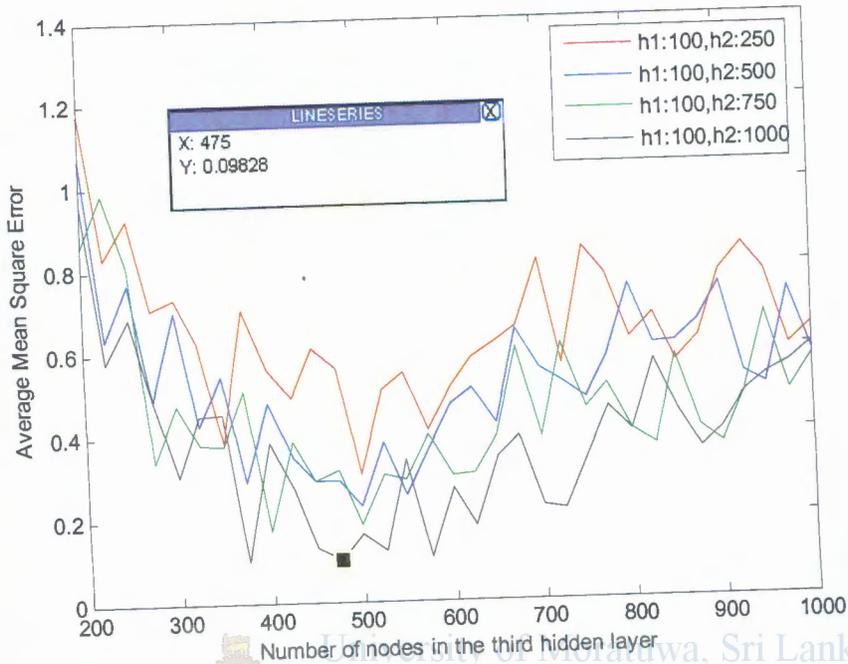
(a)

(b)

169
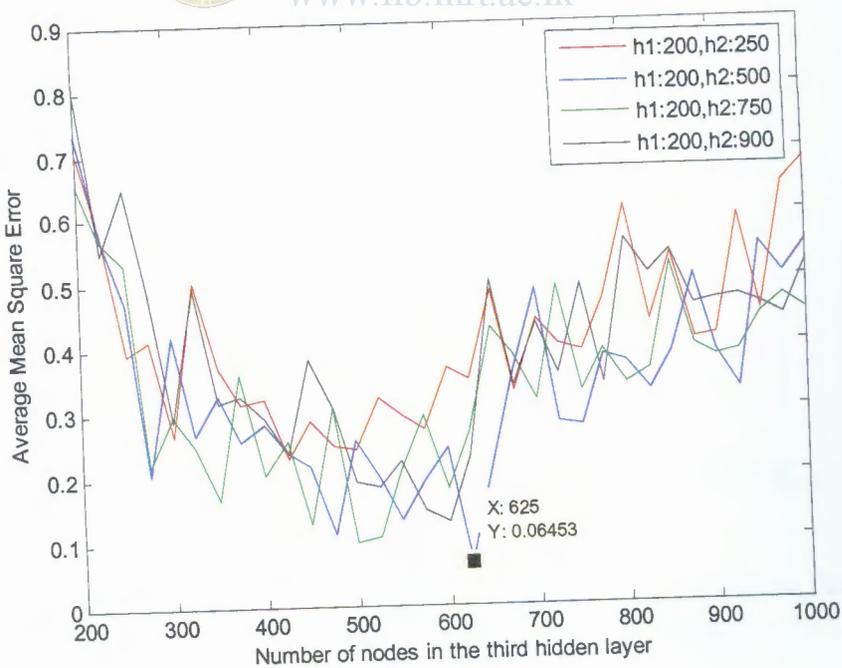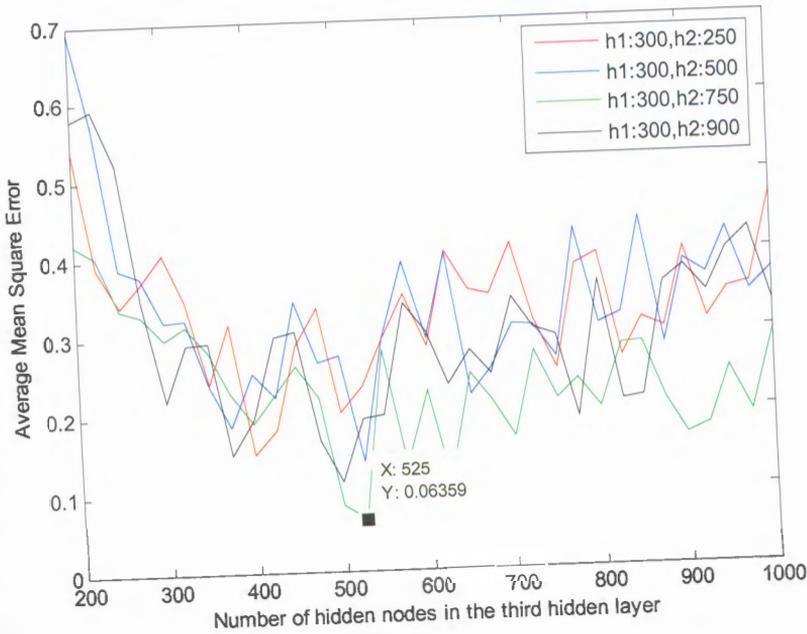
(c)

Figure 8.41 - Training Performance of three hidden layer network for 2D CASE 3
(Original is in Color)

Figure 8.42 gives the training, validation and test performance of the finalized network with 250 and 700 nodes in the respective first and second hidden layers.
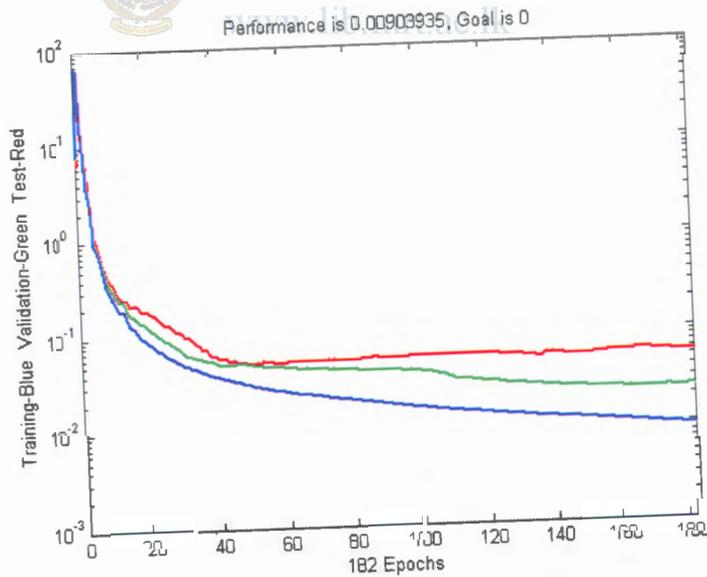
Figure 8.42 - Training, validation and Test performance of the finalized Network-2D CASE 3 *(Original is in Color)*

8.4 Simulation Results and Performance of the Two dimensional Inversion

In testing an inversion method using synthetic data, the quality of the inversion model can be gauged against the known true subsurface model. Following are the simulation

170

outputs of the optimized and trained Neural Networks for theoretical inputs, which were unseen by the networks in their training phases. In order to evaluate how strong the networks will predict for the field data, different percentages of White Gaussian Noise is added to the theoretically generated field data.

8.4.1 Two dimensional CASE1

To evaluate the Network performance on inversion of field data for the detection of an embedded 100 Ωm anomalous body in a 1000 Ωm homogeneous medium the trained network with two hidden layers with hidden nodes using the Resilient Backpropagation is used. 10 test data with different mesh assignments (different sizes, shapes and positions of the anomalous body) with different noise levels is tested with the finalized network. The network performance and the commercial software inversion results for the same test samples is evaluated and compared below.

The trained network will output the resistivity values of the 385 blocks. One such example output for test grid 1 (Figure 8.43(a)) is given in the Appendix J. Although there are changes in the individual cell values they are not clearly visualized with the color variation in the Matlab's cell based output. This is due to manner of color distribution in the color bar. Therefore with a separate Matlab routine a smoothed output was generated (Figure 8.43(d) and Figure 8.44(d)).
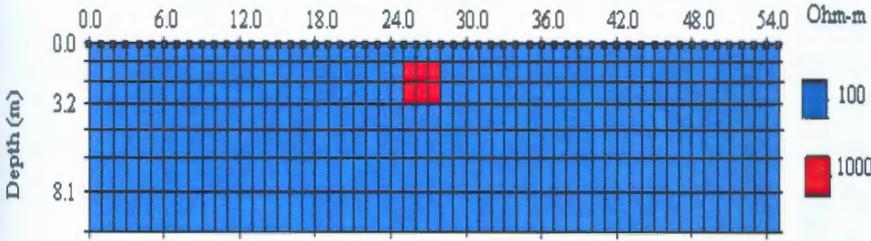
(a)
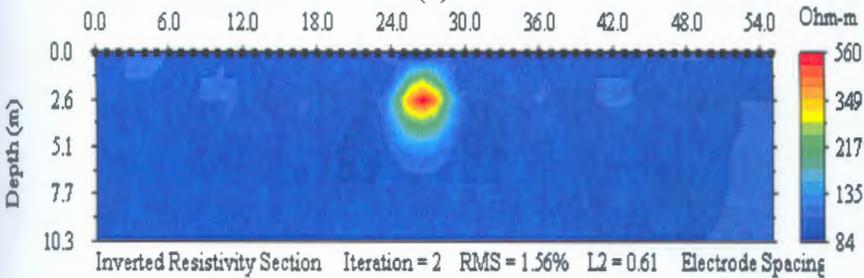
(b)
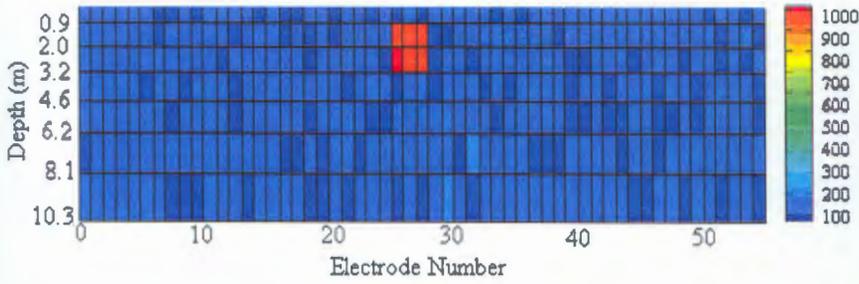
(c)
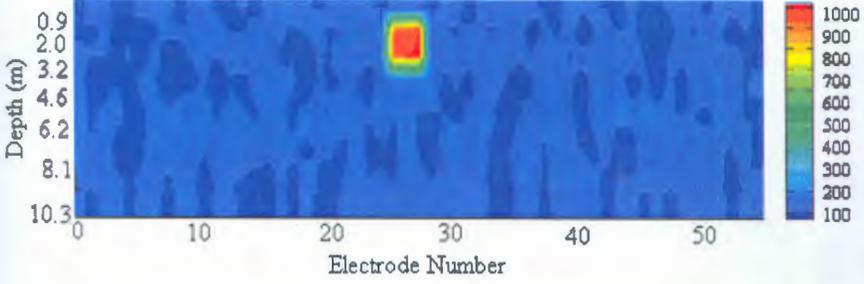
(d)

Figure 8.43 - (a) Test grid 1
(b) The smooth inversion output of the commercial program
(c) Block based inversion from the neural network output for 1.5% noise
(d) Smoothed output of (c) *(Original is in Color)*

(a)

Inverted Resistivity Section   Iteration = 3   RMS = 2.11%   L2 = 1.11   Electrode Spacing

(b)

(c)

(d)
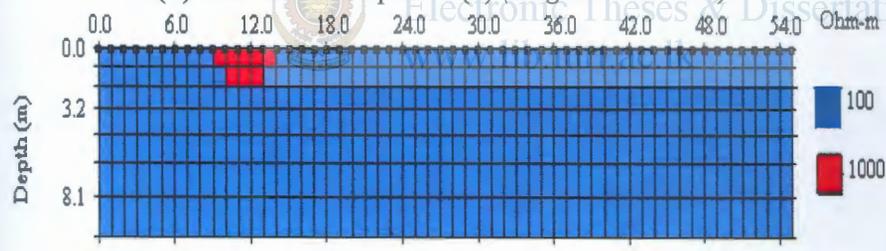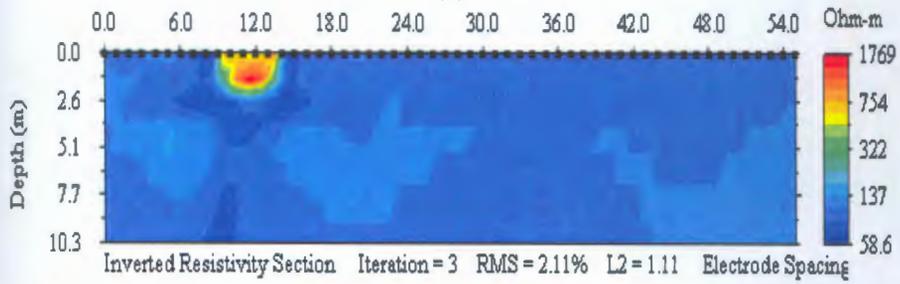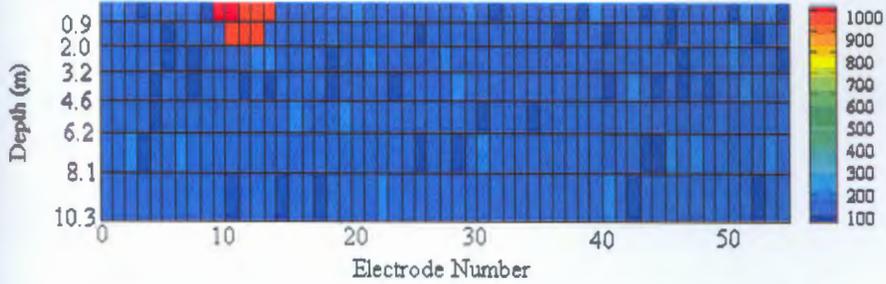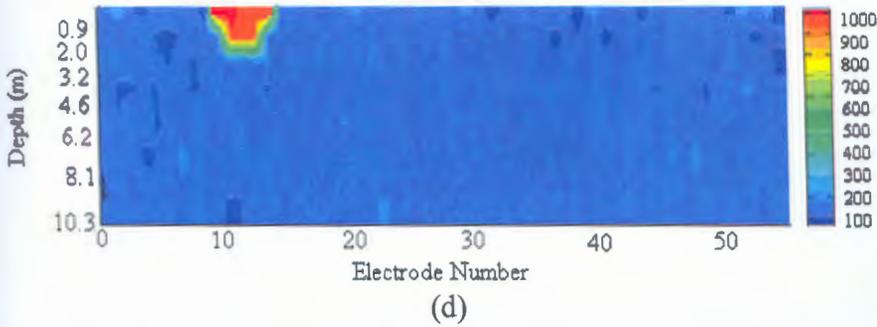
Figure 8.44 - (a) Test grid 2
(b) The smooth inversion output of the commercial program
(c) Block based inversion from the neural network output for 1% noise
(d) Smoothed output of (c) *(Original is in Color)*

(a)

Inverted Resistivity Section   Iteration = 1   RMS = 1.17%   L2 = 0.34   Electrode Spacing

(b)

(c)
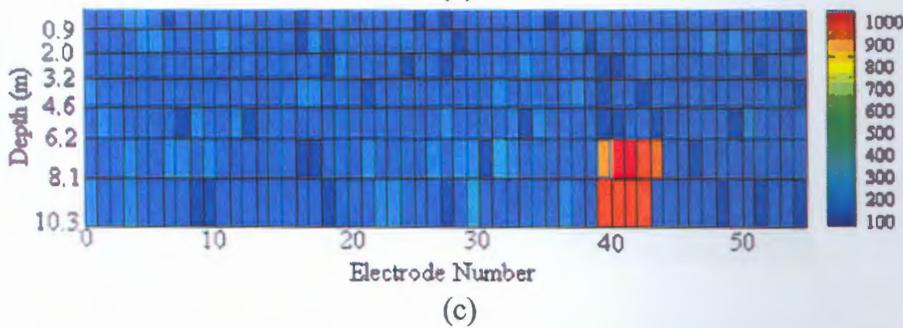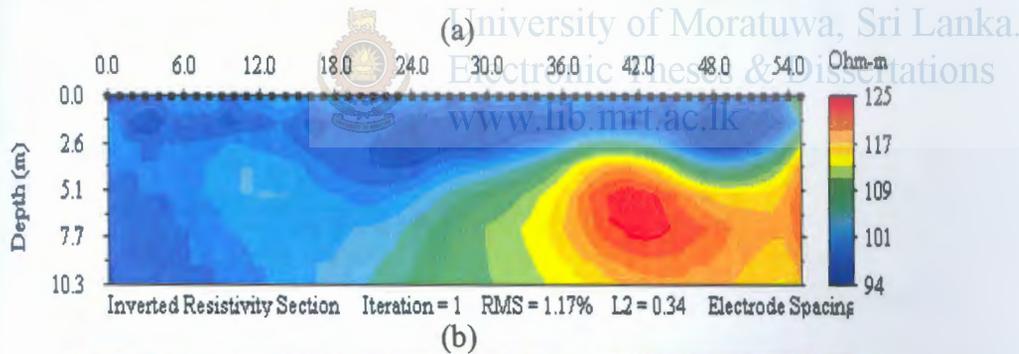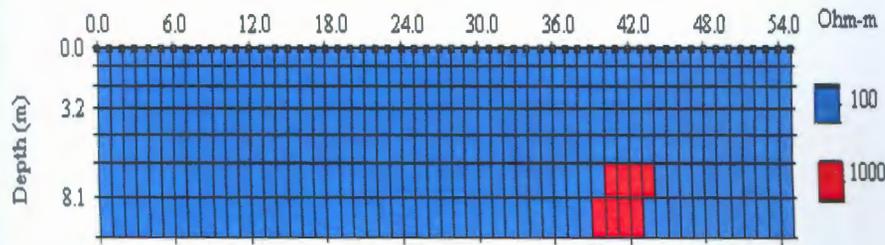
Figure 8.45 - (a) Test grid 3
(b) The smooth inversion output of the commercial program
(c) Block based inversion from the neural network output for 2.0% noise
*(Original is in Color)*

173
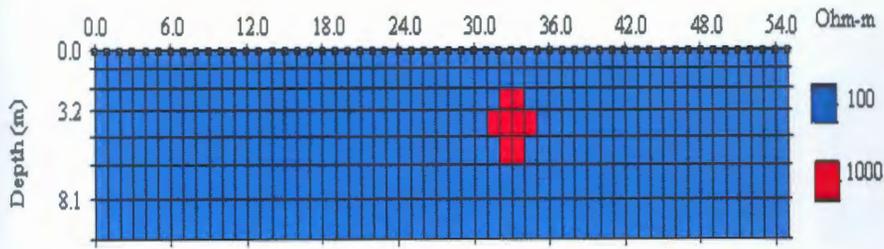
(a)
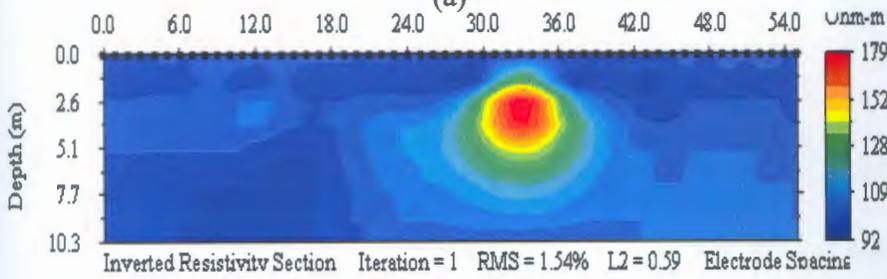
(b)
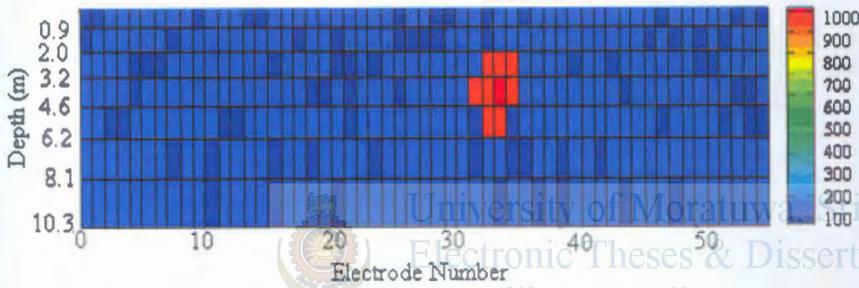
(c)

Figure 8.46 - (a) Test grid 4
(b) The smooth inversion output of the commercial program
(c) Block based inversion from the neural network output for 2.0% noise
(Original is in Color)

(a)

(b)

174

(c)
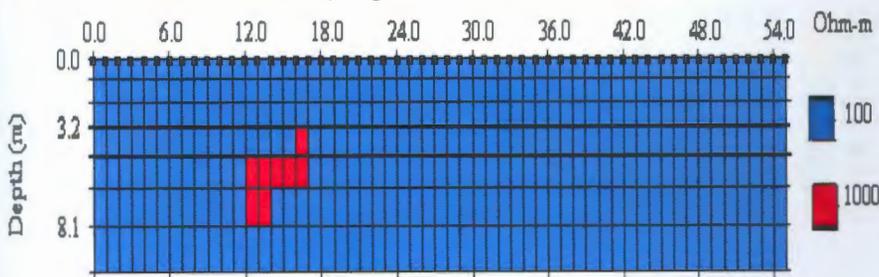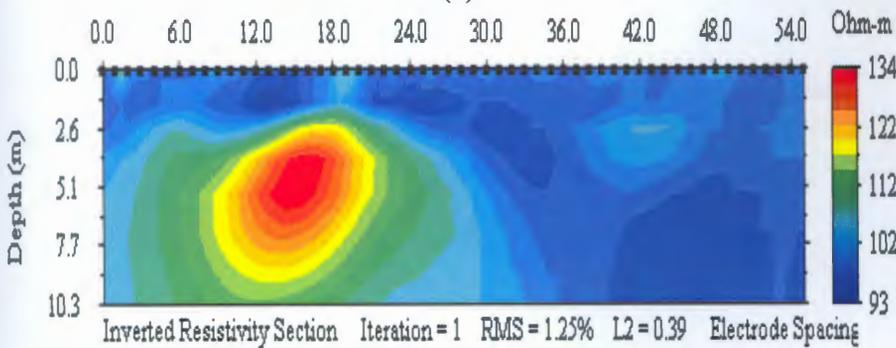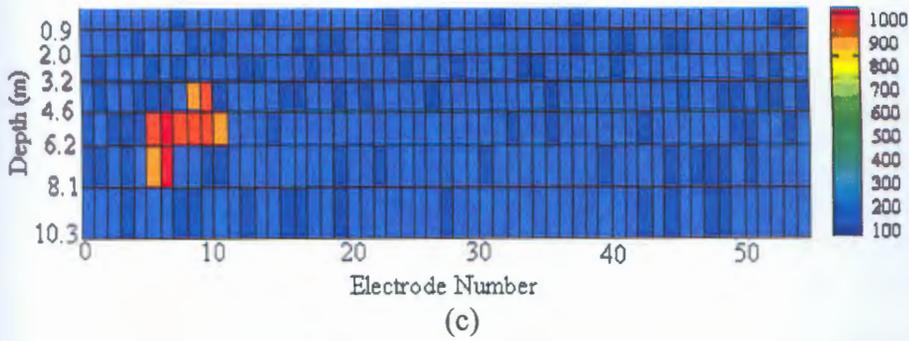
Figure 8.47 - (a) Test grid 5
(b) The smooth inversion output of the commercial program
(c) Block based inversion from the neural network output for 1.5% noise
(Original is in Color)

(a)

Inverted Resistivity Section   Iteration = 1   RMS = 1.26%   L2 = 0.39   Electrode Spacing
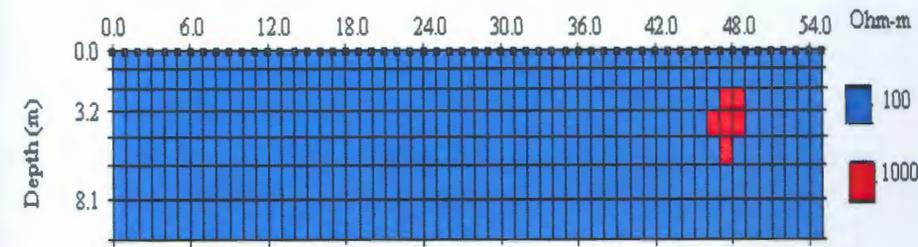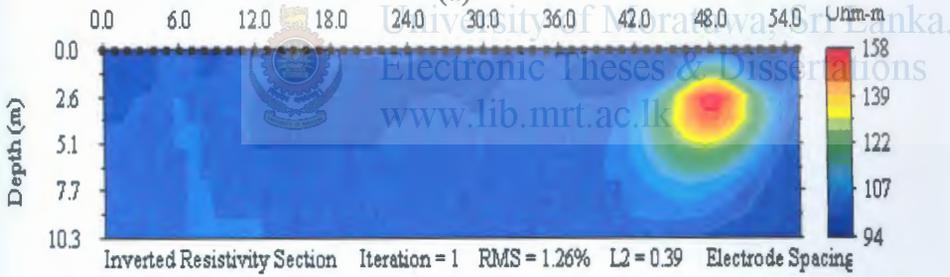
(b)
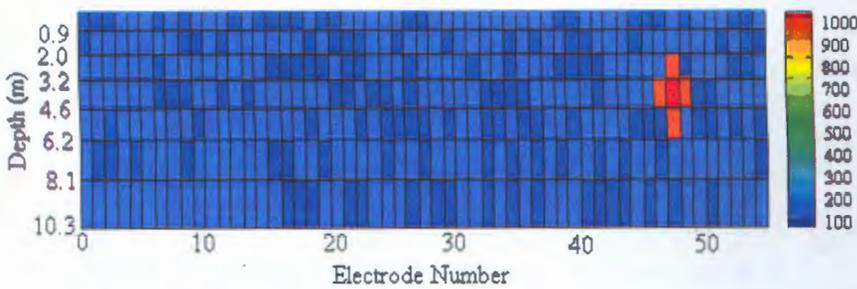
(c)

Figure 8.48 - (a) Test grid 6
(b) The smooth inversion output of the commercial program
(c) Block based inversion from the neural network output for 1% noise
(Original is in Color)

175

(a)

Inverted Resistivity Section   Iteration = 1   RMS = 1.08%   L2 = 0.29   Electrode Spacing

(b)

Electrode Number
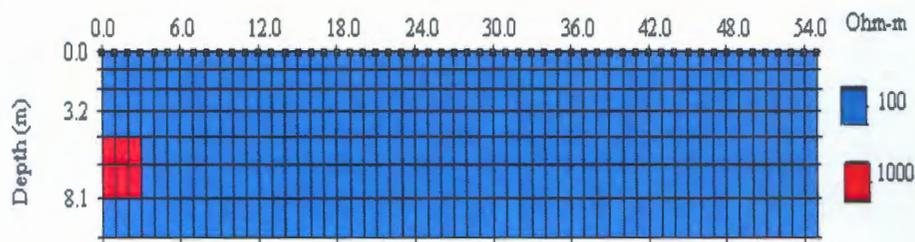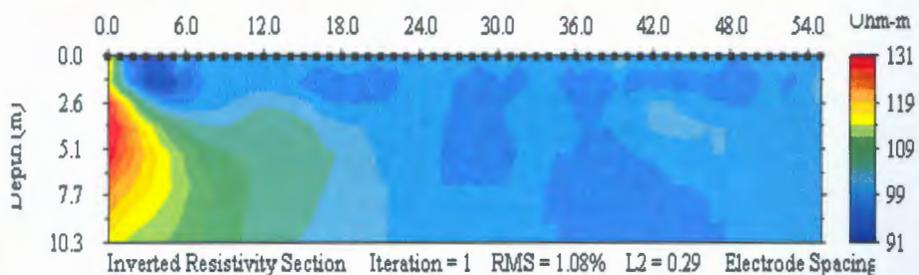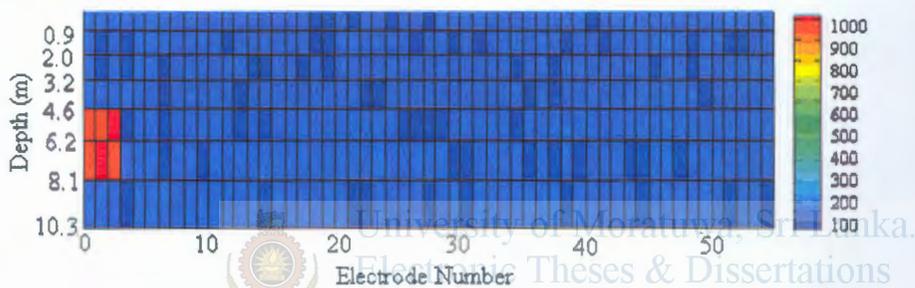
(c)

Figure 8.49 - (a) Test grid 7
(b) The smooth inversion output of the commercial program
(c) Block based inversion from the neural network output for 2.5% noise
*(Original is in Color)*

(a)

Inverted Resistivity Section   Iteration = 1   RMS = 1.17%   L2 = 0.34   Electrode Spacing

(b)

176

(c)
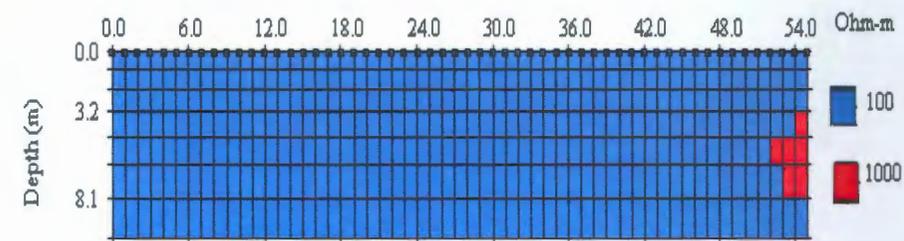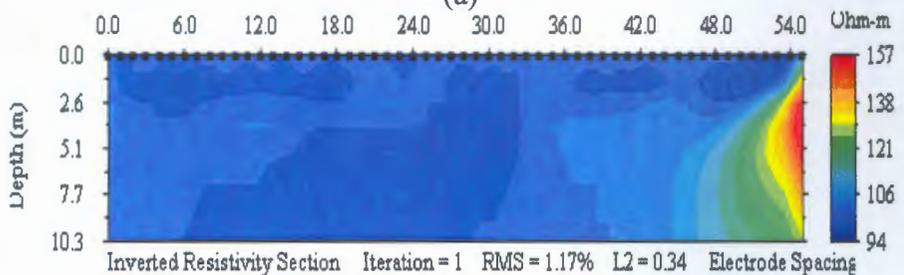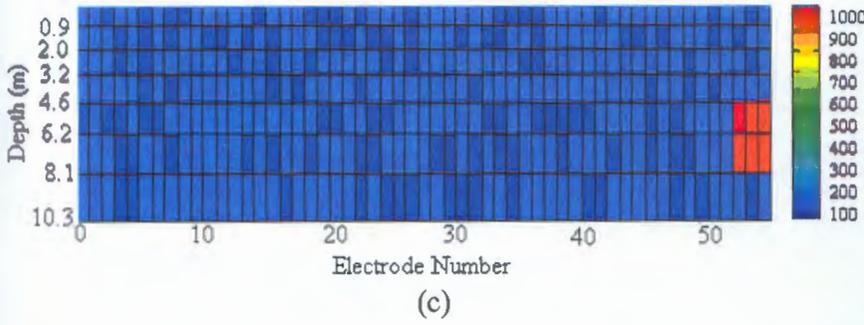
Figure 8.50 - (a) Test grid 8
(b) The smooth inversion output of the commercial program
(c) Block based inversion from the neural network output for 1.8% noise
*(Original is in Color)*

(a)

Inverted Resistivity Section   Iteration = 1   RMS = 1.17%   L2 = 0.34   Electrode Spacing

(b)

(c)
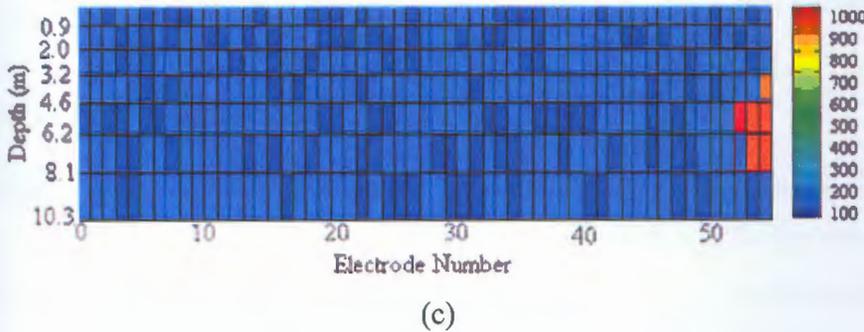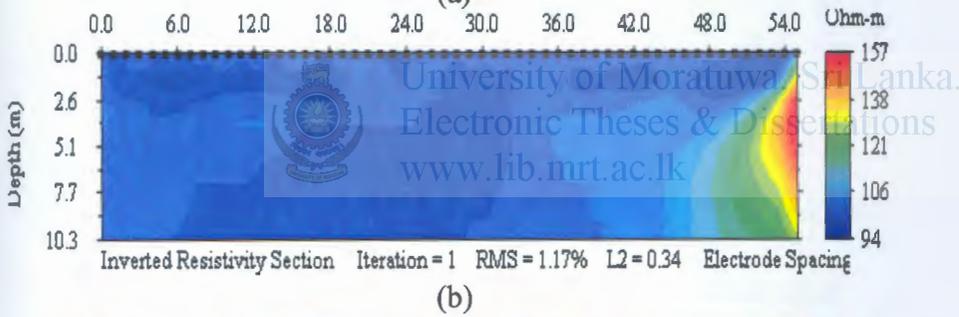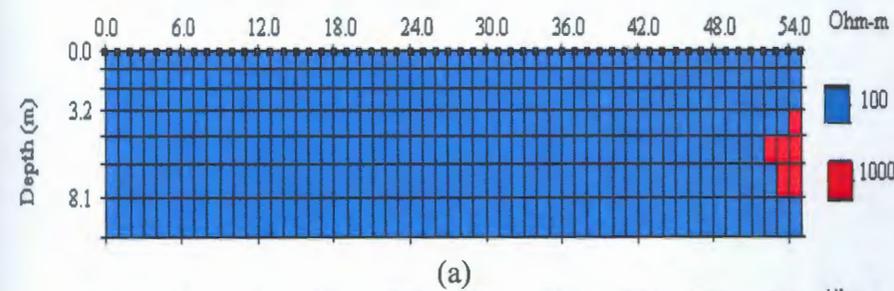
Figure 8.51 - (a) Test grid 9
(b) The smooth inversion output of the commercial program
(c) Block based inversion from the neural network output for 0.5% noise
(Original is in Color)

177
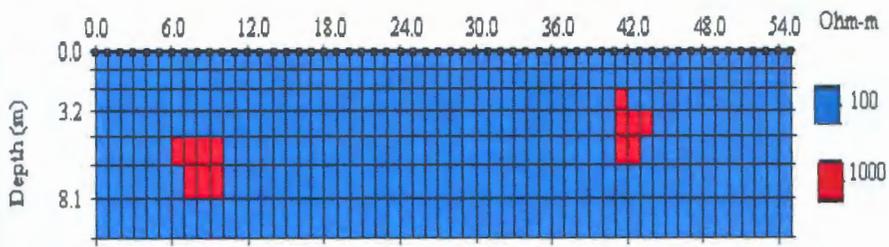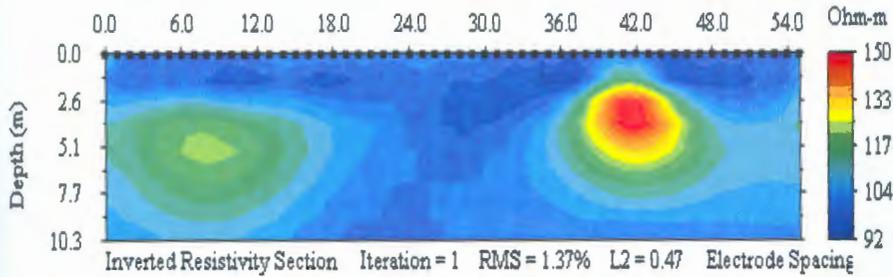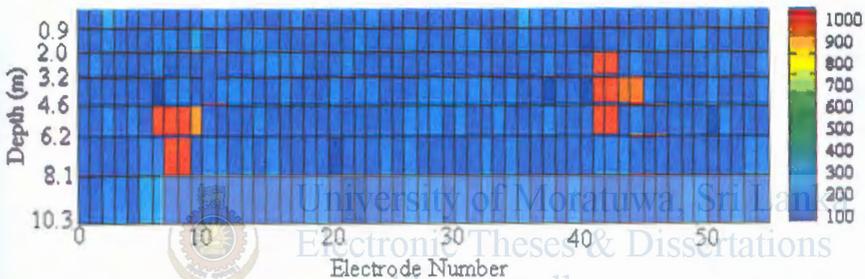
Figure 8.52 - (a) Test grid 10
(b) The smooth inversion output of the commercial program
(c) Block based inversion from the neural network output for 0% noise
(Original is in Color)

8.4.2 Two Dimensional CASE 2

To evaluate the Network performance on detection of an anomalous body with unknown resistivity embedded in a homogeneous medium with unknown resistivity the trained network with a two hidden layers with 325,800 hidden nodes in the respective hidden layers using the Resilient Backpropagation is used. 12 test data points are tested with the finalized network and the results are compared with the commercial software outputs.

1. Homogeneous medium resistivity 450 Ωm , Anomalous body resistivity 2750 Ωm

(a)

Inverted Resistivity Section   Iteration = 2   RMS = 1.73%   L2 = 0.75   Electrode Spacing

(b)

Electrode Number

(c)
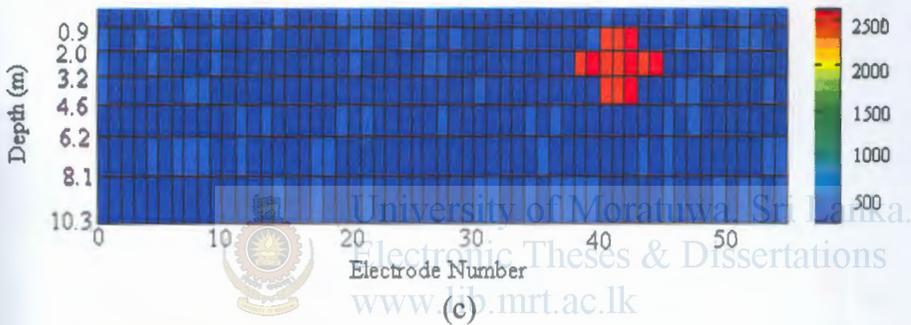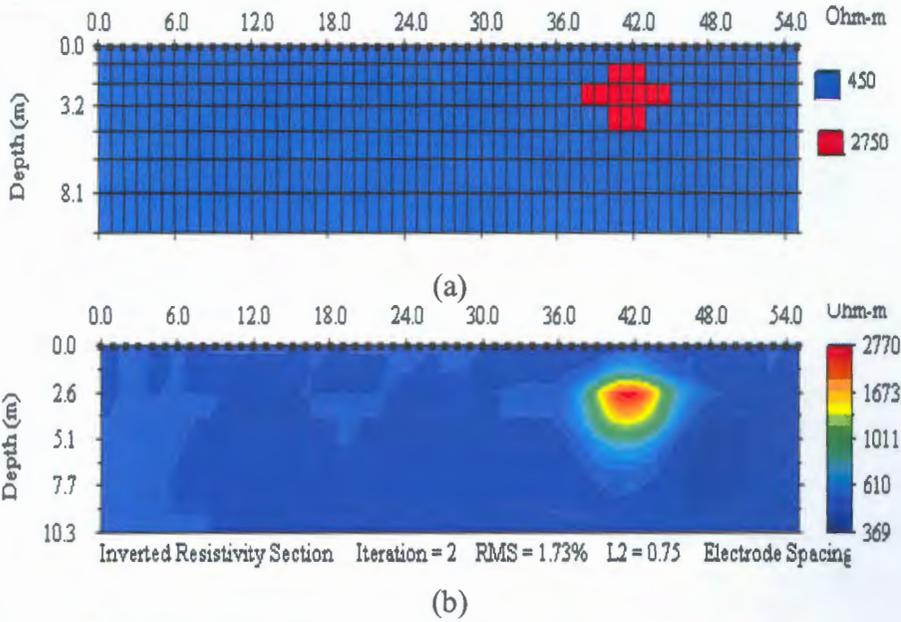
Figure 8.53 - (a) Test grid 1
(b) The smooth inversion output of the commercial program
(c) Block based inversion from the neural network output for 1% noise
(Original is in Color)

2. Homogeneous medium resistivity 200 Ωm , Anomalous body resistivity 1500 Ωm

(a)

Inverted Resistivity Section   Iteration = 1   RMS = 1.06%   L2 = 0.28   Electrode Spacing

(b)

179

(c)
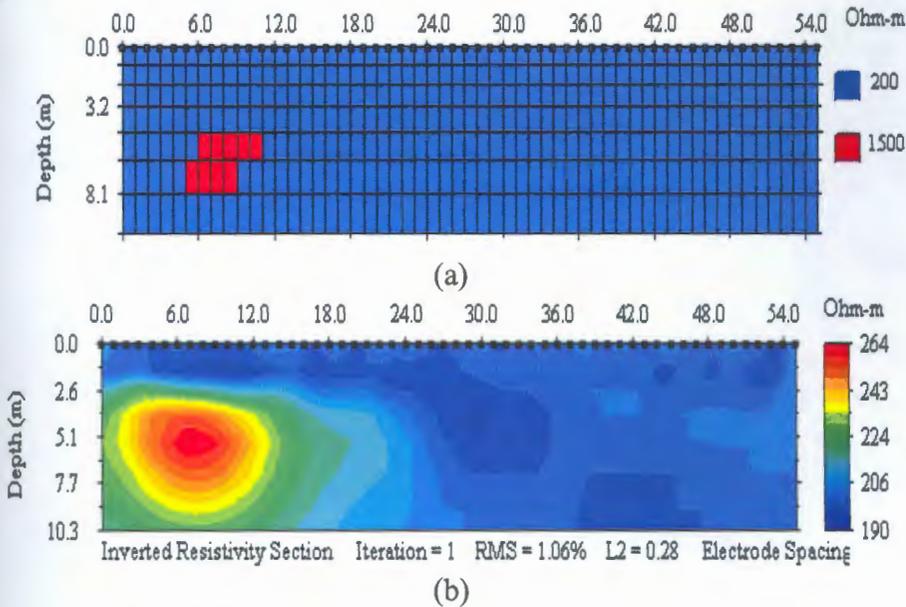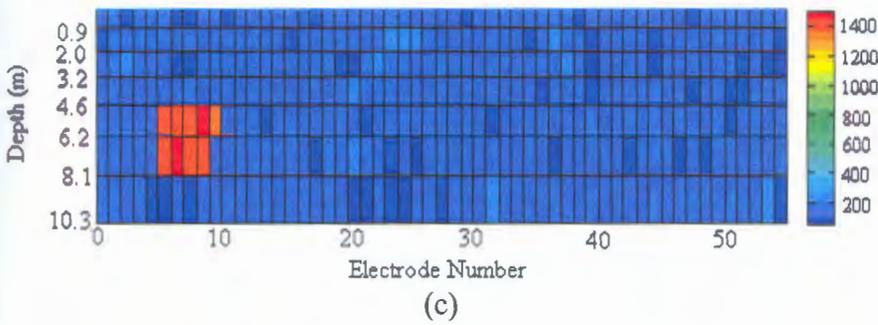
Figure 8.54 - (a) Test grid 2
(b) The smooth inversion output of the commercial program
(c) Block based inversion from the neural network output for 1.5% noise
(Original is in Color)

3. Homogeneous medium resistivity $1000\,\Omega m$, Anomalous body resistivity $100\ \Omega m$

(a)

Inverted Resistivity Section   Iteration = 2   RMS = 1.79%   L2 = 0.80   Electrode Spacing

(b)

(c)
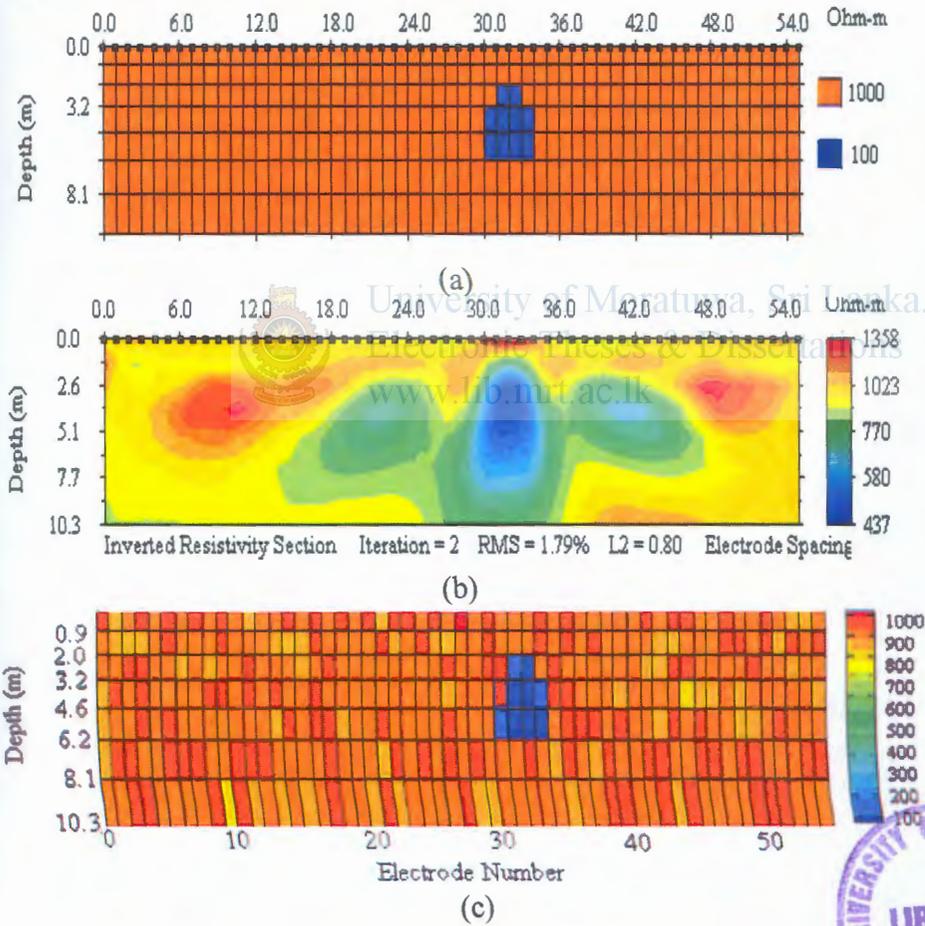
Figure 8.55 - (a) Test grid 3
(b) The smooth inversion output of the commercial program
(c) Block based inversion from the neural network output for 2% noise
(Original is in Color)

180

4. Homogeneous medium resistivity 800 Ωm, Anomalous body resistivity 7500 Ωm

(a)

Inverted Resistivity Section   Iteration = 3   RMS = 2.73%   L2 = 1.87   Electrode Spacing

(b)

Electrode Number

(c)
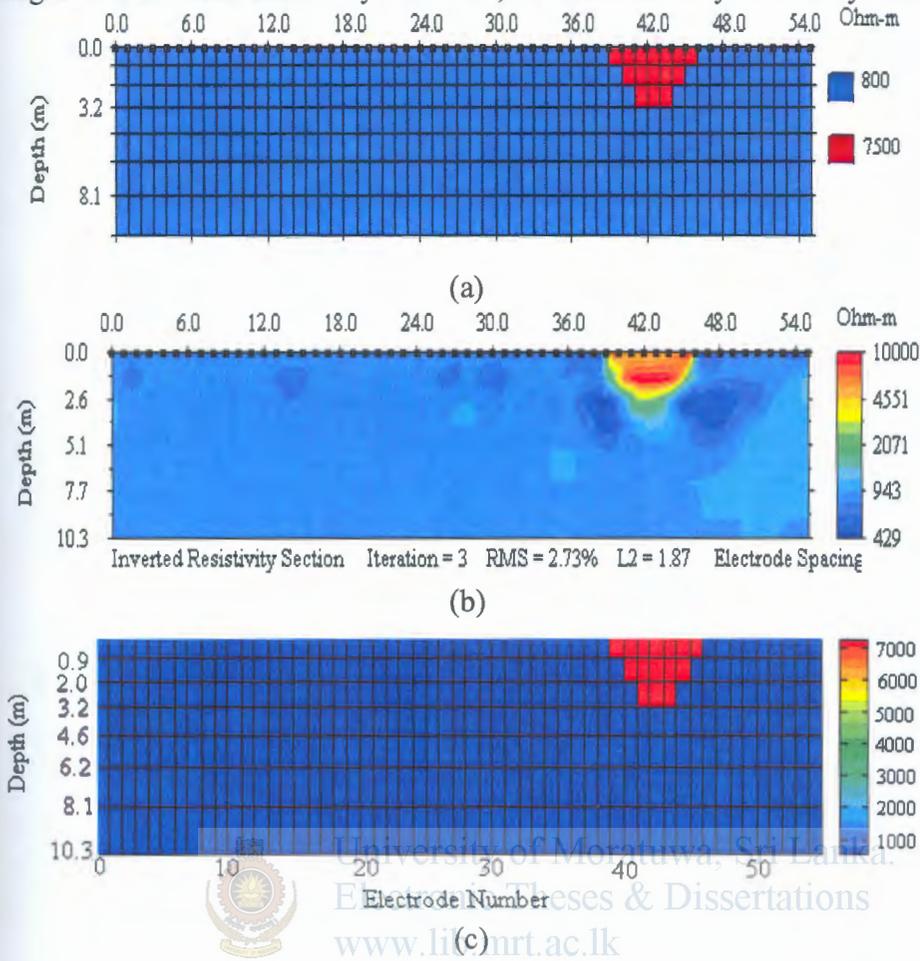
Figure 8.56 - (a) Test grid 4
(b) The smooth inversion output of the commercial program
(c) Block based inversion from the neural network output for 2% noise
(Original is in Color)

5. Homogeneous medium resistivity 670 Ωm, Anomalous body resistivity 1000 Ωm

(a)

Inverted Resistivity Section   Iteration = 1   RMS = 1.55%   L2 = 0.60   Electrode Spacing

(b)

181
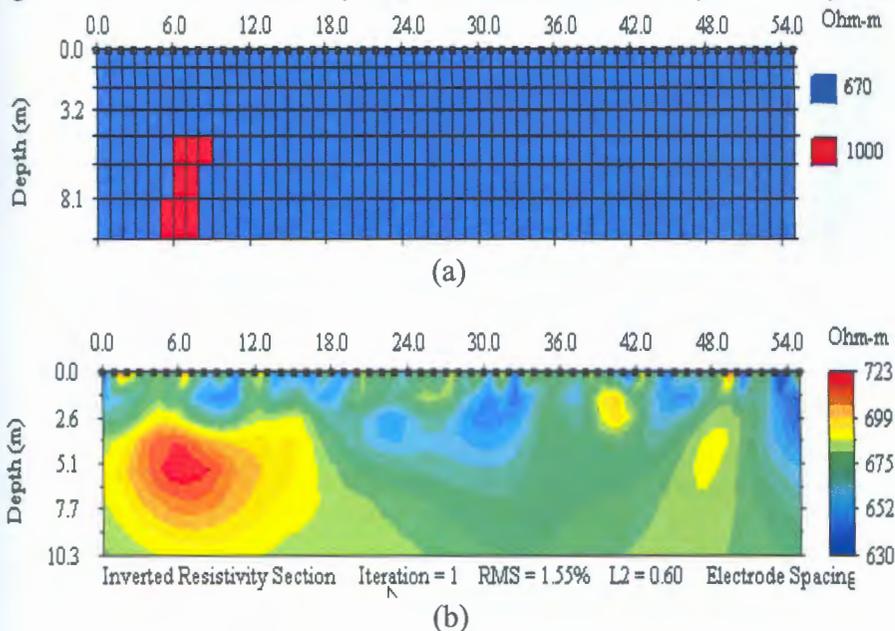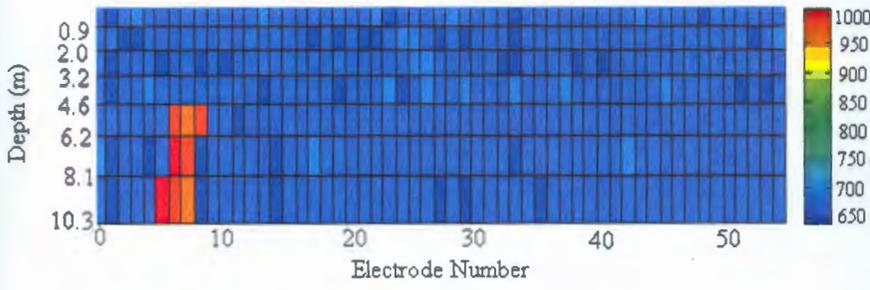
(c)

Figure 8.57 - (a) Test grid 5
(b) The smooth inversion output of the commercial program
(c) Block based inversion from the neural network output for 0.5% noise
(Original is in Color)

6. Homogeneous medium resistivity 300 Ωm , Anomalous body resistivity 8000 Ωm

(a)

Inverted Resistivity Section   Iteration = 2   RMS = 2.15%   L2 = 0.95   Electrode Spacing
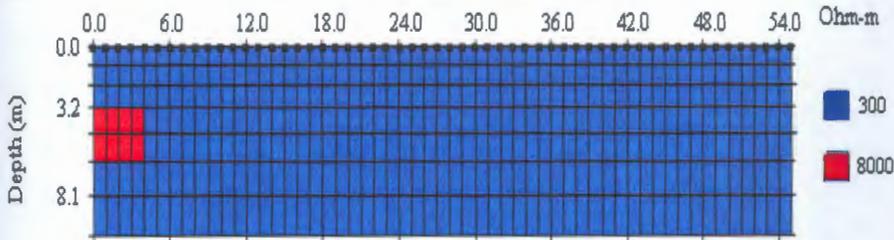
(b)
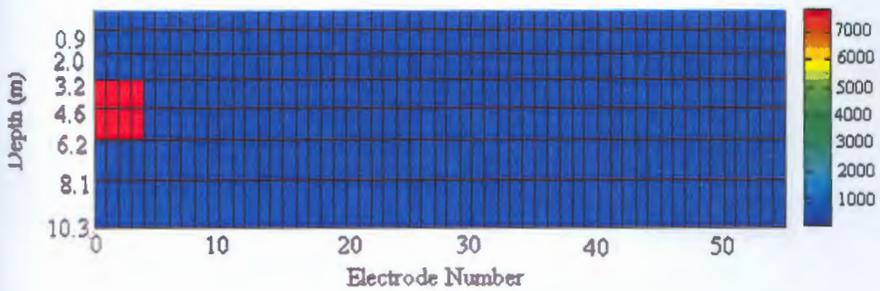
(c)

Figure 8.58 - (a) Test grid 6
(b) The smooth inversion output of the commercial program
(c) Block based inversion from the neural network output for 1.8% noise
(Original is in Color)

182

7. Homogeneous medium resistivity 100 Ωm , Anomalous body resistivity 6000 Ωm

(a)

Inverted Resistivity Section   Iteration = 1   RMS = 2.00%   L2 = 0.83   Electrode Spacing
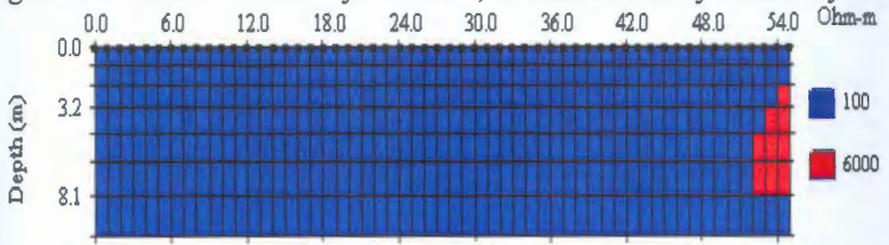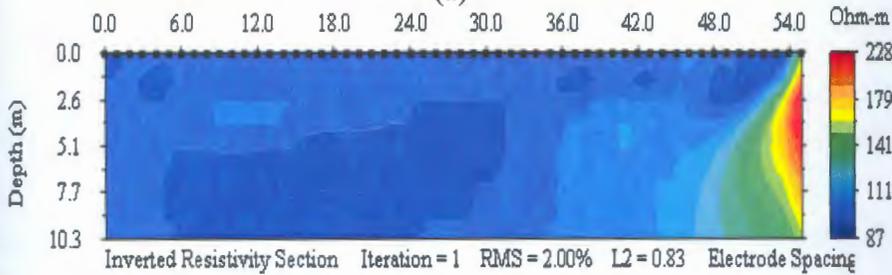
(b)
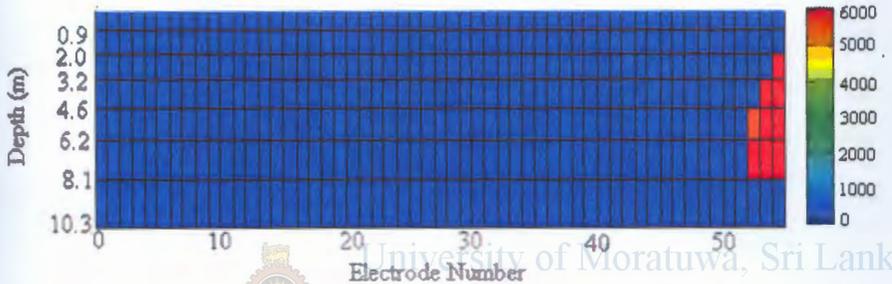
(c)

Figure 8.59 - (a) Test grid 7
(b) The smooth inversion output of the commercial program
(c) block based inversion from the neural network output for 1% noise
(Original is in Color)

8. Homogeneous medium resistivity 200 Ωm , Anomalous body resistivities 1000 Ωm and 4500 Ωm

(a)

Inverted Resistivity Section   Iteration = 1   RMS = 1.33%   L2 = 0.37   Electrode Spacing

(b)

183

(c)
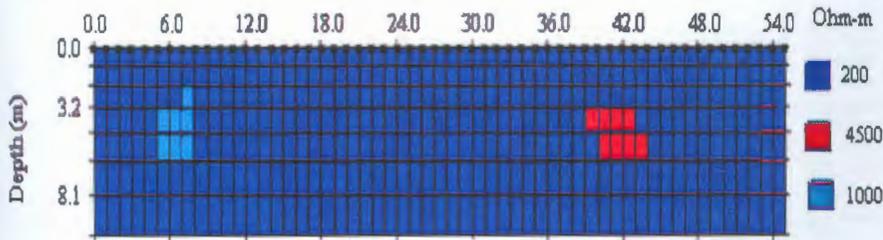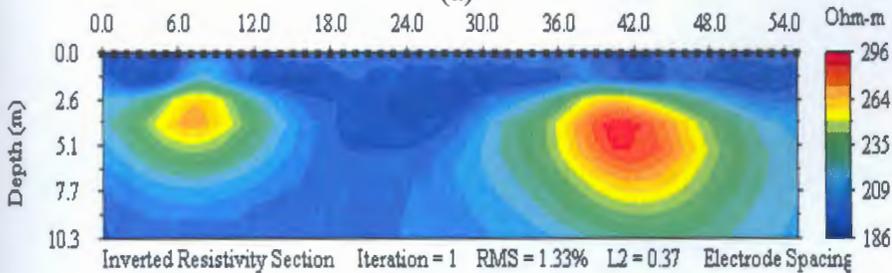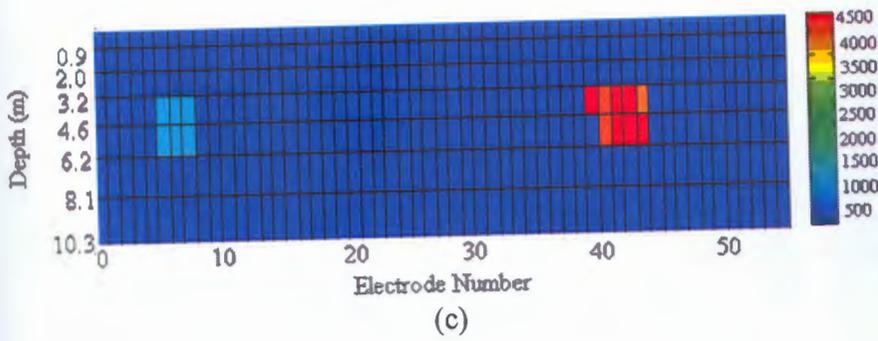
Figure 8.60 - (a) Test grid 8
(b) The smooth inversion output of the commercial program
(c) block based inversion from the neural network output for 0.75% noise
(Original is in Color)

9. Homogeneous medium resistivity 500 Ωm , Anomalous body resistivities 2500 Ωm and 10000 Ωm

(a)

Inverted Resistivity Section   Iteration = 2   RMS = 2.49%   L2 = 0.99   Electrode Spacing

(b)

(c)
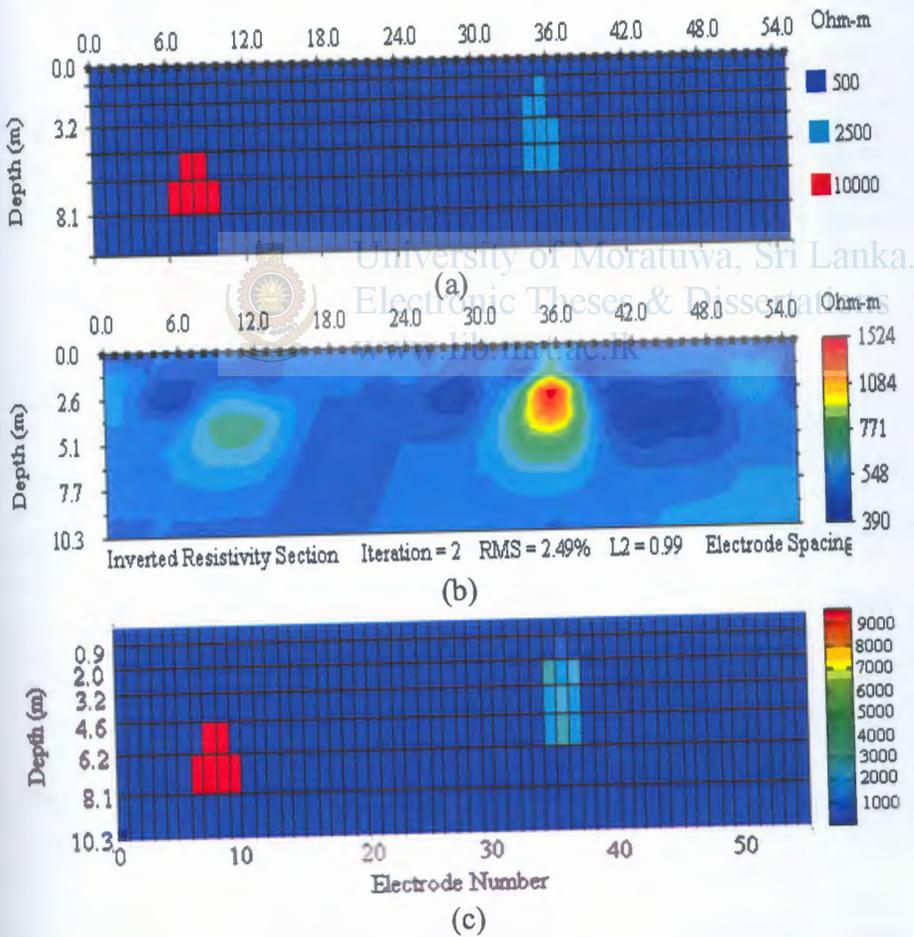
Figure 8.61 - (a) Test grid 9
(b) The smooth inversion output of the commercial program
(c) Block based inversion from the neural network output for 1.5% noise
(Original is in Color)

184

10. Homogeneous medium resistivity 100 Ωm, Anomalous body resistivities 2000 Ωm and 5000 Ωm

(a)

Inverted Resistivity Section   Iteration = 2   RMS = 1.46%   L2 = 0.34   Electrode Spacing

(b)

Electrode Number
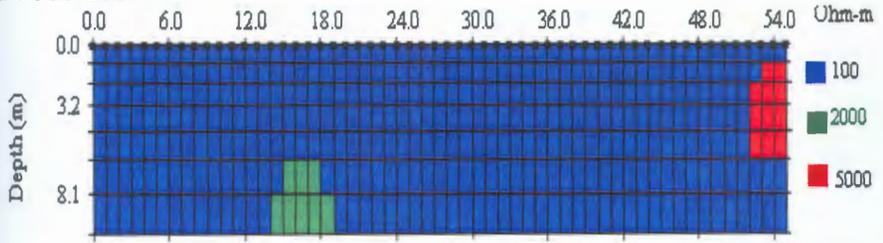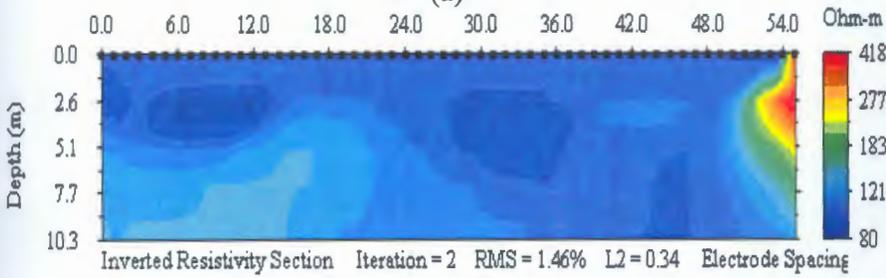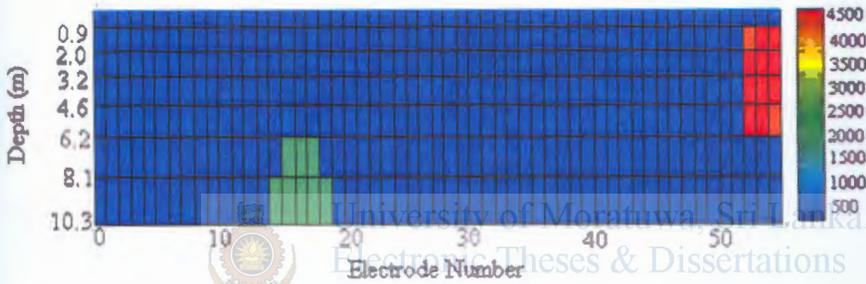
(c)

Figure 8.62 - (a) Test grid 10
(b) The smooth inversion output of the commercial program
(c) block based inversion from the neural network output for 1.5% noise
(Original is in Color)

11. Homogeneous medium resistivity 200 Ωm, Anomalous body with a resistivity gradient of 1000 Ωm, 1500 Ωm to 2000 Ωm

(a)

Inverted Resistivity Section   Iteration = 3   RMS = 2.47%   L2 = 1.52   Electrode Spacing

(b)

185

(c)
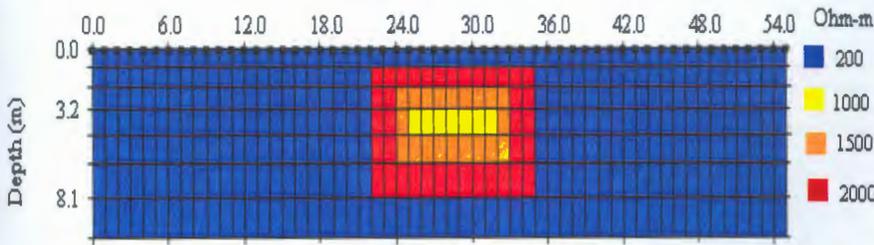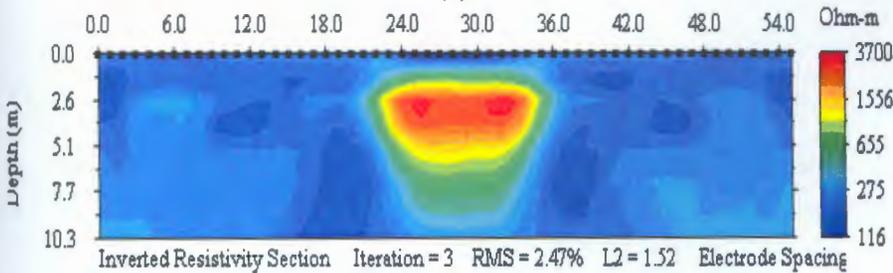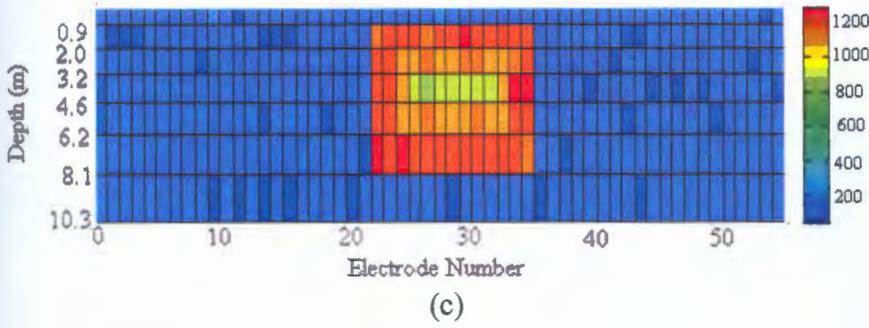
Figure 8.63 - (a) Test grid 11
(b) The smooth inversion output of the commercial program
(c) Block based inversion from the neural network output for 0.5% noise
(Original is in Color)

12. Homogeneous medium resistivity 450 Ωm , Anomalous body resistivity 2750, with 0.5m electrode spacing.


(a)
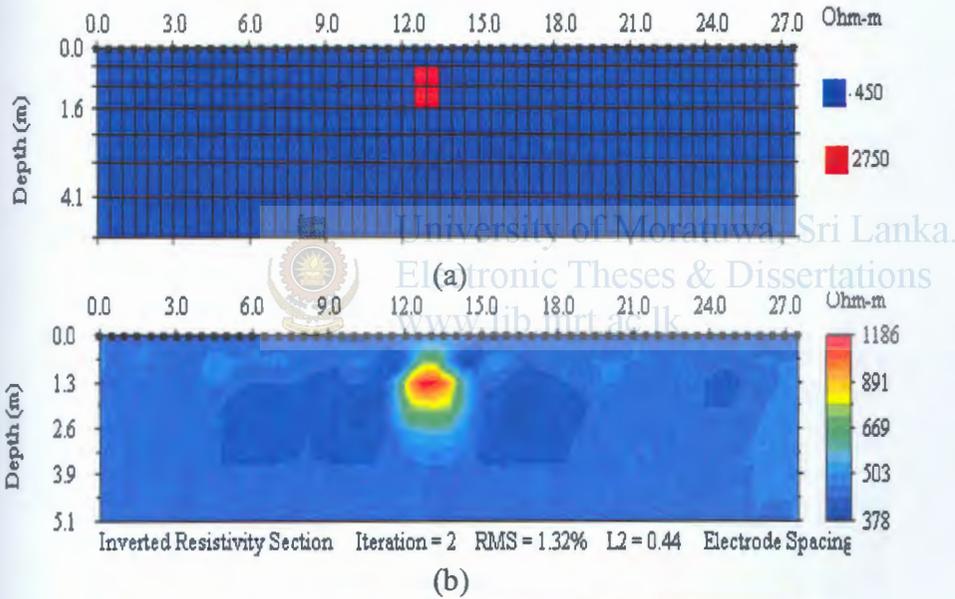
(b)
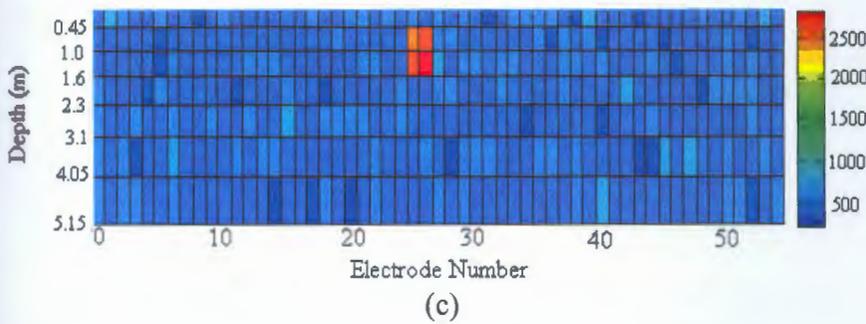
(c)

Figure 8.64 - (a) Test grid 12
(b) The smooth inversion output of the commercial program
(c) Block based inversion from the neural network output for 1% noise
(Original is in Color)

186

8.4.3 Two Dimensional CASE 3

To evaluate the Network performance on detection of an anomalous body with unknown resistivity embedded in a three layer medium with undetermined parameters the trained network with a two hidden layers with 250,700 hidden nodes in the hidden layers. 6 test grids are tested with the finalized network and the results are compared with the commercial software outputs.

1.)
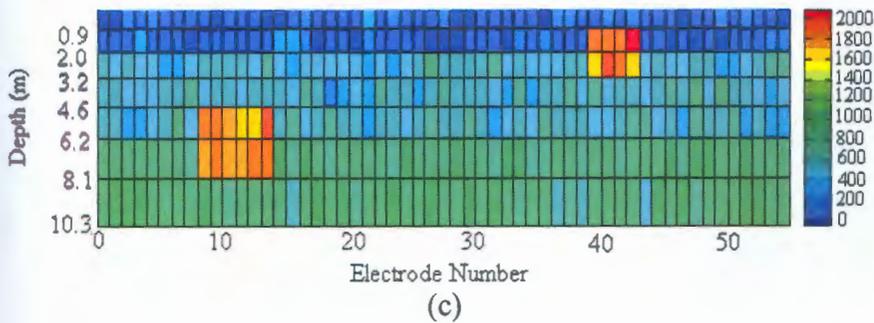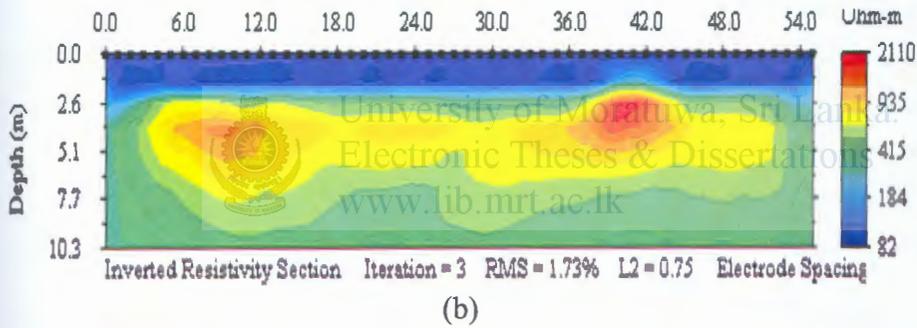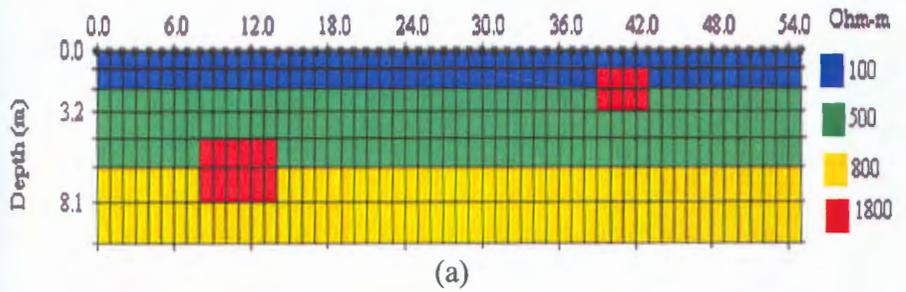
Figure 8.65 - (a) Test grid 1
(b) The smooth inversion output of the commercial program
(c) Block based inversion from the neural network output for 1.5% noise
(Original is in Color)

2.)

(a)

Inverted Resistivity Section   Iteration = 1   RMS = 1.93%   L2 = 0.93   Electrode Spacing

(b)

Electrode Number
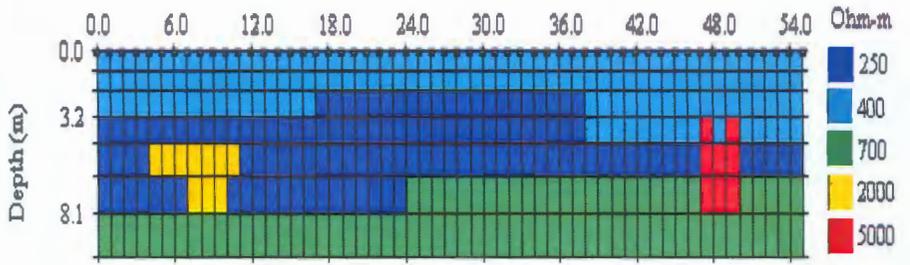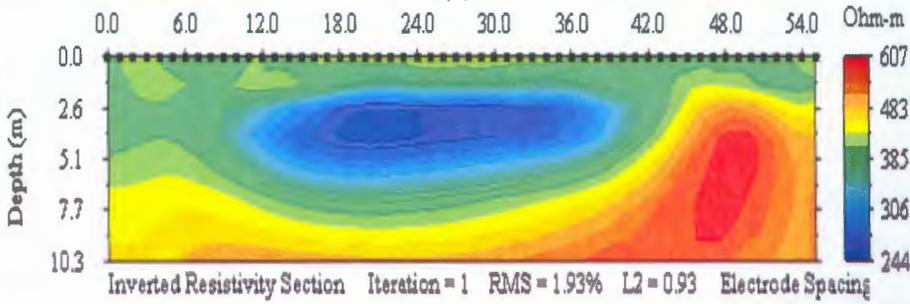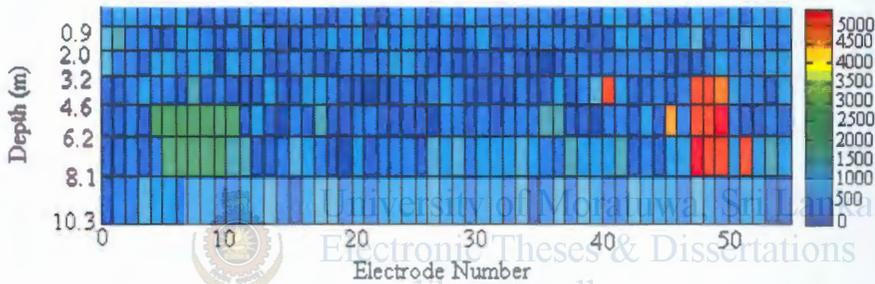
(c)

Figure 8.66 - (a) Test grid 2
(b) The smooth inversion output of the commercial program
(c) Block based inversion from the neural network output for 1% noise
(Original is in Color)

3.)

(a)

Inverted Resistivity Section   Iteration = 2   RMS = 1.94%   L2 = 0.94   Electrode Spacing

(b)

188
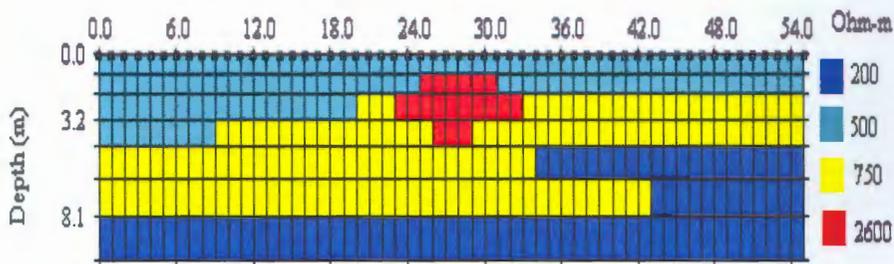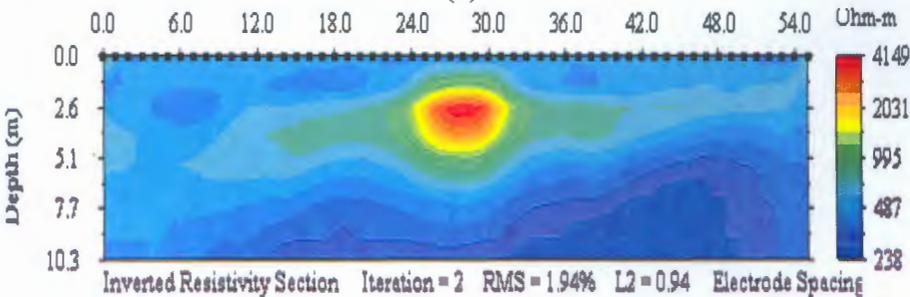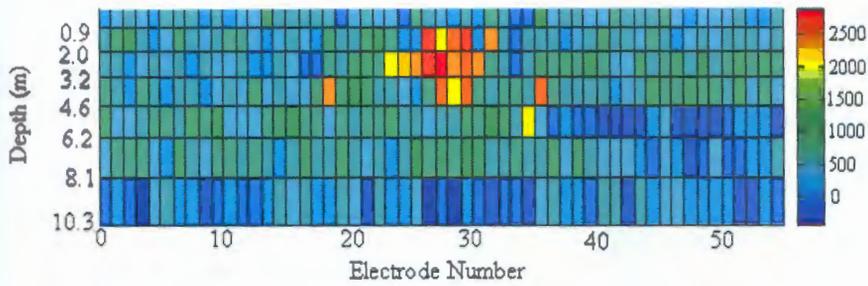
(c)

Figure 8.67 - (a) Test grid 3
(b) The smooth inversion output of the commercial program
(c) Block based inversion from the neural network output for 2.3% noise
(Original is in Color)

4.)
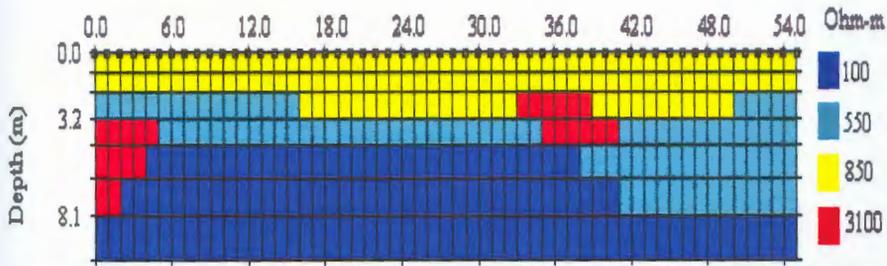
(a)
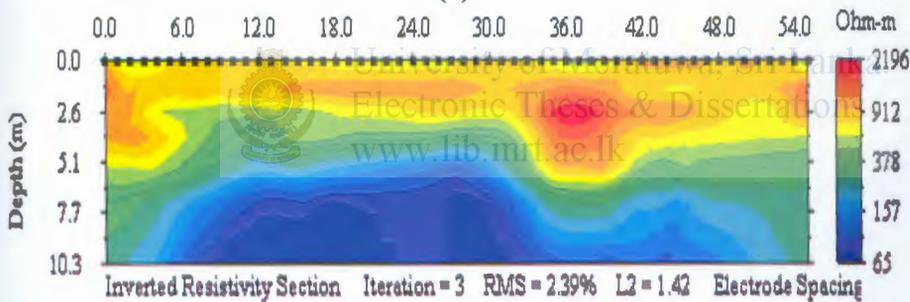
(b)
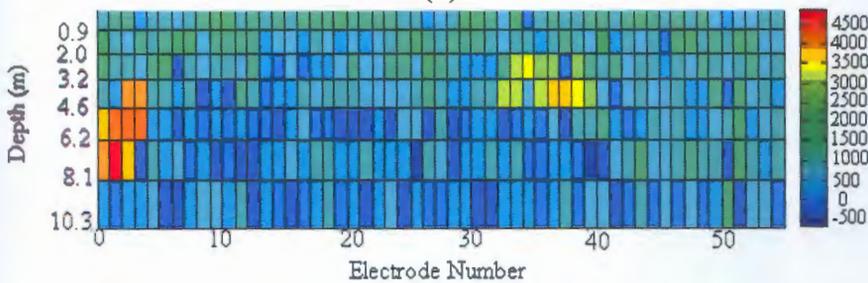
(c)

Figure 8.68 - (a) Test grid 4
(b) The smooth inversion output of the commercial program
(c) Block based inversion from the neural network output for 2% noise
(Original is in Color)

189

5.)

(a)

Inverted Resistivity Section   Iteration = 2   RMS = 1.81%   L2 = 0.82   Electrode Spacing
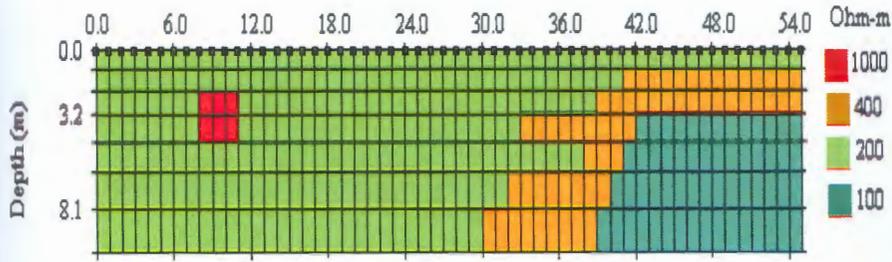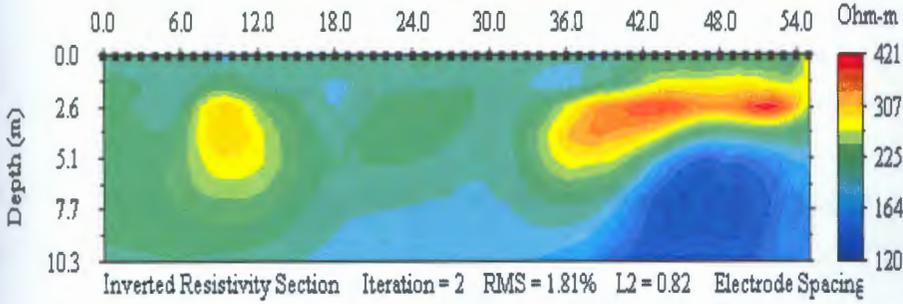
(b)
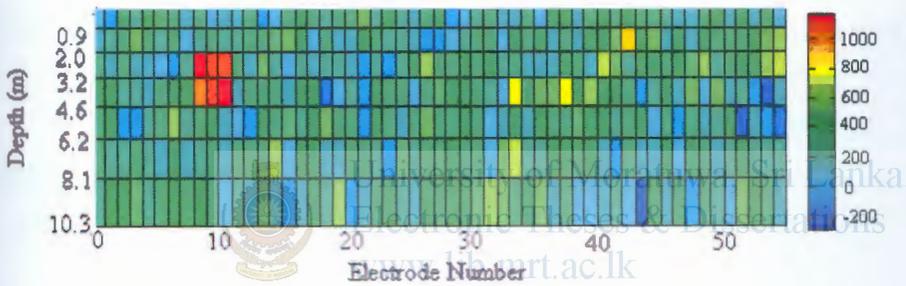
(c)

Figure 8.69 - (a) Test grid 5
(b) The smooth inversion output of the commercial program
(c) Block based inversion from the neural network output for 1.5% noise
(Original is in Color)

6.)

(a)

Inverted Resistivity Section   Iteration = 3   RMS = 1.46%   L2 = 0.53   Electrode Spacing

(b)

190
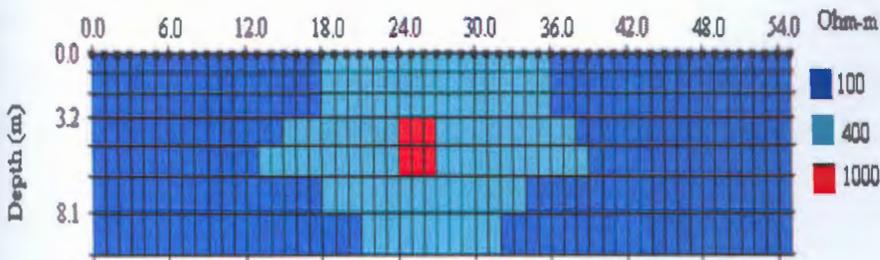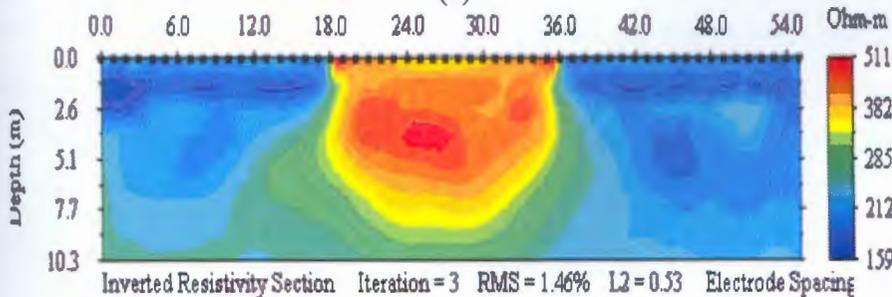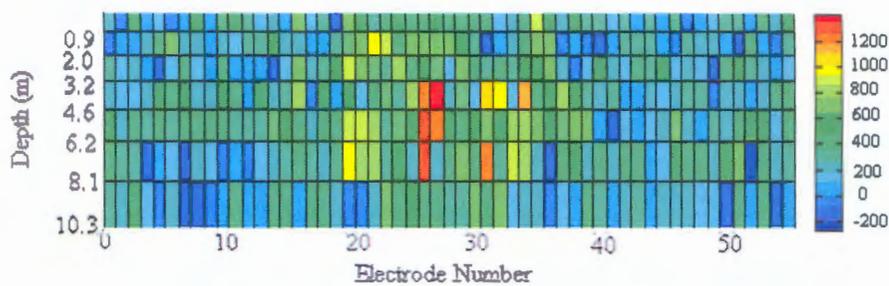
(c)

Figure 8.70 - (a) Test grid 6
(b) The smooth inversion output of the commercial program
(c) Block based inversion from the neural network output for 1% noise
(Original is in Color)

8.5 Neural Network Model Optimization Results for Three Dimensional Inversion

Similarly as the two dimensional case the 'Trainrp' function i.e. the resilient backpropagation algorithm (RPROP) of the MATLAB7s' Neural Network tool Box is used for the three dimensional resistivity data inversion too.

Model Optimization i.e. selection of Hidden layers and hidden nodes was done with evaluating the Training and Testing Errors.

In the present study since data is synthetically generated a large example database is available. Therefore in order to improve generalization or to avoid overtraining Early stopping with a Hold out cross validation is used.

First looking at Figure 8.71, that is the training error variation with varying number of single layer hidden nodes, it is seen that the training error converges around an average error 0f 0.6 after 225 single layer hidden nodes. Since this error level is not satisfactory training was preceded with two hidden layers.

Referring Figure 8.72, it is seen that though the number of first hidden layer nodes are increased the average training error preliminary reduces and finally converges with the increasing number of nodes in the second hidden layer. However the converging error level is kept nearly constant at 0.07. So two layer training was terminated at that point.
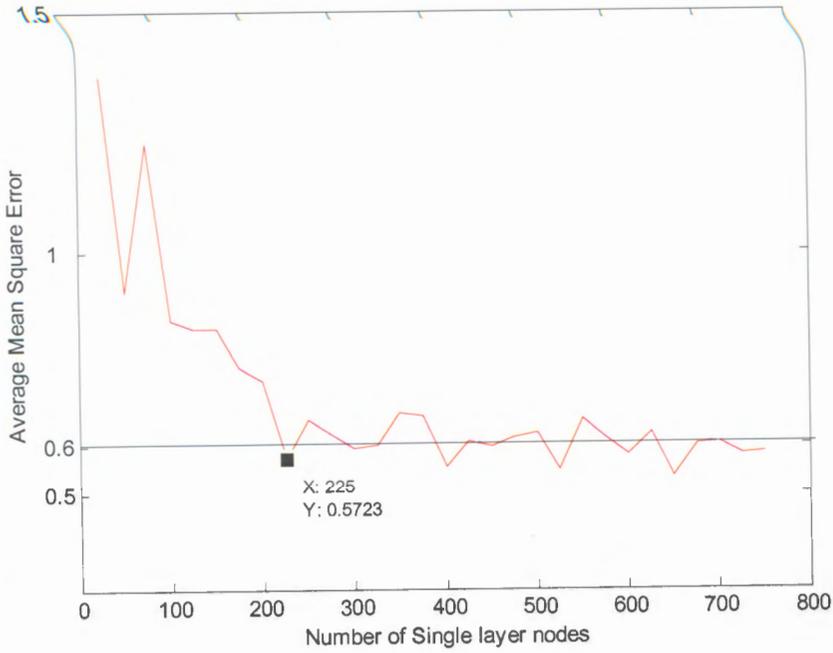
Figure 8.71 - Training Performance for the Training Function 'Trainrp' with different no of hidden nodes (single hidden layer)-3D
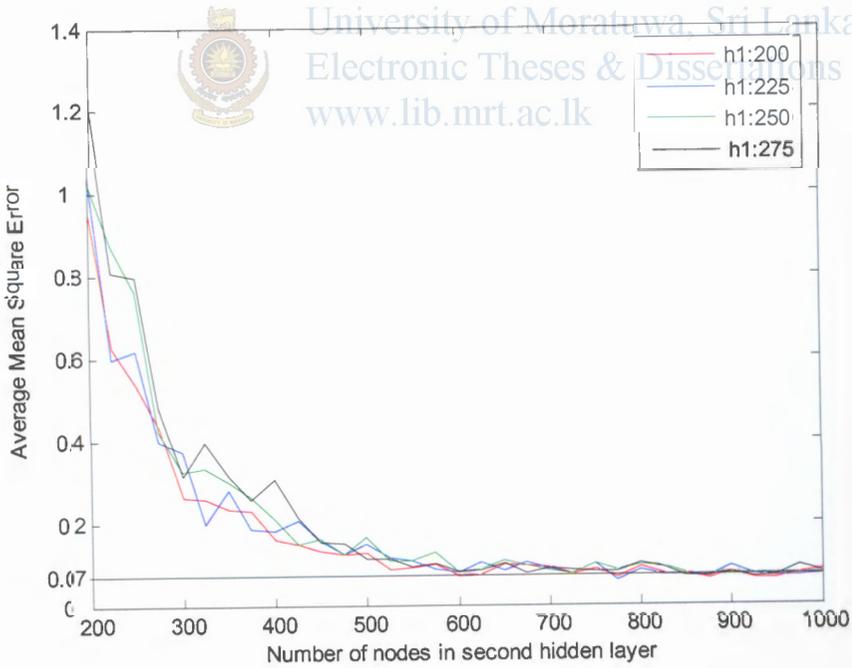
(a)
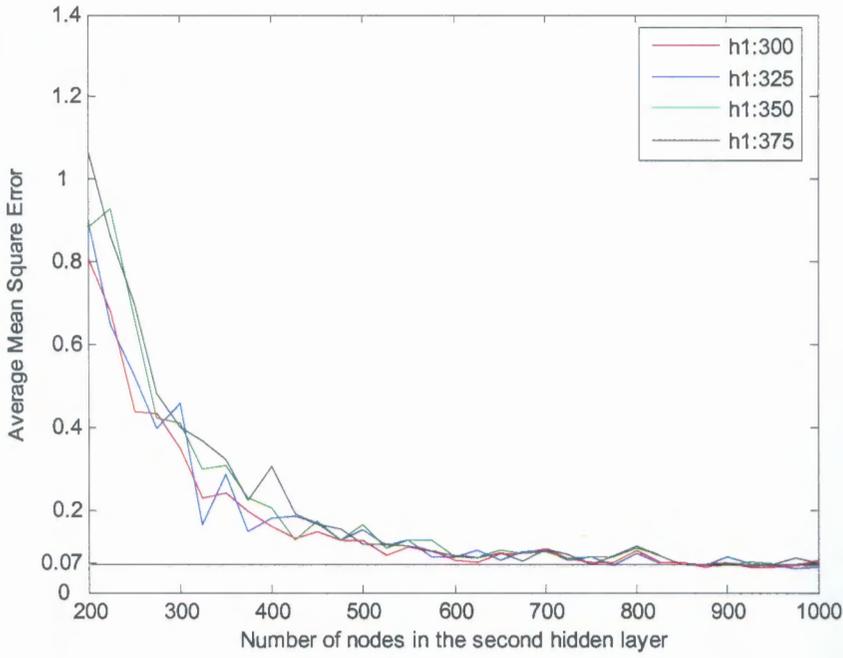
(b)

Figure 8.72 - Training Performance of two hidden layer network for 3D Case study
(Original is in Color)
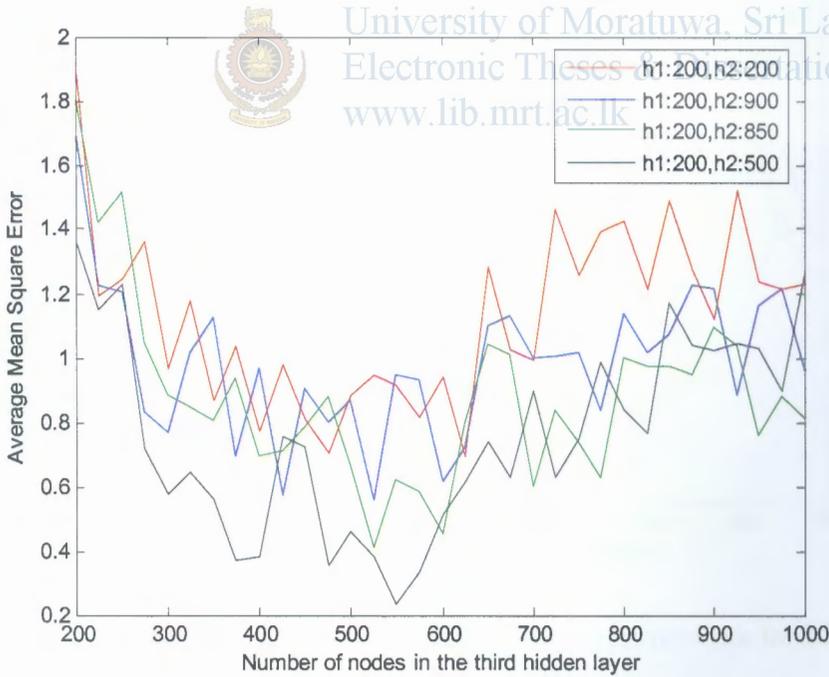
(a)
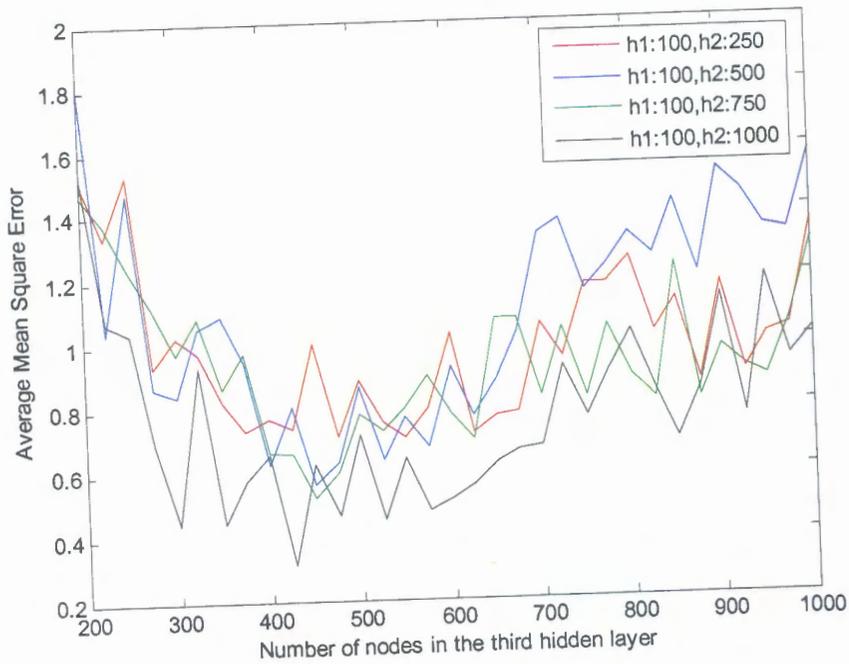
(b)
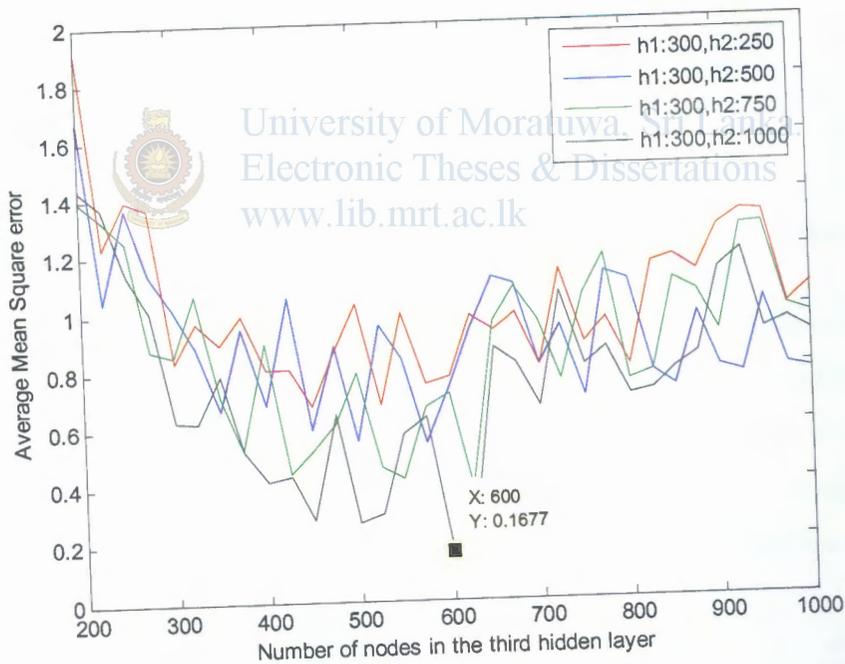
(c)

Figure 8.73 - Training Performance of three hidden layer network for 3D Case study
(Original is in Color)

Further to investigate the effect with three layers several training sessions were carried out. The results presented in Figure 8.73 shows that there is no considerable effect on the average error levels. Therefore referring Figure 8.72(a) since the two layer error levels converge around 850 nodes in the second hidden layer, the network was finalized with 200,850 numbers of nodes for first and second hidden layers

spectively. The network performance for the finalized network is shown in Figure 8.74.

Figure 8.74 - Training, validation and Test performance of the finalized Network-3D case study
(Original is in Color)

8.6 Simulation Results and Performance of the Three dimensional Inversion

To evaluate the neural network performance on detection of an anomalous body with unknown resistivity embedded in a two layer medium with undetermined parameters the trained network with a two hidden layers with 350,700 hidden nodes in the hidden layers. 3 test three dimensional scenarios are tested with the finalized network and the results are compared with the commercial software. The commercial software used for the inversion is RES3DINV [45].

195

pectively. The network performance for the finalized network is shown in Figure 8.74.

Figure 8.74 - Training, validation and Test performance of the finalized Network-3D case study
(Original is in Color)

8.6 Simulation Results and Performance of the Three dimensional Inversion

To evaluate the neural network performance on detection of an anomalous body with unknown resistivity embedded in a two layer medium with undetermined parameters the trained network with a two hidden layers with 350,700 hidden nodes in the hidden layers. 3 test three dimensional scenarios are tested with the finalized network and the results are compared with the commercial software. The commercial software used for the inversion is RES3DINV [45].

1.)

(a)

(b)

(c)

Figure 8.75 - 2D slices of the 3D (a) Test Set 1 Mesh arrangement (b) Res3dinv
smooth output (c) neural network output
(Original is in Color)

196

2.)
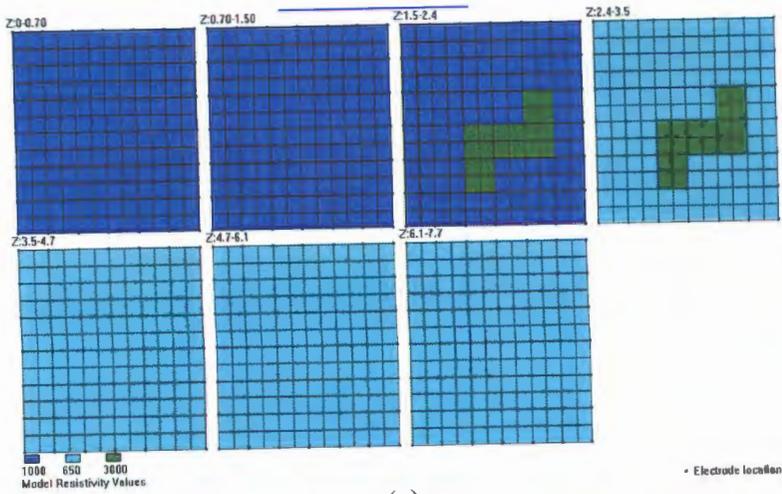
(a)
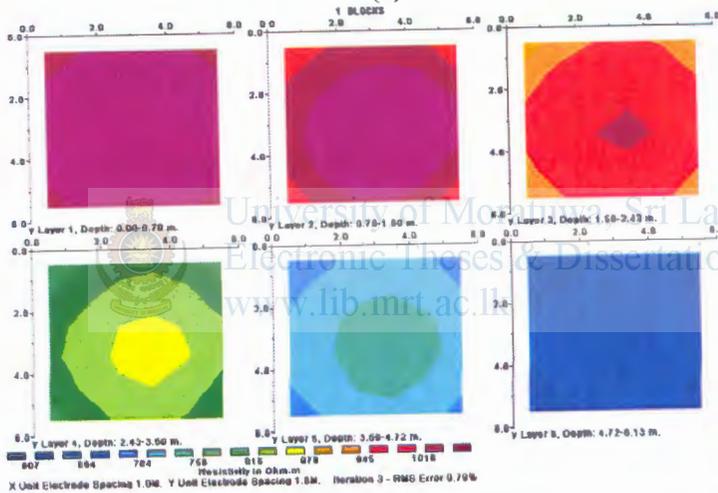
(b)
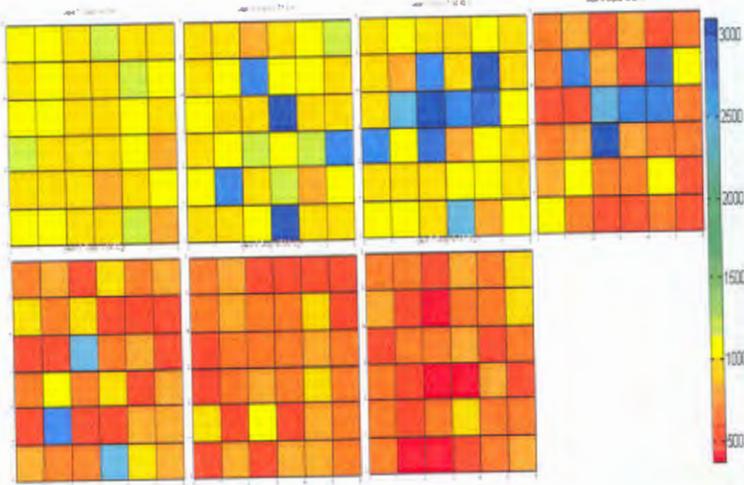
(c)

Figure 8.76 - 2D slices of the 3D (a) Test Set 2 Mesh arrangement (b) Res3dinv smooth output (c) neural network out put

(Original is in Color)

3.)
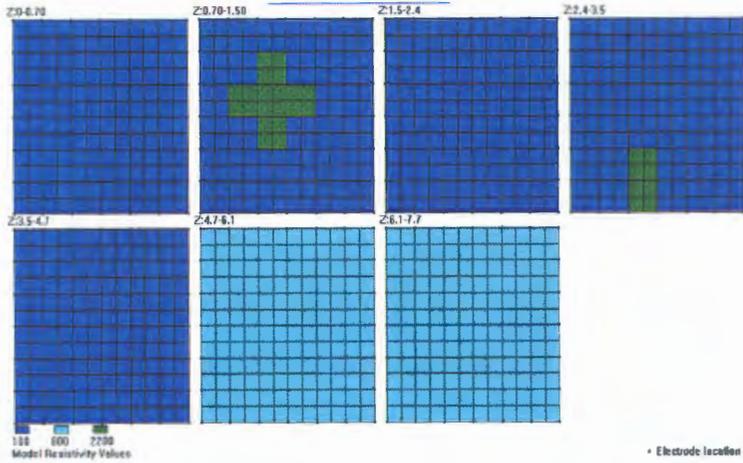
(a)
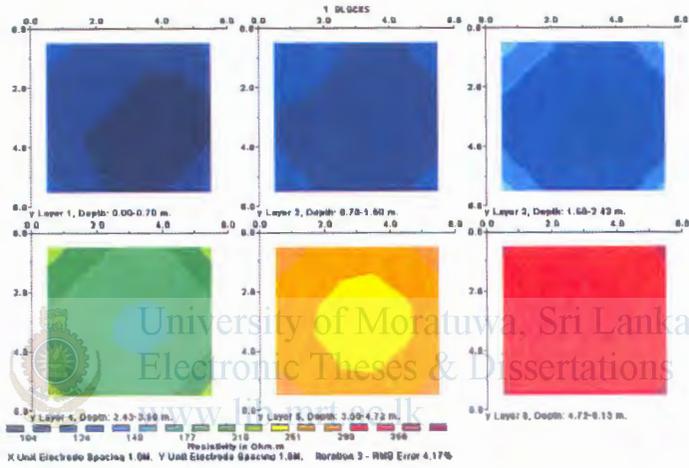
(b)
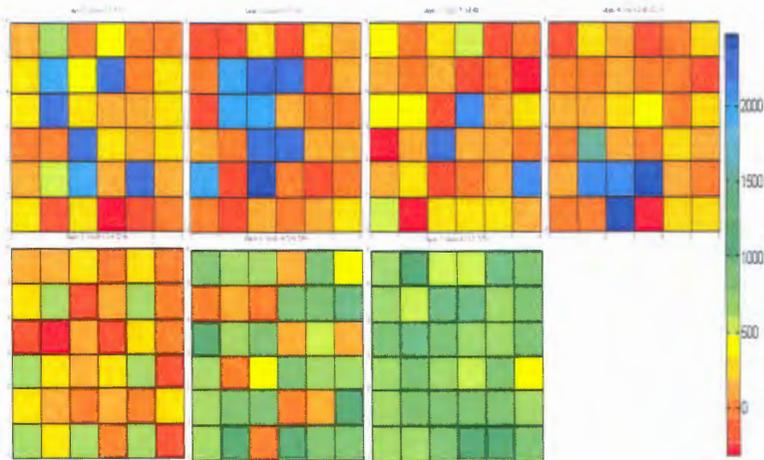
(c)

Figure 8.77 - 2D slices of the 3D model (a) Test Set 3 Mesh arrangement (b) Res3dinv smooth output (c) neural network out put

(Original is in Color)

Chapter 9
Conclusion and Recommendations

The intension of the study was to develop a user friendly, fast responding software tool with the application of artificial intelligence in order to interpret the earth resistivity field measurements. The problem was addressed with the neural networks as the inversion tool. And the study was carried out in three sections to interpret the soil structure One dimensionally, Two dimensionally and Three dimensionally, to give different details on the earth structure for the user.

It can be concluded that for the one dimensional inversion the neural networks perform promisingly. The network was first evaluated with theoretically generated field curves with parameters unknown at the stage of training. Noise added samples are used in order to evaluate the degree of predictability for field data. The performance of curve type identification and parameter estimation was satisfactory on the theoretical curves with and without noise.

In order to verify the network performance on the field data a cross calculation of an earth electrode was carried out. The theoretically calculated electrode resistance was $424.421\,\Omega$, while the measured electrode resistance was $452.01\,\Omega$. Since the electrode resistances closely match we can conclude that the neural network has classified and predicted the one dimensional earth parameters adequately. But in order to come to a thorough conclusion this type of similar tests must be performed in different sites or locations.

There is no hard and fast rule for Neural Network architecture optimization. However different heuristics exist to guide the user through this highly random process. Going back to the results obtained in Chapter 8 it is evident that a pattern cannot be recognized during the different training sessions. That is it can be concluded that the optimizations process depends heavily on the application of interest. During the study period I experienced many factors which effected this random training. Some are the contents of the database, how the database is split to obtain the training, validation and test sets and preprocessing of data are some factors directly affecting the training performance of the network. Table 9.1 gives the finalized network architectures.

Scenario	Input Nodes	Hidden Nodes	Output Nodes	Finalized network Training Error
1D Curve Identification	40	85,165	6	0.02
1D Two layer parameter Estimation	40	25, 24	3	0.0197
1D Three layer parameter Estimation	40	100,260	5	0.0136
2D CASE 1	495	500,700	385	0.0018
2D CASE 2	495	325,800	385	0.0009
2D CASE 3	495	250,700	385	0.009
3D Case	467	200,850	252	0.0536

Table 9.1 - Summarized Network Optimization results

Present proposed Neural Network based inversion it is completely automatic and the user does not even have to supply a starting model. The data inversion takes less than a minute with an optimized well-trained network.

The two dimensional and three dimensional studies are carried out on theoretical validation of the network performance. Noise is added to the synthetic models in order to resemble field data patterns. The closeness of the network output to the initial model is used to evaluate the neural network capability of inversion in the two dimensional and three dimensional cases. With the neural Network approach we cannot get smooth inversion result for the sub surface structure. However the block inversion or the cell based inversion gave satisfactory results when comparing with the commercial software's inversion results for the test data sets. In both the cases the anomaly is detected.

Referring the two dimensional outputs, it is seen that when the shapes of the anomalous bodies in the test sets resemble the body shapes presented in training data the network output gave exact matches. In some cases the arbitrary complex shapes of the structures are approximated to shapes that are seen by the network earlier.

However with the above results it is evident that a Neural Network inversion with sharp boundaries (block based) gives comparably acceptable results.

In two dimensional CASE 1 and CASE 2 the network performance on unseen data was superior. This can be due to very low training error levels obtained with the optimum architectures. In the CASE 3 a three layer medium was considered. Here the neural network output does not clearly show the sharp layer boundaries. However the results interpret a close resemblance to the initial synthetic model.

The three dimensional study considered a two layer medium with an anomaly. Here the network performance was not as satisfactory as the one dimensional or the two dimensional cases. Nevertheless the output, though does not give an exact match detect the anomaly, and layer separation is also visible. This could be due to the training error of the optimized network architecture. Referring Table 9.1 it can be seen that the highest training error for the finalized network was obtained for the three dimensional study.

Certain limitations and difficulties aroused during the study, which these factors affected boundaries on the work to be carried out. For instance, the two dimensional study was done with a 56 multi electrode array and the three dimensional study was done with a 7 by 7 electrode grid. No variation could be done to these electrode arrangements since the commercial software's used for the database generation did not facilitate these options. Many software's are available for the 2D and 3D resistivity inversion problems. But most of such available software is distributed as demo versions only. These demo versions have limited access capabilities, for instance disabling the result saving options and limitations on electrode array modifications. So some extra time was spent on finding suitable software and with it several trial and error test runs were done to verify the usability and determining the result saving formats.

Also very long hours of training were spent on the optimization training processes. And I had to limit the model resolutions since it would cause more burdens on the training session time and even the total processing speed of the computer was observed diminishing.

201

Further work is therefore desirable on harnessing the capabilities of the neural networks as a resistivity inversion tool. This can be done with varying the electrode grid sizes and model resolution. For this one would need good software for the forward solution generation that is the generation of the database.

If we consider the two dimensional study with 56 multi electrodes, if an automatic data acquisition unit is not available one would not be able to easily acquire 495 data points with a single electrode movement. In such a case data acquired at only some points also should let the user generate a 2D or 3D structure with certain accuracy. But with a neural network structure with a fixed number of inputs this cannot be achieved. Therefore studies with dynamic neural network models are proposed to be carried out with unsupervised learning.

References

[1] Telford, W.M. and Geldart, L.P. and Sheriff, R.E. *"Applied Geophysics Second Edition"*. ISBN:0-521-32693-1, Published by Cambridge University Press, Cambridge., 1990.

[2] Tarantola, Albert. *"Inverse Problem Theory and Methods for Model Parameter Estimation "*. 2005.

[3] *"Earth Resistivity Manual"*. USA:Soiltest,Inc.1968.

[4] Seedher, H.R. and Arora, J.K. "Estimation of two layer soilparameters using finite Wenner resistivity expression". *IEEE Trans.Power Delivery*, vol. 7,no. 3, 1992 , pp. 1213-1217.

[5] Yang, H.,Yuan, J. and Zong, W. "Determination of three-layer earth model from wenner four-probe test data". *IEEE Trans.Magn.*,vol. 37,no. 5, Sep.2001, pp. 3684-3687.

[6] Zohdy, A.A.F. "A new method for the automatic interpretation of Schlumberger and Wenner sounding curves". *Geophysics*, vol. 54, 1989, pp. 245-253.

[7] Takahashi, T. and Kawase, T. "Analysis of apparent resistivity in a multi layer earth structure". *IEEE Transactions on Power Deliver* , vol. 5,No. 2, April 1990, pp. 604-612.

[8] Gonos, Ioannis F. and Stathopulos, Ioannis A."Estimation of Multilayer Soil Parameters Using Genetic Algorithms". *IEEE Trans. Power Delivery*,vol. 20,no.1, Jan.2005, pp. 100-106.

[9] Stephen, J., Manoj, C. and Singh, S.B. "A direct inversion scheme for deep resistivity sounding data using artificial neural networks". *Proc. Indian Acad. Sci. (Earth Planet. Sci.), vol* 113, No. 1, March 2004, pp. 49-66.

[10] Calderon-Macias, C., Sen, M.K. and Stoffa, P. L. "Artificial neural networks for parameter estimation in geophysics". *Geophysical Prospecting*, vol 48, 2000, pp. 21–47.

[11] El-Qady, G. and Ushijima, K. "Inversion of DC resistivity data using neural networks". *Geophysical Prospecting*, vol. 49, 2001, pp. 417-430.

[12] Loke, M.H., Acworth, Ian and Dahlin, Torleif. "A comparison of smooth and blocky inversion methods in 2D electrical imaging surveys". *Exploration Geophysics*, vol. 34, 2003, pp. 182-187.

[13] Sharma, S.P. and Kaikkonen, P. "Two-dimensional non-linear inversion of VLF-R data using simulated annealing". *Geophysical Journal International*, vol. 133, 1998, pp. 649-668.

[14] Basseri, A. and Quezada, J. "Inversion of seismic data by a generalized maximum entropy method.". *71st Ann. Internat. Meeting,Soc. Of Expl. Geophysics.,Expanded Abstracts*, 2001, pp. 744-747.

[15] Ellis, R.G. & Oldenburg, D.W., "The pole–pole 3-D DC-resistivity inverse problem: a conjugate-gradient approach". *Geophys. J. Int* , vol 119,1994, pp.187–194.

[16] Zang, Z. and Zhou, Z. "Real-time quasi 2-D inversion of array resistivity logging data using neural networks". *Geophysics*, vol 67, 2002, pp. 517-524.

[17] Poulton, M.M., Sternberg, B.K. and Glass, C.E." Location of subsurface targets in geophysical data using neural networks". *Geophysics* , Vol. 57 No.12, 1992, pp. 1534-1544.

[18] Murat M.E. and Rudman A. "Automated first arrival picking: A neural network approach". *Geophysical Prospecting,* Vol 40, 1992, pp. 587–604.

[19] Nath S.K., Chakraborty S., Singh S.K. and Ganguly N. "Velocity inversion in cross-hole seismic tomography by the counter-propagation neural network, genetic algorithm and evolutionary programming techniques". *Geophysical Journal International*, Vol 138, 1999, pp. 108–124.

[20] Spichak V., Fukuoka K., Kobayashi T., Mogi T., Popova I. and Shima H. "ANN reconstruction of geoelectrical parameters of the Minou fault zone by the scalar CSAMT data". *Journal of Applied Geophysics*, Vol 49, 2002, pp. 75–90.

[21] Zhang Y. and Paulson K.V. "Magnetotelluric inversion using regularized Hopfield neural networks". *Geophysical Prospecting*, Vol 45, 2002, pp. 725–743.

[22] A. Tettamanzi, M. Tomassini, " Soft Computing: Integrating Evolutionary, Neural, and Fuzzy System ". ISBN: 3540422048 , Published by Springer-Verlag, 1969.

204

[23] Shubhabrata Datta and Malay K.Benerjee, "Optimizing parameters of supervised learning techniques (ANN) for precise mapping of the input-output relationship in TMCP steel",*Scandinavian Journal of Metallurgy*,2004,33:310-315

[24] Freeman J.A., Skapura D.M.,"Neural Networks:Algorithms,Applications, and Programming Techniques" , ISBN 81-7808-108-3, Published by Pearson Education (Singapore) Pte. Ltd., Indian Branch, 482 F.I.E. Patparganj, Delhi 110 092,India. 2002

[25] Lean Yu, Shouyang Wang, and K.K.Lai, "An Integrated Data Preparation Scheme for Neural Network Data Analysis",*IEEE Transactions on Knowledge and Data Engineering*,Vol 18,No.2, 2006, pp.217-230.

[26] Lefteri H. Tsoukalas, Robert E Uhrig ,"Fuzzy and Neural Approaches in Engineering"

[27] Stacy L. Özesmi,Uygar Özesmi, and Can O.Tan, "Methodological issues in Building,Training and Testing Artificial Neural Networks".

[28] Howard Demuth,Mak beale, Neural Network Toolbox for use with Matlab,[1994-2004] Mathwork Inc.

[29] Gosh, D.P.," The application of linear filter theory to the direct interpretation of geoelectrical resistivity sounding measurements". *Geophys. Prospecting*, vol 19, No.2, 1971, pp. 192-217.

[30] Gosh, D.P. ," Inverse filter coefficients for the computation of apparent resistivity standard curves for a horizontally stratified earth", *Geophys. Prosp.*, vol 19, No.2, 1971, pp. 769-775.

[31] Johansen, H.K. 1975 " An interactive computer/graphic-display-terminal; system for the interpretation of resistivity sounding, *Geophysical Prospecting*, vol 23, pp 449-458.

[32] Zohdy, Adel.,. "Electrical Methods in US Geological Survey, Tech Water Resources Inv", Book 2, Chap D1, 1974.

[33] Zohdy, Adel., "Automatic Interpretation of Schlumberger Sounding Curves, Using Modified DarZarrouk Functions," U.S. Geological Survey Bulletin 1313-E, 1975.

[34] D.Guptasarma, and B.Singh,"New Digital Linear Filters for Hankel J0 and J1 transforms", *Geophysical Prospecting*, vol 45,1997, pp. 745-762.

[35] Brian Borchers, Department of Mathematics,New Mexico Tech Socorro, NM 87801

[36] Anderson, W. L., "Computer Program Numerical Integration of Related Hankel Transforms of Orders 0 and 1 by Adaptive Digital Filtering". *Geophysics*, vol44(7), 1979, pp.1287-1305.

[37] Takahashi, T. and Kawase, T.,"Calculation of Eath Resistance for a Deep Driven Multi layer Earth Structure", IEEE transactions on Power Delivery, Vol 6, No.2, 1991, pp. 608-614.

[38] Li, Y. & Oldenburg, D.W., "Inversion of 3-d DC resistivity data using approximate inverse mapping", *Geophys. J. Int.,* vol 116, 1994, pp.527–537.

[39] Uchida T.,"Two-Dimensional Resistivity Inversion for schlumberger Sounding".*BUTSURI-TANSA*, Vol. 44 No. 1,1991,pp. 1-17

[40] Christopher C. Pain, J"org V. Herwanger, Michael H. Worthington and Cassiano R. E. de Oliveira, "Effective multidimensional resistivity inversion using finite-element techniques", *Geophys. J. Int.,* vol 151, 2002, pp. 710–728.

[41] Beard, L.P., Hohmann, G.W. & Tripp, A., "Fast resistivity/IP inversion using a low-contrast approximation", *Geophysics,*vol. 61, 1996, pp. 169–179.

[42] Instruction Manual for EarthImager 2D Version 2.1.7 ,Resistivity and IP Inversion Software, copyright 2002-2006 by Advanced Geosciences, Inc., 12700, Volente Rd., FM 2769, Bldg A,Austin, Texas,78726. pp. 76.

[43] Xianjin Yang , "Comparison of 2D and 3D Electrical Resistivity Imaging Methods", Mats Lagmanson, 19th Annual SAGEEP, Geophysical Applications for Environmental and Engineering Hazzards- Advances and constraints, April 2-6,2006.

[44] Dahlin, T., Bernstone, C. and Loke, M.H., "A 3-D resistivity investigation of a contaminated site at Lernacken, Sweden". *Geophysics*, vol 67, 2002, pp. 1692-1700.

[45] *RES3DINV ver. 2.15 for Windows 98/Me/2000/NT/XP Rapid 3D Resistivity & IP inversion using the least-squares method (For 3-D surveys using the pole-pole, pole-dipole, dipole-dipole, rectangular, Wenner, Wenner-Schlumberger and non-conventional arrays)On land, underwater and borehole surveys, Geoelectrical*

Imaging 2D & 3D, April 2005, GEOTOMO SOFTWARE,5 Cangkat Minden Lorong 6, Minden Heights, 11700 Gelugor,Penang, MALAYSIA

Appendix A

Potentials in Homogeneous media

The basic building block of the resistivity method is the potential build up in the earth due to a point electrode. To evaluate this, consider a continuous current (dc or low frequency ac) flowing in an isotropic homogeneous medium from a point source on the surface of a half-space.

If δA is an element of surface and J the current density in amperes per meters, then the current passing through δA is $J.\delta A$.

The current density J and the Electric field E are related through Ohm's law,

$$J = \sigma E \tag{A.1}$$

Where E is in V/m and σ is the conductivity of the medium in S/m.

The electric field is the gradient of a scalar potential

$$E = -\nabla V \tag{A.2}$$

Thus we have,

$$J = -\sigma \nabla V \tag{A.3}$$

Divergence of current density is equivalent to the rate of accumulation of charge density Q which is also referred as the equation of continuity,

$$\nabla . J = -\frac{\delta Q}{\delta t} \tag{A.4}$$

In regions of finite conductivity, charges do not accumulate to any extent during current flow, hence $Q = 0$ so that $\nabla . J = 0$. So,

$$\nabla .(\sigma \nabla V) = 0 \tag{A.5}$$

$$\nabla \sigma .\nabla V + \sigma \nabla^2 V = 0 \tag{A.6}$$

If σ is constant throughout finally the Laplace's Equation is achieved

$$\nabla^2 V = 0 \tag{A.7}$$

In order to evaluate the potential build up we can write the Laplace's equation either in spherical coordinates or with the Cartesian coordinate system.

Since the electric potential depends only on distance it is appropriate to write Laplace's equation in spherical coordinates with a r dependence only. Where r is the distance from the electrode.

$$\frac{1}{r^2}\left[\frac{\partial}{\partial r}\left(r^2 \frac{\partial V}{\partial r}\right)\right] = 0 \tag{A.8}$$

This gives the solution

$$V = -\frac{A}{r} + B \tag{A.9}$$

Where A and B are constants to be determined. Since potential should be zero at a great distance of r (i.e. $r \rightarrow \infty$) it is obvious that $B = 0$.

Now,

$$V = -\frac{A}{r} \tag{A.10}$$

From (A.2) and (A.3)

$$E = \frac{\partial V}{\partial r} = \frac{A}{r^2} = \rho J \tag{A.11}$$

Since the current flows radially outwards in all the directions the total current I crossing a hemi- spherical surface is given by,

$$I = 2\pi r^2 J \tag{A.12}$$

Thus,

If σ is constant throughout finally the Laplace's Equation is achieved

$$\nabla^2 V = 0 \tag{A.7}$$

In order to evaluate the potential build up we can write the Laplace's equation either in spherical coordinates or with the Cartesian coordinate system.

Since the electric potential depends only on distance it is appropriate to write Laplace's equation in spherical coordinates with a r dependence only. Where r is the distance from the electrode.

$$\frac{1}{r^2}\left[\frac{\partial}{\partial r}\left(r^2\frac{\partial V}{\partial r}\right)\right] = 0 \tag{A.8}$$

This gives the solution

$$V = -\frac{A}{r} + B \tag{A.9}$$

Where A and B are constants to be determined. Since potential should be zero at a great distance of r (i.e. $r \to \infty$) it is obvious that $B = 0$.

Now,

$$V = -\frac{A}{r} \tag{A.10}$$

From (A.2) and (A.3)

$$E = \frac{\partial V}{\partial r} = \frac{A}{r^2} = \rho J \tag{A.11}$$

Since the current flows radially outwards in all the directions the total current I crossing a hemi- spherical surface is given by,

$$I = 2\pi r^2 J \tag{A.12}$$

Thus,

$$\frac{A}{r^2} = \rho J = \frac{I\rho}{2\pi r^2} \qquad \text{(A.13)}$$

Therefore,

$$A = -\frac{\rho I}{2\pi} \qquad \text{(A.14)}$$

Hence,

$$V = \frac{\rho I}{2\pi r} \qquad \text{(A.15)}$$

Which is the voltage at a distance r from a point source of current (electrode) at the surface of a half-space.

Appendix B

Potentials in Non-Homogeneous media

B.1 Determining the potential at a point in a non homogeneous medium

The analogy between the electrical case and optics is based on the fact that current density, like light intensity, decrease with the inverse square of distance from a point source in a medium of resistivity ρ_1, separated by an adjacent medium ρ_2 by a plane boundary.

In the optics the analogous case would be a point source of light in one medium separated from another by a semitransparent mirror having reflection and transmission coefficient k and $k-1$ respectively .Then the light intensity at a point in the first medium is partly due to the point source and partly to its image in the second medium diminished by the reflection from the mirror. On the other hand the intensity at a point in the second medium is only due to the source in the fiest medium diminished by transmission through the mirror.

So to evaluate the potential of a given point in a non homogeneous medium involving two mediums the following argument (Figure B.1) is used. The point source of light and the light intensity at a point is now replaced by a point source of current and a potential. Now the problem is in the electrical domain.
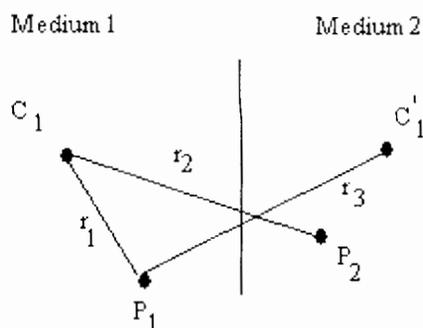
Figure B.1 Optical Image arrangement to analyze the potential development

- The potential of a point P_1 is due to the current source C_1 and the image of the current source C_1' effected by the reflection coefficient k of the boundary. Therefore the potential at P_1 in the first medium is,

$$V_1 = \frac{I\rho_1}{4\pi}\left(\frac{1}{r_1} + \frac{k}{r_2}\right)$$ (B.1)

- While the potential P_2 in the second medium is only due to the current source C_1 effected by the transmission coefficient $(1-k)$ at the boundary.

$$V_2 = \frac{I\rho_2}{4\pi}\left(\frac{1-k}{r_3}\right)$$ (B.2)

Applying the boundary condition these potentials must be equal at the interface when $r_1 = r_2 = r_3$. Thus,

$$\frac{\rho_1}{\rho_2} = \frac{1-k}{1+k} \text{ or } k = \frac{\rho_2 - \rho_1}{\rho_2 + \rho_1}$$ (B.3)

Where,

k - Reflection Coefficient and $-1 < k < 1$.

k depends on the relative resistivities in the two media.

B.2 Potential at a point on the surface of a half-space with horizontal beds

With this argument the potential at a point on the surface (with two layers) where the current electrode is fixed, can be shown to be affected by infinite set of images above and below the current electrode,(Figure B.2) due to three layers involved, namely air, medium 1 and medium 2.
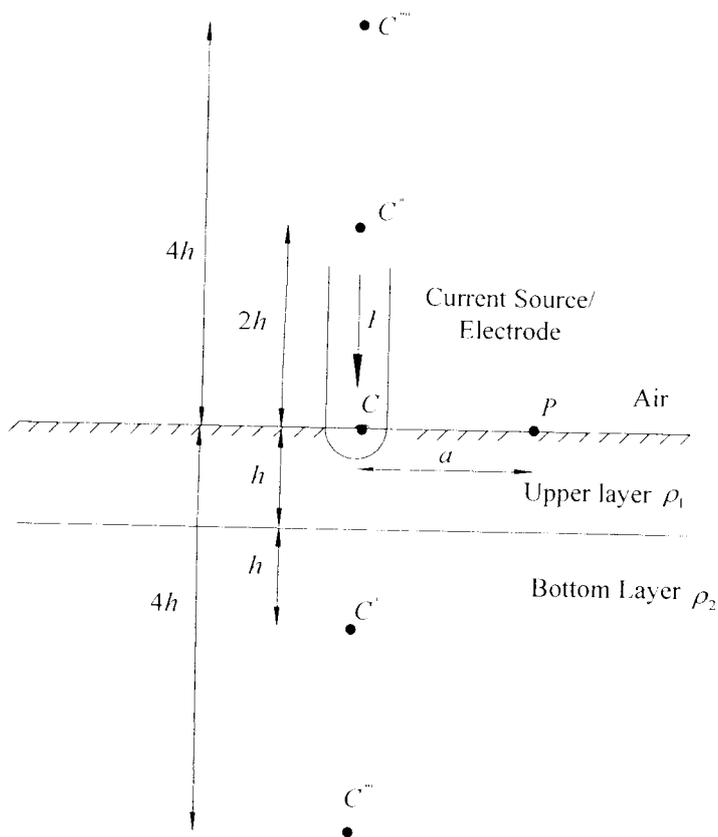
Figure B.2 Infinite set of images due to current source C ($C', C'', C''', C'''', ..$)

- C - Current source

- C' - Original image of current source C from the interface between the two medias at a $2h$ depth below C

- C'' -Image of C' from the interface between air and upper layer $2h$ above C

- C''' - Image of C'' from the interface between the two medias at $4h$ depth below C

- C'''' - Image of C''' from the interface between air and upper layer $4h$ above C

This effect of each successive image on the potential at P reduces by the reflection coefficient between the boundaries.

Potential at P due to the current source C and its first image C' is,

$$V_1 = \frac{I\rho_1}{2\pi}\left(\frac{1}{a} + \frac{k}{r_1}\right)$$

(B.4)

213

Where,

$$k = \frac{\rho_2 - \rho_1}{\rho_2 + \rho_1} \quad \text{Reflection Coefficient at the boundary of the two layers}$$

The effect on potential at P due to $C^{'}$ is,

$$V_2 = \frac{I\rho_1}{2\pi}\left(\frac{k \times k_a}{r_1}\right) \qquad (B.5)$$

Where,

k_a - Reflection coefficient at the surface boundary.

Since resistivity of the air is essentially infinite $k_a = 1$.

The potential due to the third image $C^{''}$, $4h$ below the surface will further reduce, as will that of its image $C^{'''}$, $4h$ above the surface,

$$V_3 + V_4 = \frac{I\rho_1}{2\pi}\left(\frac{k \times k}{r_2} + \frac{k \times k \times k_a}{r_2}\right)$$

$$= \frac{I\rho_1}{2\pi}\left(\frac{2k^2}{r_2}\right) \qquad (B.6)$$

Therefore the surface potential at a point on a horizontal bed is an equation with infinite series of the form,

$$V = V_1 + V_2 + V_3 + V_4 + \dots V_m + \dots$$

$$V = \frac{I\rho_1}{2\pi}\left\{\frac{1}{a} + \frac{2k}{r_1} + \frac{2k^2}{r_2} + \dots + \frac{2k^m}{r_m} + \dots\right\} \qquad (B.7)$$

Where,

$$r_1 = \left\{ a^2 + (2h)^2 \right\}^{1/2}$$

$$r_2 = \left\{ a^2 + (4h)^2 \right\}^{1/2}$$

$$r_m = \left\{ a^2 + (2mh)^2 \right\}^{1/2}$$

This can be written in the compact form,

$$V = \frac{I\rho_1}{2\pi} \left[\frac{1}{a} + 2\sum_{m=1}^{\infty} \frac{k^m}{\left\{ a^2 + (2mh)^2 \right\}^{1/2}} \right]$$

$$V = \frac{I\rho_1}{2\pi a} \left[1 + 2\sum_{m=1}^{\infty} \frac{k^m}{\left\{ 1 + (2mh/a)^2 \right\}^{1/2}} \right] \qquad (B.8)$$

i.e. for two layer earth with upper medium of resistivity ρ_1 and height h with bottom layer of resistivity ρ_2 and infinite depth the surface potential at a distance a from the current electrode is given by the equation (B.8).

Appendix C

Methods of Resistivity surveys and Electrode Arrays

C.1 Types of resistivity Surveys

There are two basic field procedures used with the resistivity surveys, Electrical Sounding and Electrical profiling or mapping. The survey type selection depends on whether one is interested in resistivity variation with depth or with lateral extent. The first is called Vertical Electric Sounding (VES) the second lateral profiling.

C.1.1 Vertical Electrical Sounding (VES)

Since the fraction of total current that flows at depth varies with the current electrode separation [refer the big book] the field procedure is to use a fixed center with an expanding spread. The presence of horizontal or gently dipping beds of different resistivities is best detected by the expanding spread. Hence the method is applicable in estimation of depth to bedrock, to a water baring layer, to sand or gravel; estimating the thickness of a layer; estimation of the variation of resistivity with the depth and determining the sequence of high and low resistivity zones.

C.1.2 Lateral Profiling

This method is particularly useful in mineral exploration where the detection of isolated bodies of anomalous resistivity is required. Lateral exploration by resistivity measurements is best suited for 2D resistivity surveys for detection of steeply dipping contacts and dikes of contrasting resistivities that is locating faults or faulty zones; prospecting sand and gravel deposits; delineating the boundaries of and gravel deposits and prospecting for ore bodies.

C.2 Electrode Arrays

The resistivity imaging method uses standard arrays developed for electrical resistivity sounding and profiling techniques. A line of electrodes is placed at intervals along the desired profile. Four electrodes are used at one time. Two inject current into the ground and two read the electrical potential between them. The short electrode intervals look at the shallow earth, and the longer intervals look more deeply.

C.2.1 Wenner Array

This is the most commonly used point electrode array (Figure C.1). In the wenner array the electrodes are uniformly spread in a line. Setting $r_1 = r_4 = a$ and $r_2 = r_3 = 2a$ in equation (2.15) the apparent resistivity of the wenner array is,

$$\rho_a = 2\pi a \, \Delta V / I \qquad\qquad\qquad (C.1)$$

Where,

      a - Electrode Spacing

      ΔV - voltage difference between the current electrodes

      I – Current injected by the current electrodes
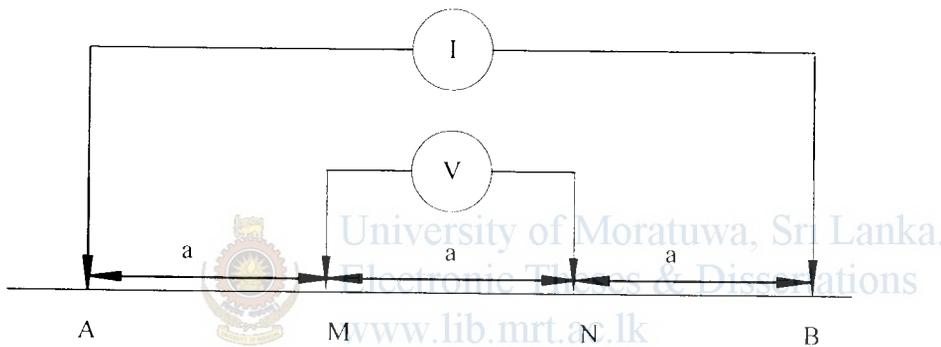
Figure C.1 Wenner Array Electrode arrangement

Wenner array can be used for both resistivity profiling and depth sounding. For depth exploration the electrodes are expanded about a fixed center increasing the spacing a in steps. For lateral exploration or mapping the spacing remains constant and all four electrodes are moved along the line, then along another line and so on. In mapping the apparent resistivity for each array position is plotted against the centre of the spread.

Therefore, in this array all four electrodes are moved making it less time efficient for profiling, but since the distances between the electrodes are small, mistakes are less likely. In the Wenner array near-surface conditions differ at all four electrodes for each reading, giving a rather high noise level. A very much smoother curve can be produced using offsetting techniques. Offsetting is achieved by setting out five equal-spaced electrodes, two readings are then taken at each expansion and averaging of the two produces a curve in which local effects are suppressed, while differencing provides estimates of the significance of those effects.

Because the signal-contribution contours for the Wenner array at depth are slightly flatter than those of the Schlumberger array we will often use Wenner array for locating flat laying interfaces.

C.2.2 Schlumberger Array

In this array the current electrodes are spaced much further apart than the potential electrodes (Figure C.2). Here $r_1 = r_4 = L - l$ and $r_2 = r_3 = L + l$ and equation (2.15) gives,

$$\rho_a = \frac{\pi}{2l}\left(L^2 - l^2\right)\frac{\Delta V}{I} \qquad (C.2)$$

Where,

L - Spacing between the current electrodes $\left(\frac{AB}{2}\right)$

l - Spacing between the current electrodes $\left(\frac{MN}{2}\right)$

ΔV - voltage difference between the current electrodes

I – Current injected by the current electrodes

Or with alternate symbols frequently found in literature i.e. using A, B, M and N for C_1, C_2, P_1 and P_2 equation (C.2) can be re-written as,

$$\rho_a = \frac{\pi}{4MN}\left(AB^2 - MN^2\right)\frac{\Delta V}{I} \qquad (C.3)$$
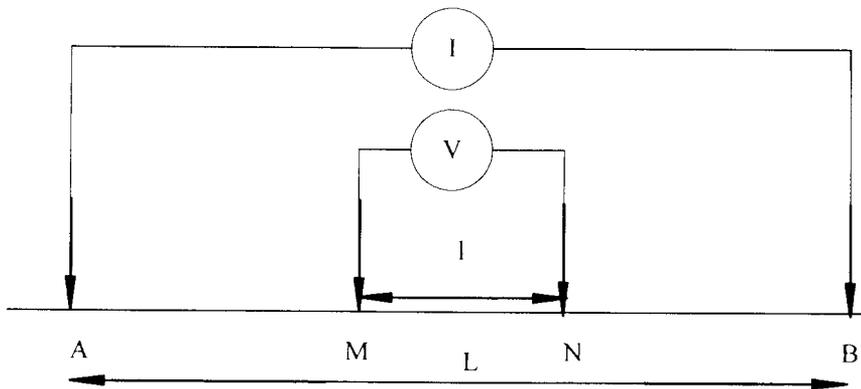
Figure C.2 Schlumberger Array Electrode Arrangement

In vertical sounding the potential electrodes remain fixed while the current electrode spacing is expanded symmetrically about the centre of the spread. Even though portability is less important in resistivity depth sounding than in profiling the Schlumberger array will be used were appropriate because of speed and convenience. However for large values of L it is necessary to increase l in order to maintain a measurable potential.

Site selection is extremely important with the Shlumberger array because it is sensitive to conditions around the closely-spaced inner electrodes. Therefore, locations where the upper layer is very inhomogeneous may not be suitable for the Schlumberger array and the offset Wenner array will be used.

C.2.3 Pole-Pole array

In the Pole-Pole array one of the current electrodes and one of the potential electrodes are placed so far away that they can be considered at infinity (Figure C.3). Setting $r_2 = r_3 = r_4 = \infty$ and $r_1 = a$ in equation (2.15) the apparent resistivity of the Pole-Pole array is,

$$\rho_a = 2\pi a \frac{\Delta V}{I}$$
(C.4)

Where,

a - Electrode Spacing between the first current and first Potential electrode

ΔV - voltage difference between the current electrodes

I Current injected by the current electrodes
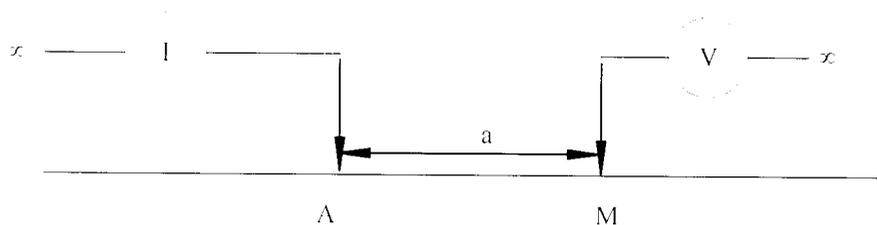
Figure C.3 Pole-pole Array Electrode Arrangement

This array can actually be achieved for surveys of small overall dimension when it is possible to put the distant electrodes some practical distance away. For a survey in an area of a few square meters "infinity" can be on the order of a hundred meters.

C.2.4 Pole-dipole Array

In this array type only one of the current electrodes is placed at "infinity" (Figure C.4). Setting $r_1 = b$, $r_3 = a+b$ and $r_2 = r_4 = \infty$ in equation (2.15) the apparent resistivity of the Pole-dipole array is,

$$\rho_a = 2\pi \frac{b(b+a)}{a} \Delta V/I \qquad\qquad (C.5)$$

Where,

a - Electrode Spacing between the Potential electrodes

b - Electrode Spacing between the first current and the first Potential electrode

ΔV - Voltage difference between the current electrodes

I - Current injected by the current electrodes
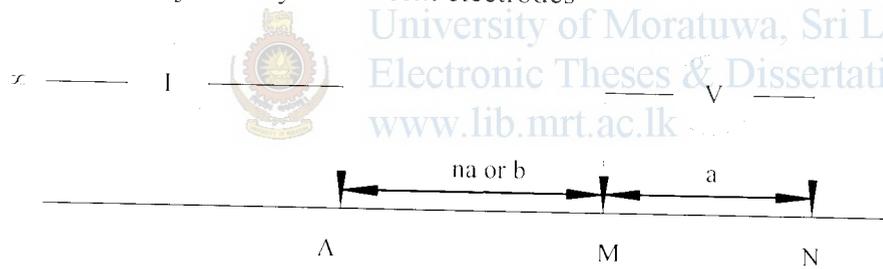
(a)
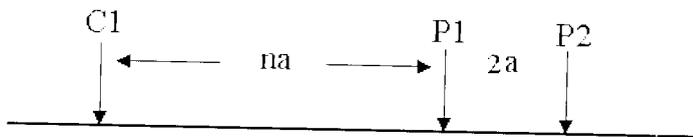
(b)
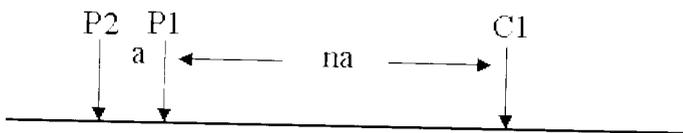
(c)

Figure C.4 Pole-dipole Array Electrode Arrangement
(a) "forward" direction, (b) with a larger spacing between the potential electrodes
And (c) in the "reverse" direction.

This array is used frequently in resistivity surveying and the spacing are usually described, and taken, in integer multiples of the voltage electrode spacing b. The standard nomenclature is to call the potential electrode spacing a so the apparent resistivity become.

$$\rho_a = 2\pi a n(n+1) \Delta V / I \qquad (C.6)$$

When used in two dimensional resistivity surveys, this array is an attractive alternative to the pole-pole array for surveys with medium and large survey grids (12 by 12 and above). It has a better resolving power than the pole-pole array, and is less susceptible to telluric noise since both potential electrodes are kept within the survey grid. Compared to the dipole-dipole array, it has significantly stronger signal strength.

Unlike other common arrays, it is an asymmetrical array. Over symmetrical structures the apparent resistivity anomalies are also asymmetrical. In some situations, the asymmetry in the measured apparent resistivity values could influence the model obtained after inversion. One method to eliminate the effect of this asymmetry is to repeat the measurements with the electrodes arranged in the reverse manner (Figure C.4(c)). By combining the measurements with the "forward" and "reverse" pole-dipole arrays, any bias in the model due to the asymmetrical nature of this array would be removed.

The voltage measure between the potential electrodes decreases with the square of the n factor. For large values of the n factor, the signal to noise ratio might become too small for a reliable measurement to be made. To increase the signal strength, the distance between the P1 and P2 electrodes is increased (Figure C.4 (b)). One possible field technique is to make all the possible measurements with the P1-P2 spacing equals to 1a (i.e. the unit electrode spacing), followed by measurements with P1-P2 spacing equals to 2a. This will increase the data density. In some cases, particularly in noisy areas, has been found by having such redundant measurements improves the resolution of the resulting inversion model.

C.2.5 Dipole-dipole Array

In the dipole-dipole array (Figure C.5) the current and voltage spacing is the same and the spacing between them is an integer multiple. This sets $r_1 = r_4 = a(n+1)$, $r_2 = na$ and $r_3 = a(n+2)$ in equation (2.15) and the apparent resistivity of the Dipole-dipole array is.

$$\rho_a = \pi a n (n+1)(n+2) \Delta V / I \qquad\qquad (C.7)$$

(a)

(b)
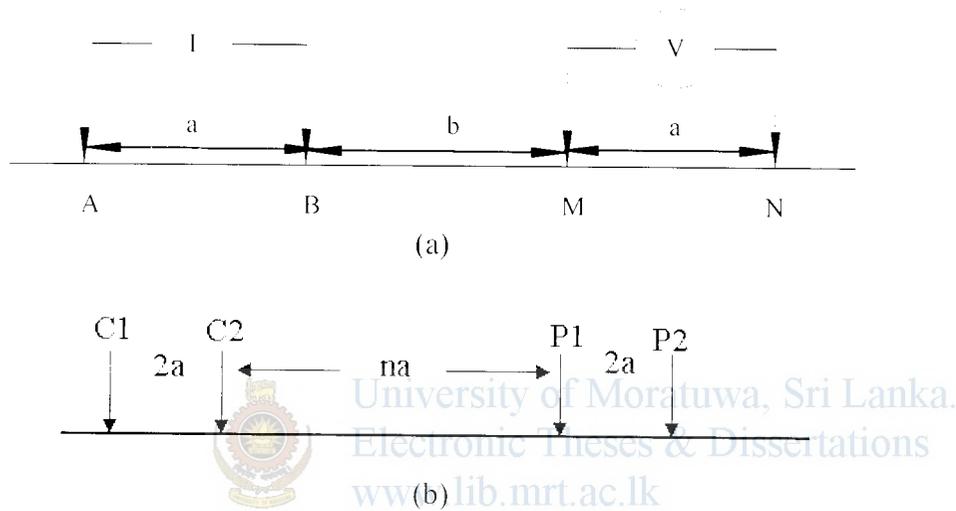
Figure C.5 (a) The arrangement of the electrodes for the dipole-dipole array.
(b) The use of a larger spacing between the C1-C2 (and P1-P2) electrodes
to increase the signal strength.

This array is mainly used in IP work where induction effects must be avoided at all costs; however it is also effective in resistivity profiling. The dipole-dipole array is logistically the most convenient in the field, especially for large spacing. It uses four moving electrodes and is therefore less desirable also the observed voltages tend to be rather small. All the other arrays require significant lengths of wire to connect the power supply and voltmeter to their respective electrodes and these wires must be moved for every change in spacing as the array is either expanded for a sounding or moved along a line.

Although theoretically possible the dipole-dipole array will not be used for resistivity depth sounding. When used in two dimensional resistivity studies, this array can is

recommended only for grids that are larger than 12 by 12 due to the poorer horizontal data coverage at the sides.

This array has the advantage of very good horizontal resolution, but its main disadvantage is its relatively low signal strength. The voltage measured by the P1-P2 pair is inversely proportional to the cube of the n factor. Normally, the maximum value for the n factor is 6. To get a deeper depth of penetration, the spacing between the C1-C2 (and P1-P2) pair is increased. One method to reduce the effect of noise is to make redundant measurements using different combinations of the n factor and the a spacing.

Appendix D
Matlab Programs for the synthetic data generation of two layers and three layers

1. This is the main program that calculates 300 training samples for training for the two layer case and save them.This calls the function 'mytest' with the layer parameters as inputs to generate the apparent resistivity curves. Variables p1 and p2 are the upper layer and bottom layer resistivities respectively. Parameter 'h' gives the values of upper layer height selected for the data generation.

```
function [resistivitydata,target]= calcresisitivity()

p1=[10 98 175 325 475 545  725 840 100 220 420 50 935 620 250];

p2=[1000 300 520 600 500 650 1000 1000 400 600 750 250 1000 700 500];

h=[1 2.5 5 3 7.5 4.25 6 8.3 9.2 10];

i=1;

[u1 v1]=size(h);
[u2 v2]=size(p1);
m=300;
n=40;
resistivitydata2=zeros(m,n);
target2=zeros(m,6);
k=1;
while i<=v2
   j=1;
   while j<=v1
      x=p1(i);
      y=p2(i);
      z=h(j);
      [distance resval]=mytest(x,y,z);
      resistivitydata2(k,:)=resval;
      target2(k,:)=[1 0 0 0 0 0];
      j=j+1;
      k=k+1;
   end
   i=i+1;
end

p1=[300 450 1000 220 500 650 900 725 1000 850 600 700 500 350 1000]
```

```
p2=[250 100 100 20 350 400 300 500 200 400 300 100 175 200 300]

h=[1 2.5 5 3 7.5 4.25 6 8.3 9.2 10];

i=1;

[u1 v1]=size(h);
[u2 v2]=size(p1);
while i<=v2
    j=1;
    while j<=v1
        x=p1(i);
        y=p2(i);
        z=h(j);
        [distance resval]=mytest(x,y,z);
        resistivitydata2(k,:)=resval;
        target2(k,:)=[0 1 0 0 0 0]
        j=j+1;
        k=k+1;
    end
    i=i+1;
end
save ('D:\MATLAB7\work\1D\appresdata2.mat','resistivitydata2')
save ('D:\MATLAB7\work\1D\target2.mat','target2')
```

2. This function takes the two layer parameters as the inputs and returns the apparent resistivity data points of 40 successive points to the main program. Variable 'B' gives wenner spread spacings used for the data generation, spacing is varied from 0.001 to 390m in 10m steps.

```
function [B,integral]= mytest(p1,p2,h)

B=[0.001 10:10:390];
B1=2*B;

ourvec=zeros(size(B));
ourvec1=zeros(size(B1));

for i=1:length(B),
    ourvec(i)=hankel('twolayerh',B(i),p1,p2,h);
end;

for i=1:length(B1),
    ourvec1(i)=hankel('twolayerh',B1(i),p1,p2,h);
end;

for i=1:length(B),
    integral(i)=p1*((ourvec(i)-ourvec1(i))*(4*B(i))+1);
end;
```

3.This function calculates the infinite integral in the equation 2.45 with digital filter operations.

funname   The name of the function to be transformed.

B   The transform argument. (the electrode spacing in this application)

z0   The value of the transform of order 0.

function z0=hankel(funname,B,p1,p2,h)

YBASE=[];   - The 801 sampling points

WT0=[ ];   - The 801 filter weights

Y=YBASE/B;   - Get the points at which to evaluate F.

YF=feval(funname,p1,p2,h,Y);   - Evaluate F at these points.

z0=WT0.'*YF;   - Compute the dot product.

z0=z0/B;   - Finally correct for the factor of 1/B.

The 801 parameters of the J_0 filter is given later in the Appendix A.

4. This is the function that illustrates the resistivity forward modeling kernel function for two layers.

function f=twolayerh(p1,p2,h,g)

k=(p2-p1)/(p2+p1);

f=(k*exp(-2*h*g))./(1-(k*exp(-2*h*g)));

5. This is the main program that calculates 600 training samples for training for the three layer case and save them.This calls the function 'mytest3' with the five layer parameters as inputs to generate the apparent resistivity curves. Variables p1, p2 and p3 are the first layer , second layer and bottom layer resistivities respectively. Parameter h1 gives the values of first layer height and h2 gives the values of second layer heights selected for the data generation.

function [resistivitydata,target]= calcresisitivity3()

% Type A curve generation for condition P1<P2<P3
p1=[10 100 120 210 300 125 175 500 350 475 250 220 420 50 400];

```matlab
p2=[300 235 400 456 350 543 700 642 377 532 500 240 800 400 675];

p3=[1000 300 520 600 500 650 1000 1000 400 600 750 250 1000 700 800];

h1=[1 2.5 5 3 7.5 4.25 6 8.3 9.2 10];
h2=[4 6.75 3.8 9.4 2 10 3.5 7.4 8.3 10];

i=1;

[u1 v1]=size(h1);
[u2 v2]=size(p1);
m=600;
n=40;
resistivitydata3=zeros(m,n);
target3=zeros(m,6);
k=1;
while i<=v2
    j=1;
    while j<=v1
        x=p1(i);
        y=p2(i);
        a=p3(i);
        z=h1(j);
        b=h2(j);
        [distance resval]=mytest3(x,y,a,z,b);
        resistivitydata3(k,:)=resval;
        target3(k,:)=[0 0 1 0 0 0];
        j=j+1;
        k=k+1;
    end
    i=i+1;
end


%Type H curve generation for condition P1>P2<P3

p1=[300 450 500 220 500 650 900 725 452 850 600 700 500 350 750];
p2=[100 100 100 20 350 400 300 500 200 400 300 100 175 200 300];
p3=[700 800 1000 467 879 743 1000 865 678 975 700 1000 775 920 1000];
h1=[1 2.5 5 3 7.5 4.25 6 8.3 9.2 10];
h2=[4 6.75 3.8 9.4 2 10 3.5 7.4 8.3 10];

i=1;
[u1 v1]=size(h1);
[u2 v2]=size(p1);
while i<=v2
    j=1;
    while j<=v1
        x=p1(i);
        y=p2(i);
        a=p3(i);
```

```matlab
            z=h1(j);
            b=h2(j);
            [distance resval]=mytest3(x,y,a,z,b);
            resistivitydata3(k,:)=resval;
            target3(k,:)=[0 0 0 1 0 0];
            j=j+1;
            k=k+1;
        end
        i=i+1;
end


%Type K curve generation for Condition P1<P2>P3
%75 examples each for small h2 and large h2
p1=[245 350 725 120 685 400 100 195 720 500 830 900 200 475 540];
p2=[500 450 1000 800 950 575 300 660 1000 750 950 1000 620 800 720];
p3=[100 20 400 10 350 100 25 78 200 340 250 620 20 300 210];
h1=[2 5.5 8 1.5 9.25 6.4 3.6 4.4 7 10];
h21=[1 1.5 4 2 5 ];
h22=[20 15 9 100 50];


i=1;
[u1 v1]=size(h1);
[u2 v2]=size(h21);
[u3 v3]=size(p1);
while i<=v3
    j=1;
    if rem(i,2)==1
        l=1;
    end
    if rem(i,2)==0
        l=5;
    end

    while j<=v2
        x=p1(i);
        y=p2(i);
        a=p3(i);
        z=h1(l);
        b=h21(j);

        [distance resval]=mytest3(x,y,a,z,b);
        resistivitydata3(k,:)=resval;
        target3(k,:)=[0 0 0 0 1 0];

        l=l+1;
        j=j+1;
        k=k+1;
    end
    i=i+1;
end
i=1;
```

```
[u1 v1]=size(h1);
[u2 v2]=size(h22);
[u3 v3]=size(p1);

while i<=v3
   j=1;
   if rem(i,2)==1
      l=1;
   end
   if rem(i,2)==0
      l=5;
   end

   while j<=v2
      x=p1(i);
      y=p2(i);
      a=p3(i);
      z=h1(l);
      b=h22(j);

      [distance resval]=mytest3(x,y,a,z,b);
      resistivitydata3(k,:)=resval;
      target3(k,:)=[0 0 0 0 1 0];

      l=l+1;
      j=j+1;
      k=k+1;
   end
   i=i+1;
end

%Type Q curve generation for Condition P1>P2>P3
%75 examples each for small h2 and large h2
p1=[800 750 1000 975 1000 998 800 700 675 900 700 1000 700 1000 750];
p2=[300 420 600 750 600 800 450 100 350 675 100 750 500 700 560];
p3=[100 250 345 472 560 630 200 20 70 300 10 420 150 485 100];
h1=[4 6 7.2 1 10 7.5 3.25 4.4 5 2.67];
h21=[1 1.5 4 2 5 ];
h22=[20 15 30 100 45];

i=1;

[u1 v1]=size(h1);
[u2 v2]=size(h21);
[u3 v3]=size(p1);

while i<=v3
   j=1;
   if rem(i,2)==1
      l=1;
```

```
end
if rem(i,2)==0
    l=5;
end

while j<=v2
    x=p1(i);
    y=p2(i);
    a=p3(i);
    z=h1(l);
    b=h21(j);

    [distance resval]=mytest3(x,y,a,z,b);
    resistivitydata3(k,:)=resval;
    target3(k,:)=[0 0 0 0 0 1];

    l=l+1;
    j=j+1;
    k=k+1;
end
i=i+1;
end
i=1;

[u1 v1]=size(h1);
[u2 v2]=size(h22);
[u3 v3]=size(p1);

while i<=v3
    j=1;
    if rem(i,2)==1
        l=1;
    end
    if rem(i,2)==0
        l=5;
    end

    while j<=v2
        x=p1(i);
        y=p2(i);
        a=p3(i);
        z=h1(l);
        b=h22(j);

        [distance resval]=mytest3(x,y,a,z,b);
        resistivitydata3(k,:)=resval;
        target3(k,:)=[0 0 0 0 0 1];

        l=l+1;
        j=j+1;
        k=k+1;
```

```
    end
    i=i+1;
  end
save ('D:\MATLAB7\work\1D\appresdata3.mat','resistivitydata3')
save ('D:\MATLAB7\work\1D\target3.mat','target3')
```

6. This function takes the three layer parameters as the inputs and returns the apparent resistivity data points of 40 successive points to the main program

```
function [B,integral]= mytest3(p1,p2,p3,h1,h2)

B  [0.001 1.25:1.25:48.75];
B1=2*B;

ourvec=zeros(size(B));
ourvec1=zeros(size(Bi));

for i=1:length(B),
  ourvec(i)=hankel03('threelayerh',B(i),p1,p2,p3,h1,h2);
end;

for i=1:length(B1),
  ourvec1(i)=hankel03('threelayerh',B1(i),p1,p2,p3,h1,h2);
end;

for i=1:length(B),
  integral(i)=p1*((ourvec(i)-ourvec1(i))*(4*B(i))+1);
end;
```

7. This function calculates the infinite integral with digital filter operations . This is similar to the function **hankel** given in 3, except the number of arguments passed to the function are different.

```
%  funname     The name of the function to be transformed.
%  B           The transform argument.
%  z0          The value of the transform of order 0.
```

```
function z0=hankel03(funname,B,p1,p2,p3,h1,h2)

YBASE=[ ];                  - The 801 sampling point

WT0=[ ];                    - The 801 weights

Y =YBASE/B;                 -Get the points at which to evaluate F.

YF=feval(funname,p1,p2,p3,h1,h2,Y);- Evaluate F at these points.

z0=WT0.'*YF;                - Compute the dot product.
```

231

z0=z0/B;   - Finally correct for the factor of 1/B.

8. This is the function that illustrates the resistivity forward modeling kernel function for three layers.

function f=threelayerh(p1,p2,p3,h1,h2,x)

```
k1=(p2-p1)/(p2+p1);
k2=(p3-p2)/(p3+p2);

i=k2*exp((-2)*h2*x);
j=k1*k2*exp((-2)*h2*x);
k=k1+i;
l=1+j;

K31=k./l;

m=K31.*exp((-2)*h1*x);
n=1-m;

f=m./n;
```

Parameters of the 801 –point J_0 filter

Sampling Points 1 to 192

8.9170998013274418e-14	1.0835205199155280e-11	1.3165903076505279e-09	1.5997943798373573e-07
9.8549193740052245e-14	1.1974753677488471e-11	1.4550573190356333e-09	1.7680462234971138e-07
1.0891370292130841e-13	1.3234149515479672e-11	1.6080870331313015e-09	1.9539932680224871e-07
1.2036825704856076e-13	1.4625997169973058e-11	1.7772110227512649e-09	2.1594965339340473e-07
1.3302749714952345e-13	1.6164226720110948e-11	1.9641219376281762e-09	2.3866127669890702e-07
1.4701812115404443e-13	1.7864233284247930e-11	2.1706904450210516e-09	2.6376150227843728e-07
1.6248015192957209e-13	1.9743031099469828e-11	2.3989839519819520e-09	2.9150154162607256e-07
1.7956833867707590e-13	2.1819423805797136e-11	2.6512872966606394e-09	3.2215902637935327e-07
1.9845370571306282e-13	2.4114192639334462e-11	2.9301256157327411e-09	3.5604078695002664e-07
2.1932526413842005e-13	2.6650304417866294e-11	3.2382896168163261e-09	3.9348592338593700e-07
2.4239190352504162e-13	2.9453141400488783e-11	3.5788635088117363e-09	4.3486919919827997e-07
2.6788448255287407e-13	3.2550755321790057e-11	3.9552558697009004e-09	4.8060479212078480e-07
2.9605813952117967e-13	3.5974148143038491e-11	4.3712337607414382e-09	5.3115043933968360e-07
3.2719484585839035e-13	3.9757582330231206e-11	4.8309604284818817e-09	5.8701201868132178e-07
3.6160622818693727e-13	4.3938923764369768e-11	5.3390369719324459e-09	6.4874861160747570e-07
3.9963668718722961e-13	4.8560020715924429e-11	5.9005483919104070e-09	7.1697809869053571e-07
4.4166684447542096e-13	5.3667122676390673e-11	6.5211144834374116e-09	7.9238334356995170e-07
4.8811735199247527e-13	5.9311343238745088e-11	7.2069460805369272e-09	8.7571902728105488e-07
5.3945310203017795e-13	6.5549171659463761e-11	7.9649072163486862e-09	9.6781920135651654e-07
5.9618788002944785e-13	7.2443038221987792e-11	8.8025838206794284e-09	1.0696056352944216e-06
6.5888950671771899e-13	8.0061939059983487e-11	9.7283596425381269e-09	1.1820970419372223e-06
7.2818552104963217e-13	8.8482126693838504e-11	1.0751500157513941e-08	1.3064192730922673e-06
8.0476946082781583e-13	9.7787873191515278e-11	1.1882245299770154e-08	1.4438165874351013e-06
8.8940780386232124e-13	1.0807231359173195e-10	1.3131911946747030e-08	1.5956641034684996e-06
9.8294763913816720e-13	1.1943837803073370e-10	1.4513007182274982e-08	1.7634815621706371e-06
1.0863251447666186e-12	1.3199982190169224e-10	1.6039353471673310e-08	1.9489485370736003e-06
1.2005749575703847e-12	1.4588236435691521e-10	1.7726227001629019e-08	2.1539212439998211e-06
1.3268405280766938e-12	1.6122494654737812e-10	1.9590510569407677e-08	2.3804511186939235e-06
1.4663855645544968e-12	1.7818112219246310e-10	2.1650862551562963e-08	2.6308053482811660e-06
1.6206066806315702e-12	1.9692059439719362e-10	2.3927903643240499e-08	2.9074895620382204e-06
1.7910473730731204e-12	2.1763091409794871e-10	2.6444423237025737e-08	3.2132729085731429e-06
1.9794134696161976e-12	2.4051935713527238e-10	2.9225607506844726e-08	3.5512157703953872e-06
2.1875902014670364e-12	2.6581499874015355e-10	3.2299291479658129e-08	3.9247003932525885e-06
2.4176610713286156e-12	2.9377100619593265e-10	3.5696237617766722e-08	4.3374647367828189e-06
2.6719287057960000e-12	3.2466717262156566e-10	3.9450443699873716e-08	4.7936398852710157e-06
2.9529379008172425e-12	3.5881271723520049e-10	4.3599483082281089e-08	5.2977913929290109e-06
3.2635010908665675e-12	3.9654938012404428e-10	4.8184880745668262e-08	5.8549649774966190e-06
3.6067264967338821e-12	4.3825484249401899e-10	5.3252528891055793e-08	6.4707370194807025e-06
3.9860492336431492e-12	4.8434650663021337e-10	5.8853146244378082e-08	7.1512703724455683e-06
4.4052656910401313e-12	5.3528567339924565e-10	6.5042785666539686e-08	7.9033760429228480e-06
4.8685715281339743e-12	5.9158215910338558e-10	7.1883395149287240e-08	8.7345813572541237e-06
5.3806036654647833e-12	6.5379939789346253e-10	7.9443437811532343e-08	9.6532052976029776e-06
5.9464866927629101e-12	7.2256008080722362e-10	8.7798577101256825e-08	1.0668441761124589e-05
6.5718841575654077e-12	7.9855238787053352e-10	9.7032434060731539e-08	1.1790451575578641e-05
7.2630552479033658e-12	8.8253687563437822e-10	1.0723742423401342e-07	1.3030464192308714e-05
8.0269174363595134e-12	9.7535408908045947e-10	1.1851568259277232e-07	1.4400890074365673e-05
8.8711157124588670e-12	1.0779329740778886e-09	1.3098008573741623e-07	1.5915444904593194e-05
9.8040990962934688e-12	1.1913001745856734e-09	1.4475538160404734e-07	1.7589286856791647e-05

Sampling points 193 to 384

1.9439168303816350e-05	2.3620614568136901e-03	2.8701507382234348e-01	3.4875321454323611e-01
2.1483603480955747e-05	2.6104816287778878e-03	3.1720071263778915e-01	3.8543191029858157e-01
2.3743053782621043e-05	2.8850283782960702e-03	3.5056100280015512e-01	4.2596813816033411e-01
2.6240132546858776e-05	3.1884494615157647e-03	3.8742982530616715e-01	4.7076759832163077e-01
2.8999831377238596e-05	3.5237816186211822e-03	4.2817617572350458e-01	5.2027865883738443e-01
3.2049770267221755e-05	3.8943809665496639e-03	4.7320785722246539e-01	5.7499684304247886e-01
3.5420474030339066e-05	4.3039565881380203e-03	5.2297556200716211e-01	6.3546978891585546e-01
3.9145677802784465e-05	4.7566076538702283e-03	5.7797738199458315e-01	7.0230273002547406e-01
4.3262664675996812e-05	5.2568644477534125e-03	6.3876379388591276e-01	7.7616455290928698e-01
4.7812638838370288e-05	5.8097337079228714e-03	7.0594316852237804e-01	8.5779449151653139e-01
5.2841137960621061e-05	6.4207487357601564e-03	7.8018785966510817e-01	9.4800952570955843e-01
5.8398488952101537e-05	7.0960247750331065e-03	8.6224093313756223e-01	1.0477125578728921e-02
6.4540311649424626e-05	7.8423202153108801e-03	9.5292360367804285e-01	1.1579014494637693e-02
7.1328075478483034e-05	8.6671042321983371e-03	1.0531434539328173e+00	1.2796790079449971e-02
7.8829714661124184e-05	9.5786315413559676e-03	1.1639035178482904e+00	1.4142640240527066e-02
8.7120308123675967e-05	1.0586025014468731e-02	1.2863123193718711e-00	1.5630034698636896e-02
9.6282830912076270e-05	1.1699366984012178e-02	1.4215949669322265e+00	1.7273859797446769e-02
1.0640898463402168e-04	1.2929800150624660e-02	1.5711054147362089e+00	1.9090567491054267e-02
1.1760011523947924e-04	1.4289639103000504e-02	1.7363400135976372e+00	2.1098340000673559e-02
1.2996822732501724e-04	1.5792493566432742e-02	1.9189524869191834e-00	2.3317271788416559e-02
1.4363710511345378e-04	1.7453404613518231e-02	2.1207704817120212e+00	2.5769570669423729e-02
1.5874355132796403e-04	1.9288995200267688e-02	2.3438138603014083e+00	2.8479780075142304e-02
1.7543875635971472e-04	2.1317636534236600e-02	2.5903149157877352e-00	3.1475024692237560e-02
1.9388981143211579e-04	2.3559631939745231e-02	2.8627407135861755e+00	3.4785281935573863e-02
2.1428138090594562e-04	2.6037420060372587e-02	3.1638177826465683e+00	3.8443681972258412e-02
2.3681755046234149e-04	2.8775799432443259e-02	3.4965594034715681e-00	4.2486839299489054e-02
2.6172386966089197e-04	3.1802176677114019e-02	3.8642957660407120e-00	4.6955219194748827e-02
2.8924960931543914e-04	3.5146840795050052e-02	4.2707072994710522e-00	5.1893542705903837e-02
3.1967025628016629e-04	3.8843266308924096e-02	4.7198615069887930e+00	5.7351234234481581e-02
3.5329027061462893e-04	4.2928448287690518e-02	5.2162536748687147e-00	6.3382916191693528e-02
3.9044613272236350e-04	4.7443272605669898e-02	5.7648518627701284e-00	7.0048955677885772e-02
4.3150971095986065e-04	5.2432925142121424e-02	6.3711466257477705e+00	7.7416068656769369e-02
4.7689198342006658e-04	5.7947344016710048e-02	7.0412059655722290e+00	8.5557987671209173e-02
5.2704715113927156e-04	6.4041719386992838e-02	7.7817360613311877e-00	9.4556199783295187e-02
5.8247718389374341e-04	7.0777045810065886e-02	8.6001483871237632e-00	1.0450076212424869e-03
6.4373684408196633e-04	7.8220732696592687e-02	9.5046338885843706e+00	1.1549120321646080e-03
7.1143923897318674e-04	8.6447278966843177e-02	1.0504244960619703e+01	1.2763751908839718e-03
7.8626195689103691e-04	9.5539018660927705e-02	1.1608986046819572e-01	1.4106127415182191e-03
8.6895384874522254e-04	1.0556944965543910e-01	1.2829913767290970e-01	1.5589681785928965e-03
9.6034252278312515e-04	1.1669162090437306e-01	1.4179247577028352e+01	1.7229262931862318e-03
1.0613426275713101e-03	1.2896418580662142e-01	1.5670492062326328e+01	1.9041280332173003e-03
1.1729650061058051e-03	1.4252746762678220e-01	1.7318572099218340e+01	2.1043869266043412e-03
1.2963268126685603e-03	1.5751721224808804e-01	1.9139982226652432e-01	2.3257072316617105e-03
1.4326626936829910e-03	1.7408344207293611e-01	2.1152951729381048e+01	2.5703039963907459e-03
1.5833371444703617e-03	1.9239195749751564e-01	2.3377627082769912e+01	2.8406252274246667e-03
1.7498581655775839e-03	2.1262599629790035e-01	2.5836273585494951e+01	3.1393763905017645e-03
1.9338923553535471e-03	2.3498806753529980e-01	2.8553498198135060e-01	3.4695474876758481e-03
2.1372815898255564e-03	2.5970197833480957e-01	3.1556495817904278e-01	3.8344429822617740e-03

Sampling Points 385 to 576

4.2377148710149695e+03	5.1492650330238225e+05	6.2568934407734923e+07	7.6027773435862408e+09
4.6833992345424385e+03	5.6908179639617680e+05	6.9149366682411388e+07	8.4023684167359400e+09
5.1759566317540530e+03	6.2893265138330159e+05	7.6421869060750201e+07	9.2860532171338844e+09
5.7203167426353639e+03	6.9507807573703467e+05	8.4459227190926239e+07	1.0262675959279177e+10
6.3219277061418234e+03	7.6818007509655319e+05	9.3341881654555663e+07	1.1342011011829447e+10
6.9868106470046323e+03	8.4897027884187771e+05	1.0315873304307374e+08	1.2534860722767656e+10
7.7216199371708199e+03	9.3825726248661662e+05	1.1400803170473446e+08	1.3853163532931507e+10
8.5337097949943000e+03	1.0369346401734781e+06	1.2599836106711893e+08	1.5310113459941998e+10
9.4312078887249972e+03	1.1459900082649642e+06	1.3924972437657478e+08	1.6920292148366428e+10
1.0423096680944496e+04	1.2665148295397097e+06	1.5389474573104006e+08	1.8699814807718300e+10
1.1519303328070666e+04	1.3997153569188234e+06	1.7007999742659190e+08	2.0666491498890625e+10
1.2730799034675721e+04	1.5469247060505589e+06	1.8796746690225038e+08	2.2840005383231522e+10
1.4069708856989137e+04	1.7096161975797976e+06	2.0773617796471399e+08	2.5242109718238716e+10
1.5549433054535755e+04	1.8894181026362628e+06	2.2958398251878911e+08	2.7896845571472111e+10
1.7184781204437102e+04	2.0881299391192668e+06	2.5372954073575363e+08	3.0830782431638401e+10
1.8992120420636886e+04	2.3077404818776865e+06	2.8041450947784531e+08	3.4073284124964363e+10
2.0989539161478522e+04	2.5504476670371005e+06	3.0990596088136274e+08	3.7656802698239258e+10
2.3197028265075980e+04	2.8186805896832864e+06	3.4249905530437142e+08	4.1617203209806610e+10
2.5636681024340771e+04	3.1151238150622859e+06	3.7851999539077419e+08	4.5994122679122765e+10
2.8332914304083228e+04	3.4427442466117009e+06	4.1832929081601185e+08	5.0831366787370079e+10
3.1312712913202311e+04	3.8048208197275074e+06	4.6232536638906646e+08	5.6177348299437775e+10
3.4605899677722984e+04	4.2049773184515880e+06	5.1094854962186480e+08	6.2085571595145073e+10
3.8245433917662871e+04	4.6472186435204167e+06	5.6468547767501700e+08	6.8615168159057838e+10
4.2267741314984989e+04	5.1359708947577253e+06	6.2407396778608418e+08	7.5831488388260895e+10
4.6713078474065944e+04	5.6761256689692009e+06	6.8970839992525887e+08	8.3806755641097107e+10
5.1625935823323234e+04	6.2730890166874416e+06	7.6224566554988432e+08	9.2620789072812759e+10
5.7055482890376610e+04	6.9328355477427216e+06	8.4241174199494874e+08	1.0236180249249139e+11
6.3056060407206925e+04	7.6619682271663100e+06	9.3100895829826319e+08	1.1312728723650484e+11
6.9687724170466376e+04	8.4677844598838333e+06	1.0289240251791439e+09	1.2502498789457556e+11
7.7016846100076829e+04	9.3583491255965196e+06	1.1371369095373254e+09	1.3817398065384482e+11
8.5116778511712779e+04	1.0342575294807941e+07	1.2567306422910707e+09	1.5270586505337646e+11
9.4068588251431182e+04	1.1430313433829404e+07	1.3889021577146211e+09	1.6876608107657605e+11
1.0396186803991429e+05	1.2632449991557652e+07	1.5349742727587159e+09	1.8651536476342874e+11
1.1489563314653141e+05	1.3961016354714479e+07	1.6964089262472496e+09	2.0613135691081287e+11
1.2697931236743495e+05	1.5429309262008933e+07	1.8748218104523966e+09	2.2781038096130206e+11
1.4033384322573253e+05	1.7052023882367507e+07	2.0719985414859231e+09	2.5176940787416525e+11
1.5509288235486683e+05	1.8845400889123969e+07	2.2899125303454008e+09	2.7824822764365344e+11
1.7140414317912661e+05	2.0827389002136763e+07	2.5307447334747562e+09	3.0751184919785828e+11
1.8943087427924512e+05	2.3017824624610133e+07	2.7969054805094066e+09	3.3985315269713715e+11
2.0935349323906592e+05	2.5438630372484632e+07	3.0910585976653914e+09	3.7559582077719836e+11
2.3137139232536239e+05	2.8114034483345896e+07	3.4161480682074847e+09	4.1509757807371277e+11
2.5570493407266162e+05	3.1070813300769802e+07	3.7754274968232164e+09	4.5873377145070300e+11
2.8259765674555639e+05	3.4338559260968812e+07	4.1724926727921586e+09	5.0700132676483929e+11
3.1231871175151330e+05	3.7949977063839935e+07	4.6113175578536234e+09	5.6032312176626892e+11
3.4516555739862355e+05	4.1941210992593758e+07	5.0962940589514427e+09	6.1925281890144031e+11
3.8146693595832947e+05	4.6352206657889292e+07	5.6322759839148350e+09	6.8438020638623755e+11
4.2158616382857127e+05	5.1227110786931656e+07	6.2246276199985800e+09	7.5635710100467944e+11
4.6592476772641251e+05	5.6614713058756173e+07	6.8792774214728651e+09	8.3590387171037695e+11

9.2381664932114575e+11	1.1225334676977153e+14	1.3639951033870320e+16	1.6573961450606881e
1.0209752944638193e+12	1.2405913430661245e+14	1.5074477206609342e+16	1.8317060192517601e
1.1283522035151340e+12	1.3710654735730897e+14	1.6659873813938872e+16	2.0243482229411579e
1.2470220406715007e+12	1.5152616881705944e+14	1.8412008037975264e+16	2.2372507840526853e
1.3781724935494902e+12	1.6746231510403516e+14	2.0348415826945328e+16	2.4725445029769687e
1.5231161599626948e+12	1.8507448052659994e+14	2.2488477400850208e+16	2.7325842783379528e
1.6833036848418264e+12	2.0453893355595603e+14	2.4853611215221080e+16	3.0199726756098365e
1.8603382787767620e+12	2.2605048098024984e+14	2.7467488324221096e+16	3.3375859744670935e
2.0559917634869844e+12	2.4982441759638447e+14	3.0356269288511564e+16	3.6886029555582029e
2.2722223048088804e+12	2.7609868095271022e+14	3.3548865998935916e+16	4.0765367148108068e
2.5111940106775947e+12	3.0513623270798212e+14	3.7077231036440888e+16	4.5052698236765440e
2.7752985902466255e+12	3.3722769044002506e+14	4.0976677464246272e+16	4.9790931872111176e
3.0671792909169141e+12	3.7269423624413281e+14	4.5286232252850760e+16	5.5027489888943135e
3.3897573528452603e+12	4.1189083123143062e+14	5.0049026875070080e+16	6.0814781519961702e
3.7462612456976733e+12	4.5520976809898188e+14	5.5312728980313968e+16	6.7210727924986010e
4.1402589802589175e+12	5.0308459732695450e+14	6.1130019468443072e+16	7.4279341885389363e
4.5756938182836924e+12	5.5599446629754788e+14	6.7559119737921448e+16	8.2091368465530675e
5.0569237379856543e+12	6.1446891476304075e+14	7.4664374385141264e+16	9.0724993053136814e
5.5887650501481416e+12	6.7909317465761662e+14	8.2516895186770448e+16	1.0026662386494198e
6.1765406013813154e+12	7.5051402729526438e+14	9.1195272810315088e+16	1.1081175674916358e
6.8261330469601016e+12	8.2944627657455900e+14	1.0078636337593507e+17	1.2246593094004847e
7.5440437264154141e+12	9.1667990297633300e+14	1.1138615774168800e+17	1.3534578533000223e
8.3374577311253535e+12	1.0130879699558496e+15	1.2310074221230024e+17	1.4958022583082809e
9.2143158151247129e+12	1.1196353618452902e+15	1.3604736028656150e+17	1.6531171550741899e
1.0183393868840340e+13	1.2373884407605195e+15	1.5035558606966758e+17	1.8269770039599454e
1.1254390751152201e+13	1.3675257190914975e+15	1.6616862109441658e+17	2.0191218527695090e
1.2438025358832957e+13	1.5113496544604105e+15	1.8364472753028080e+17	2.2314747517318812e
1.3746143904869607e+13	1.6702996851533248e+15	2.0295881212439261e+17	2.4661610000341512e
1.5191838479344713e+13	1.8459666365023652e+15	2.2430417672705789e+17	2.7255294165301002e
1.6789578079474348e+13	2.0401086424003345e+15	2.4789445292164490e+17	3.0121758475087553e
1.8555353420195434e+13	2.2546687412956410e+15	2.7396574012127472e+17	3.3289691467965432e
2.0506836974615496e+13	2.4917943227741685e+15	3.0277896853110349e+17	3.6790798882106413e
2.2663559846063445e+13	2.7538586193560145e+15	3.3462251062551731e+17	4.0660120977274061e
2.5047107241936324e+13	3.0434844586042220e+15	3.6981506727678112e+17	4.4936383229520880e
2.7681334505709973e+13	3.3635705132645935e+15	4.0870885742048762e+17	4.9662383908768727e
3.0592605869234598e+13	3.7173203121568085e+15	4.5169314318104928e+17	5.4885422418279211e
3.3810058314828449e+13	4.1082743021675935e+15	4.9919812573787520e+17	6.0657772682979369e
3.7365893187990141e+13	4.5403452822331500e+15	5.5169925092337018e+17	6.7037206324472250e
4.1295698479287656e+13	5.0178575639460460e+15	6.0972196764462810e+17	7.4087570858843619e
4.5638805000929469e+13	5.5455902507190850e+15	6.7384698675270400e+17	8.1879428704062800e
5.0438680022752680e+13	6.1288250686585730e+15	7.4471609299199475e+17	9.0490763392378634e
5.5743362307269414e+13	6.7733992278544400e+15	8.2303856819767232e+17	1.0000776005572131e
6.1605942897748391e+13	7.4857638431407750e+15	9.0959829002668813e+17	1.1052566799547061e
6.8085096471220516e+13	8.2730484990213790e+15	1.0052615772688342e+18	1.2214975396947848e
7.5245668574367812e+13	9.1431326049478160e+15	1.1109858602563712e+18	1.3499635573716302e
8.3159324619549984e+13	1.0104724255097566e+16	1.2278292631485970e+18	1.4919404640690720e
9.1905267136338875e+13	1.1167447381907442e+16	1.3569611939940810e+18	1.6488492123894242e
1.0157102845705528e+14	1.2341938075624136e+16	1.4996740485594657e+18	1.8222601978247286e

Sampling Points 769 to 801

2.0139089758026668e+20	4.9534167824711496e+20	1.2183439329023096e+21	2.9966425278257165e+21
2.2257136317086207e+20	5.4743721730949612e+20	1.3464782828575407e+21	3.3118021736216768e+21
2.4597939777289005e+20	6.0501169204271369e+20	1.4880886400345899e+21	3.6601074487063940e+21
2.7184927686435983e+20	6.6864132714134700e+20	1.6445922884849697e+21	4.0450443093423623e+21
3.0043991489038549e+20	7.3896294938012195e+20	1.8175555693250643e+21	4.4704653330125727e+21
3.3203745656597683e+20	8.1668036119031775e+20	2.0087095572044880e+21	4.9406282763108614e+21
3.6695814070852361e+20	9.0257138455105503e+20	2.2199673854830119e+21	
4.0555146526217175e+20	9.9749564569309793e+20	2.4534433935122555e+21	
4.4820368519071852e+20	1.1024031785271021e+21	2.7114742876545719e+21	

Filter Weights 1 to 144

0.21035620538389819885E-28	0.10954511874715580138E-11	0.13166195190543400137E-09
-0.12644693616088940552E-13	0.11858893754914550946E-11	0.14550289515667290553E-09
0.46157312567885668321E-13	0.13346662261643230004E-11	0.16081145810919829686E-09
-0.27987033742576678494E-13	0.14516734901185850330E-11	0.17771842706736448843E-09
0.54657649654108409156E-13	0.16270332417806469835E-11	0.19641479168712890847E-09
-0.26529331099287291499E-13	0.17761192965262209981E-11	0.21706652163468219836E-09
0.56749134340673213135E-13	0.19843094598657728049E-11	0.23990084518390418007E-09
-0.21572768289772080733E-13	0.21722251127126358340E-11	0.26512635046403231588E-09
0.58318460867739760925E-13	0.24208558013562638359E-11	0.29301487204485379059E-09
-0.15465892848687829700E-13	0.26558665246211218806E-11	0.32382671796405940321E-09
0.60573024556529743179E-13	0.29542133130007581834E-11	0.35788852978338560143E-09
-0.85025312590830646706E-14	0.32464334551104291636E-11	0.39552347102192978760E-09
0.63880180611476449908E-13	0.36058072230543221354E-11	0.43712543089936042400E-09
-0.56596576350102877128E-15	0.39676082798212998573E-11	0.48309404739375797825E-09
0.68485006047914070374E-13	0.44018068787207206107E-11	0.53390563500721587301E-09
0.85728977321682762439E-14	0.48483162182209038194E-11	0.59005295736900699180E-09
0.74650681546818133979E-13	0.53741760778847699533E-11	0.65211327580989620296E-09
0.19208372932613381433E-13	0.59238861421284167256E-11	0.72069283339348376395E-09
0.82693454289757706437E-13	0.65619559488550109069E-11	0.79649244503723412979E-09
0.31701165629228998860E-13	0.72374683888302430790E-11	0.88025670846750671949E-09
0.93000040396952081623E-13	0.80128318647926483616E-11	0.97283758951862838429E-09
0.46490696394179916916E-13	0.88417664804021047188E-11	0.10751484374562240226E-08
0.10604419444905640479E-12	0.97850472788000974558E-11	0.11882260626931209546E-08
0.64112165895974571186E-13	0.10801152249024990298E-10	0.13131897062580609792E-08
0.12240608340017008854E-12	0.11949741288775620211E-10	0.14513021636655630472E-08
0.85217767515070225126E-13	0.13194249255521529763E-10	0.16039339435115999074E-08
0.14279579404871719178E-12	0.14593803746893311587E-10	0.17726240632935599375E-08
0.11060266069684630524E-12	0.16117088182600741411E-10	0.19590497332198700268E-08
0.16808202030984049793E-12	0.17823362499440759998E-10	0.21650875406672578739E-08
0.14123670281595459178E-12	0.19686960839662181492E-10	0.23927891159868709863E-08
0.19932710117763080694E-12	0.21768042712348459703E-10	0.26444435360147638239E-08
0.17830320429641190908E-12	0.24047127453754399616E-10	0.29225595734392348364E-08
0.23782981967994220694E-12	0.26586169224245549843E-10	0.32299302912485969586E-08
0.22324626027650970672E-12	0.29372566166660639848E-10	0.35696226515762041770E-08
0.28517768171070357866E-12	0.32471120715874496926E-10	0.39450454481729238111E-08
0.27782855757859949941E-12	0.35876995485484108464E-10	0.43599472612559631445E-08
0.34331077352335570256E-12	0.39659090711123993131E-10	0.48184890913636877388E-08
0.34420197641399489491E-12	0.43821451522206353096E-10	0.53252519017629532640E-08
0.41459976123278392377E-12	0.48438566886024388833E-10	0.58853155833436851597E-08
0.42499381982249688902E-12	0.53524764256840081139E-10	0.65042776355473761329E-08
0.50194116319499513568E-12	0.59161909123775483693E-10	0.71883404192425699700E-08
0.52341213107734220974E-12	0.65376353273289546079E-10	0.79443429030829021263E-08
0.60887371932475596308E-12	0.72259490983916676274E-10	0.87798585629591097164E-08
0.64337432538102752823E-12	0.79851856505621554776E-10	0.97032425780220928695E-08
0.73972052807969328662E-12	0.88256972132554113981E-10	0.10723743227689399320E-07
0.78966429788659195358E-12	0.97532219231111761839E-10	0.11851567478400949647E-07
0.89976265596232089469E-12	0.10779639493701439540E-09	0.13098009332253010086E-07
0.96812431295714248033E-12	0.11912700941828918848E-09	0.14475537424021579590E-07

Filter Weights 145 to 288

0.15997944513720238914E-07	0.19439168303884759854E-05	0.23620581621746139576E-03
0.17680461540553181382E-07	0.21483603476946079820E-05	0.26104771814107751186E-03
0.19539933354871179973E-07	0.23743053781113989137E-05	0.28850223750643329973E-03
0.21594964684505000780E-07	0.26240132540945578888E-05	0.31884413578705622606E-03
0.23866128306162058448E-07	0.28999831372928098690E-05	0.35237068000135917308E-03
0.26376149610345229076E-07	0.32049770257732388059E-05	0.38943662007281590462E-03
0.29150154762698309478E-07	0.35420474020978068237E-05	0.43039366566958368833E-03
0.32215902055657983021E-07	0.39145677786671023699E-05	0.47565807487700027594E-03
0.35604079260985092872E-07	0.43262664657480666650E-05	0.52568281303167982161E-03
0.39348591789544360374E-07	0.47812638810077579977E-05	0.58096846836193664822E-03
0.43486920453657868292E-07	0.52841137925459449193E-05	0.64206825611437718954E-03
0.48060478694380069026E-07	0.58398488901504216978E-05	0.70959354469423893946E-03
0.53115044437493142888E-07	0.64540311583956847791E-05	0.78421996374912559657E-03
0.58701201380017479006E-07	0.71328075387126483640E-05	0.86669414659246905939E-03
0.64874861635712681668E-07	0.78829714540444842174E-05	0.95784118347590099622E-03
0.71697809408859342572E-07	0.87120307957926337232E-05	0.10585728435434579864E-02
0.79238334805050121668E-07	0.96282830690788715692E-05	0.11698966653840010659E-02
0.87571902294266750180E-07	0.10640898433258409191E-04	0.12929259749833240008E-02
0.96781920558355529704E-07	0.11760011483484689510E-04	0.14288909657393959393E-02
0.10696056312048640378E-06	0.12996822677619209683E-04	0.15791508896276298946E-02
0.11820970459254829996E-06	0.14363710437469910021E-04	0.17452075486231769744E-02
0.13064192692376749733E-06	0.15874355032820411062E-04	0.19287201026563420645E-02
0.14438165911984879199E-06	0.17543875501207770228E-04	0.21315214730933669356E-02
0.15956640998357920017E-06	0.19388980961051210830E-04	0.23556362776736309780E-02
0.17634815657222329376E-06	0.21428137844875080257E-04	0.26033007312297349808E-02
0.19489485336503760544E-06	0.23681754714302638776E-04	0.28769842725422829777E-02
0.21539212473518470874E-06	0.26172386518181301401E-04	0.31794136300501061286E-02
0.23804511154682969141E-06	0.28924960326686671307E-04	0.35135987233342810820E-02
0.26308053514448537707E-06	0.31967024811679323171E-04	0.38828616256736492134E-02
0.29074895589985508713E-06	0.35329025959273332330E-04	0.42908672540316900729E-02
0.32132729115584617374E-06	0.39044611784553647914E-04	0.47416579734868603835E-02
0.35512157675298091583E-06	0.43150969087563300697E-04	0.52396893384671194144E-02
0.39247003960676882480E-06	0.47689195631023510063E-04	0.57898709851889693795E-02
0.43374647340783931675E-06	0.52704711454198507913E-04	0.63976070720003401851E-02
0.47936398879211592319E-06	0.58247713449355698436E-04	0.70688437831027441105E-02
0.52977913903701991577E-06	0.64373677739542765810E-04	0.78101127966257229834E-02
0.58549649799821895163E-06	0.71143914895687183756E-04	0.86285849757206656285E-02
0.64707370170465826468E-06	0.78626183537770216584E-04	0.95321125348557418644E-02
0.71512703747583724585E-06	0.86895368472094227166E-04	0.10529286971052299882E-01
0.79033760405820345763E-06	0.96034230136811580777E-04	0.11629470426845669312E-01
0.87345813593705873095E-06	0.10613423286950590218E-03	0.12842853010275019979E-01
0.96532052953043588492E-06	0.11729640026571620215E-03	0.14180454004084899408E-01
0.10668441762993300587E-05	0.12963262680752149015E-03	0.15654168426849128515E-01
0.11790451573234470162E-05	0.14326619585462989793E-03	0.17276700258609969246E-01
0.13030464193827640161E-05	0.15833361521503999387E-03	0.19061578784670331344E-01
0.14400890071820729325E-05	0.17498568260644121238E-03	0.21022951738450229575E-01
0.15915444905568059534E-05	0.19338905472215898854E-03	0.23175536220878610594E-01
0.17589286853766969218E-05	0.21372791490647819607E-03	0.25534136813168170632E-01

Filter Weights 290 to 432

0.28113470567056909888E-01	-0.16951351027511458308E-01	0.68558909586342899260E-05
0.30927161344728969217E-01	-0.88285242013749955919E-02	-0.66573078263653524112E-05
0.33987341082207328524E-01	0.16167873561835501006E-01	0.64646106359474119065E-05
0.37302669043183162012E-01	-0.15564117559925290737E-01	-0.62775967052488337714E-05
0.40877565846017260842E-01	0.12513111252163700016E-01	0.60960690045641779074E-05
0.44708454582277110112E-01	-0.92993152469780984010E-02	-0.59198350149128057049E-05
0.48782456555642082774E-01	0.66505259967794931597E-02	0.57487213891732378171E-05
0.53070463888373879680E-01	-0.46677074086718837662E-02	-0.55825764283683409239E-05
0.57525214796560822372E-01	0.32488855455568548675E-02	0.54212557290731716876E-05
0.62068889249144526543E-01	-0.22555291085446750252E-02	-0.52646114832336199488E-05
0.66590986905823254527E-01	0.15668752111009150857E-02	0.51124978277574427215E-05
0.70926870977039285782E-01	-0.10911324863680910667E-02	-0.49647806501954759280E-05
0.74857621553299974471E-01	0.76253830490409491537E-03	0.48213365261592663842E-05
0.78074664211727651253E-01	-0.53525405778204085232E-03	-0.46820435304229967753E-05
0.80188872113380424422E-01	0.37771045672146697511E-03	0.45467775878200409083E-05
0.80676406709186576638E-01	-0.26825282115352968703E-03	-0.44154180000760036035E-05
0.78917673064227769619E-01	0.19202652749967551236E-03	0.42878525031129105819E-05
0.74124063016304961304E-01	-0.13882137232089440237E-03	-0.41639746681098469138E-05
0.65458647531413310938E-01	0.10159989178100049974E-03	0.40436784078298272207E-05
0.51957717257333460581E-01	-0.75497250626312589804E-04	-0.39268575265170754164E-05
0.32847972741848592559E-01	0.57141729200529359656E-04	0.38134098513603608910E-05
0.74970763258312700383E-02	-0.44191609676806338589E-04	-0.37032392398348510301E-05
-0.23866128698945488634E-01	0.35017761995785832974E-04	0.35962529271829669603E-05
-0.60174943784761181220E-01	-0.28484969541399899885E-04	-0.34923586009061261710E-05
-0.98178997988506697125E-01	0.23801048173241150913E-04	0.33914651799141980567E-05
-0.13281477972726110637E+00	-0.20412749240321660898E-04	0.32934854312419398030E-05
-0.15546285697725620301E+00	0.17933634897918600856E-04	0.31983363564463991755E-05
-0.15639821579874499391E+00	-0.16093677807779768610E-04	-0.31059371103484061739E-05
-0.12430498665290500016E+00	0.14703946920177649808E-04	0.30162076790696608685E-05
-0.54868159863436967438E-01	-0.13632085400878389976E-04	-0.29290699115622908088E-05
0.46862558991703072431E-01	0.12785408514801159958E-04	0.28444489540948809787E-05
0.15112182958062059246E+00	-0.12099103232765920005E-04	-0.27622729358204111026E-05
0.21193155344105990556E+00	0.11527807463720849231E-04	0.26824715684158770123E-05
0.16951341358877961008E+00	-0.11039642499677090445E-04	-0.26049757091405561401E-05
0.13861974203314799889E-01	0.10612147244787119201E-04	0.25297182336640620443E-05
-0.18693504518381348634E+00	-0.10229546722558040478E-04	-0.24566346909850541750E-05
-0.24558896069253360883E+00	0.98808019172690629615E-05	0.23856627938558707926E-05
-0.53092694018998139172E-01	-0.95581362683731644660E-05	-0.23167415846242317899E-05
0.25199984157985949595E+00	0.92559894628748428139E-05	0.22498114158806991699E-05
0.19682248760574280744E+00	-0.89703680398349605195E-05	-0.21848145526023768863E-05
-0.20143336189691599114E+00	0.86984392262176360162E-05	0.21216953789870668849E-05
-0.24584508272586030886E+00	-0.84381998993781744882E-05	-0.20603999269499001719E-05
0.34335593140766357267E+00	0.81881850397080960968E-05	0.20008754358939798722E-05
-0.47700665106262918336E-01	-0.79472759767526677708E-05	-0.19430704833474811314E-05
-0.20966284735074519618E+00	0.77146204892770847038E-05	0.18869353395796189952E-05
0.25090851237942479734E+00	-0.74895903346701209313E-05	-0.18324219538318030139E-05
-0.16764126613351920669E+00	0.72717128455631313132E-05	0.17794835990689859392E-05
0.74951997868967626393E-01	-0.70605952027200397989E-05	-0.17280746718615620423E-05

Filter Weights 433 to 576

0.16781508408187099176E-05	0.41088331789010578938E-06	0.10060186649751670646E-06
-0.16296692208678659180E-05	-0.39901295702377770089E-06	-0.97695492950586510549E-07
0.15825882749397249515E-05	0.38748552999527151342E-06	0.94873084124749734212E-07
-0.15368675777174579453E-05	-0.37629112895780040410E-06	-0.92132214283314405060E-07
0.14924677441823879966E-05	0.36542013202237861199E-06	0.89470527774724840543E-07
-0.14493505440316709914E-05	-0.35486319617658597678E-06	-0.86885737009431156146E-07
0.14074789632159439540E-05	0.34461124894551899091E-06	0.84375620484431720137E-07
-0.13668170916979060623E-05	-0.33465547948734137742E-06	-0.81938020868743667602E-07
0.13273299804037580486E-05	0.32498733079349469753E-06	0.79570843154679285033E-07
-0.12889836283545319635E-05	-0.31559849314212400870E-06	-0.77272052863928245642E-07
0.12517450527435769451E-05	0.30648089749286697872E-06	0.75039674297478696595E-07
-0.12155822896230419416E-05	-0.29762670812339488137E-06	-0.72871788831488877790E-07
0.11804642977313919266E-05	0.28902831526969758359E-06	0.70766533266929795021E-07
-0.11463608782321180614E-05	-0.28067832866533619338E-06	-0.68722098232649864085E-07
0.11132426817551759487E-05	0.27256957173628210936E-06	0.66736726633350816695E-07
-0.10810812413606430626E-05	-0.26469507560502209121E-06	-0.64808712137167796518E-07
0.10498489463079790445E-05	0.25704807272840818962E-06	0.62936397705674278282E-07
-0.10195189699197359345E-05	-0.24962199077868072385E-06	-0.61118174170089166613E-07
0.99006522696480728454E-06	0.24241044716871418470E-06	0.59352478851276259248E-07
-0.96146238238294861780E-06	-0.23540724388966429376E-06	-0.57637794217708362227E-07
0.93368585903962674737E-06	0.22860636218196940360E-06	0.55972646579199561646E-07
-0.90671180391877650539E-06	-0.22200195709699679458E-06	-0.54355604818630417116E-07
0.88051703794158972103E-06	0.21558835236008589946E-06	0.52785279162883091201E-07
-0.85507903355065637431E-06	-0.20936003566018609291E-06	-0.51260319990189909104E-07
0.83037591856657379114E-06	0.20331165407816460064E-06	0.49779416670227040800E-07
-0.80638646950736030707E-06	-0.19743800942055008854E-06	-0.48341296436233499673E-07
0.78309007959684342440E-06	0.19173405358761880565E-06	0.46944723290471018939E-07
-0.76046672516600126341E-06	-0.18619488421725469657E-06	-0.45588496942848318593E-07
0.73849695280747625374E-06	0.18081574059851621267E-06	0.44271451780258727462E-07
-0.71716187755802708277E-06	-0.17559199964945570756E-06	-0.42992455864451837250E-07
0.69644316956135183135E-06	0.17051917187001359107E-06	0.41750409958276353087E-07
-0.67632302736954520768E-06	-0.16559289739464161294E-06	-0.40544246580819631899E-07
0.65678415552512063648E-06	0.16080894226704971095E-06	0.39372929090650920317E-07
-0.63780975556830963862E-06	-0.15616319488355259655E-06	-0.38235450795273419860E-07
0.61938351997573715339E-06	0.15165166247713490835E-06	0.37130834085523768675E-07
-0.60148961697207375561E-06	-0.14727046762624959541E-06	-0.36058129594866006882E-07
0.58411266955661727328E-06	0.14301584488191908927E-06	0.35016415383563508384E-07
-0.56723774005096348097E-06	-0.13888413756276189610E-06	-0.34004796146768310693E-07
0.55085032232163946943E-06	0.13487179465891340034E-06	0.33022402445156628786E-07
-0.53493633333997110944E-06	-0.13097536777476139733E-06	-0.32068389957362020693E-07
0.51948209868244907623E-06	0.12719150812468619494E-06	0.31141938754091167181E-07
-0.50447433644131324069E-06	-0.12351696364172060964E-06	-0.30242252593599009938E-07
0.48990014588904722006E-06	0.11994857620999400758E-06	0.29368558237615870861E-07
-0.47574699997612418437E-06	-0.11648327897320799497E-06	-0.28520104786762129308E-07
0.46200273605516768571E-06	0.11311809368621049480E-06	0.27696163034962460481E-07
-0.44865554313913170035E-06	-0.10985012813125349456E-06	-0.26896024842649531045E-07
0.43569394953682061395E-06	0.10667657363213940060E-06	0.26119002528299780677E-07
-0.42310681390672771474E-06	-0.10359470265995370341E-06	-0.25364428277531399452E-07

Filter Weights 577 to 720

0.24631653569082881086E-07	0.60308856947513333758E-08	0.14766195927971890460E-08
-0.23920048617305701087E-07	-0.58566542688268000505E-08	-0.14339602637660350412E-08
0.23229001830889051246E-07	0.56874563638996400563E-08	0.13925333566546899287E-08
-0.22557919287333441164E-07	-0.55231465622676621705E-08	-0.13523032669700050132E-08
0.21906224222551861542E-07	0.53635836473256503502E-08	0.13132354188275479691E-08
-0.21273356535101449785E-07	-0.52086304821955339059E-08	-0.12752962352352419048E-08
0.20658772304732728872E-07	0.50581538918636123925E-08	0.12384531092355140920E-08
-0.20061943324939738367E-07	-0.49120245487234261852E-08	-0.12026743758811379070E-08
0.19482356649058811450E-07	0.47701168614250102390E-08	0.11679292850206920657E-08
-0.18919514149424371449E-07	-0.46323088669346301918E-08	-0.11341879748702300079E-08
0.18372932089200169455E-07	0.44984821257128528939E-08	0.11014214463484779337E-08
-0.17842140706600119178E-07	-0.43685216199214189850E-08	-0.10696015381534739059E-08
0.17326683811178871537E-07	0.42423156545711511770E-08	0.10387009025592480307E-08
-0.16826118391794460252E-07	-0.41197557615253826557E-08	-0.10086929819117270958E-08
0.16340014235853439520E-07	0.40007366062763786183E-08	0.97955198580366660312E-09
-0.15867953559529469194E-07	-0.38851558974150727748E-08	-0.95125286890900208679E-09
0.15409530648689289756E-07	0.37729142987165276171E-08	0.92377130945756002788E-09
-0.14964351510224189348E-07	-0.36639153437652961865E-08	-0.89708368883163302057E-09
0.14532033533448680711E-07	0.35580653530469988486E-08	0.87116706876449941479E-09
-0.14112205161252269515E-07	-0.34552733534349709264E-08	-0.84599917663709281674E-09
0.13704505570744190592E-07	0.33554510000030559535E-08	0.82155838131493233922E-09
-0.13308584363144380637E-07	-0.32585125000973940249E-08	-0.79782367707710818756E-09
0.12924101262648650824E-07	0.31643745396017359674E-08	0.77477466505309300292E-09
-0.12550725823983490048E-07	-0.30729562113327868796E-08	-0.75239153569281363935E-09
0.12188137148392460070E-07	0.29841789455041530200E-08	0.73065505174126690031E-09
-0.11836023607829919776E-07	-0.28979664421992758989E-08	-0.70954653170499806391E-09
0.11494082577135149689E-07	0.28142446057953132032E-08	0.68904783379622916597E-09
-0.11162020173950579471E-07	-0.27329414812814390995E-08	-0.66914134034083904798E-09
0.10839551006143939185E-07	0.26539871924168161407E-08	0.64980994263679380996E-09
-0.10526397926519000691E-07	-0.25773138816751668664E-08	-0.63103702625001653087E-09
0.10222291794616780561E-07	0.25028556519244291169E-08	0.61280645673505631634E-09
-0.99269712454067339727E-08	-0.24305485097912959499E-08	-0.59510256576828648337E-09
0.96401824646609211080E-08	0.23603303106619080563E-08	0.57791013768171107199E-09
-0.93616789708108062008E-08	-0.22921407052714058628E-08	-0.56121439638580773724E-09
0.90912214031028235422E-08	0.22259210878365399183E-08	0.54500099267016873900E-09
-0.88285773158782117222E-08	-0.21616145456867578372E-08	-0.52925599187102496775E-09
0.85735209788006156203E-08	0.20991658103504500059E-08	0.51396586189505248004E-09
-0.83258331828536520172E-08	-0.20385212100542671023E-08	-0.49911746158916965897E-09
0.80853010519388850005E-08	0.19796286235947108123E-08	0.48469802944632955612E-09
-0.78517178599159764754E-08	-0.19224374355423869606E-08	-0.47069517263760014005E-09
0.76248828529317467947E-08	0.18668984927404269626E-08	0.45709685636110621144E-09
-0.74046010768841071059E-08	-0.18129640620596530537E-08	-0.44389139349867930081E-09
0.71906832098687622728E-08	0.17605877893741759270E-08	0.43106743457132480471E-09
-0.69829453994641022983E-08	-0.17097246597221680675E-08	-0.41861395798487421376E-09
0.67812091047173317459E-08	0.16603309586176070024E-08	0.40652026055743952578E-09
-0.65853009426977313290E-08	-0.16123642344797300183E-08	-0.39477594832052842209E-09
0.63950525394835678792E-08	0.15657832621478869464E-08	0.38337092758591272230E-09
-0.62103003854524726628E-08	-0.15205480074504270167E-08	-0.37229539627057491552E-09

Filter weights 721 to 801

0.36153983547227521766E-09	-0.16383451179612808855E-09	0.74242848583018786633E-10
-0.35109500128849910154E-09	0.15910135616182540748E-09	-0.72097983319807716229E-10
0.34095191687175519511E-09	-0.15450494071744330869E-09	0.70015082938317186447E-10
-0.33110186471439289704E-09	0.15004131505843449035E-09	-0.67992357322650702613E-10
0.32153637915631239045E-09	-0.14570664290687508993E-09	0.66028068126905105916E-10
-0.31224723910912398970E-09	0.14149719881436189859E-09	-0.64120527350693063962E-10
0.30322646099050710905E-09	-0.13740936496016368823E-09	0.62268096049913068230E-10
-0.29446629186269331473E-09	0.13343962804187350973E-09	-0.60469183303296924744E-10
0.28595920276917881651E-09	-0.12958457625588848896E-09	0.58722245716347976830E-10
-0.27769788226393698380E-09	0.12584089636512460714E-09	-0.57025788118346391824E-10
0.26967523012757238777E-09	-0.12220537085144369393E-09	0.55378366976800887211E-10
-0.26188435126501301881E-09	0.11867487515034671199E-09	-0.53778600071222512844E-10
0.25431854977949852574E-09	-0.11524637496555659739E-09	0.52225190653632309517E-10
-0.24697132321776888896E-09	0.11191692366118209830E-09	-0.50716985205207501023E-10
0.23983635698150977934E-09	-0.10868365972922199935E-09	0.49253109171572777739E-10
-0.23290751890024982077E-09	0.10554380433023220449E-09	-0.47833283755322262690E-10
0.22617885396104611209E-09	-0.10249465890504320142E-09	0.46458563164427748566E-10
-0.21964457919042880688E-09	0.99533602855475026004E-10	-0.45133048314954522821E-10
0.21329907868420528750E-09	-0.96658091292055187607E-10	0.43867868281155817508E-10
-0.20713689878085250208E-09	0.93865652846806834872E-10	-0.42690428488605550129E-10
0.20115274337434959303E-09	-0.91153887549225778384E-10	0.41665890740660430845E-10
-0.19534146936242159446E-09	0.88520464763624569567E-10	-0.40947061319725302450E-10
0.18969808222628370222E-09	-0.85963121186075071965E-10	0.40890256062850869212E-10
-0.18421773173808480806E-09	0.83479658899239781350E-10	-0.42324395200868817252E-10
0.17889570779236339873E-09	-0.81067943483446593655E-10	0.47175970286618397865E-10
-0.17372743635793169822E-09	0.78725902182445575131E-10	-0.59920514722972034865E-10
0.16870847554670939670E-09	-0.76451522122414838220E-10	0.90953607290146280299E-10

Appendix E

Resistivity Values of Rock Materials

Material	Nominal Resistivity (Ωm)
Sulphides:	$1.2 \times 10^{-5} - 3 \times 10^{-1}$
Chalcopyrite	$2.9 \times 10^{-5} - 1.5$
Pyrite	$7.5 \times 10^{-6} - 5 \times 10^{-2}$
Pyrrhotite	$3 \times 10^{-5} - 3 \times 10^{2}$
Galena	$1.2 \times 10^{-5} - 3 \times 10^{-1}$
Sphalerite	1.5×10^{7}
Oxides	
Hematite	$3.5 \times 10^{-3} - 10^{7}$
Limonite	$10^{3} - 10^{7}$
Magnetite	$5 \times 10^{-5} - 5.7 \times 10^{3}$
Ilmenite	$10^{-3} - 5 \times 10$
Quartz	$3 \times 10^{2} - 10^{6}$
Rock Salt	$3 \times 10 - 10^{13}$
Anthratic	$10^{-3} - 2 \times 10^{5}$
Lignite	$9 - 2 \times 10^{2}$
Granite	$3 \times 10^{2} - 1 \times 10^{6}$
Granite (Weathered)	$3 \times 10 - 5 \times 10^{2}$
Syenite	$10^{2} - 10^{6}$
Diorite	$10^{4} - 10^{5}$
Gabbro	$10^{3} - 10^{6}$
Basalt	$10 - 1.3 \times 10^{7}$
Schists (Calcareous & mica)	$20 - 3 \times 10^{4}$
Schist (Graphite)	$10 - 10^{2}$
Slates	$6 \times 10^{2} - 4 \times 10^{7}$
Marble	$10^{2} - 2.5 \times 10^{8}$
Consolidated Shales	$20 - 2 \times 10^{3}$
Conglomerates	$2 \times 10^{3} - 10^{4}$
Sandstones	$1 - 7.4 \times 10^{8}$
Limestones	$5 \times 10 - 10^{7}$
Dolomite	$3.5 \times 10^{2} - 5 \times 10^{3}$
Marls	$3 - 7 \times 10$
Clays	$1 - 10^{2}$
Alluvium & Sand	$10 - 8 \times 10^{2}$
Moraine	$10 - 5 \times 10^{3}$

Sherwood Sandstone	$100-400$
Soil (40% clay)	8
Soil (20% clay)	33
Top Soil	250-1700
London Clay	4-20
Lias Clay	10-15
Boulder Clay	15-35
Clay (very dry)	50-150
Mercia Mudstone	20-60
Coal measures Clay	50
Middle Coal measures	>100
Chalk	50-150
Coke	0.2-8
Gravel (dry)	1400
Gravel(Saturated)	100
Quaternary/recent sand	50-100
Ash	4
Colliery Spoil	10-20
Pulverized Fuel Ash	50-100
Laterite	800-1500
Lateritic Soil	120-750
Dry Sand Soil	80-1050
Sand Clay/clayey Sand	30-215
Sand and Gravel	30-225
Unsaturated landfill	30-100
Saturated landfill	15-30
Acid Peat waters	100
Acid Mine waters	20
Rainfall payoff	20-100
Landfill payoff	<10-50
Glacier ice(temperate)	$2 \times 10^{6} - 1.2 \times 10^{8}$
Glacier ice(polar)	$5 \times 10^{4} - 3 \times 10^{5}$
Permafrost	$10^{3} - > 10^{4}$

Database of Mesh assignments used for 2D case studies
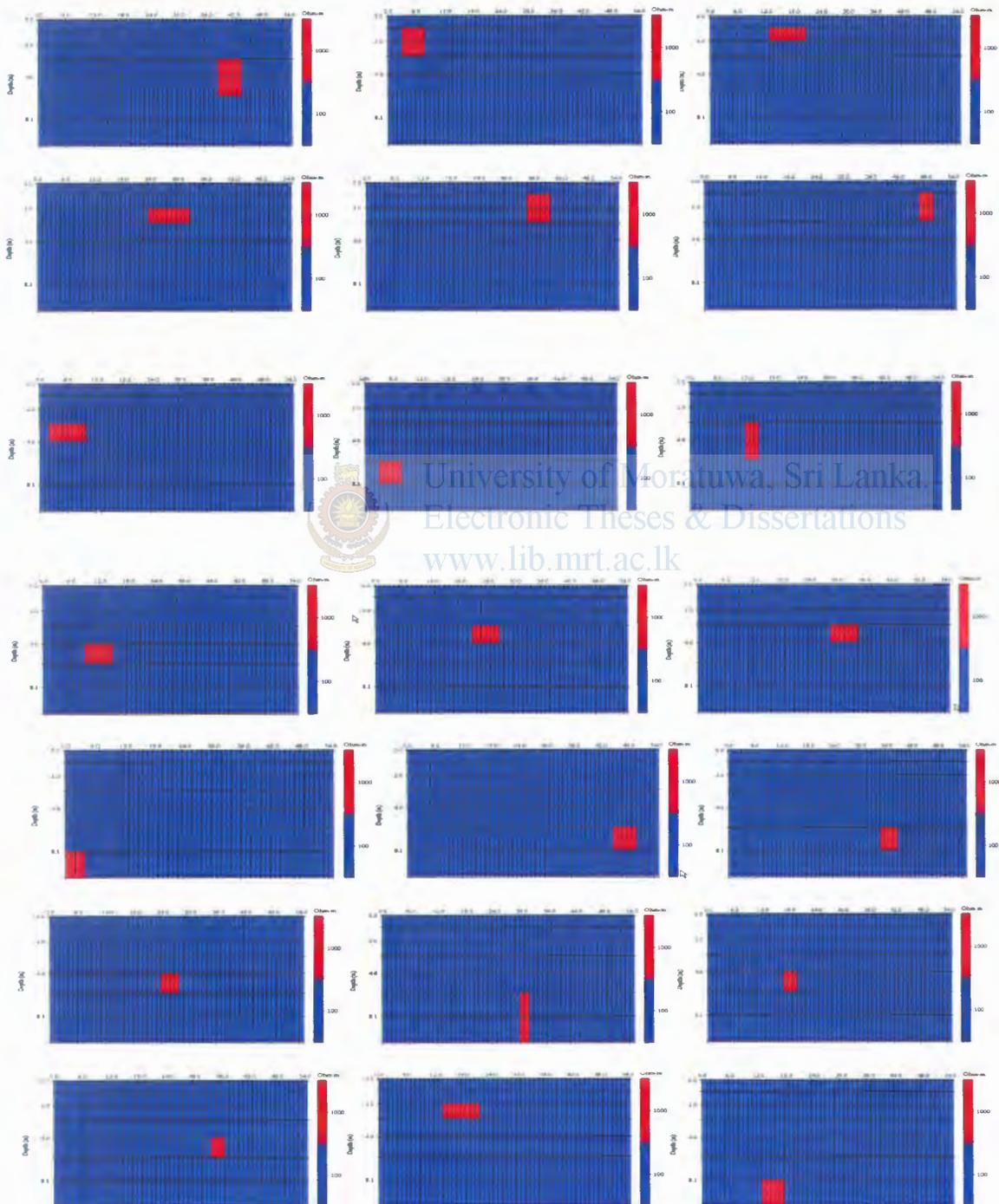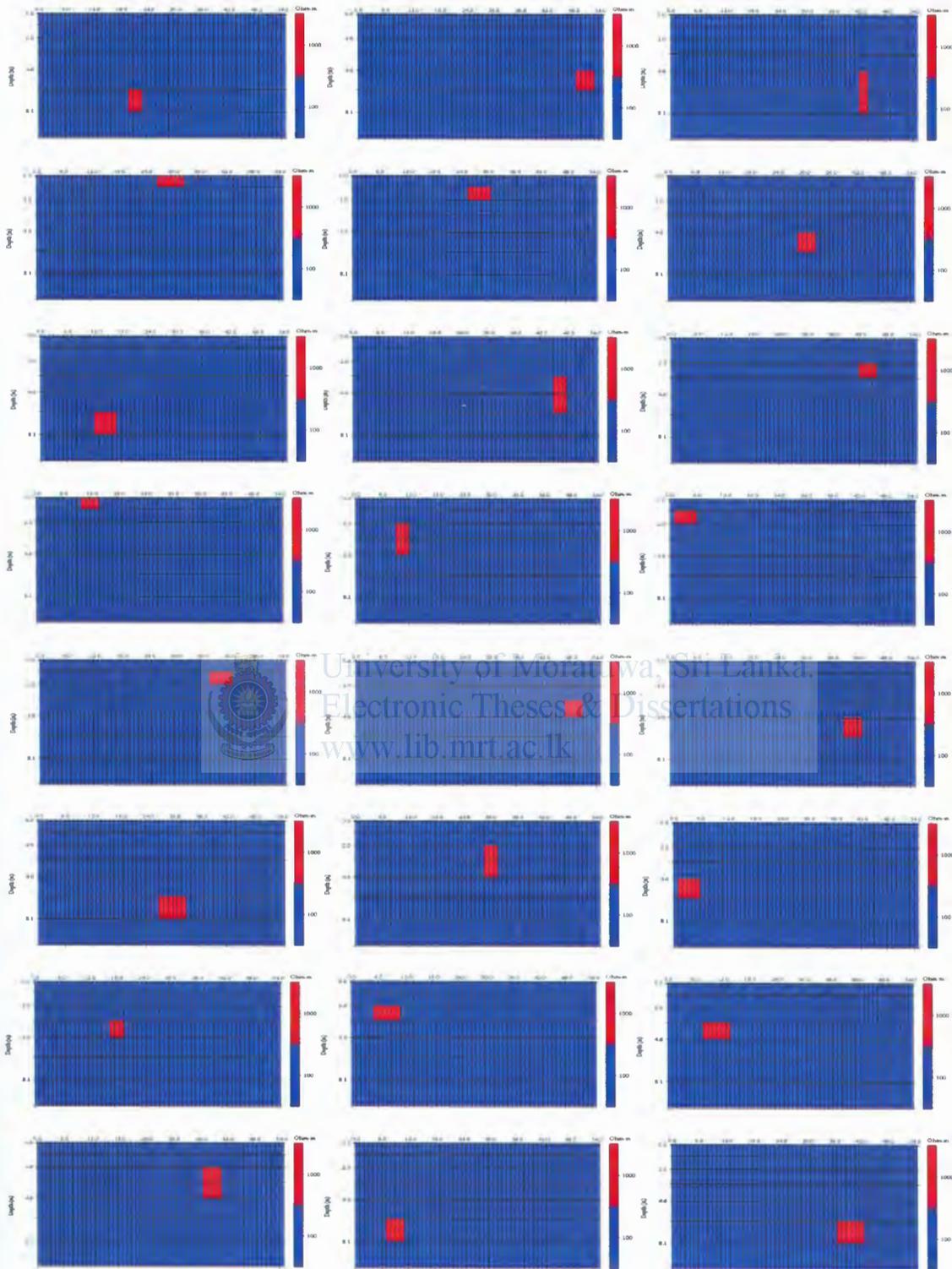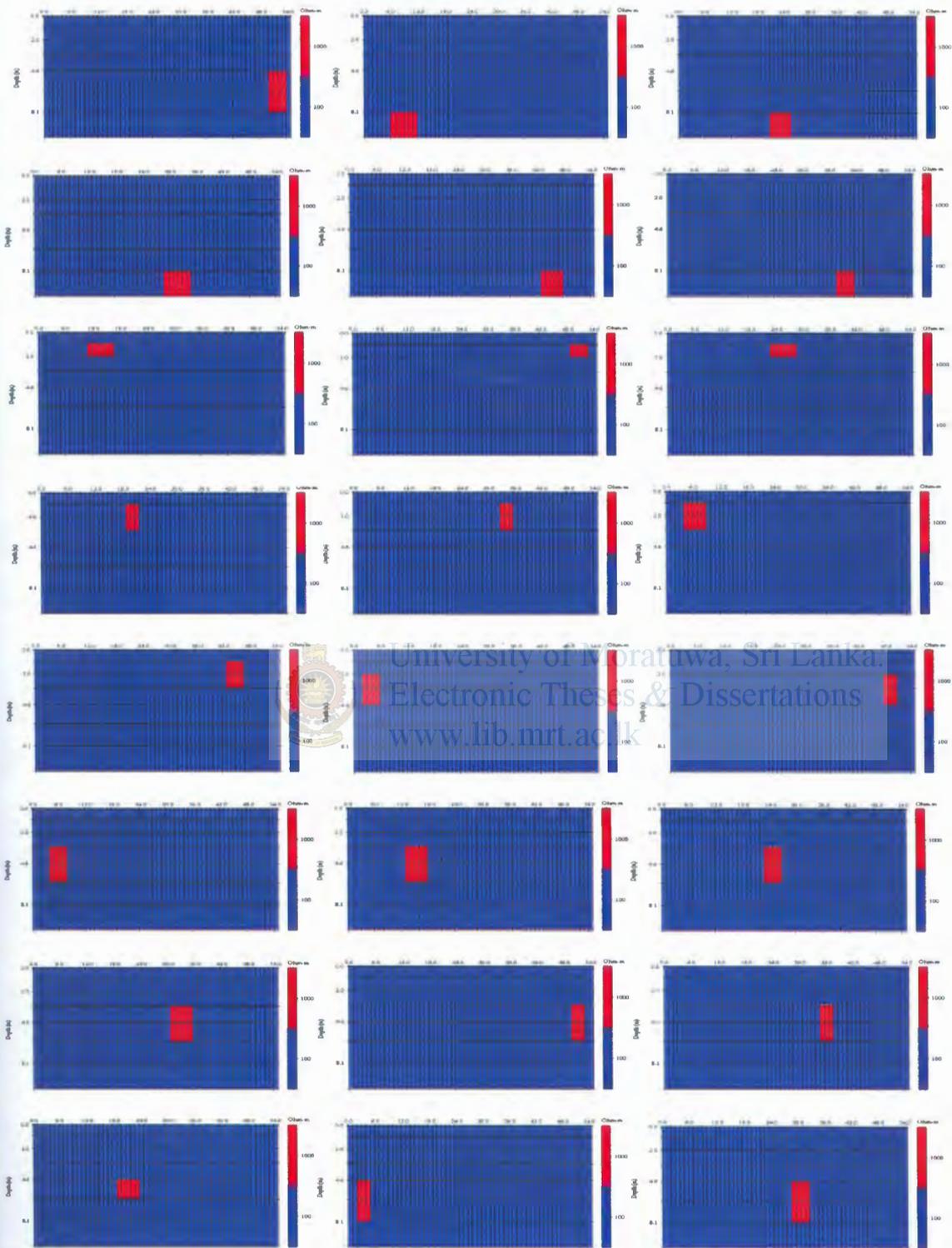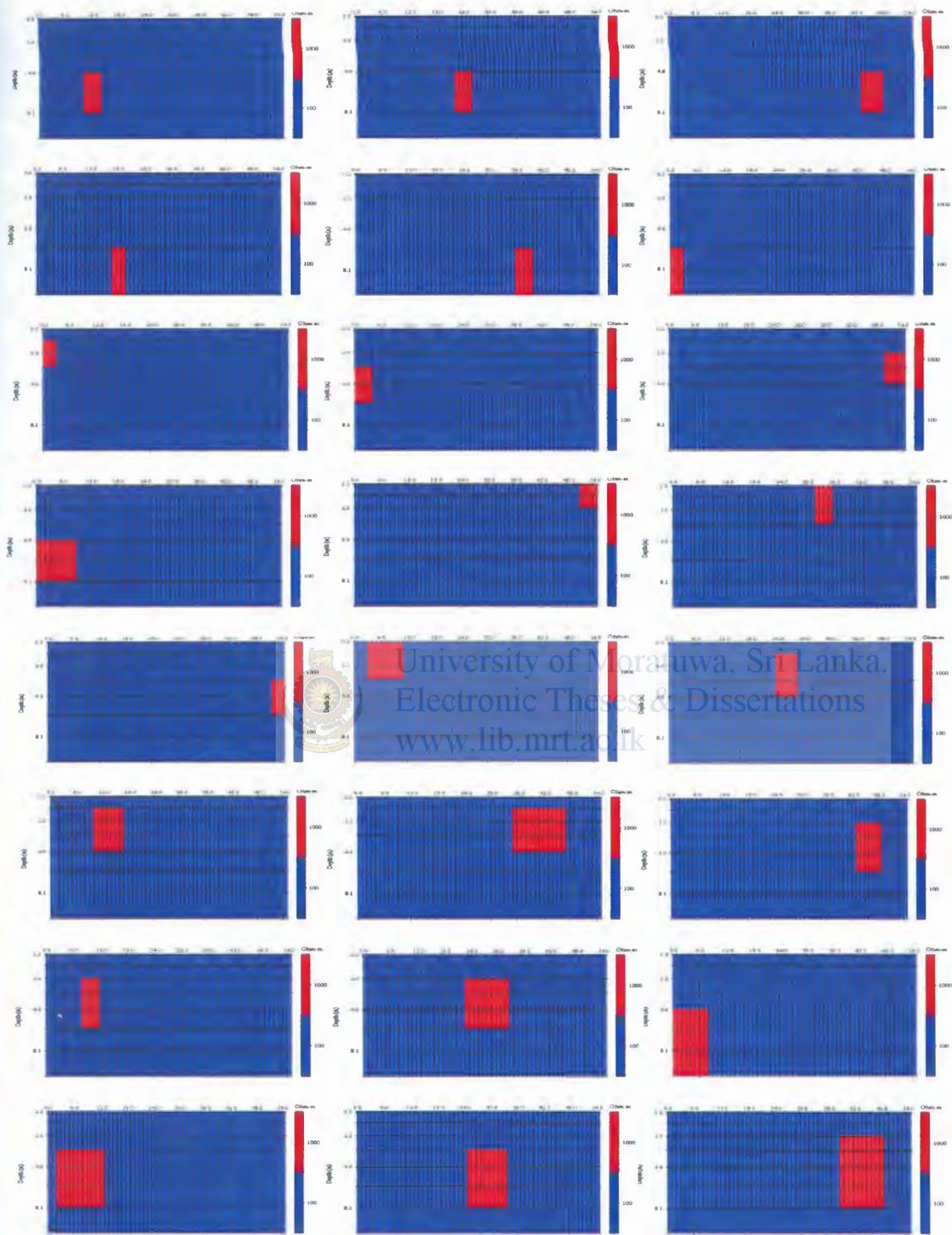
Database of Layer height assignments used for 2D case3
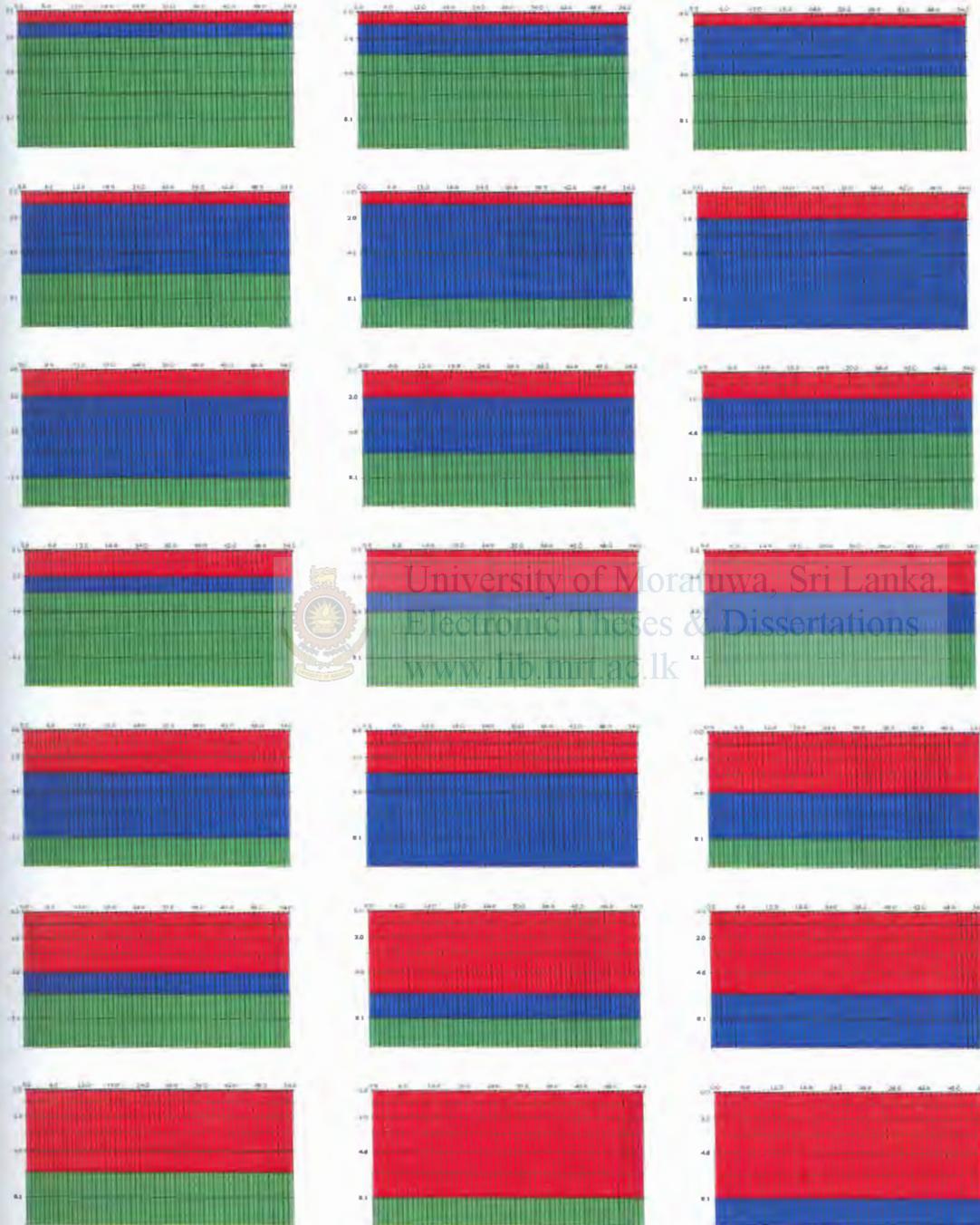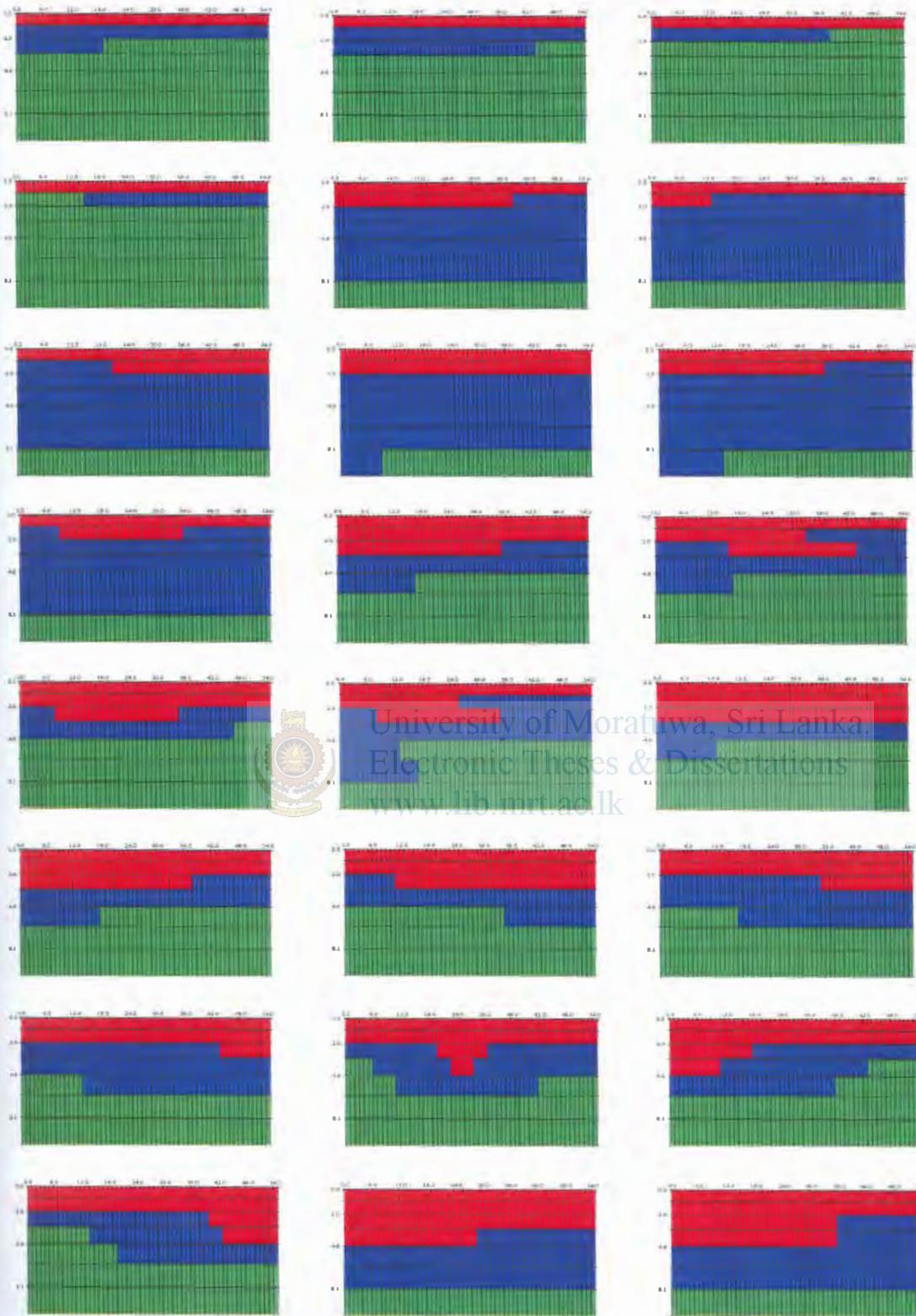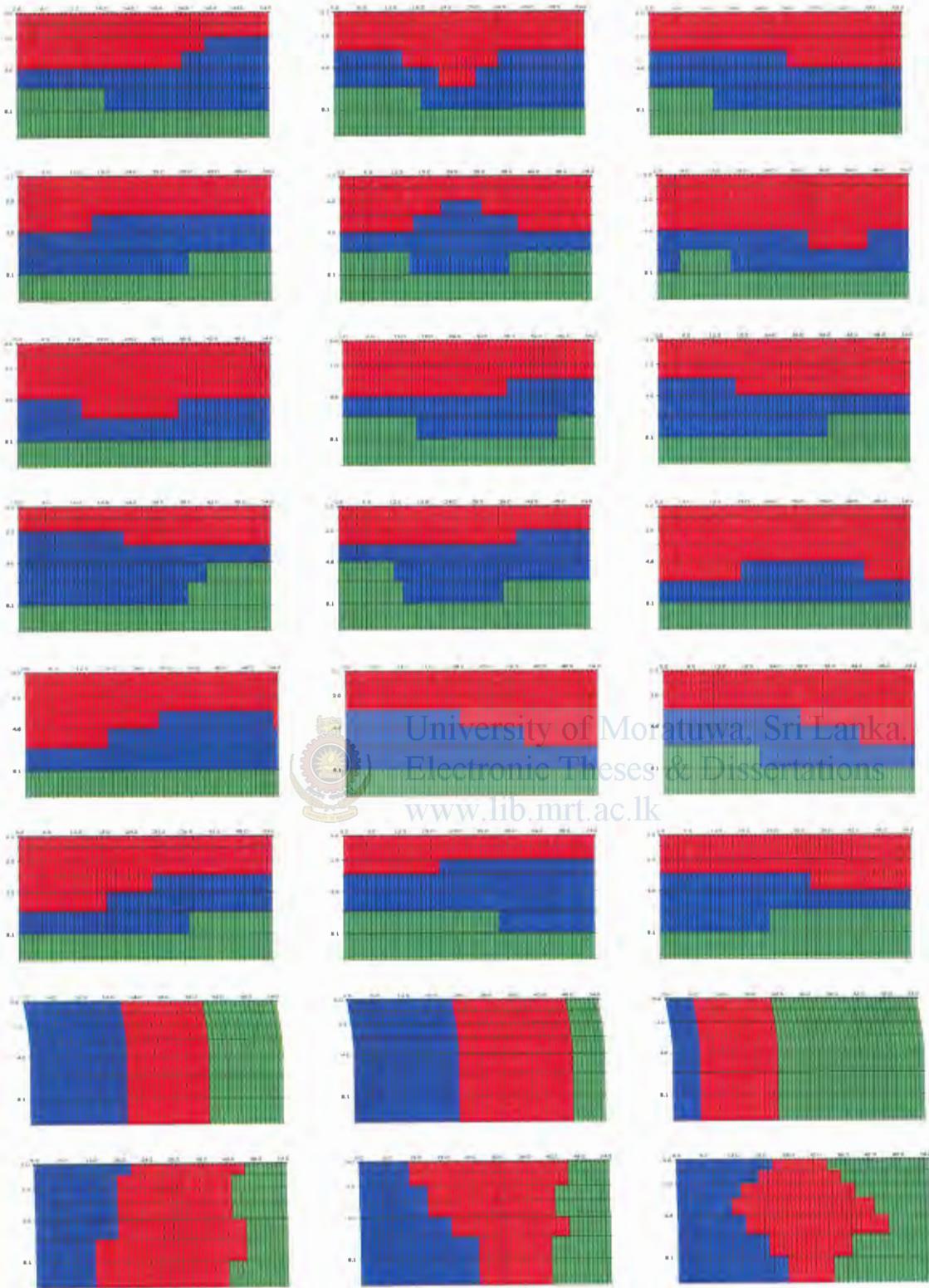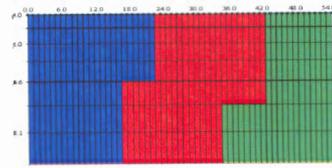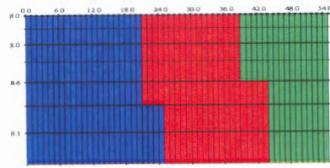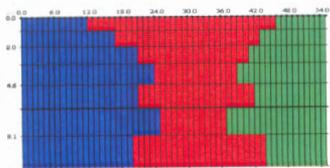
Database of Mesh assignments used for 2D case studies

H.1 Sample Model File used for mesh assignments

Figure H.1 – First half of the model file

```
LEVEL 6
111111111111
111111111111
111111111111
111111111111
111111111111
111111111111
111111111111
111111111111
111111111111
111111111111
111111111111
111111111111
LEVEL 7
111111111111 ⌐
111111111111
111111111111
111111111111
111111111111       Resistivity blocks for
111111111111       Layer 7- Last layer
111111111111
111111111111
111111111111
111111111111
111111111111
111111111111 ⌐
1                  1 means user defined layer depths are used
0.70
1.505
2.4307
3.4954             Depths to the base of each model layer
4.72
6.1276
7.7468
0                  Followed by few zeros
0
0
0
```

Figure H.2 – Second half of the model file

H.2 Database of Mesh Assignments

The 2D slices for each 3D model used for the generation of the training database is given below. Each set consists of seven 2D meshes representing the 7 layers. Here the top layer height is set to 1.5m (bark blue), while the bottom layer (light blue) extends to infinity. The anomalous body is shown with dark green.
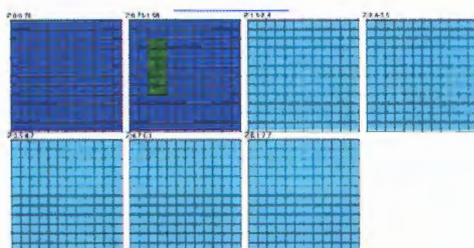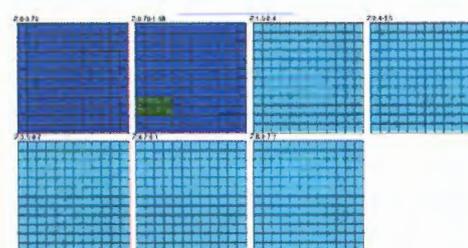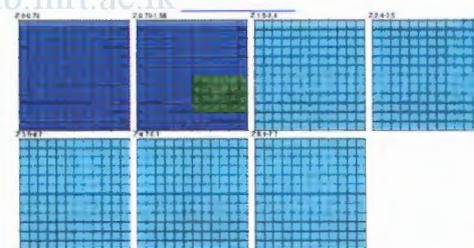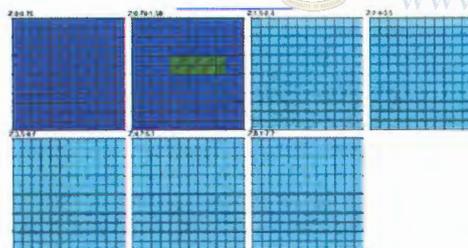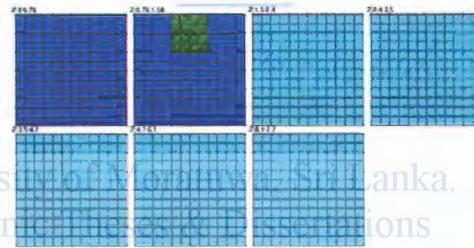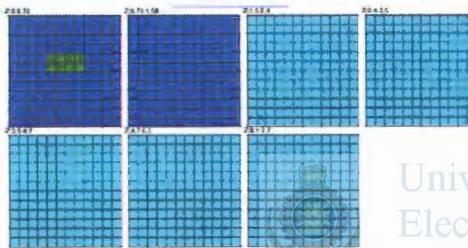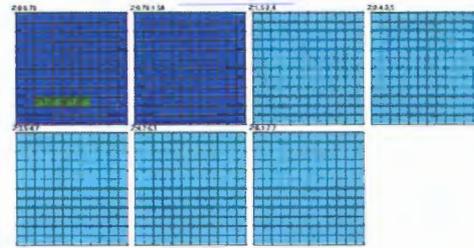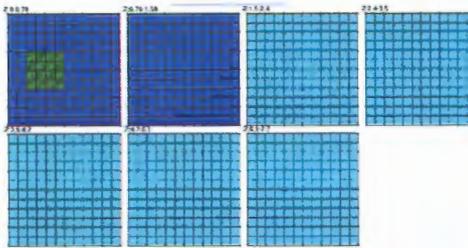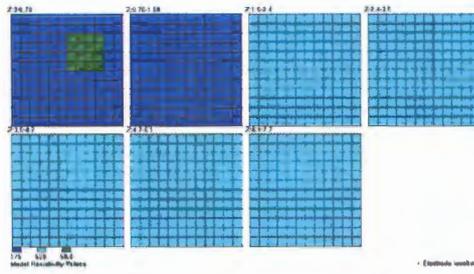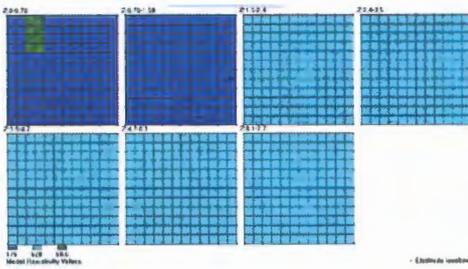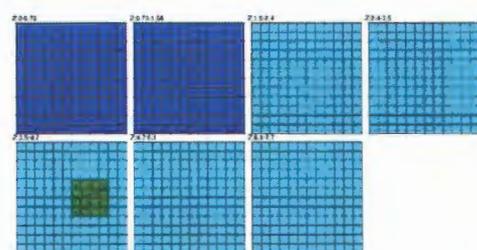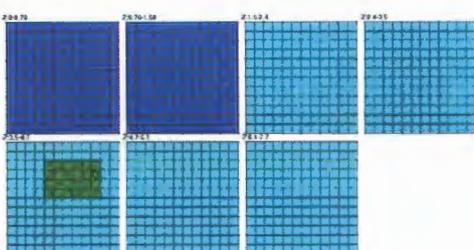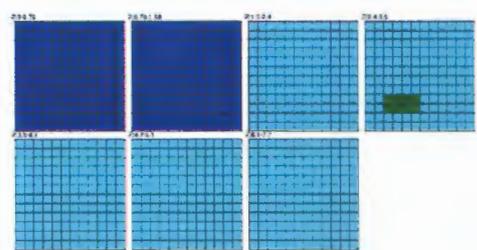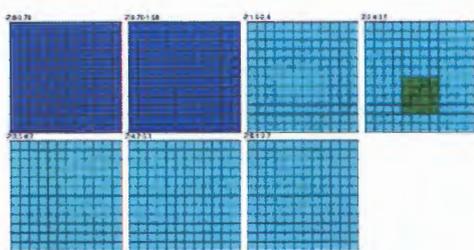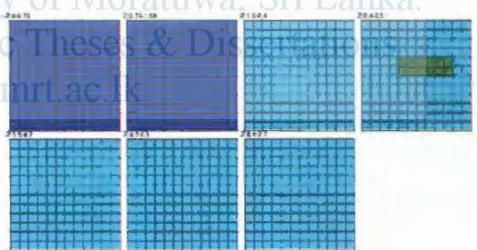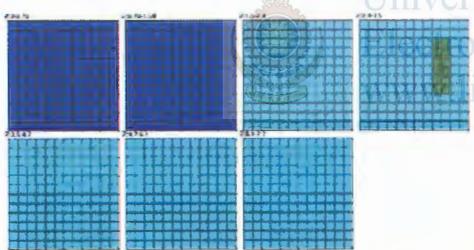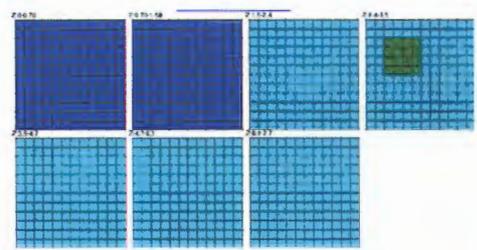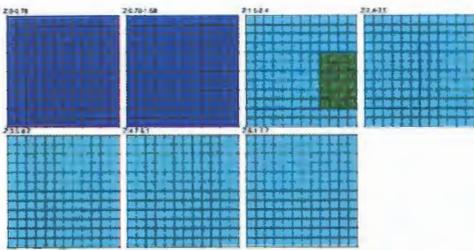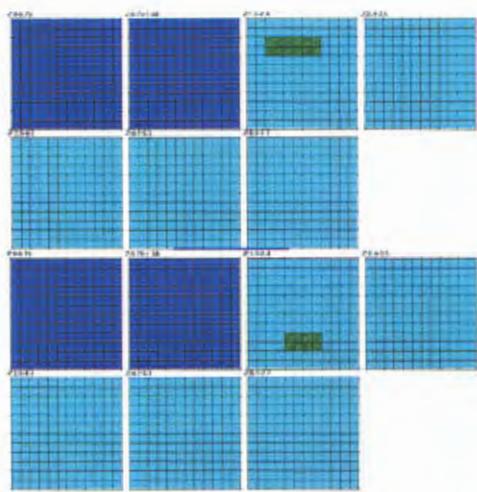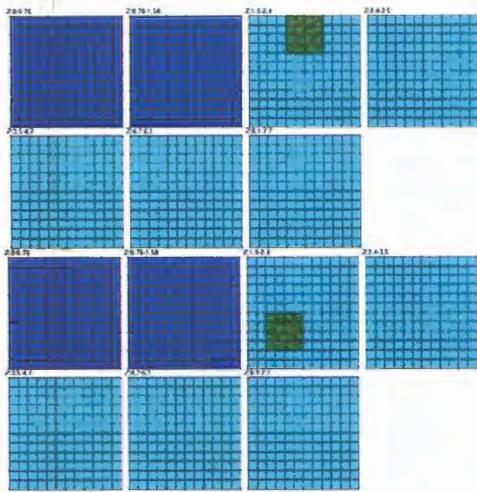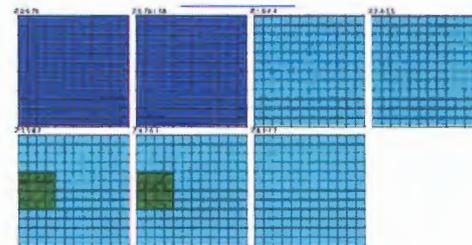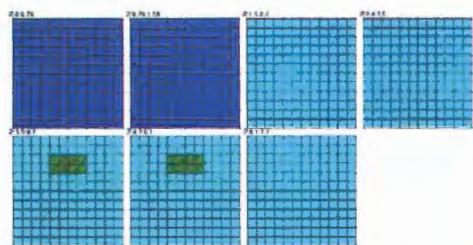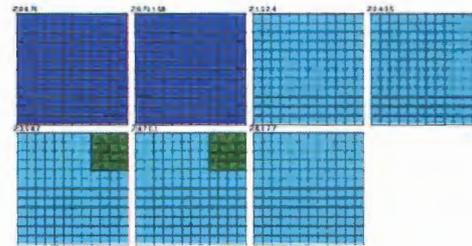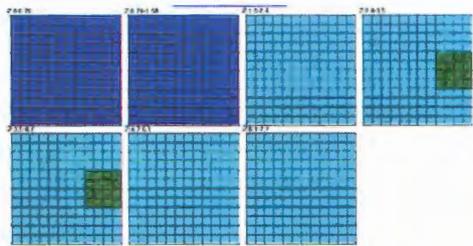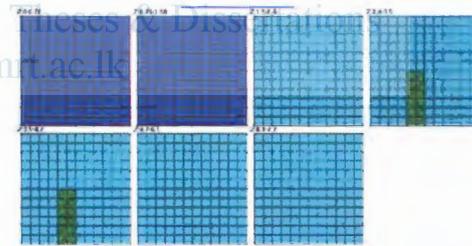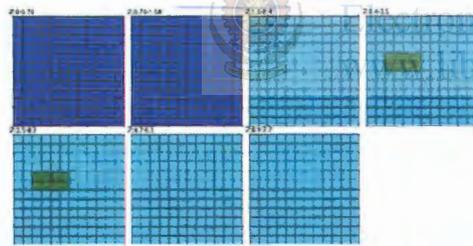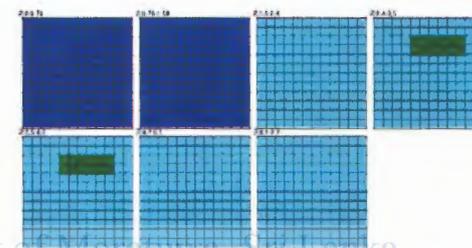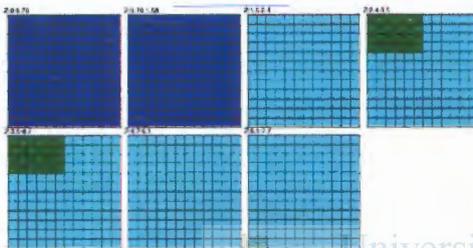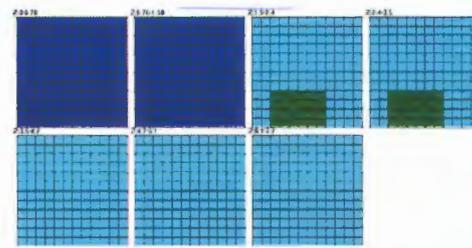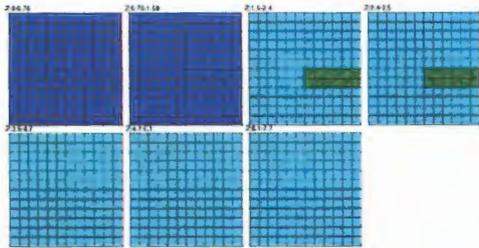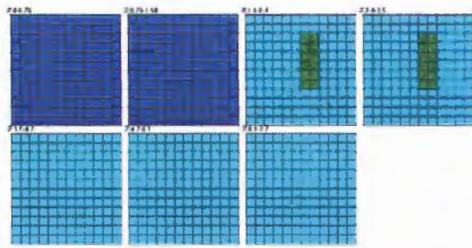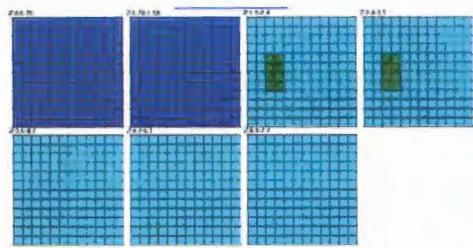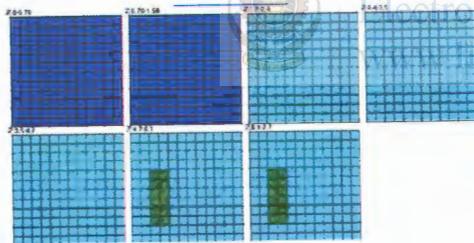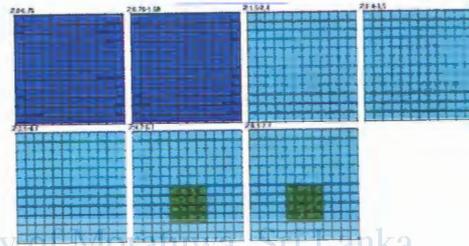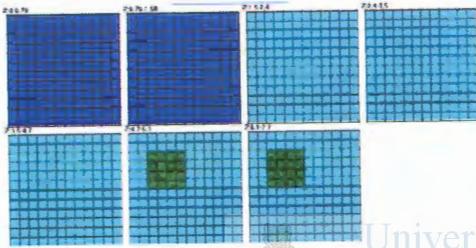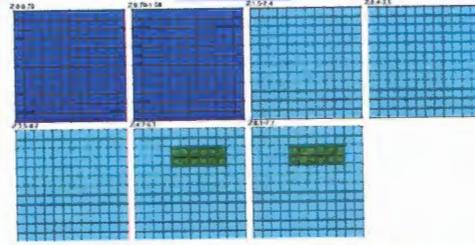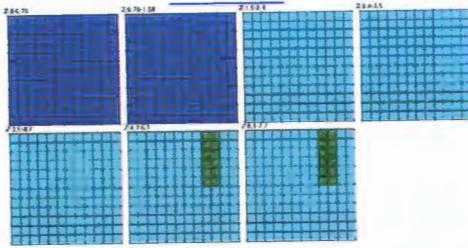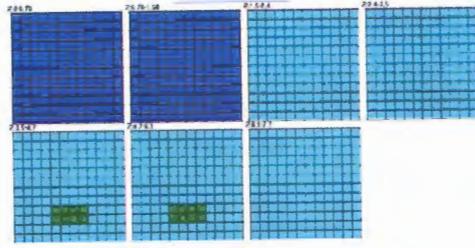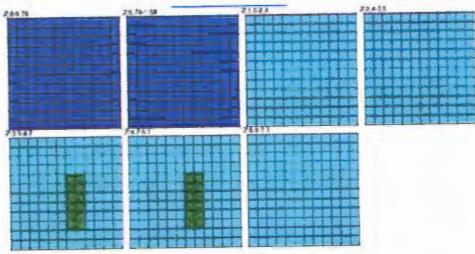
Commands on Mathematica Editor for Electrode Resistance Calculations

---

```
In[1]:= p1 = 800.45
        p2 = 593.05
        h = 5.71
        a = 0.0254
        1 = 1.4
        k1 = (p2 - p1) / (p1 + p2)

Out[1]= 800.45

Out[2]= 593.05

Out[3]= 5.71

Out[4]= 0.0254

Out[5]= 1.4

Out[6]= -0.148834
```

$$p[\lambda\_, t\_, h\_, k1\_, a\_] := \frac{Exp[-\lambda t] + k1 \, Exp[-2 \lambda h] \, Exp[\lambda t]}{1 - k1 \, Exp[-2 \lambda h]} \, BesselJ[0, \lambda a]$$

```
g = NIntegrate[p[λ, t, h, k1, a], {λ, 0, ∞},
     {t, 0, 1.40208}]
```

NIntegrate::slwcon :
  Numerical integration converging too slowly; suspect one
    of the following: singularity, value of the integration
    being 0, oscillatory integrand, or insufficient
    WorkingPrecision. If your integrand is oscillatory try
    using the option Method->Oscillatory in NIntegrate. More...

NIntegrate::ncvb :
  NIntegrate failed to converge to prescribed accuracy
    after 13 recursive bisections in λ near
    (λ, t) = {97768.3, 5.5520×10⁻⁶}. More...

```
Out[8]= 4.66413
```

$$R = \frac{1}{2 \pi 1} \, p1 \, g$$

```
Out[10]= 424.421
```

Figure I.1 - Mathematica editor commands for electrode resistance calculations

Individual cell outputs for Test Grid 1 of 2D case 1

99.8	78.8	61.8	72.6	110.8	99.2	123.4	1
98	126	80.1	113.5	86.2	57.6	76.4	2
122.4	119.6	112.2	101.1	121.7	63.3	88.6	3
126.1	109.1	123	126.5	112.6	69.2	123.5	4
101.2	108.9	87.8	95.4	84.9	95.3	104.5	5
86.1	125.9	131.2	110.3	104.8	124	115.2	6
100.5	122.7	97.6	87	75.9	99.3	83	7
104.2	129.2	102.4	100.3	93.8	89.2	137.2	8
112.6	80	94.2	124.3	69.2	98.7	99.3	9
34.3	87.2	88.9	128.2	87.6	145.1	151.8	10
129.7	124.1	105.2	101.7	95.7	104.2	86.2	11
64.6	121.9	111.5	150.9	121.6	103.8	68.5	12
82.5	121.9	95.9	98.3	96.6	105.7	87.8	13
68.5	102.7	46.2	125.7	83.8	69.4	107.5	14
84.1	105.1	143.1	105	99.9	52.6	125.5	15
73.4	93.5	80.9	93.4	76.7	59.4	88.2	16
108.1	99.2	138.5	136.9	87.1	124.4	145	17
128.8	127.5	120.3	105.7	131.4	92.7	99.7	18
82.2	106.2	46.5	94.6	102.6	87.3	114.7	19
86.4	104.9	99.9	96.4	83.9	95.5	87.2	20
75.4	108.1	105	106.5	98	103.6	128.9	21

Table J.1 - Neural network output mesh values for test grid 1 of 2D CASE1 – (Columns 1 to 21)

113.9	66.8	115.8	99.9	86.6	117.9	76.8	**22**
76.1	140.9	111.8	101.3	85.9	75.4	113.7	**23**
98.1	89.3	111.5	96.6	95.6	102.5	114.6	**24**
82.6	142.7	105.8	80.8	91	116.1	110.3	**25**
92.2	99.5	108.2	99.4	1003	978.7	133.9	**26**
106.2	112.8	133.5	69.2	1032	959.8	86.5	**27**
113.6	90.2	110.3	96.8	994.1	1005	168.3	**28**
73.1	132.3	96.5	101.8	93	103	92.1	**29**
78.3	102.2	100.2	106.7	117.5	152.2	124.1	**30**
84.4	100.4	112.6	118.4	116.4	98.9	106.2	**31**
84.8	111.3	99.3	76.6	111.9	99.7	90.3	**32**
111.3	122.3	84.1	75.7	100.8	89.7	93.4	**33**
87.9	79.4	79.2	140.3	77.5	124.1	115.5	**34**
82.5	73	106	154.1	113.6	102.2	93.3	**35**
52.1	114.3	119.5	118.3	94.6	133.9	141.9	**36**
92.2	105.9	126.1	88.6	103.3	109.1	107.8	**37**
108.8	65.1	118	111.8	90.5	121.3	86.9	**38**
117.7	119.2	85.4	103.9	109	97.4	98.9	**39**
114.2	88	116.4	58.6	94.6	103.8	108.5	**40**
86.9	109.7	79.9	101.4	88.6	90.9	98.5	**41**
83.9	123.4	97.5	97.6	71.7	87.6	115.7	**42**

Table J.2 - Neural network output mesh values for test grid 1 of 2D CASE1 - (Columns 22 to 42)

126.6	118.8	72.9	109.1	78.9	61.5	97.3	**43**
47.5	86.8	126.6	101.8	135.3	71.5	112.7	**44**
124.1	99.3	109	29.9	142.2	105.4	131.6	**45**
102.7	118.5	118.5	77.4	79.5	92.7	99.4	**46**
80.5	124.7	97.5	70.6	97.8	80.3	106.3	**47**
110.7	111.8	106.1	84.2	101.3	127.3	139.7	**48**
83.8	130.7	78.4	62.9	91.2	117.3	87.1	**49**
123.6	118.7	73.9	94.7	136.7	91.4	106.3	**50**
135.3	110.6	79.4	81.5	111.2	119.4	131.8	**51**
133.9	85.7	136.1	111.8	87.6	77.1	80.5	**52**
97	105.9	107.3	86	75.1	141	77	**53**
82.6	115.1	93.6	111.7	101.9	100.2	70.3	**54**
82.8	121.1	89.9	72.2	101.3	114.9	80.7	**55**

Table J.3 - Neural network output mesh values for test grid 1 of 2D CASE1 - (Columns 43 to 55)